National Renewable Energy Laboratory
A national laboratory of the U.S. Department of Energy
Office of Energy Efficiency & Renewable Energy
Innovation for Our Energy Future

Model Development and Loads Analysis of an Offshore Wind Turbine on a Tension Leg Platform, with a Comparison to Other Floating Turbine Concepts

April 2009

Denis Matha
University of Colorado - Boulder

Thesis Supervisors:

Jason Jonkman, Ph.D., NREL
Tim Fischer, MSc Dipl.-Ing(FH),
University Stuttgart, Germany

Subcontract Report
NREL/SR-500-45891
February 2010

NREL is operated for DOE by the Alliance for Sustainable Energy, LLC Contract No. DE-AC36-08-GO28308

Model Development and Loads Analysis of an Offshore Wind Turbine on a Tension Leg Platform, with a Comparison to Other Floating Turbine Concepts

April 2009

Denis Matha
University of Colorado - Boulder

Thesis Supervisors:

Jason Jonkman, Ph.D., NREL
Tim Fischer, MSc Dipl.-Ing(FH),
University Stuttgart, Germany

NREL Technical Monitor: J. Jonkman

Prepared under Subcontract No. KXEA-3-33606-3

Subcontract Report
NREL/SR-500-45891
February 2010

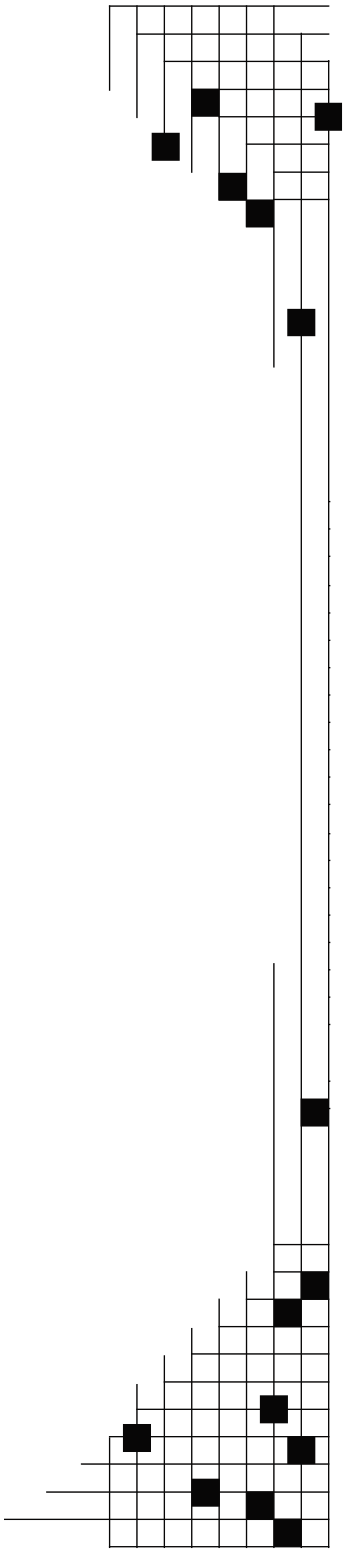

National Renewable Energy Laboratory
1617 Cole Boulevard, Golden, Colorado 80401-3393
303-275-3000 • www.nrel.gov

NREL is a national laboratory of the U.S. Department of Energy
Office of Energy Efficiency and Renewable Energy
Operated by the Alliance for Sustainable Energy, LLC

Contract No. DE-AC36-08-GO28308

Available electronically at http://www.osti.gov/bridge

Available for a processing fee to U.S. Department of Energy
and its contractors, in paper, from:
U.S. Department of Energy
Office of Scientific and Technical Information
P.O. Box 62
Oak Ridge, TN 37831-0062
phone: 865.576.8401
fax: 865.576.5728
email: mailto:reports@adonis.osti.gov

Available for sale to the public, in paper, from:
U.S. Department of Commerce
National Technical Information Service
5285 Port Royal Road
Springfield, VA 22161
phone: 800.553.6847
fax: 703.605.6900
email: orders@ntis.fedworld.gov
online ordering: http://www.ntis.gov/ordering.htm

This publication received minimal editorial review at NREL

Printed on paper containing at least 50% wastepaper, including 20% postconsumer waste

Acknowledgments

I am grateful to many people for help—both direct and indirect—in writing this report.

I would like to express my deepest appreciation to my thesis adviser at NREL, Dr. Jason Jonkman, for his support throughout each stage of the project and for giving me the opportunity to work on a truly exciting project. Dr. Jonkman's help in the facilitation of my six-month stay at NREL (in Boulder, CO), his guidance and persistent aid during the research process, and his review of the thesis during its final stages all are very much appreciated. On many occasions he provided guidance, motivation, and new ideas, and I am very thankful for Dr. Jonkman's patience and willingness to address my questions and share his knowledge to help me thoroughly understand the subject.

Thanks also are due to Tim Fischer (MSc. Dipl. Ing.), my thesis adviser from the University of Stuttgart. He provided valuable advice, motivation, and support during the entire project, and helped review my thesis. Without Mr. Fischer, this project would have been not possible.

Very special thanks go to my professor and thesis supervisor Dr. Martin Kühn of the Endowed Chair of Wind Energy at the University Stuttgart for his role in my education, his advice on important decisions in the course of the project, and for giving me the opportunity to pursue this project at NREL.

Thank you José Azcona Armendáriz from the Departamento de Energía Eólica at Centro Nacional de Energías Renovables (CENER), for supporting me during the building of the TLP model in FAST and for valuable help in overcoming the challenges we encountered.

Special thanks to Dr. Gary Pawlas of the University of Colorado, Boulder, for both his time and his valuable role in providing the resources and support to work on this project, and also for his assistance with immigration and visa issues.

My gratitude also goes to several colleagues at the National Renewable Energy Laboratory's National Wind Technology Center. I thank Marshall L. Buhl Jr. for providing me support in the load case simulations and especially in adding fatigue calculation capability to the postprocessor MCrunch. Without his help, several parts of the project would have been impossible to accomplish in my limited time frame. I also thank Dr. Gunjit Bir for his support in the stability analysis process. The efforts of Cynthia Szydlek in solving the mandatory formalities prior to and during my stay in the United States at NREL are very much appreciated. The leaders of the offshore wind energy program—Sandy Butterfield and Walter Musial—are greatly appreciated for making my stay possible and for supporting me with valuable advice. Thank you also to the directors of the NWTC, Dr. Robert Tresher and Dr. Michael Robinson. Special thanks to Kathleen O'Dell and Lisa Teman for editing this work to make it much more readable.

I also am very much indebted to all the individuals mentioned above, and to colleagues including Dr. Shuangwen Sheng, Francisco Oyague, Billy Hoffman, Dr. Patrick Moriarty, and those whose names are not included here. Finally, I want to thank my family and friends in Germany for the support you've given me—without you, this endeavor would not have been possible.

Nomenclature

Latin Symbols

Symbol	Unit	Description
A_0	[m^2]	Water-plane area of the support platform when it is not displaced
A_2	[m^2]	Rotor area
A_{ij}	[kg, kg·m, kg·m^2]	(i,j) Component of the impulsive hydrodynamic added mass
a_i	[m/s^2]	Component of the undisturbed fluid-particle acceleration in Morison's equation in the direction of the i^{th} translational degree of freedom of the support platform
$A_{Radiation}$	[kg·m^2]	Added inertia (added mass) associated with hydrodynamic radiation in pitch
B_{ij}	[kg/s, kg·m/s, kg·m^2/s]	(i,j) Component of the hydrodynamic-damping matrix
$B_{Radiation}$	[kg·m^2/s]	Damping associated with hydrodynamic radiation in pitch
C_A	[-]	Normalized hydrodynamic-added-mass coefficient in Morison's equation
C_D	[-]	Normalized viscous-drag coefficient in Morison's equation
C_{ij}^{Lines}	[kg/s^2, kg·m/s^2, kg·m^2/s^2]	(i,j) Component of the linear restoring matrix from all mooring lines
$C_{ij}^{Hydrostatic}$	[kg/s^2, kg·m/s^2, kg·m^2/s^2]	(i,j) Component of the linear hydrostatic-restoring matrix from the water-plane area and the center of buoyancy
C_x	$[\frac{kg}{ms}]$	Effective damping in the equation of motion for the platform pitch in terms of the translation of the hub
D	[m]	Diameter of cylinder in Morison's equation
D_C	[m]	Effective diameter of a mooring line
D^{Life}	[-]	Lifetime damage
DEL^{Life}	[N·m]	Lifetime damage equivalent load
$dF_i^{Platform}$	[N/m]	i^{th} Component of the total external load acting on a differential element of cylinder in Morison's equation, other than those loads transmitted from the wind turbine and the weight of the support
dz	[m]	Length of a differential element of cylinder in Morison's equation

$E[H_s \mid V_{hub}]$	[m]	Expected value of the significant wave height conditioned on the mean hub-height wind speed, based on the long-term joint-probability distribution of metocean parameters
EA	[N]	Extensional stiffness of a mooring line
$F_i^{Hydrostatic}$	[N, N·m]	i-th Component of the total hydrostatic load on the support platform
F_i^{Lines}	[N, N·m]	ith Component of the total load on the support platform from the contribution of all mooring lines
$F_i^{Lines,0}$	[N, N·m]	ith Component of the total load on the support platform in its undisplaced position from the contribution of all mooring lines
F_i^{Wave}	[N, N·m]	ith Component of the total excitation force on the support platform from incident waves
$F_i^{Cylinder}$	[N, N·m]	ith Component of the total load on a cylindrical structure from Morison's equation
$F_i^{Viscous}$	[N, N·m]	ith Component of the total viscous-drag load acting on the support platform from Morison's equation
f_{waves}	[Hz]	Incident-wave frequency
g	[m/s^2]	Gravitational acceleration constant
H_F	[N]	Horizontal component of the effective tension in a mooring line at the fairlead
H_s	[m]	Significant wave height
H_{s1}	[m]	Significant wave height based on a 3-hour reference period, with a recurrence period of 1 year
H_{s50}	[m]	Significant wave height based on a 3-hour reference period, with a recurrence period of 50 years
I_{Mass}	[m^2 kg]	Pitch inertia associated with wind turbine and platform mass
$I_{yy,\ sys,\ \&\ a/m}$	[m^2 kg]	Pitch inertia associated with wind turbine and platform mass, including added mass
j	[-]	Imaginary number, $\sqrt{-1}$
k	[-]	Wave number of an incident wave
K_{ij}	[N/(m/s^2, Nm/(m/s^2), Nm^2/(m/s^2)]	(i,j) Component of the matrix of wave-radiation-retardation kernels or impulse-response functions of the radiation problem
K_x	[N/m]	Effective stiffness in the equation of motion for the platform pitch in terms of the translation of the hub
L	[m]	Total unstretched length of a mooring line
L_{ij}	[N/(m/s, Nm/(m/s), Nm^2/(m/s)]	(i,j) Component of the matrix of alternative formulations of the wave-radiation-retardation kernels or impulse-response functions of the radiation problem
L_k^{RF}	[N·m]	kth Load range at fixed mean

L_l	[N·m]	l^{th} Load range
L^{MF}	[N]	Fixed load mean
L^{M}	[N]	l^{th} load mean bin
L^{Ult}	[N]	Ultimate load
$M_{sys\ \&\ a/m}$	[kg]	Mass of the wind turbine and platform, including added mass
M_x	[kg]	Effective mass in the equation of motion for the platform pitch in terms of the translation of the hub
n	[-]	Discrete-time-step counter
N_k^F	[-]	Number of cycles to failure in the k^{th} load range bin at fixed load mean
$n_j^{Life,eq}$	[-]	Number of equivalent lifetime cycles in the j^{th} wind speed bin
$n_{jk}^{Life,eq}$	[-]	Number of equivalent lifetime cycles in the k^{th} load range bin and j^{th} wind speed bin
$n_j^{ST,eq}$	[-]	Number of equivalent short-term lifetime cycles in the j^{th} wind speed bin
p	[Pa]	Pressure
p_j^v	[-]	Wind speed probability
p_{-2}	[Pa]	Pressure just before the rotor
p_{+2}	[Pa]	Pressure just behind the rotor
PDF_ζ	[1/m]	Probability density function
q_j	[m, rad]	j^{th} system degree of freedom
$r_{Fairleads}$	[m]	Radius from the platform center (symmetry) line to the attachment points (= fairleads) of the mooring lines
R_{Gyr}	[m]	Radius of gyration
$S_\xi^{1/2-sided}$	[m^2/(rad/s)]	One/two-sided power spectral density of the wave elevation per unit time
t	[s]	Simulation time
T	[N]	Aerodynamic rotor thrust force
T^{Life}	[s]	Lifetime
T_j^{ST}	[s]	Short-term lifetime
T_p	[s]	Peak spectral period
v	[m/s]	Velocity
v_{ref}	[m/s]	Reference velocity for wind shear equation

V	[m^3]	Volume
V_0	[m^3]	Displaced volume of fluid when the support platform is in its undisplaced position
v_1	[m/s]	Velocity far in front of rotor
v_3	[m/s]	Velocity far behind rotor
V_F	[N]	Vertical component of the effective tension in a mooring line at the fairlead
$W[k]$	[-]	Fourier transform of a realization of a white Gaussian noise time-series process with unit variance
x_f	[m]	Horizontal distance between the anchor and fairlead of a mooring line
X_i	[kg/s^2, $kg \cdot m/s^2$]	i-th Component of the frequency- and direction-dependent complex incident-wave-excitation force on the support platform per unit wave amplitude
X, Y, Z	[m]	Set of orthogonal axes making up an original reference frame (when applied to the support platform in particular, X, Y, Z represents the set of orthogonal axes of an inertial reference frame fixed with respect to the mean location of the platform, with the XY-plane designating the still-water level and the Z-axis directed upward opposite gravity along the centerline of the undeflected tower when the platform is undisplaced)
x, y, z	[m]	Set of orthogonal axes making up a transformed reference frame (when applied to the support platform in particular, x, y, z represents the set of orthogonal axes of a body-fixed reference frame within the platform, with the xy-plane designating the still-water level when the platform is undisplaced and the z-axis directed upward along the centerline of the undeflected tower)
z_{COB}	[m]	Body-fixed vertical location of the center of buoyancy of the support platform (relative to the still-water level and negative downward along the undeflected tower centerline when the support platform is in its undisplaced position)
z_F	[m]	Vertical distance between the anchor and fairlead of a mooring line
z_{ref}	[m]	Reference height for wind shear equation

Greek Symbols

Symbol	Unit	Description
α	[deg]	Angle of attack
β	[deg]	Incident-wave propagation heading direction
Γ	[-]	Peak shape parameter in the Joint North Sea Wave Project (JONSWAP) spectrum

δ_{ij}	[-]	(i,j) Component of the Kronecker-Delta function (i.e., identity matrix), equal to unity when i=j and zero when i≠j
ζ	[m]	Instantaneous elevation of incident waves
θ	[deg]	For the blade-pitch controller, the full-span rotor-collective blade-pitch angle
η_i	[m, rad]	i-th Translatory or rotational platform displacement
μ	[kg/m]	Mass of mooring line per unit length
ν	[m^2/s]	Kinematic viscosity
ξ_i	[m, rad]	i-th Platform degree of freedom
π	[-]	The ratio of a circle's circumference to its diameter
ρ	[kg/m^3]	Density
σ	[-]	Scaling factor in the Joint North Sea Wave Project (JONSWAP) spectrum
σ^2_{zeta}	[m^2]	Variance of the instantaneous elevation of incident waves (≡ RMS value)
τ	[s]	Dummy integration variable using the same units as the simulation time
φ	[m^2/s^2]	Velocity potential function
ω	[rad/s]	For hydrodynamics, this is the frequency of incident waves or frequency of oscillation of a particular mode of motion of the platform
ω	[N/m]	For mooring systems, this is the apparent weight of a line in fluid per unit length of line

List of Acronyms and Abbreviations

ADAMS	Automatic Dynamic Analysis of Mechanical Systems (MSC Software)
BEM	blade element momentum
CENER	Centro Nacional de Energías Renovables
CFD	computational fluid dynamics
CM	center of mass
COB	center of buoyancy
COG	center of gravity
DEL	damage equivalent load
DLC	design load case
DOF	degree of freedom
DOWEC	Dutch Offshore Wind Energy Converter project

ECD	extreme coherent gust with direction change
ECN	Energy Research Center of the Netherlands
EOG	extreme operating gust
ESS	extreme sea state
ETM	extreme turbulence model
EWEA	European Wind Energy Association
EWM	turbulent extreme wind model
EWS	extreme wind shear
FEM	finite element method
FAST	Fatigue, Aerodynamics, Structures, and Turbulence (NREL Design Code)
FLEX	DTU design code
GDW	generalized dynamic wake
IEC	International Electrotechnical Commission
JONSWAP	Joint North Sea Wave Project
LSS	low-speed shaft
MIT	Massachusetts Institute of Technology
MSL	mean sea level
NREL	National Renewable Energy Laboratory
NSS	normal sea state
NTM	normal turbulence model
NWTC	National Wind Technology Center
OC3	Offshore Code Comparison Collaboration
OWC	oscillating water column
PDF	probability density function
PI	proportional integral
PID	proportional integral derivative
PSD	power spectral density
PSF	partial safety factor
RAO	response amplitude operator
RECOFF	recommendations for design of offshore wind turbines project
RMS	root mean square
sec	second(s)
SIMPACK	“SIMulation PACKage”; multi-body systems software package (SIMPACK AG)
S/N	stress against number of cycles to failure
ST	short term
SWL	still water level
TLP	tension leg platform
ULF	ultimate load factor
WAMIT	Wave Analysis at MIT
WGN	white Gaussian noise
WindPACT	Wind Partnerships for Advanced Component Technology project
WT	wind turbine

Executive Summary

This report presents results of the analysis of a 5-MW wind turbine located on a floating offshore tension leg platform (TLP) that was conducted using the fully coupled time-domain aero-hydro-servo-elastic design code FAST with AeroDyn and HydroDyn. The report also provides a description of the development process of the TLP model. The model has been verified via comparisons to frequency-domain calculations. Important differences have been identified between the frequency-domain and time-domain simulations, and have generated implications for the conceptual design process. An extensive loads and stability analysis for ultimate and fatigue loads according to the procedure of the IEC 61400-3 offshore wind turbine design standard was performed with the verified TLP model. This report compares the loads for the wind turbine on the TLP to those of an equivalent land-based turbine. Major instabilities for the TLP are identified and described.

A comprehensive analysis of three floating-platform concepts for offshore wind turbines—including the TLP—is also presented. In addition to the TLP, models were made of a 5-MW turbine supported on land and a 5-MW turbine located offshore on a barge and spar buoy. A loads and stability analysis according to the procedures of the IEC 61400-3 offshore wind turbine design standard was performed for each model using FAST with AeroDyn and HydroDyn. The concepts are compared based on the statistics, extreme event tables, instabilities, and fatigue-lifetime calculations. The results will help resolve the fundamental design trade-offs between the basic floating-system concepts.

Table of Contents

List of Figures

List of Tables

1 Introduction

1.1 Background

Wind power has emerged as an alternative to conventional power generation. It has established itself as a major source of non-polluting, inexhaustible renewable energy and—according to the World Wind Energy Association [36]—by the end of 2008 a capacity of 121,188 MW was installed worldwide. This capacity equals more than 1.5% of global electricity consumption. The turnover of the wind sector worldwide reached U.S. $ 40 billion in 2008, and the market for new wind turbines showed a 42% increase and reached an overall size of 27,261 MW.

In the wind energy industry, offshore technology is a relatively new field, having only 1,486 MW installed (Nov. 2008 [10]). These fixed-bottom offshore wind turbines are erected in shallow water in the North Sea and Baltic Sea in depths ranging from 10 m to a maximum of 45 m. In the United States, China, Japan, Spain, Norway, and many other countries, such shallow-water areas are scarce. Additionally, space requirements onshore and the public pressure to place wind turbines out of visual range further push the demand for offshore wind plants in deeper coastal waters. Huge potential sources for supplying coastal areas with offshore wind energy therefore are wind turbines located on floating support platforms in deep offshore waters (in depths of approximately 60 m to 900 m). Even at transitional depths of 30 m to 60 m, floating structures could provide a viable alternative to conventional monopile, tripod, and jacket structures. The European Wind Energy Association (EWEA) reports that, by 2015, 30,882 MW [10] of new offshore wind energy capacity will be installed in Europe alone, with Norway having installed the first full-scale floating offshore wind turbine in 2009 with a 3-MW capacity 10 km off Karmoy in water depths around 120 m using the so-called Hywind spar buoy floating concept. The U.S. potential 5 to 50 nautical miles off the coast is estimated to be more than 900,000 MW, with major metropolitan areas located on the U.S. coastline providing a huge future market for floating offshore wind turbines.

A requirement for deep-water floating offshore wind turbines is the development of reliable, viable floating-platform support structures. To develop cost-effective, high-performance floating wind turbines with structural and dynamic integrity and reliability, the IEC 61400-3 design standard for offshore wind turbines requires that integrated loads analysis be performed before a turbine is certified. Such analysis also is crucial for conceptual design and preliminary analysis. It is conducted using numerical aero-hydro-servo-elastic simulation tools like FAST (Fatigue, Aerodynamics, Structures, and Turbulence), GH Bladed, or FLEX, which are based on a combined modal and multibody structural-dynamics formulation in the time domain. These design codes are suited for performing numerous design-load case simulations within short computing time and can simulate fixed-bottom offshore support structures. Hydrodynamic loads in these codes usually are simulated using Morison's equation, which only is valid for slender cylinders. Important effects for offshore floating platforms, like free-surface memory or atypical added-mass-induced couplings between modes of motion in the radiation problem, are ignored and the diffraction problem is simplified using G.I. Taylor's long-wavelength approximation.

More-complex simulation codes like MSC. ADAMS or SIMPACK employ higher-fidelity multibody-dynamics and can incorporate more advanced aerodynamics formulations (e.g. CFD, free vortex wake models,…) and structural (FEM) models. But due to significant computing time, they are currently not suited for the extensive load case simulations required for a loads

analysis according to the IEC 61400-3 design standard. The loads analyses for this project were performed with FAST with AeroDyn and HydroDyn, because it provides unique capabilities in simulating floating-platform wind turbine designs, incorporating sophisticated hydrodynamic and mooring-system modules in a fully coupled integrated simulation environment. The work presented here investigates the tension leg platform (TLP) floating concept by developing the FAST model and performing a thorough loads analysis. Further, the results from the TLP are compared to results from the loads analysis of a barge and a spar-buoy floating concept.

1.2 Previous Research

Several studies have been conducted on floating wind turbines using a linear frequency-domain approach. Bulder et al. [3] investigated a tri-floater design for a 5-MW turbine with linear frequency-domain analysis, based on finding response amplitude operators (RAOs) for the platform's six rigid-body modes. This technique was also used by Lee [23] to analyze a 1.5-MW turbine, and by Wayman et al. [33], and Jonkman [34] to analyze various TLP and barge designs. Vijfhuizen [32] investigated a 5-MW barge design with an oscillating water column (OWC) wave-energy device. Tracy [31] (from MIT) used a frequency-domain approach described in Wayman [34] and conducted a parametric study determining the optimal TLP and slack and taut catenary spar-buoy designs with best overall performance in combination with low cost. These studies did not model the wind turbine realistically, however, and instead included the turbine's structural and aerodynamic properties by augmenting the mass, damping, and restoring matrix of the platform with the proper turbine values at an initial condition with defined platform displacement and rotor thrust. The linearized mooring system's restoring properties also were derived at that static equilibrium platform displacement.

Thus, these linear frequency-domain analyses have the important limitation that they do not capture nonlinear structural-dynamics, aerodynamics, and hydrodynamics and transient effects. To overcome these limitations, time-domain simulations were used by several research teams. Henderson and Patel [15] used a so-called state-domain technique to study the effects of platform motion on turbine fatigue loads. Withee [35] used a aero-servo-elastic design code which was modified to include platform motion and hydrodynamic loading based on Morison's equation. The so-called Hywind spar buoy concept is investigated by Nielsen, Hanson, and Skaare [28], and by Larson and Hansen [21]. They use a combined aero-servo-elastic hydrodynamic and mooring program. The technical feasibility of floating wind turbines was demonstrated by Zambrano et al. [37], but they used an unsophisticated aerodynamic and structural model for the turbine. Further limitations (not mentioned here) exist in these time-domain studies.

To overcome these limitations, Jason Jonkman [18] at NREL developed a fully coupled aero-hydro-servo-elastic simulation tool which overcomes most limitations of previously developed floating wind turbine codes. It consists of the sophisticated GL-certified [24] aero-servo-elastic design code FAST with AeroDyn, and is augmented by the coupled hydrodynamics module HydroDyn. HydroDyn has the capability of simulating time-domain hydrodynamic effects from linear hydrostatic restoring, nonlinear viscous drag, and sea currents. It accounts for added-mass and damping contributions from linear radiation, including free-surface memory effects, and incident-wave excitation from linear diffraction, and includes a quasi-static mooring line module. Jonkman applied the tool in a loads analysis of a barge concept, the ITI Energy barge, where he characterized the dynamic response and identified extreme loads and instabilities resulting from the dynamic coupling between the turbine and the floating barge. Important results include the

influence of increased pitch motion on the extreme loads and the identification of instabilities in yaw and tower side-to-side motions. In addition to the barge concept, Jonkman specified and developed a preliminary FAST model of the so-called OC3-Hywind spar buoy concept within the Benchmark Exercise of Aero-Elastic Offshore Wind Turbine Codes (OC3 stands for Offshore Code Comparison Collaboration) [17].

1.3 Floating Support Platform Concepts

Several support platform configurations are possible for floating offshore wind turbines, particularly considering the variety of the mooring systems, tanks, and ballast options that are used in the offshore oil and gas industries. The three principal concepts—classified in terms of how the concepts achieve static stability—are:

1. A shallow drafted *barge*, achieving pitch restoring via waterplane area moment;
2. A ballasted deep-drafted *spar buoy* with pitch restoring by ballasting; and
3. An unballasted *tension leg platform*, for which pitch restoring mainly is provided by the mooring system.

Figure 1 shows this classification in a simple symbolic triangle plot. In Section 3 a quantified, more detailed plot of the design space is given.

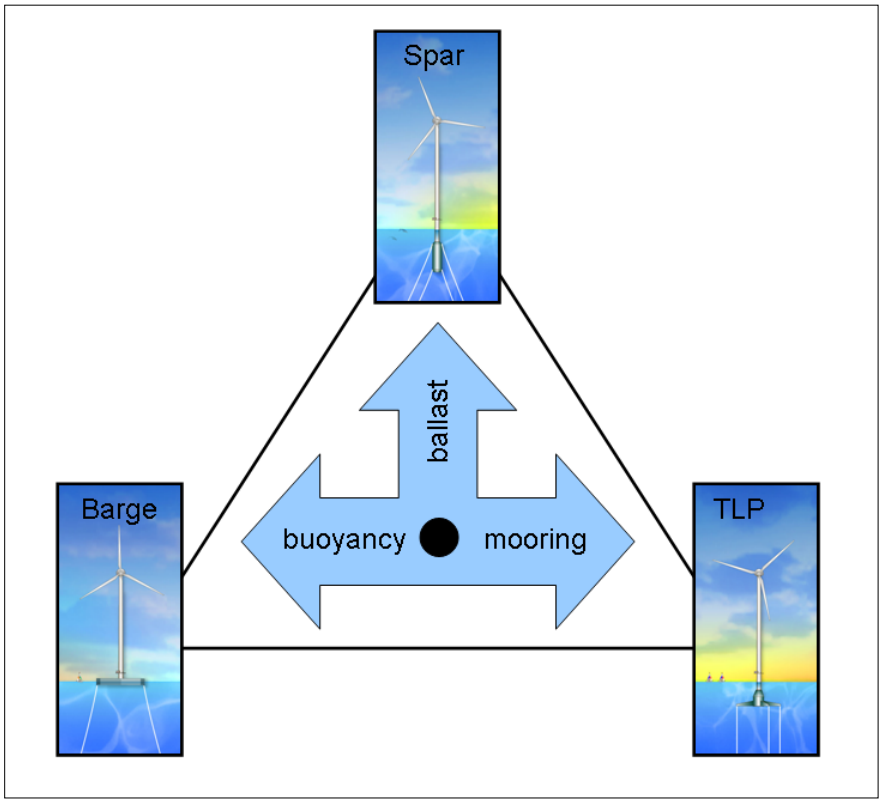

Figure 1. Floating wind turbine concepts

The barge and spar-buoy types can be anchored to the seabed either with slack catenary or with taut vertical mooring lines, but the TLP must be equipped with taut mooring lines. There are

various types of possible mooring cables, such as chains, steel or synthetic fibers, or a combination of these. Numerous anchor systems exist, ranging from simple deadweight anchors and conventional "mushroom" anchors to more sophisticated screw-in and suction anchors.

Further information on the advantages and disadvantages of each investigated concept is provided in Section 5 In addition to these basic concepts and hybrids thereof, there are conceptual unconventional floating systems being investigated which do not easily fit into these basic categories(for example, systems with an inclined tower attached to a horizontal spar buoy support platform). This report focuses on the three basic concepts.

1.4 Project Description and Software Used

This work uses the design tool FAST with AeroDyn and HydroDyn—developed and verified by Jonkman and Buhl at NREL [19]—to create a model of a TLP floating wind turbine concept. As noted in subsequent sections, the time-domain simulation tool FAST can model the aero-hydro-servo-elastic response of a variety of offshore floating wind turbines.

The aerodynamics are calculated in the FAST module AeroDyn, which uses a state-of-the art blade element-momentum approach (BEM) with empirical corrections to calculate the rotor aerodynamics. The empirical corrections consider the losses caused by the airflow around the blade tip and at the rotor hub. The effect of a turbulent-wake state that occurs if the rotor strongly decelerates the axial airflow is considered, as well as unsteady airfoil aerodynamics and wake inertia and 3-D effects such as stall delay. AeroDyn also is able to apply the generalized dynamic wake (GDW) theory to account for the effects of dynamic inflow.

The FAST module HydroDyn adds the capability of simulating time-domain hydrodynamic effects from linear hydrostatic restoring; added-mass and damping contributions from linear radiation, including free-surface memory effects; incident-wave excitation from linear diffraction; and nonlinear viscous drag, including sea current loading. The code also includes a nonlinear quasi-static mooring line module. These models are of higher fidelity than most of the models that have been used in the past to analyze floating turbines and which neglected important hydrodynamic and mooring system effects.

With these modules, FAST with AeroDyn and HydroDyn provides a fully coupled aeroelastic and hydrodynamic design code environment capable of simulating extreme and fatigue loads of two- and three-bladed horizontal-axis onshore, fixed-bottom offshore, and floating offshore wind turbines. Additionally, FAST can produce linearized representations of the nonlinear aero-elastic wind turbine model to help identify natural frequencies, damping ratios, instabilities, and in developing control systems. The software also produces input files for the multi-body code ADAMS (MSC Software), which can be used to obtain tower mode shapes and to verify the results of FAST simulations for critical load cases. Turbulent wind-inflow files are calculated with NREL's TurbSim [16] and then provided as an input for FAST. Figure 2 illustrates the various FAST modules and their interfaces. A close link between MATLAB (The Mathworks) and FAST exists, enabling the use of MATLAB's comprehensive embedded analysis functions in user-programmed MATLAB routines as a pre-processor and postprocessor or for control design purposes. For evaluating raw data from the loads analysis with FAST, the software utility Crunch/MCrunch—developed by Marshall Buhl at NREL [4]—is used.

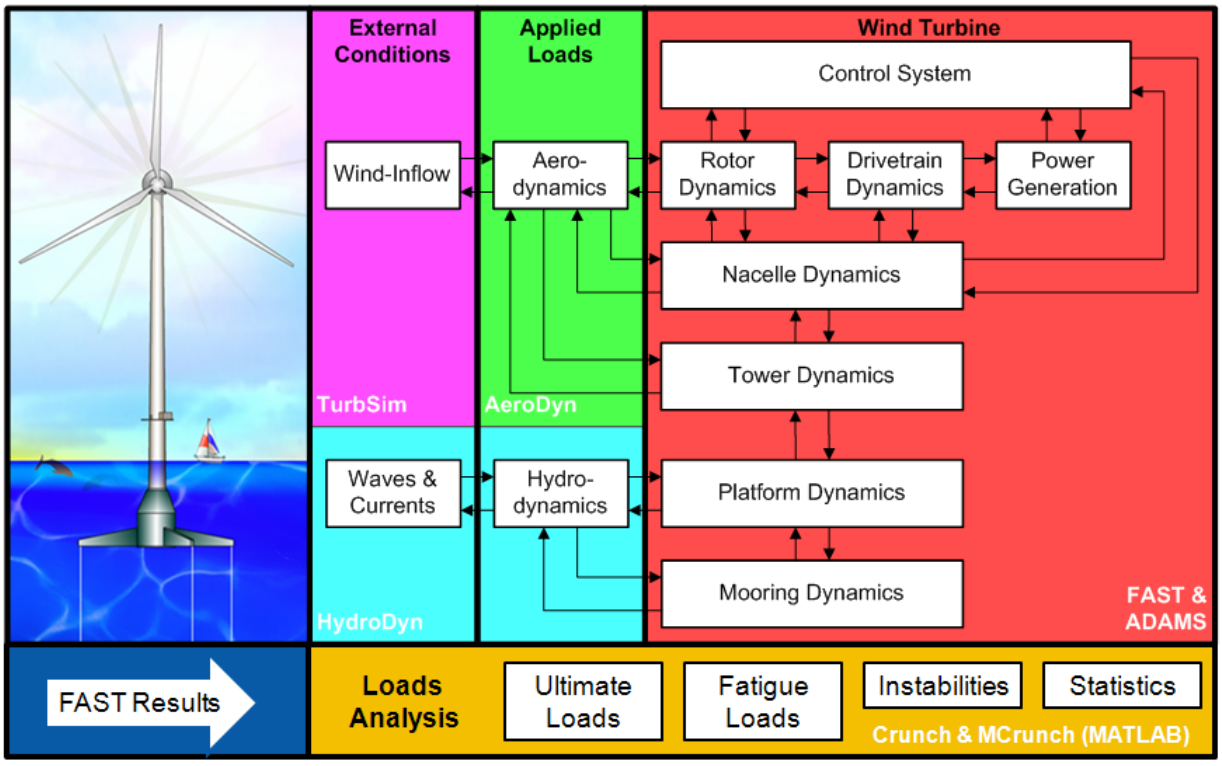

Figure 2. FAST modules

1.5 Objectives

The aim of this present study is to provide new insight in the modeling, loads, and dynamics of the TLP concept. It also is intended to provide valuable information to help clarify the advantages and disadvantages of TLP, barge, and spar-buoy floating platform concepts and to help to improve the design of floating wind turbine systems. Section 2 additionally provides a concise overview of aerodynamic and hydrodynamic loads on floating offshore wind turbines.

A FAST model of a 5-MW turbine supported by a TLP platform—modified from a MIT design derived from a parametric linear frequency-domain optimization process—is developed and compared to frequency-domain results for verification. Next, an extensive time-domain loads and stability analysis is performed in FAST for ultimate and fatigue loads according to the procedure of the IEC 61400-3 offshore wind turbine design standard, and using the verified TLP model. Major instabilities for the TLP are identified and are described. The loads for the wind turbine on the TLP are compared to those of an equivalent land-based turbine. This onshore design uses exactly the same 5-MW turbine as used on the TLP, but instead of being mounted on a floating TLP the land-based system is cantilevered to the ground. The foundation at the tower base is simulated in FAST by a rigid restraint of 0 degrees of freedom (DOF). Section 3 presents the TLP model development and Section 4 provides the results from the loads and stability analysis of the TLP.

The same design load case simulation process is performed for the OC3-Hywind concept. Including results from Jonkman, who used the same process to analyze the ITI Energy barge [18]

concept, the onshore and offshore floating concepts are compared based on the statistics, extreme event tables, and fatigue lifetime calculations. The OC3-Hywind and ITI Energy barge also use the same 5-MW wind turbine as the TLP and the land-based machine, and differ only in certain control system and tower properties. Details on the specific models and their differences are provided in Section 5. The results from the comprehensive comparison, given at the end of Section 5 and in Section 6, can help resolve fundamental design trade-offs between the floating-system concepts.

Summarized, the study had the following main objectives, which are described in this report.

- Develop a tension leg platform floating wind turbine model in the design code FAST with AeroDyn and HydroDyn;
- Verify the TLP model and compare results with frequency-domain simulations in WAMIT;
- Run a series of time-domain simulations with the TLP model and
    - analyze the ultimate loads on the turbine
    - analyze the fatigue loads on the turbine
    - identify and analyze instabilities
- Run a series of time-domain simulations with the OC3-Hywind model
- Compare ultimate and fatigue loads analysis and stability analysis results of TLP, ITI Energy barge, and OC3-Hywind floating concepts to equivalent land-based turbine
- Analyze and discuss the results for the different floating concepts and identify the fundamental design trade-offs between the floating system concepts

2 Loads on Offshore Wind Turbines

Wind turbines on floating support platforms are designed to be installed in a deep offshore environment several miles off the coast and in water depths greater than 60 m. The loads on these systems, as shown in Figure 3, are dominated by aerodynamic and hydrodynamic effects. Effects from sea ice, varying mean sea level, and marine growth constitute additional loads that must be considered in a real design process. The following section is an overview of the various loads governing the design of a floating wind turbine. The study simulated the loads using the numerical code FAST, therefore at the end of each section is a brief description the code's simplifications to the real physics and discussion of the resulting implications. Theory and derivations of aerodynamics, structural dynamics, and general descriptions of wind turbines are not provided here, but such information can be found in great detail in various textbooks ([1], [5], [12], [25]).

2.1 Aerodynamic Loads

The power production of a wind turbine depends on the interaction between the airfoils of each rotor blade and the wind. Air flowing over the blades' airfoil generates aerodynamic lift and drag forces.

The resulting aerodynamic loads on the blades and the turbine can be subdivided into three categories.

1. Steady aerodynamic forces generated by the mean wind speed.
2. Periodic aerodynamic forces generated by wind shear, rotor rotation, off-axis winds, and tower shadow.
3. Randomly fluctuating aerodynamic forces induced by gusts, turbulence, and dynamic effects.

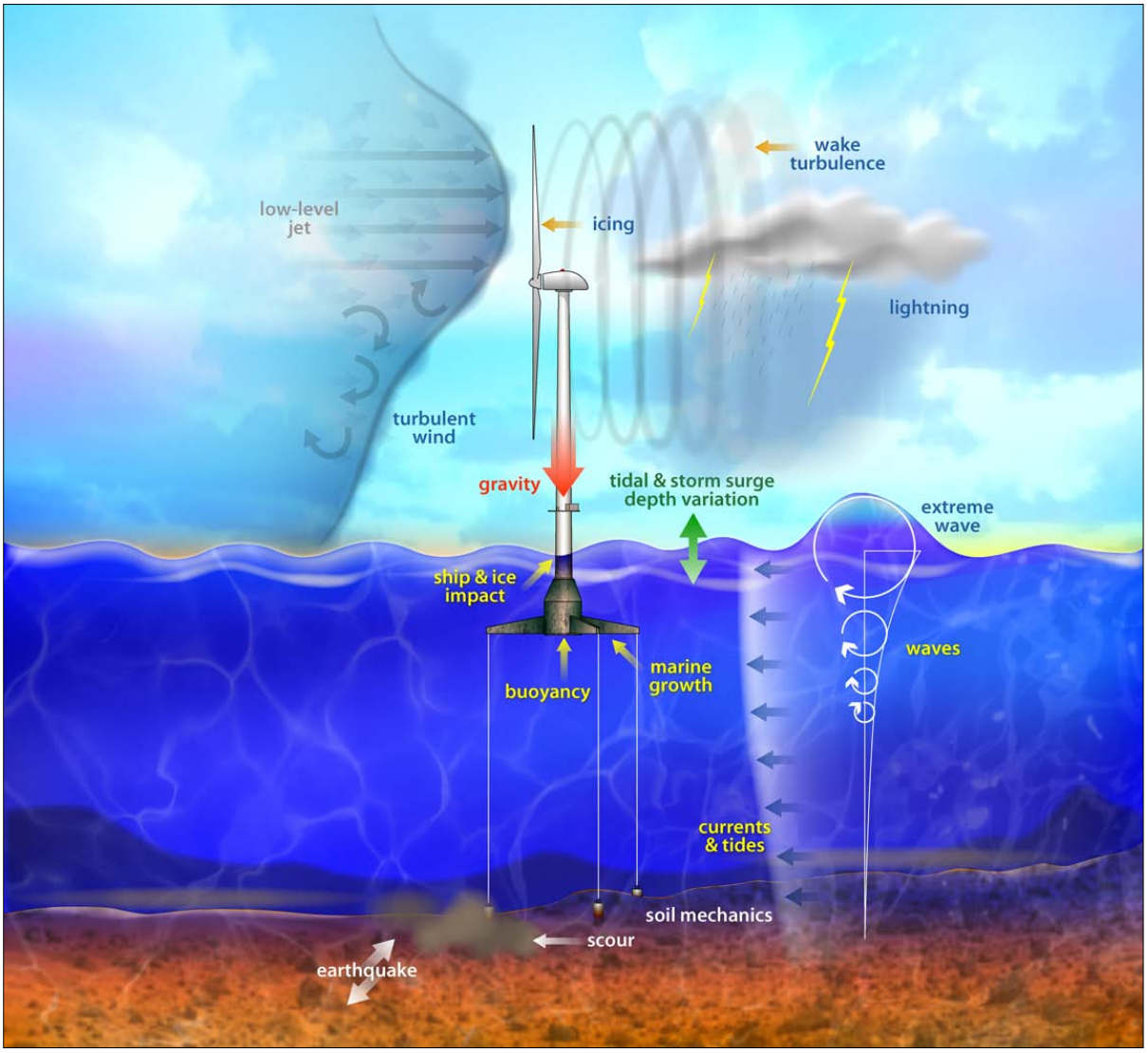

Figure 3. Loads on an offshore wind turbine [18]

2.1.1 Steady Aerodynamic Loads

Mean wind loads constitute the steady aerodynamic forces on a turbine. They occur when the wind is decelerated by the rotor, which can be represented simply as an actuator disc. According to Bernoulli's equation, this deceleration causes a discontinuity in pressure just before and behind the rotor ($p_{-2} - p_{+2}$) and, thus, a uniform thrust force over the rotor area A_2. This thrust

force T is a constant force only depending on the mean wind speed v_1 (far in front of the rotor), v_3 (far behind the rotor), the rotor area A_2, and the air density ρ [20].

$$T = A_2(p_{-2} - p_{+2}) = \frac{1}{2}\rho A_2(v_1^2 - v_3^2) \quad (1)$$

Regarding, for example, a floating TLP offshore wind turbine, this aerodynamic thrust force pushes the platform downwind to a mean offset position, where the thrust equals the restoring effect from ballast, buoyancy, and mooring lines forces in surge and pitch. For the TLP, the aerodynamic thrust force primarily is balanced by the mooring-line forces. At the mean offset position in surge the effective tension deflections on the tethers generate a negative moment which takes the positive moment from the wind thrust so as to be at equilibrium. This tension deflection becomes positive at the windward side and becomes negative at the leeward side. This is why, for TLPs, the leeward-side line tension is the critical one that is most likely to go slack. For other concepts with slack catenary mooring lines, thrust is balanced by ballast and buoyancy of the platform and the gravity of the mooring lines.

2.1.2 Periodic Aerodynamic Loads

The wind speed is not constant over the height of the turbine, it increases with increasing height above ground. The rate of that increase depends on the surface roughness. Due to the lower ground roughness length parameter z_0 offshore, the wind speed $v(z)$ increases more rapidly with increasing height than it does onshore. Figure 4 illustrates the difference in wind profiles for a typical onshore and typical offshore location, using the logarithmic wind shear description.

$$v(z) = v_{ref}\frac{ln(z/z_0)}{ln(z_{ref}/z_0)}$$

Often the vertical power shear law for the wind-speed profile is used instead, its basic form being the following [20].

$$v(z) = v_{ref}\left(\frac{z}{z_{ref}}\right)^{\alpha} \quad (2)$$

In the present research, according to the IEC 61400-3 offshore design standard [8], a shear exponent of $\alpha = 0.14$ was used for all normal wind conditions and $\alpha = 0.11$ in extreme 1- and 50-year wind conditions. Instead of utilizing different wind shear exponents for the onshore machine as advised in the IEC 61400-1 [9] onshore design standard, the IEC 61400-3 shear exponent values are used for both onshore and offshore locations to produce results that are easier to compare.

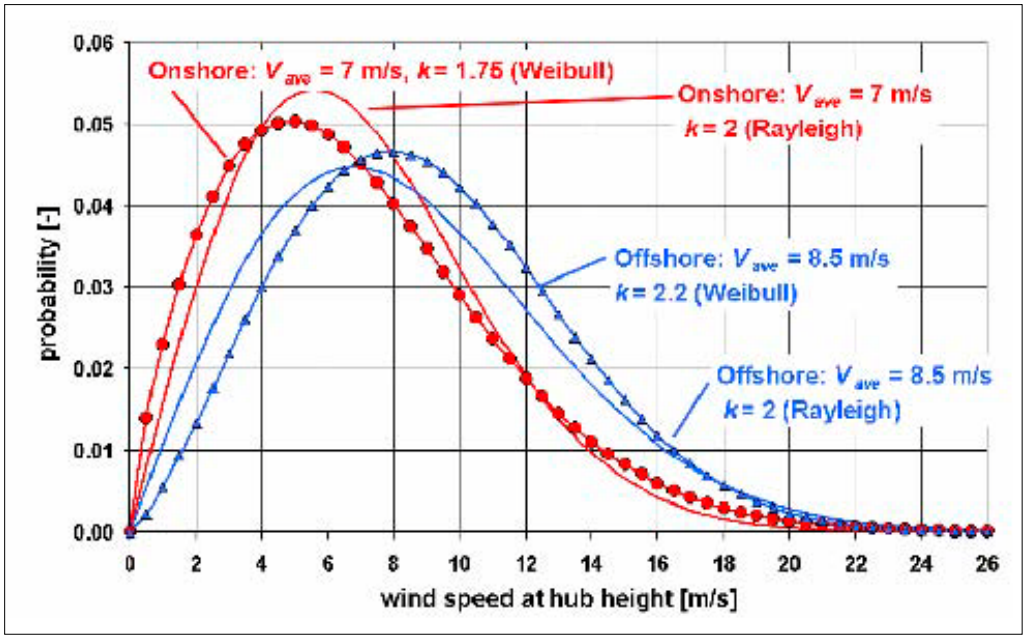

Figure 4. Differences between onshore and offshore wind shear [20]

The wind shear generates loads on the spinning rotor blades which change periodically at the rotor frequency because each blade experiences periodically changing wind speeds during each full rotation. Constant off-axis winds cause a similar periodically changing load on the turbine and the blades. Additionally, the tower poses an obstacle for the incoming airflow, a stagnation point and associated boundary layer forms and the flow in front of the tower is decelerated. So that each time a blade passes the tower, the aerodynamic forces on that passing blade drop. This oscillation excites the blade at a strong 1P (and multiples 2P, 3P, ...) frequency and the tower and nacelle at a 3P (and multiples 6P, 9P, ...) frequency. Here, the abbreviations 1P, 2P, 3P, etc., refer to the rotor frequency and multiples thereof. Wind turbines generally are designed so that the major natural frequencies of the tower and platform modes are well above (usually 10%) or below these 1P and 3P frequencies to avoid resonances which negatively affect the lifetime of the turbine.

2.1.3 Randomly Fluctuating Aerodynamic Loads

In addition to these steady and periodic loads which are very predictable, randomly fluctuating, stochastic aerodynamic loads occur on an operating or idling (parked) wind turbine. The main stochastic aerodynamic load contribution comes from turbulence. It is characterized as a random variation of wind speed in space and time around a mean value. The turbulence varies in intensity and introduces fluctuating loads on the blades. A exemplary turbulent wind field generated with TurbSim [16] is shown in Figure 5. Loads due to turbulence generally are the defining factor for the fatigue life of an onshore turbine. Regarding extreme peak loads from aerodynamics, high-speed gusts typically are the most important effect. A gust is a sudden increase in wind speed that lasts between 3 sec and 20 sec and imposes high loads on the blades and the turbine. In addition to gusts affecting the whole rotor, partial gusts which only affect part of the rotor area, also can occur. This so-called eddy slicing or rotational sampling generates great eccentric transient loads on the rotor. The turbulence level—which increases with rougher sea conditions—as well as the 50-year gust speed both generally are less offshore than onshore.

Gusts also can trigger aerodynamic states in which the airfoils stall, which subsequently changes the loads on the blades rapidly and can lead to extreme load changes.

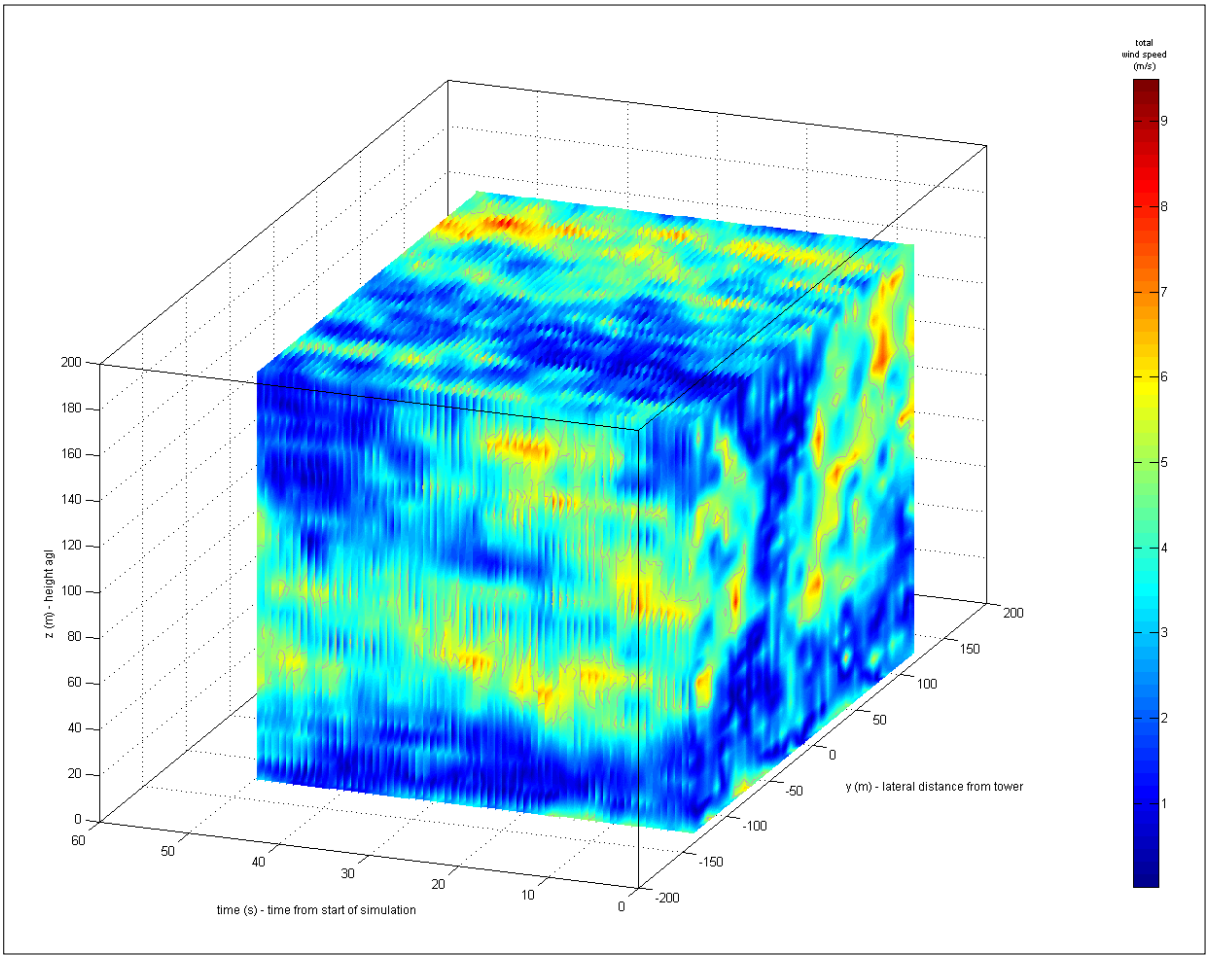

Figure 5. Turbulent wind field

In sum, the steady aerodynamic loads are important for long-term power production estimations. Periodic loads mainly are associated with resonance issues and govern the design of the system's natural frequencies. Lastly, fluctuating loads due to turbulence affect the fatigue lifetime and gusts—which are short-term effects—dominate the ultimate loads. The required strength of most of the system's components usually is governed by fatigue loads.

AeroDyn—the aerodynamics module of FAST—models these aerodynamic effects that cause the loads described above. Nevertheless, to calculate the aerodynamics in acceptable computation time, substantial simplifications are made to account for the various effects. AeroDyn uses the blade element momentum (BEM) theory to calculate the aerodynamic forces and moments on the blades. This theory captures the primary features of the air flow in and around wind turbines: The induced velocities due to power production and the rotation of the expanding turbine wake downwind. Empirical corrections are required to overcome the simplicity of the BEM theory, which is based on the assumption of uniform induction on radial annuli and steady two-

dimensional aerodynamics, but neglects, for example, the interdependence of the airflows at adjacent radial blade sections.

The corrections include the Prandtl tip-loss model to capture the effect of reduced lift at the blade tips. Further losses from the airflow around the rotor hub also are modeled. A dynamic inflow model based on the generalized dynamic wake (GDW) theory is implemented to consider unsteady, turbulent wind inflow. The airfoil data is augmented to account for some rotational 3D effects and unsteady airfoil aerodynamics. The effect of turbulent-wake-state that occurs if the rotor strongly decelerates the axial airflow also is considered, as is wake inertia or some 3-D effects such as stall delay. The dynamics of stalled blades during turbine operation are simulated using a Beddoes-Leishman dynamic stall model.

The actual flow field and aerodynamics, however, are more complex and the capabilities of the correction models to account for the various influences that are not captured by simple BEM theory are limited. These limitations include:

- The correct modeling of the rotor wake, especially when the rotor is misaligned in yaw with the mean wind direction;
- Simplifications when the turbine is operating in or near the blade stall region or in other aerodynamically greatly unsteady, nonlinear wind regimes; and
- Neglecting aerodynamic tower damping, which becomes important in high wind speeds.

The consequences of neglecting these more-complex aerodynamic effects and interactions are that, in some cases, actual fatigue and ultimate loads on the turbine differ from AeroDyn's prediction. These known limitations always must be considered when reviewing simulation results, and are reflected in the partial safety factors applied on the calculated loads.

2.2 Hydrodynamic Loads

Onshore and shallow-water fixed-bottom offshore turbine loads mainly are dominated by aerodynamics. For offshore floating turbines, hydrodynamic loads become more important. The significance of hydrodynamic loads depends on the particular floating concept and the investigated turbine component, as well as on the severity of the wind and wave conditions. Aerodynamics and hydrodynamics are related in terms of the long-term statistical correlation of wind speed, wave height, and wave period, which are expressed in the long-term joint probability density distribution. Although no short-term correlation exists, long-term statistics show the correlation: In the long term, the wind generates the waves. Therefore load cases with high wind speeds and increased aerodynamic loads usually are accompanied by increased wave heights resulting in greater loads on the floating platform.

In the equations presented in the next sections, a right-hand Cartesian coordinate system (X, Y, Z) fixed to the mean position of the wind turbine is used as shown in Figure 6. The positive Z-axis is vertically upwards through the center of gravity of the platform in its undisplaced position; the origin of the CS is in the plane of the undisturbed free surface, the mean sea level; and the X-axis is parallel to the nominal downwind direction. The incident-wave-propagation heading direction β is zero for waves propagating along the positive X-axis, and positive for positive rotations about the Z-axis. The translatory displacements are η_1, η_2, η_3, respectively

surge, sway, and heave. The rotational displacements are η_4, η_5, η_6, respectively roll, pitch, and yaw. In all derivations, the angles of the platform rotations are assumed to be small.

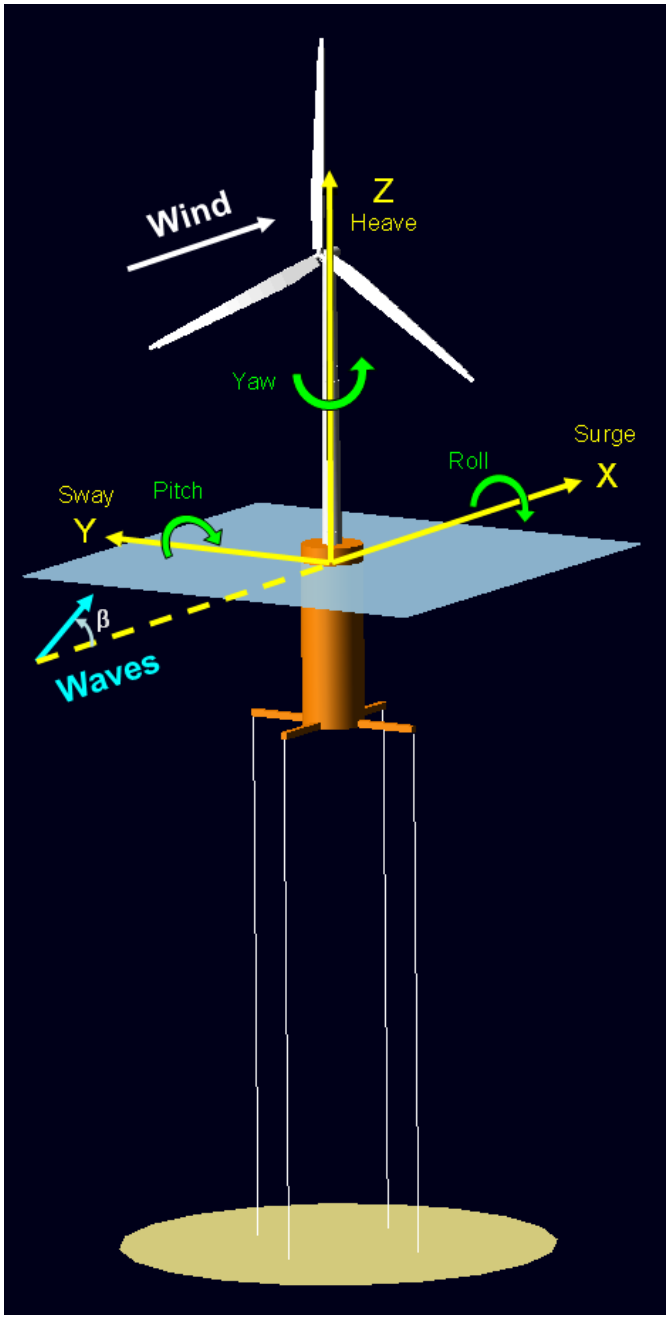

Figure 6. Coordinate system

The following sections describe the hydrodynamic loads on floating offshore wind turbines and assume knowledge in general aspects of free-surface fluid flow, potential theory, the Bernoulli equation, and basic fluid mechanics. More-detailed information on basic theories and the topics described below are found in Newman [27], Faltinsen [11], Cummins [6], Oglivie [29], and Anderson [1].

First an introduction to linear, steady-state hydrodynamic loads on floating offshore structures resulting from periodic (regular) sinusoidal incident-waves is provided. These linear hydrodynamic forces and moments can be expressed as the sum of three separate contributions from hydrostatics, diffraction, and radiation, which are discussed separately. It is followed by sections on non-steady-state, transient linear hydrodynamic loads from irregular incident-waves, which go beyond the steady-state linear theory, the so-called true linear hydrodynamic model. Next, a concise section on the numerical implementation of hydrodynamics within FAST's HydroDyn is presented. HydroDyn is capable of simulating irregular waves and non-steady-state hydrodynamic loads. Additionally, because it still is widely used in the wind turbine offshore industry, an overview of the Morison equation is presented, specifically including the viscous drag equation which is used in HydroDyn. The mooring system also is discussed in this section. Finally, the general limitations of the described potential flow–based theories are described.

2.2.1 Steady-State Hydrodynamic Loads

The total time-dependent external load $F_i^{Platform}(t)$ from a periodic, regular wave with amplitude A, frequency ω, and direction β, acting on a floating support platform with a mooring system, can be expressed as shown in Eq. 3.

$$F_i^{Platform}(t) = -A_{ij}(\omega)\ddot{\eta} + Re\{AX_i(\omega,\beta)e^{j\omega t}\} - [C_{ij}^{Lines} + C_{ij}^{Hydrostatic}]\eta_j - B_{ij}(\omega)\dot{\eta}_j + \rho g V_0 \delta_{i3} + F_i^{Lines,0} \quad (3)$$

This expression is equal to the time-domain representation of the frequency-domain hydrodynamic problem. Except C_{ij}^{Lines} and $F_i^{Lines,0}$ representing the mooring system forces, each term in Eq. 3 represents a different type of hydrodynamic load. Each term is described below; but first a concise introduction on regular wave theory is provided.

2.2.1.1 Regular Wave Theory

Linear, regular wave theory, which also is termed Airy wave theory, is based on potential flow. When applied to hydrodynamics of floating bodies on the water surface, the velocity potential ϕ must satisfy the linearized free-surface boundary condition (Eq. 4).

$$\frac{\partial^2 \phi}{\partial t^2} + g\frac{\partial \phi}{\partial z} = 0 \; on \; z = 0 \quad (4)$$

Equation 4 fulfills the linearized kinematic and dynamic free-surface conditions. It states that the vertical velocities of the free surface and fluid particles are equal to each other and that the water pressure is equal to the constant atmospheric pressure on the free surface. A simple linear, periodic solution for the free-surface condition in Eq. 4 is the two-dimensional plane progressive wave system; that is, a regular, sinusoidal wave. After solving Eq. 4 for the velocity potential, the free-surface elevation (ζ) at the time (t) and position (x) for a regular wave can be derived as shown in Eq. 5.

$$\zeta(x,t) = A \cdot sin(\omega t - kx) \quad (5)$$

Where A is the wave amplitude, ω is the wave's radian frequency, and k is the wave number (the number of waves per unit distance) with λ denoting the wavelength (Eq. 6).

$$k = \frac{2\pi}{\lambda} \tag{6}$$

The equations for the velocity potential, pressures, velocities, and accelerations for plane progressive waves which satisfy the free-surface boundary condition can be found in Faltinsen [11]. Nonlinear, higher-order wave kinematic effects—such as steep crests and flatted troughs—are not examined here and can be accounted for by using nonlinear, higher-order representations. Nevertheless, Figure 7 shows that for deep water—where floating offshore platforms are installed—and up to a certain dimensionless wave steepness, the linear, regular wave theory gives a valid approximation. Figure 11 in Section 2 indicates the location within the diagram of the sea states used in the present study for all three investigated floating concepts. In Figure 7 and Figure 11, the dimensionless wave steepness is $\frac{H}{gT^2}$. The dimensionless water depth—dimensionalized by both gravity and wavelength squared—is represented by $\frac{d}{gT^2}$.

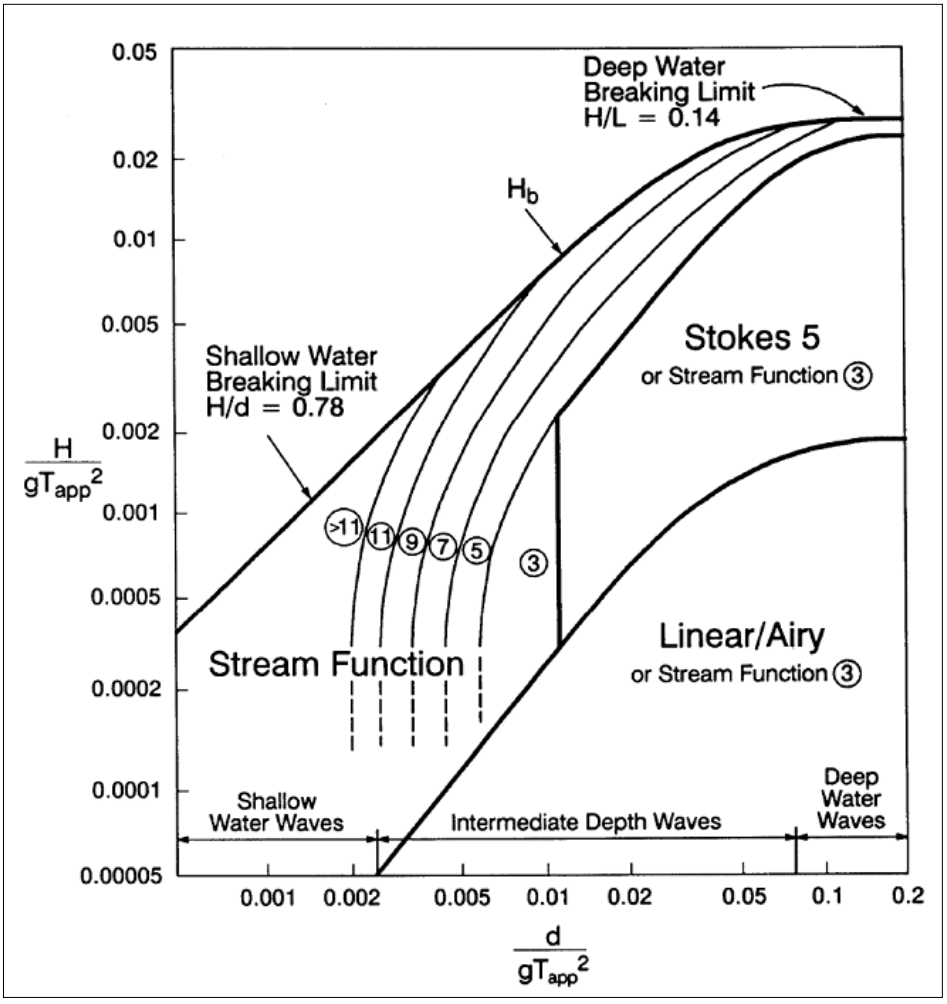

Figure 7. Validity of different wave theories [20]

2.2.1.2 Total Hydrostatic Forces

The third term in Eq. 3 includes the hydrostatic restoring matrix $C_{ij}^{Hydrostatic}$. Together with the buoyancy term, these two terms constitute the total hydrostatic force on the floating body [18].

$$F_i^{Hydrostatic}(q) = \rho g V_0 \delta_{i3} - C_{ij}^{Hydrostatic} q_j \tag{7}$$

$$\mathbf{C}_{\mathbf{ij}}^{Hydrostatic} = \begin{pmatrix} 0 & 0 & 0 & 0 & 0 & 0 \\ 0 & 0 & 0 & 0 & 0 & 0 \\ 0 & 0 & \rho g A_0 & 0 & 0 & 0 \\ 0 & 0 & 0 & \rho g \iint_{A_0} y^2 dA + \rho g V_0 z_{COB} & 0 & 0 \\ 0 & 0 & 0 & 0 & \rho g \iint_{A_0} x^2 dA + \rho g V_0 z_{COB} & 0 \\ 0 & 0 & 0 & 0 & 0 & 0 \end{pmatrix}. \tag{8}$$

Here the structure is assumed to be symmetrical around its body-fixed xz-plane and yz-plane. The total hydrostatic forces $F_i^{Hydrostatic}$ in Eq. 7 acting on a semi-submerged body consist of a buoyancy force from Archimedes' principle (first term in Eq. 7), linear restoring forces from water-plane area effects, and effects from the change of the COB position (second term in Eq. 7).

The term in C(3,3) in Eq. 8 simply is the change in the vertical buoyancy force when the structure is vertically displaced from its mean position. The term A_0 denotes the water plane area of the undisplaced platform in calm water. The first terms in matrix entries C(4,4) and C(5,5) represent the restoring moments from the water plane area effect. When the platform is perturbated in pitch or roll, one side of the structure is submerged and the other side is elevated from the water. According to Archimedes' law, the buoyancy force acting in z-direction on the submerged side of the body is increased and on the elevated side it is decreased. This yields a restoring moment counteracting the moment exerted on the body to displace it in pitch or roll. Due to the symmetry of the examined TLP structure, the moments from waterplane area restoring effects are equal for pitch and roll. The last terms in C(4,4) and C(5,5) represent the hydrostatic moments about the platform reference point due to the change in the position of the COB in z-direction z_{COB} when the platform is displaced. Note that, due to the upward orientation of the coordinate system's z-axis, z_{COB} is negative ($z_{COB} < 0$). In the literature [11], however, the last terms in C(4,4) and C(5,5) often are augmented by the restoring moment due to the weight of the platform.

$$(z_{COB}) \rightarrow (z_{COB} - z_{COG})$$

When adding this effect to the hydrostatic restoring matrix C_{ij}, the sum in Eq. 7 comprises not only hydrostatic restoring but the full static restoring forces and moments on the support platform, including the gravity (ballast) contribution. This formulation makes it easier to identify the forces and moments from the effect when the center of gravity does not coincide with the

center of buoyancy. For a structure displaced in roll or pitch, the separation between the COB and COG yields a moment because the horizontally offset vertical buoyancy and gravitational forces acting at the COB and COG produce a moment aggravating or counteracting the pitch or roll movement. Nevertheless, because it constitutes no contribution from hydrostatic effects, it is not included in $C_{ij}^{Hydrostatic}$ here.

2.2.1.3 Radiation (Added Mass and Damping) Forces and Moments

$A_{ij}(\omega)$ in the first term and $B_{ij}(\omega)$ in the third from last term of Eq. 3 represent the 36-element oscillation-frequency dependent hydrodynamic added-mass and damping matrices. When the structure is forced to oscillate with the wave excitation frequency and no incident-waves are present, hydrodynamic loads defined as added mass and damping are acting on the floating body. The oscillating structure generates outgoing waves which change the fluid pressure field. Integration of the changing fluid pressure surrounding the floating body over its surface yields the hydrodynamic radiation loads on the structure. More simply explained, added mass is the inertia added to a system because an accelerating or decelerating body must move some volume of surrounding fluid as it moves through it; the object and fluid cannot occupy the same physical space simultaneously. The two matrices are influenced by body form, frequency of oscillation, forward speed, finite water depth, and restricted water area.

2.2.1.4 Diffraction Forces and Moments

In the second term of Eq. 3, $X_i(\omega, \beta)$ represents the wave frequency and direction-dependent hydrodynamic wave excitation force vector. *Re* denotes the real value of the argument with the harmonic exponential e^{jwt}.

When a floating structure is restrained from oscillating and there are incident regular waves, so-called diffraction or wave excitation forces and moments are acting on the structure. These forces occur because of the varying, unsteady fluid pressure around the fixed structure in incident regular waves. In ocean-engineering literature a distinction typically is made between forces due to the corresponding undisturbed pressure field (i.e., the pressure field in the fluid only due to the waves ignoring the structure), the so-called Froude-Kriloff forces, and additional forces, which are called wave scattering forces and are due to the structure changing the undisturbed pressure field. Note that, in common ocean engineering literature [11], the scattering forces instead often are called diffraction forces, and the sum of scattering and Froude-Kriloff forces are called wave excitation forces.

The potential flow theory to calculate the diffraction forces assumes that no flow separation occurs. For a cylindrical structure such as a TLP, flow separation occurs when the Keulegan-Carpenter number K exceeds 2 [13]. The Keulegan-Carpenter number is defined as shown in Eq. 9.

$$K = \frac{VT}{D}, \tag{9}$$

Where T is the wave period, D is the cylinder diameter, and V is the amplitude of the fluid velocity normal to the cylinder. This means that for a TLP-like cylinder with a large diameter, flow separation occurs only in the upper section of the cylinder and only in extreme sea states. Therefore for TLPs the potential flow theory in general is valid.

2.2.2 True Linear Hydrodynamic Model

The linear, steady-state hydrodynamic problem described in the previous section assumes that the incident wave propagates at a single amplitude, frequency, and direction and that the platform motions are oscillating at the same frequency as the incident wave. To overcome these limitations for transient analyses in which optional nonlinear effects, transient behavior, and irregular sea states are important, the steady-state solution is extended and a irregular wave formulation is introduced. The total forces in the time domain acting on a semi-submerged platform with a mooring system in irregular incident waves are shown in Eq. 10.

$$F_i^{Platform}(\eta) = -A_{ij}\ddot{\eta}_j + F_i^{Waves} + \rho g V_0 \delta_{i3} - C_{ij}^{Hydrostatic}\eta_j - \int_0^t K_{ij}(t-\tau)\dot{\eta}_j(\tau)d\tau + F_i^{Lines} \quad (10)$$

Following Jonkman's nomenclature [18] within the thesis, this formulation is called the true linear hydrodynamic model in the time domain. Although the previously described steady-state, respectively frequency-domain solution in Eq. 3 cannot be directly applied, it is valuable for determining important parameters for the true linear hydrodynamic-loading equations. The parameters derived from the frequency domain are the added mass and damping matrices A_{ij} and B_{ij}, and the wave excitation load vector X_i, which is part of the wave excitation force term F_i^{Waves}. To obtain these matrices, the frequency-domain potential flow panel method code WAMIT (described in Section 3) is used. The hydrostatics for the true time-domain representation remain unchanged.

2.2.2.1 Irregular Waves

To obtain a description of random, irregular waves, multiple linear wave components are summed. This approach assumes that the sea can be described as a stationary random process, which generally is valid for the limited periods of no more than a few hours used in a typical wind turbine loads analysis. Expressing the time-dependent wave elevation $\zeta(t)$ by an appropriate wave spectrum $S(\omega)$ yields the expression shown in Eq. 11 [18].

$$\zeta(t)|_{t=n\Delta t} = \frac{1}{N}\sum_{k=-\frac{N}{2}+1}^{\frac{N}{2}} W[k]\sqrt{\frac{2\pi}{\Delta t}S_\zeta^{2-sided}(\omega)|_{\omega=k\Delta\omega}}\cdot e^{j\frac{2\pi kn}{N}} \quad (11)$$

$$for\ n = 0,1,...,N-1$$

Where j is the imaginary number, n and k are the discrete time-step and frequency-step counters, and N is the number of discrete steps. $W[k]$ represents the discrete Fourier transform of a realization of white Gaussian noise and is calculated using the Box-Muller method. It ensures a Gaussian-distributed wave elevation but causes the actual variance of the wave elevations to vary among realizations. Further information on the calculation and effect of $W[k]$ is found in Jonkman [18]. Here, $S_\zeta^{2-sided}$ is the two-sided power spectral density of the wave elevation per unit time.

Figure 8 illustrates the relationship between the time-domain solution $\zeta(t)$ of the waves and the frequency-domain representation of the waves by a wave spectrum $S(\omega)$. Basically, multiple

regular waves of different frequencies and with random phase angles are summed with respect to their probability spectral density according to the wave spectrum used for the specific site.

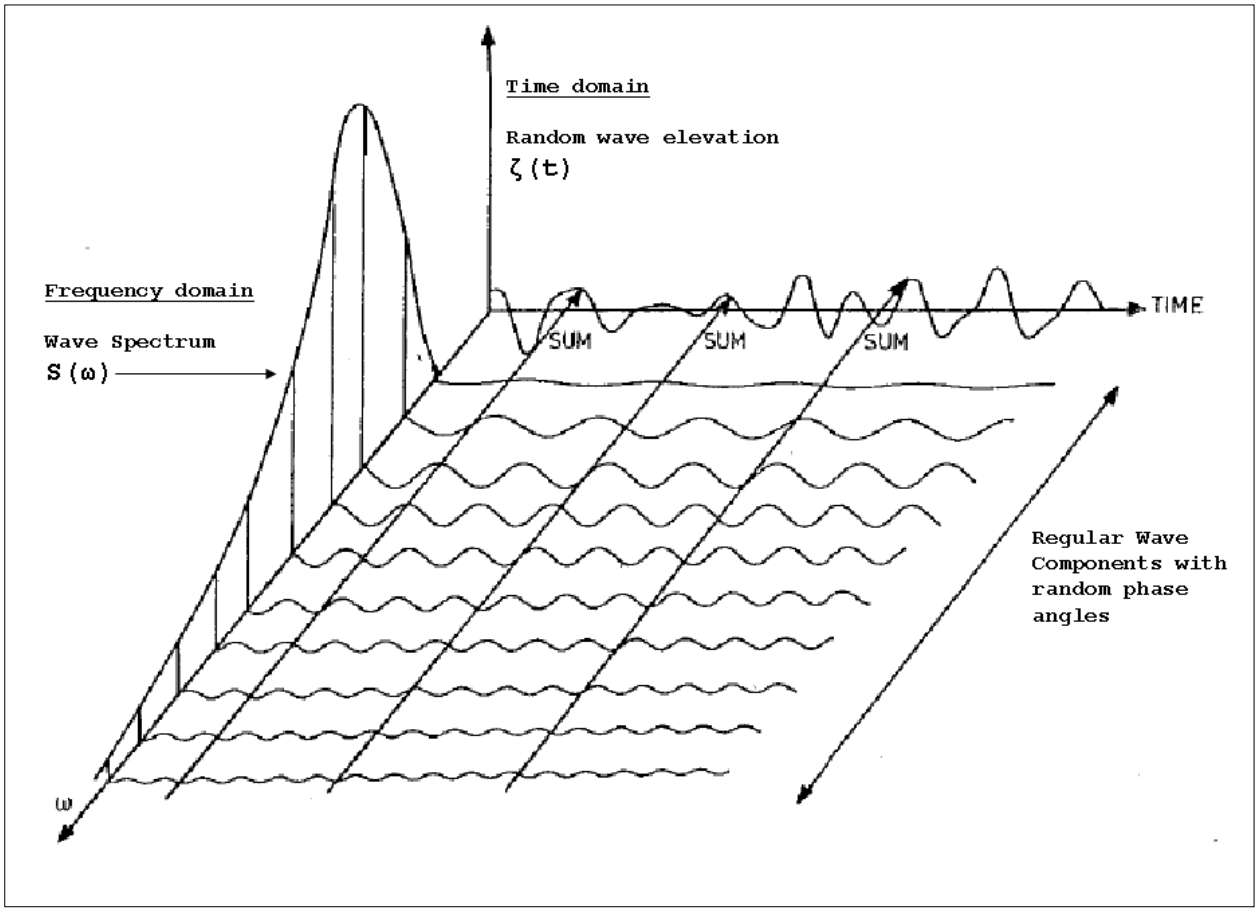

Figure 8. Wave elevation of irregular waves in the time domain as a combination of regular waves and a typical wave spectrum [11]

A typical wave spectrum implemented in FAST and used in the analysis of the TLP is the JONSWAP spectrum presented in Figure 9, defined from the IEC 61400-3 design standard [8].

$$S_{\zeta}^{1-sided}(\omega) = \frac{1}{2\pi}\frac{5}{16}H_s^2 T_p \left(\frac{\omega T_p}{2\pi}\right)^{-5} exp\left[-\frac{5}{4}\left(\frac{\omega T_p}{2\pi}\right)\right]^{-4}\left[1-0.287ln(\gamma)\right]\gamma^{exp\left[-0.5\left[\frac{\frac{\omega T_p}{2\pi}-1}{\sigma(\omega)}\right]\right]^{-4}} \quad (12)$$

The two-sided spectrum, as used in Eq. 11, is defined as shown in Eq. 13 and Eq. 14.

$$S_\zeta^{2-sided}(\omega >= 0) = \frac{1}{2} S_\zeta^{1-sided}(\omega), \tag{13}$$

$$S_\zeta^{2-sided}(\omega < 0) = \frac{1}{2} S_\zeta^{1-sided}(-\omega) \tag{14}$$

In Eq. 12, H_s is the significant wave height (i.e., the mean of the one-third highest waves), T_p is the peak spectral period, γ is the peak-shape parameter, and σ is a scaling factor. The figure also presents a Pierson-Moskovitz spectrum, which is a reduced JONSWAP spectrum with the peak-shape parameter γ set to unity. Further information on the JONSWAP spectrum is provided by the IEC 61400-3 design standard [8].

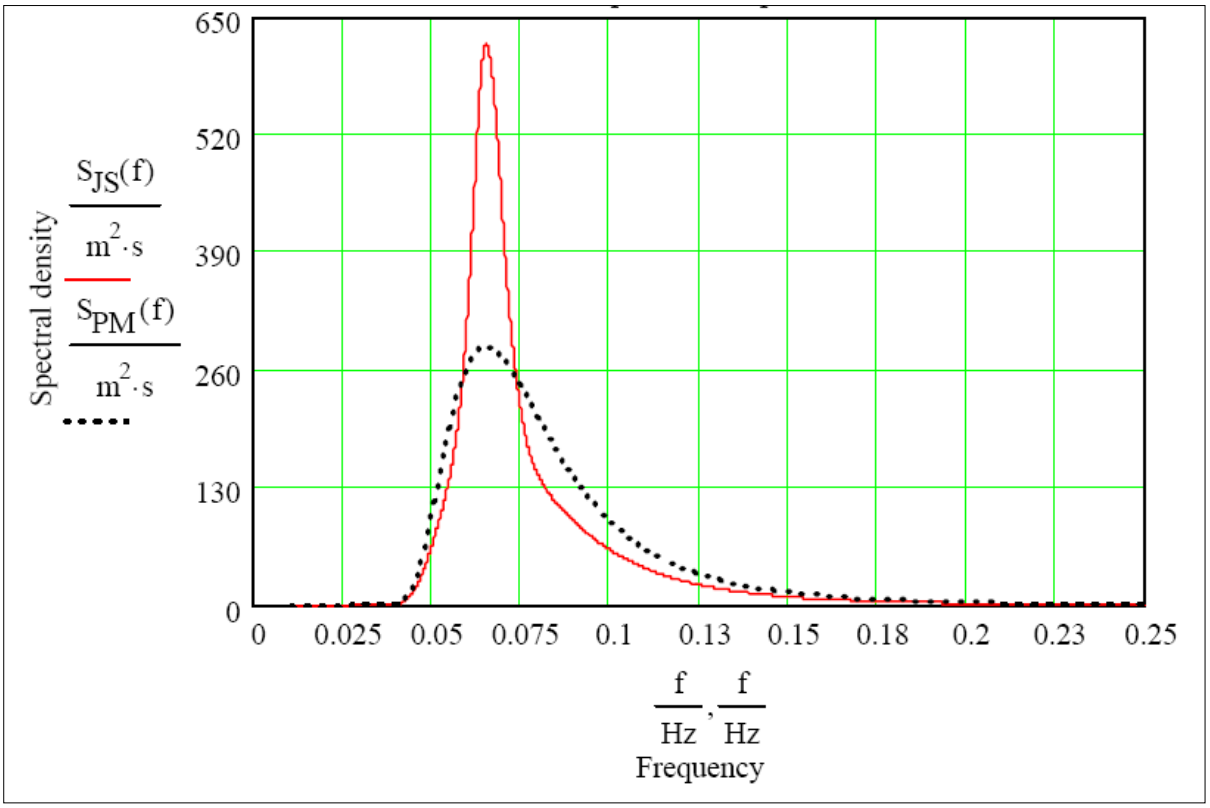

Figure 9. Typical JONSWAP and Pierson-Moskovitz wave spectra [8]

2.2.2.2 True Linear Radiation (Added Mass and Damping) Forces and Moments

The wave radiation loads in Eq. 10 consist of the impulsive hydrodynamic added-mass components A_{ij} and an additional wave-radiation contribution from added mass and damping. It is not included in A_{ij} and can be expressed as the convolution integral $-\int_0^t K_{ij}(t-\tau)\dot{q}_j(\tau)d\tau$.

The velocity and acceleration forms of the convolution integral are related by Jonkman [18].

$$-\int_0^t K_{ij}(t-\tau)\dot{q}_j(\tau)d\tau = -\int_0^t L_{ij}(t-\tau)\ddot{q}_j(\tau)d\tau, \quad (15)$$

Here, L_{ij} represents an alternative form of the wave radiation retardation kernel. The wave radiation retardation kernel K_{ij} depends on both added mass and damping, which are intrinsically related [18].

$$K_{ij} = \frac{2}{\pi}\int_0^\infty \omega[A_{ij}(\omega) - A_{ij}(\infty)]sin(\omega t)d\omega, \quad (16)$$

$$K_{ij} = \frac{2}{\pi}\int_0^\infty B_{ij}(\omega)cos(\omega t)d\omega. \quad (17)$$

Each component (i,j) of the wave radiation kernel represents the hydrodynamic force at a time (t) in the direction of DOF (i) resulting from a unit impulse in velocity at time zero of DOF (j). That essentially means that an impulse in platform velocity causes a force for infinite lasting subsequent time because the pressure field induced by the resulting outgoing waves exists as long as the waves radiate away. More detailed information is given by Jonkman [18].

The wave radiation retardation kernel $K_{ij}(t)$ can be assumed to be of finite energy. For B_{ij}, the infinite-frequency limit is zero, whereas the infinite-frequency limit of $A_{ij}(\infty)$ in Eq. 16 yields the following [18].

$$A_{ij} = lim_{\omega\to\infty} A_{ij}(\omega) = A_{ij}(\infty) \quad (18)$$

The impulsive added mass term A_{ij} in the true linear hydrodynamic loading equation Eq. 10 therefore is not frequency dependent.

In FAST's hydrodynamics module, HydroDyn, the wave-radiation loads are calculated by summation of A_{ij} and K_{ij}, therefore accounting for all radiation effects including surface memory effects. Equation 17 is used to caclculate K_{ij}; that is, the radiation loads in FAST's true linear hydrodynamic model in the time domain are computed utilizing the damping matrix B_{ij} calculated from the frequency-domain representation in WAMIT.

2.2.2.3 True Linear Diffraction Forces and Moments

When extending the diffraction formulation from periodic to irregular waves, the expression for the total wave excitation load from Eq. 10 is given by the following.

$$F_i^{waves}|_{t=n\Delta t} = \frac{1}{N}\sum_{k=-\frac{N}{2}+1}^{\frac{N}{2}} W[k]\sqrt{\frac{2\pi}{\Delta t}S_\zeta^{2-sided}(\omega)|_{\omega=k\Delta\omega}}\cdot X_i(\omega,\beta)|_{\omega=k\Delta\omega}\cdot e^{j\frac{2\pi kn}{N}}, \quad (19)$$

$$for\ n = 0,1,...,N-1$$

Equation 19 consists of the irregular wave elevation presented in Eq. 11 and X_i, representing the wave frequency and direction dependent hydrodynamic wave excitation vector obtained from the

frequency domain. The difference from the steady-state to the true linear diffraction formulation is the addition of the irregular wave representation. Modern numerical potential flow panel codes like WAMIT calculate the excitation force and moments X_i from direct integration of hydrodynamic pressure over the surface [22].

2.2.3 Morison's Representation

Nonlinear viscous drag from incident-wave kinematics, sea currents, and platform motion also must be taken into account. The viscous drag term of the Morison's representation with a fixed-drag coefficient C_D is used for this purpose (Eq. 20).

$$dF_i^{viscous}(t,z) = \frac{1}{2} C_D \rho (Ddz)[v_i(t,0,0,z) - \dot{q}_i(z)]\sqrt{[v_1(t,0,0,z) - \dot{q}_1(z)]^2 + [v_2(t,0,0,z) - \dot{q}_2(z)]^2} \quad (20)$$

$$for\ i = 1,2$$

The diameter of the cylinder is denoted by D; dz is the height of a differential strip around the cylinder; C_D is the viscous drag coefficient; v_i are the components of the undisturbed fluid-particle velocity in the direction of DOF i = 1 or 2; the translational velocities $\dot{q}_i(z)$ are related to the rigid-body platform surge, sway, roll, and pitch velocities by the following expressions.

$$\dot{q}_1(z) = \dot{\eta}_1 + \dot{\eta}_5 z$$

$$\dot{q}_2(z) = \dot{\eta}_2 - \dot{\eta}_4 z$$

An overview of the complete Morison's representation is provided here because it is used widely in the analysis of fixed-bottom monopile offshore wind turbines. Morison's representation, when combined with strip theory, gives a straightforward equation to calculate wave loads and viscous forces on slender vertical, bottom-mounted surface-piercing cylinders. The total load on a cylinder in surge and sway according to Morison's representation is shown in Eq. 21.

$$dF_i^{Cylinder}(t,z) = -C_A \rho (\frac{\pi D^2}{4} dz)\ddot{q}_i(z) + (1 + C_A)\rho (\frac{\pi D^2}{4} dz) a_i(t,0,0,z) + dF_i^{viscous}(t,z) \quad (21)$$

$$for\ i = 1,2$$

Here a_i represents the components of the undisturbed fluid-particle acceleration in the direction of DOF i = 1 or 2. Similar equations apply to the pitch and roll moments (i = 4: $-dF_2^{Cylinder} \cdot z$; i = 5: $dF_1^{Cylinder} \cdot z$, [18]). The heave force and yaw moment are zero by definition.

Equation 21 ignores radiation damping forces and moments and off-diagonal terms in the added-mass matrix other than those which couple surge and pitch or sway and roll, and uses a simplified solution of the diffraction problem for long wave length approximation. It only is valid for cylindrical structures and does not compute heave forces or other end effects. Taking all these simplifications and neglected effects into account, Morison's equation mainly is applicable to a narrow range of floating platforms (e.g., the spar-buoy concept). For most other concepts the true linear hydrodynamic loading equations described above must be applied.

2.3 Numerical Hydrodynamics Modeling in HydroDyn

In the present study, the added mass, damping, and excitation force matrices A_{ij}, B_{ij}, and X_i are calculated using the software WAMIT (Wave Analysis at MIT) [22]. WAMIT works for any shape and it uses the panel method (as do other similar numerical codes for wave loads). This method is based on potential flow theory and it neglects flow separation.

For the analysis, first the surface of the structure is discretized with an appropriate number of panels. The velocity potential then is computed using the source distribution method. After the velocity potential is calculated, the force matrices are obtained by integration of the pressure over the structure's surface. A view of a discretized cylinder with flat panels is shown in Figure 10. More information on WAMIT and on numerical panel methods in general can be found in the *WAMIT User Manual* [22] and in Faltinsen [11].

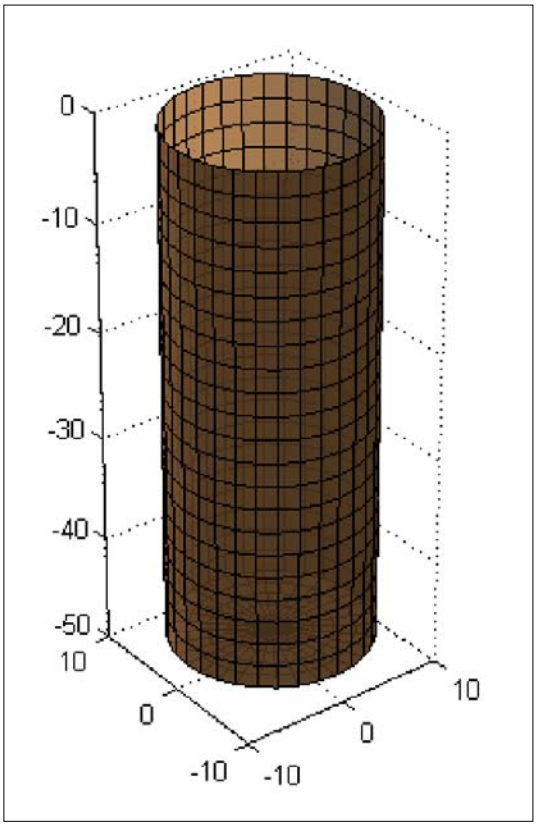

Figure 10. Visualization of a grid for potential flow panel method [22]

All potential flow–based theories, including higher-order representations, inherently neglect viscous effects and do not capture the effects of turbulence, flow separation, free-surface tension, boundary layers, breaking waves, or multiphase flow. Additional drag originating from wave slamming also is excluded from this simplified model. To account for some of these effects, extensions to the potential flow theory exist [11]. In the present study, however, only viscous drag is added using a simple approach based on Morison's equation (described in Section 2.2.3).

The first-order linear theory also neglects several effects which second-order (and higher) potential flow solutions are able to capture. Second-order theory accounts more properly for the

zero-normal flow condition through the body at the instantaneous position of the body, and also approximates the free-surface pressure condition more accurately. Improvements also include a better consideration for non-linearities in the velocities of fluid particles on the free surface. In addition to the linear solution, the second-order solution for the problem results in mean drift forces and forces oscillating with difference and sum frequencies. Further information on second-order (and higher) solutions of the hydrodynamic problem is provided by Faltinsen [11]. Despite improvements being possible with higher-order representations, the inherent limitations of potential flow theory remain. Very detailed data that captures all existent hydrodynamic effects only can be obtained with experiments and, to some extent, with next generation CFD solvers.

Figure 11 shows the location and flow regime of all investigated concepts for all simulated stochastic wave conditions. The plotted points from the different simulations are drawn using the significant wave height ($H = H_s$) and peak spectral wave period ($T = T_p$). The lines constituting the limits of linear theory and breaking waves use the periodic wave height $H = H_{periodic}$ and wave period $T = T_{periodic}$. If the average values for wave height and period would be used for the simulated stochastic wave conditions, the points mostly would fall within the linear limit. Therefore, although some points given here are out of the range of valid linear theory, the error is considerably small. For the structures and flow regimes investigated in the present study, the linear theory incorporated in HydroDyn therefore provides a great degree of accuracy—and it is more than sufficient for use here.

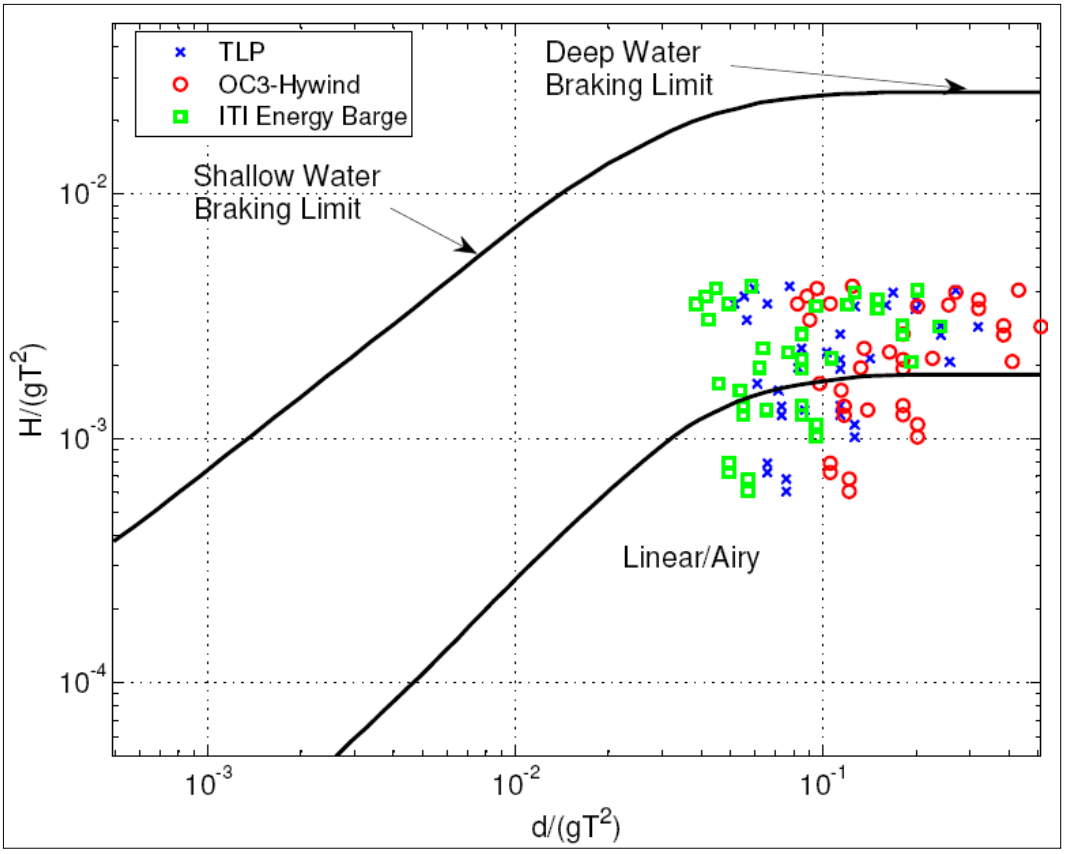

Figure 11. Validity of linear theory for investigated floating concepts

2.4 Mooring System

An integral part of all floating-platform concepts is the mooring system. A tension leg platform obtains stability mainly due to stiffness provided by the taut mooring lines, therefore the mooring system especially is critical for a TLP design. Mooring systems consist of cables attached to the floating platform at fairlead connections with the lower ends anchored to the seabed. There are various types of cables available, such as chains, steel, synthetic fibers, or a combination of these. Numerous anchor systems exist, ranging from simple dead-weight moorings and conventional "mushroom" moorings, to more sophisticated screw-in and suction anchors. For the purpose of the study, anchors simply were regarded as rigidly fixed to the seabed and the mooring lines were regarded as consisting of a single material with a constant elasticity.

2.5 Quasi-Static Mooring System in HydroDyn

When ignoring mooring inertias and damping, and assuming linearity, the mooring line forces on a floating platform can be described as shown in Eq. 22.

$$F_i^{Lines} = F_i^{Lines,0} - C_{ij}^{Lines} q_j \tag{22}$$

Here $F_i^{Lines,0}$ represents the mooring system load acting on the platform in its undisplaced, static position as a result of pre-tension from excess buoyancy. The linearized restoring matrix is C_{ij}^{Lines} due to the elastic stiffness of the cables and the effective stiffness from the weight of the cables in water. For taut lines of a TLP with no part of the cables lying on the seabed, the linearity assumption is a relatively good approximation and Eq. 22 therefore illustrates the basic functionality of a mooring system very accurately.

Nevertheless, in reality mooring system dynamics are not linear. In the present study, a quasi-static mooring system calculation procedure implemented in FAST was used. An analytical formulation for an elastic cable suspended between two points hanging under its own weight in water was utilized to compute the actual location of all parts of the line and to determine whether any part rests on the seabed. For the TLP, the mooring lines are supposed to be taut under all conditions, therefore this report uses only the equation for the effective horizontal and vertical line tensions H_F and V_F (effective actual cable wall tension plus hydrostatic pressure) for a line with no part resting on the seabed. These equations also are valid for catenary lines as long as no part is resting on the seabed. The fairlead location relative to the anchor of each mooring line is represented by x_f and z_f, EA represents the line's extensional stiffness, and L is the overall unstretched line length. The implicit Eq. 23 and Eq. 24 are solved for the effective fairlead tensions H_F and V_F with a Newton-Raphson iteration scheme. From the fairlead tensions, a balance of external forces on the line yields the anchor tensions.

$$x_f(H_F,V_F) = \frac{H_F}{\omega}\{ln[\frac{V_F}{H_F} + \sqrt{1+(\frac{V_F}{H_F})^2}] - ln[\frac{V_F-\omega L}{H_F} + \sqrt{1+(\frac{V_F-\omega L}{H_F})^2}]\} + \frac{H_F L}{EA} \tag{23}$$

$$z_f(H_F, V_F) = \frac{H_F}{\omega}\left[\sqrt{1+\left(\frac{V_F}{H_F}\right)^2} - \sqrt{1+\left(\frac{V_F-\omega L}{H_F}\right)^2}\right] + \frac{1}{EA}\left(V_F L - \frac{\omega L^2}{2}\right) \quad (24)$$

The apparent weight of the line in fluid is determined as shown in Eq. 25.

$$\omega = \left(\mu_c - \rho\frac{\pi D_c^2}{4}\right)g \quad (25)$$

This quasi-static approach assumes the line to be in static equilibrium at each calculated time-step. It neglects (increased) different anchor and fairlead tensions because of inertia effects due to the line's acceleration and deceleration—which can be significant for a TLP where large waves can lead to quick changes of line tensions in short periods. The numerical model allows the line tension to drop to zero and then tauten again, but it must be noted that in reality this event probably would cause the line to snap. A more detailed description with additional equations for lines resting on the seabed and details on the numerical scheme is found in Jonkman [18].

3 Tension Leg Platform Model Design in FAST

To perform a thorough loads analysis in the design code FAST, the floating wind turbine model first must be created. This section provides information about the 5-MW wind turbine used in the study and the properties of the TLP design. Each step necessary to develop a valid, viable FAST model of the floating platform is explained. The model design process described here is not limited to the TLP but can be applied to almost any floating-platform design. Summarized, the steps performed in the present study to create the TLP model in FAST are listed below.

- Defined geometry and structural properties of wind turbine and blades
- Defined geometry and structural properties of TLP platform and mooring system
- Obtained hydrodynamic frequency-domain properties with WAMIT
- Obtained tower mode shapes with ADAMS
- Created FAST model with the TLP floating platform and NREL's 5-MW baseline turbine
- Compared MIT's published predicted performance with results from FAST model for MIT's extreme sea state reference-load case
- Validated time-domain FAST model with frequency-domain results in terms of response amplitude operators and PDFs for MIT's extreme sea state reference-load case
- If there were problems with the original design, redesigned the TLP and repeated the validation process to meet desired design capabilities

3.1 NREL 5-MW Baseline Turbine Properties

The NREL 5-MW baseline wind turbine represents a typical state-of-the-art multi-megawatt turbine. This section gives an overview of its properties without providing details that are out of the scope of this work. An in-depth description of the turbine can be found in Jonkman [18]. The

baseline turbine's properties presented in Table 1 are derived from publicly available data on the Multibrid M5000 and REpower 5-MW machines and from conceptual models used in the WindPACT, RECOFF, and DOWEC projects.

Table 1. NREL 5-MW Baseline Turbine Specifications

Property	Specification
Rated power	5 MW
Rotor orientation	Upwind
Rotor configuration	3 blades, 61.5-m length
Rotor, hub diameter	126 m, 3 m
Hub height	90 m
Wind speed:	
Cut-in V_{In},	3 m/s,
Rated,	11.4 m/s,
Cut-out V_{Out}	25 m/s
Cut-in rotor speed	6.9 rpm,
Rated rotor speed	12.1 rpm
Drivetrain concept	Geared,
Gearbox ratio	97:1
Rated generator speed	1173.7 rpm,
Generator efficiency	94.4 %
Rated tip-speed	80 m/s
Overhang	5 m,
Shaft tilt	5°,
Precone	2.5°
Rotor mass	110,000/kg
Nacelle mass	240,000/kg
Tower mass	347,460/kg
Tower diameter base,	6 m,
Tower top diameter	3.87 m
CM location	-0.2 m, 0.0 m, 64.0 m
Control system	Variable-speed generator torque & collective active pitch (PI)

To accurately approximate the blades' smoothly changing cross-section geometry, each blade is subdivided into 17 sections with different airfoils over the blade's length (Cylinder (1–3), DU40 (4), DU35 (5–6), DU30(7), DU25 (8–9), DU21(10–11), NACA64 (12–17)). Detailed airfoil geometries and diagrams of lift and drag versus angle of attack for each airfoil are provided in Jonkman [18]. The quality of this airfoil data is critical for the calculation of lift and drag coefficients and the overall accuracy of the BEM-based aerodynamic model.

Very important for the final loads on the wind turbine is the baseline turbine's control system, schematically presented in Figure 13. The incorporated so-called "baseline controller" operates in five regions: 1, 1½, 2, 2½, and 3 (presented in Figure 12). Region 1 is before cut-in wind speed; the generator torque is zero and and no power is generated. In this region the rotor is accelerating for start-up. The next region (1½) is a linear transition between regions 1 and 2.

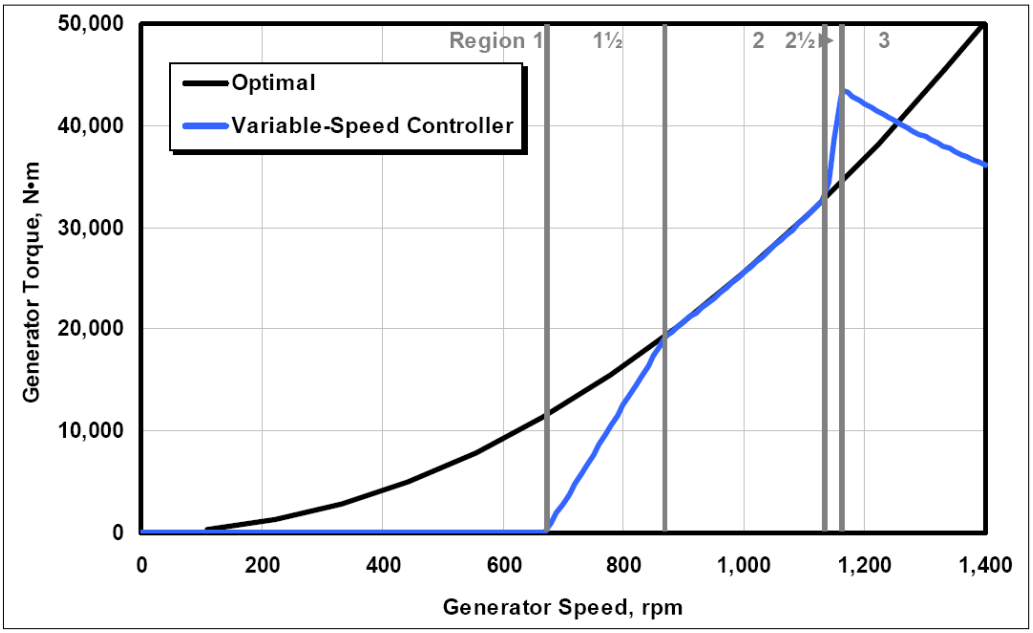

Figure 12. Torque versus generator-speed diagram of baseline controller [18]

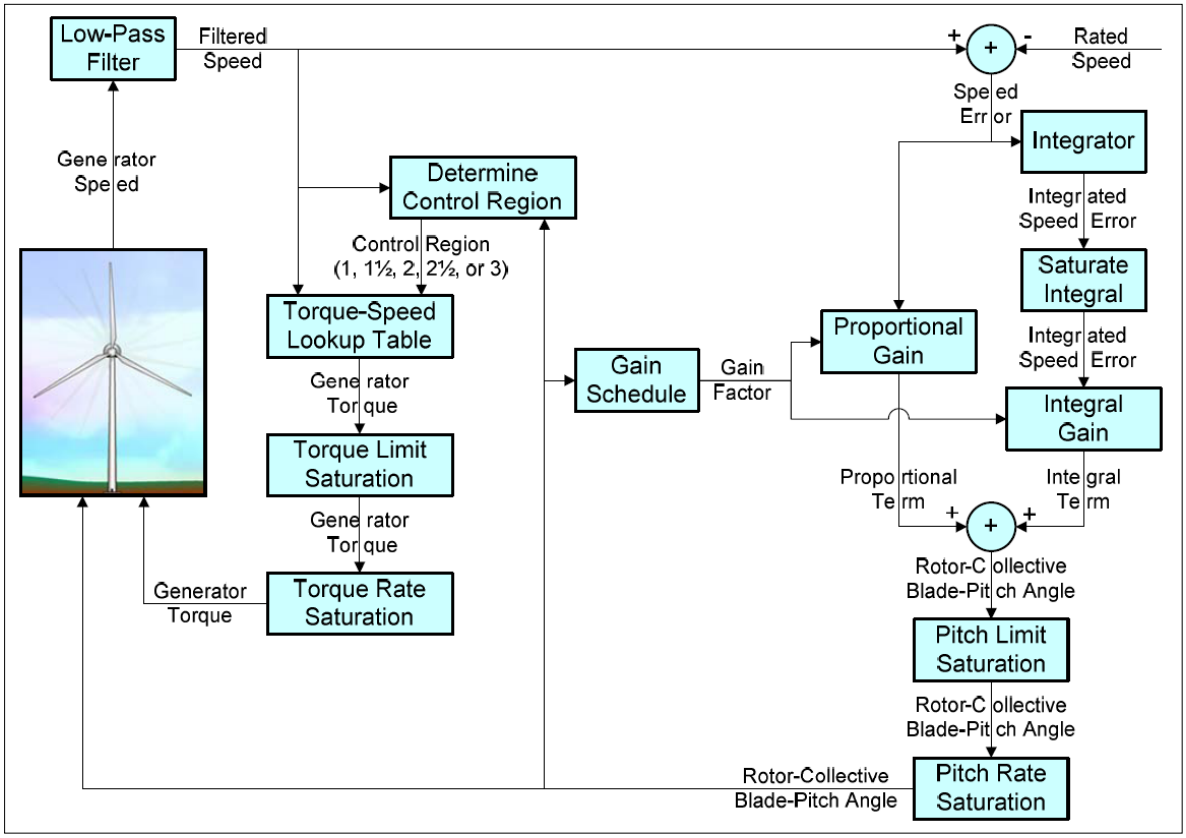

Figure 13. Flowchart of baseline control system [18]

In region 2, the turbine starts producing power that is less than the rated power. This region is optimized for power capture. The controller maintains an optimal, constant tip-speed ratio of

$\lambda = 7.55$ to sustain the maximum power coefficient of $c_p = 0.482$. Control in this region is achieved by adjusting generator torque while the rotor collective pitch angle is $\alpha_p = 0°$. Region 2½ assures smooth transition between region 2 and region 3, and is used to limit tip-speed and noise emissions.

In region 3, collective active pitch is used to hold the generator speed—respectively the power generation—constant at rated speed. The blade-pitch commands are calculated using a gain-scheduled proportional-integral (PI) controller on the speed error between the filtered and the rated generator speed. Hansen et al. [14] describe methods and equations to obtain viable gains. Note that this baseline controller uses collective pitch, has no start-up and shut-down routines, and is not optimized to limit ultimate and fatigue loads by applying sophisticated control algorithms and techniques. This task currently is investigated by several dedicated control research teams for this and other floating wind turbine concepts.

3.2 Platform Properties MIT TLP#1

As a basis for the development of the FAST model, a TLP design from Tracy's "Parametric Design of Floating Wind Turbines" [31] (conducted at the Mechanical Engineering Department at MIT) was selected. Tracy's thesis contains a parametric optimization study conducted for several different floating-platform concepts for NREL's 5-MW baseline wind turbine. The study resulted in a number of designs that show Pareto fronts for mean-square acceleration of the turbine versus multiple cost drivers, including platform displacement and total mooring line tension. The report concludes that the TLP represents the most attractive choice because of its low root mean square (RMS) accelerations and negligible heave and pitch motions. For the present study, the tension leg platform design (TLP#1) for the 10-m sea state was chosen. The properties of this TLP#1 are listed in Table 2. (Tensions provided in Tracy [31] were rendered using the uncommon unit kg, and were converted to kN using $g = 9.81$ for the gravity constant.)

Table 2. Static Properties of MIT TLP#1 [31]

Static Properties	Value
Platform diameter	18 m
Platform draft	47.89 m
Water depth	200 m
Mooring system angle	90°
Average mooring system tension per line	3,931 kN
Ballast at platform bottom:	
Concrete mass	8,216,000 kg
Concrete height	12.6 m
Total displacement	12,187,000 kg
Wind Speed (constant, no shear)	11.0 m/s
Sea state significant wave height	10.0 m
Peak spectral wave period	17.6394 sec
Windward static line tension	5,290 kN
Leeward static line tension	2,570 kN
Steady state surge offset	4.394 m
Steady state pitch offset	0.438°

Note that the concrete ballast at the platform bottom (cf. Table 2), which is uncommon for typical TLP designs, is due to constraints of Tracy's optimization process. The next section briefly explains these design constraints.

In addition to this information, Mr. Sungho Lee (of MIT) provided further data on the mooring system, platform wall thicknesses, and steel and concrete properties (presented in Table 4). The TLP investigated uses a vertical tension leg mooring system; stability primarily is generated by the excess buoyancy of the platform. This buoyancy exceeding the system weight must be great enough that the mooring lines stay taut under all wind and wave conditions. Additionally, to sustain tension in the mooring lines, the position of the fairleads is an important factor. Moving the fairlead positions further from the center line of the structure leads to reduced line tension oscillating amplitudes and therefore decreases the probability of the lines going slack under heavy wind and wave conditions.

Table 3. Dynamic Properties of MIT TLP#1 in 10-m Sea State at 11-m/s Windspeed [31]

Dynamic Properties	Value
Nacelle RMS acceleration	0.031 g
RMS surge displacement	2.095 m
RMS heave displacement	0.067 m
RMS pitch displacement	0.224°
Windward RMS tension	779 kN
Leeward RMS tension	767 kN
Static plus 3σ dynamic windward line tension	7,626 kN
Static minus 3σ dynamic windward line tension	2,956 kN
Static plus 3σ dynamic leeward line tension	4,871 kN
Static minus 3σ dynamic leeward line tension	268 kN

Based on the data in Table 2, Table 3, and Table 4, and following the steps described in the subsequent sections, a model of the TLP#1 was created in FAST.

Table 4. Properties of MIT TLP#1 Platform and Mooring System

Properties	Value
Number of mooring lines	8
Fairlead distance from center	18 m
Unstretched mooring-line length	151.73 m
Line diameter	0.127
Line mass per unit length	116.03 kg/m
Line extensional stiffness	1,500,000,000 N
Average steel density	7850 kg/m^3
Average concrete density	2562.5 kg/m^3
Steel-wall thickness	0.015 m

3.2.1 Center of Gravity and Inertias

Using FAST requires input of the basic inertial properties of the support platform. With the available data on the selected TLP#1 design, the center of gravity and the inertias of the platform have been calculated using a custom-built MATLAB script.

Table 5. Properties of MIT TLP#1 Center of Mass and Center of Buoyancy

Properties	Value [m]
Center of mass (platform)	-40.612
Center of mass (full system)	-32.7957
Center of buoyancy	-23.945

Due to the large amount of concrete ballast at the bottom of the TLP, the center of mass of the full system—the wind turbine and the platform—is well below the center of buoyancy, as shown in Table 5. Therefore this particular design is statically stable without the mooring system. This is uncommon for generic TLPs because the main contribution in restoring is provided by the mooring system. One of MIT's constraints in its design optimization, however, was that the structure would be minimally stable without the mooring system so that the whole system with the tower and the blades could be assembled at a coastal facility and then towed by boat to the installation site at sea [31]. The platform would be additionally ballasted with water during towing and unballasted when the mooring system would be attached to the platform. For MIT's analysis, the TLP needed to provide enough stability to not exceed 10 degrees of pitch during towing.

In summary, the MIT TLP#1 can be considered a hybrid design of a deeply drafted, ballast-stabilized spar buoy and an unballasted generic TLP for which all restoring is provided by the mooring system. Note that, without the moorings, this design is stable only in calm sea states when the turbine is not operating. When anchored to the seabed, most of the restoring still is provided by the mooring system, despite the large amount of ballast. Other TLP designs solve the on-site installation problem alternatively and therefore do not need to ballast the lower section of the platform to achieve stability without a mooring system. Regarding costs, this second option might be preferable.

3.2.2 Hydrodynamic Properties with WAMIT

When FAST's HydroDyn is calculating the hydrostatic and hydrodynamic loads on the platform, it requires the inputs for hydrostatic, added mass, damping, and wave-excitation forces matrices C_{ij}, A_{ij}, B_{ij}, and X_i. These matrices are calculated using the potential flow hydrodynamic code WAMIT. The potential flow–based approach for the TLP is valid, as the calculation of the Keulegan-Carpenter number in Figure 14 illustrates for different sea states with associated periodic wave periods (T) and wave heights (H) defined in the OC3 definition [17]. Except for the most extreme sea state 8 (with T=17s, H=15.24m), the Keulegan-Carpenter number remains less than 2, which marks the limit for potential flow theory validity as described in Section 2.2.1.4. Accordingly, no flow separation occurs at the main tank of the TLP for Sea States 1-7, but separation on the spokes is still possible.

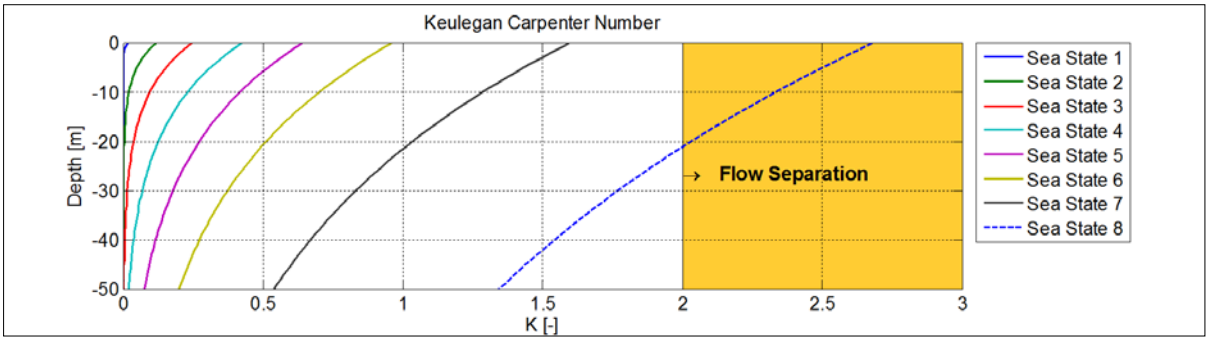

Figure 14. Keulegan-Carpenter number for TLP in different sea states

Because the code is a panel code (as described in the previous section), the support platform is discretized into flat panels. WAMIT takes advantage of the symmetry of the platform which makes it sufficient to calculate only a quarter of the cylinder. The utilized discretization with 3,024 panels for one quarter of the cylinder is presented in Figure 15 (here displayed as a full cylinder with 4 · 3,024 = 12,096 panels).

The WAMIT-calculated coefficients for added mass $A_{ij}(\omega)$, damping $B_{ij}(\omega)$, and wave-excitation forces $X_i(\omega)$ are shown in Figure 16, Figure 17, and Figure 18. Most of the wave energy is concentrated between (*c.f.* Figure 9):

$$0.04Hz(0.25\frac{rad}{s}) < f_{waves} \cdot \text{and}$$

$$< 0.2Hz(1.25\frac{rad}{s}).$$

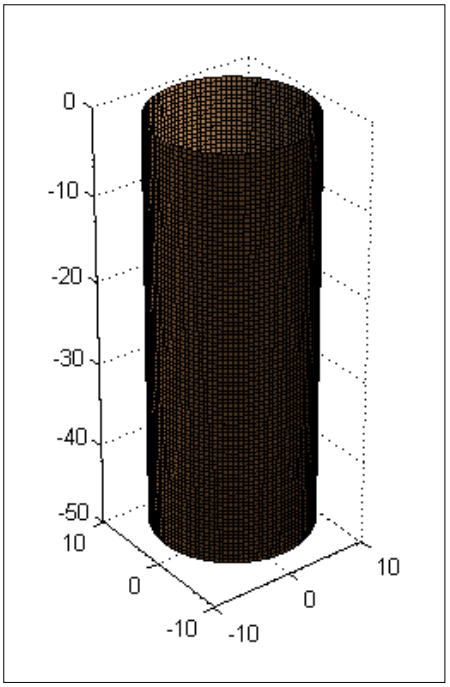

Figure 15. Tension leg platform discretization with flat panels

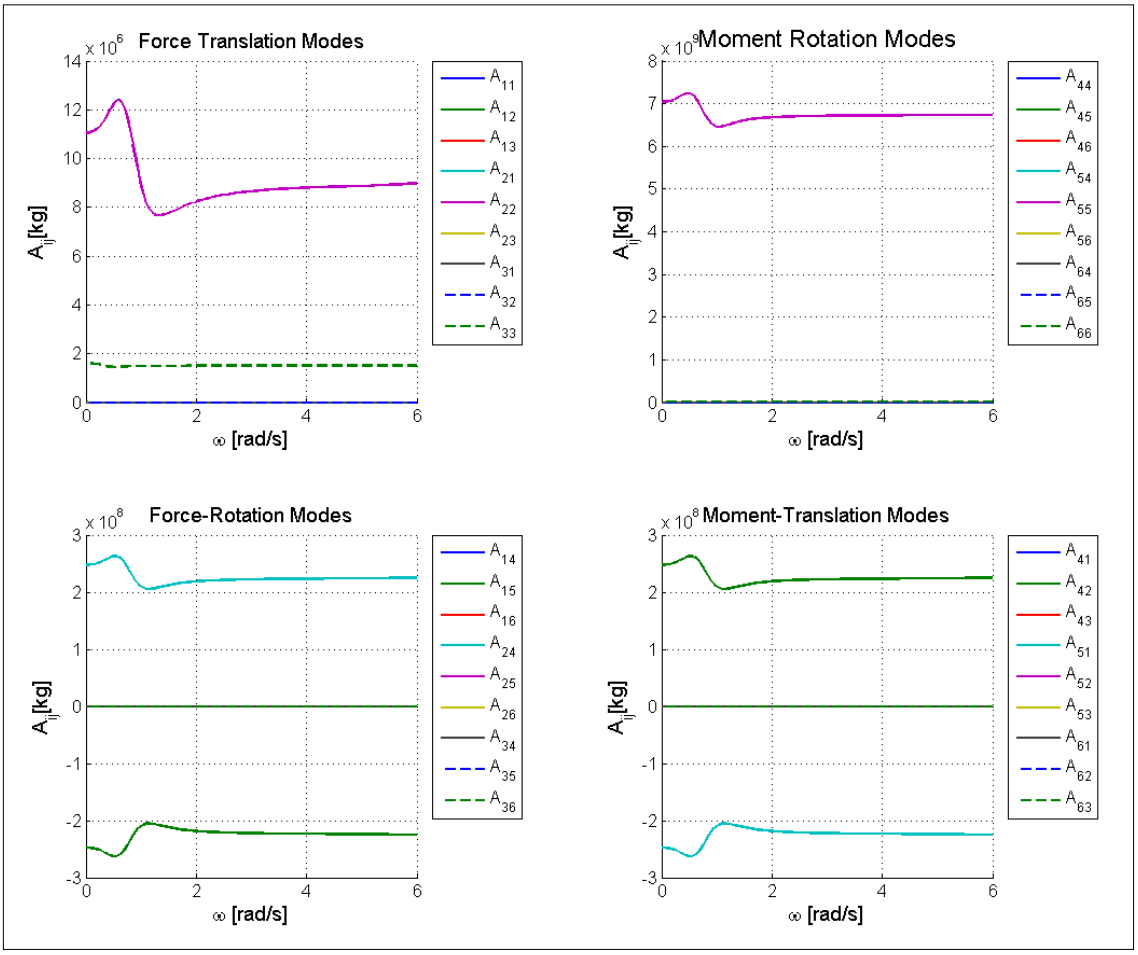

Figure 16. Tension leg platform added-mass coefficients

Figure 16 presents the 36 frequency-dependent coefficients of the added mass matrix calculated with WAMIT. The upper-left diagram shows the force-translation modes. Because the TLP is axisymmetrical, the coefficients in surge and sway are equal. They are significantly greater than the added mass in heave, because wetted surface and subsequently the amount of displaced water from motions in these directions apparently is much greater. All off-diagonal translational coefficients are zero. This similarly is true for the moment rotation modes displayed in the upper-right corner. Here, only pitch and roll coefficients are non zero. From the remaining coupled modes, only surge-pitch and sway-roll modes are not zero. For HydroDyn calculations, especially the infinite-frequency limits of the added-mass coefficients are important.

Hydrodynamic damping coefficients, presented in Figure 17, are non-zero in the same modes as added mass coefficients. Conforming with theory [11], the damping vanishes in all coefficients at the low- and high-frequency limits. The maxima in damping occur here at the upper-frequency limit of the energy-rich wave spectrum range, that is, for small waves with short periods the damping is increased.

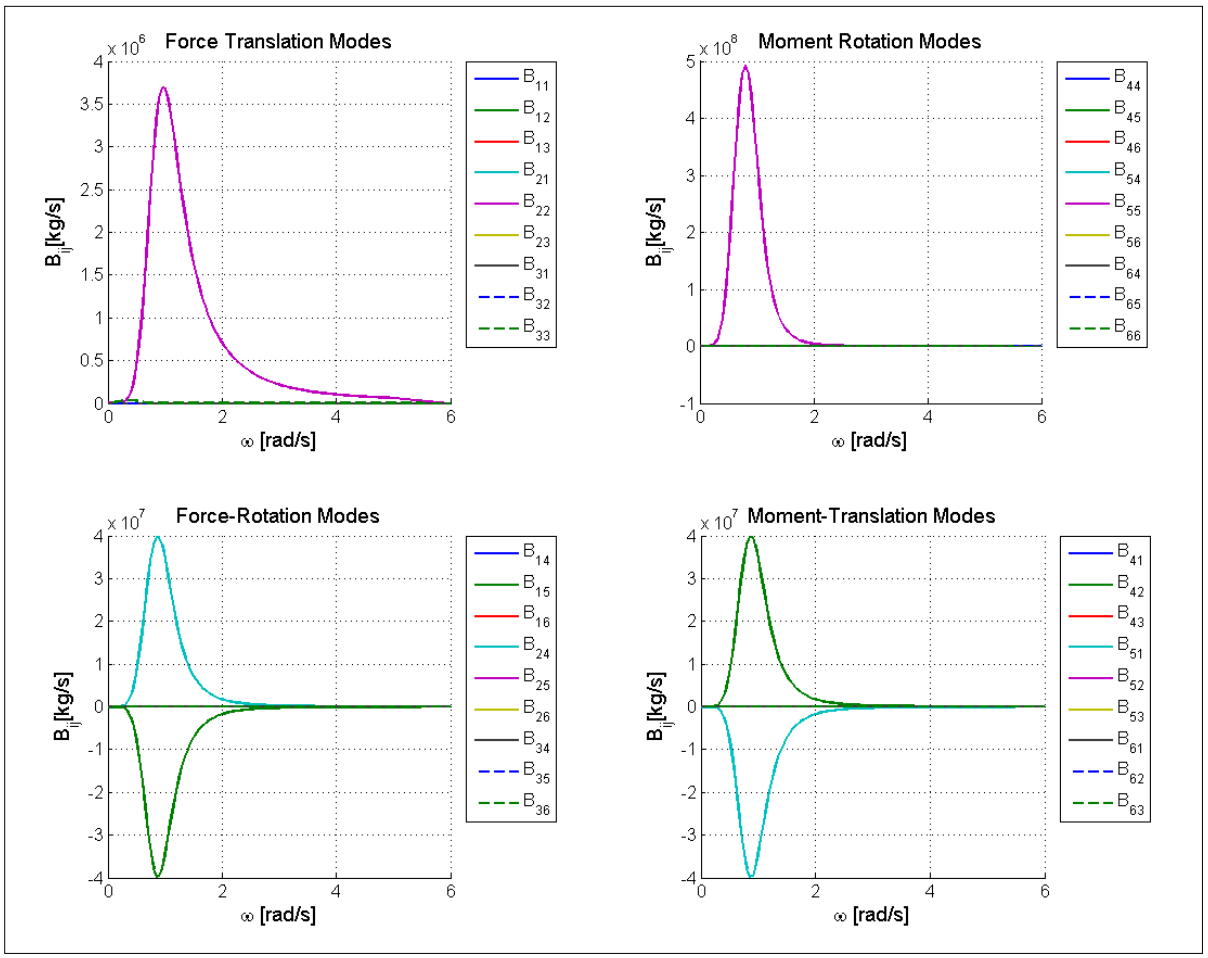

Figure 17. Tension leg platform hydrodynamic damping coefficients

Figure 18 presents the exciting forces and moments with associated phase angles over frequency from incident-waves in surge-direction $\beta = 0°$. In Figure 18, depending on the incident-wave direction, only surge, heave, and pitch are excited and show non-zero values. Corresponding to theory, the infinite frequency limit is zero for all coefficients.

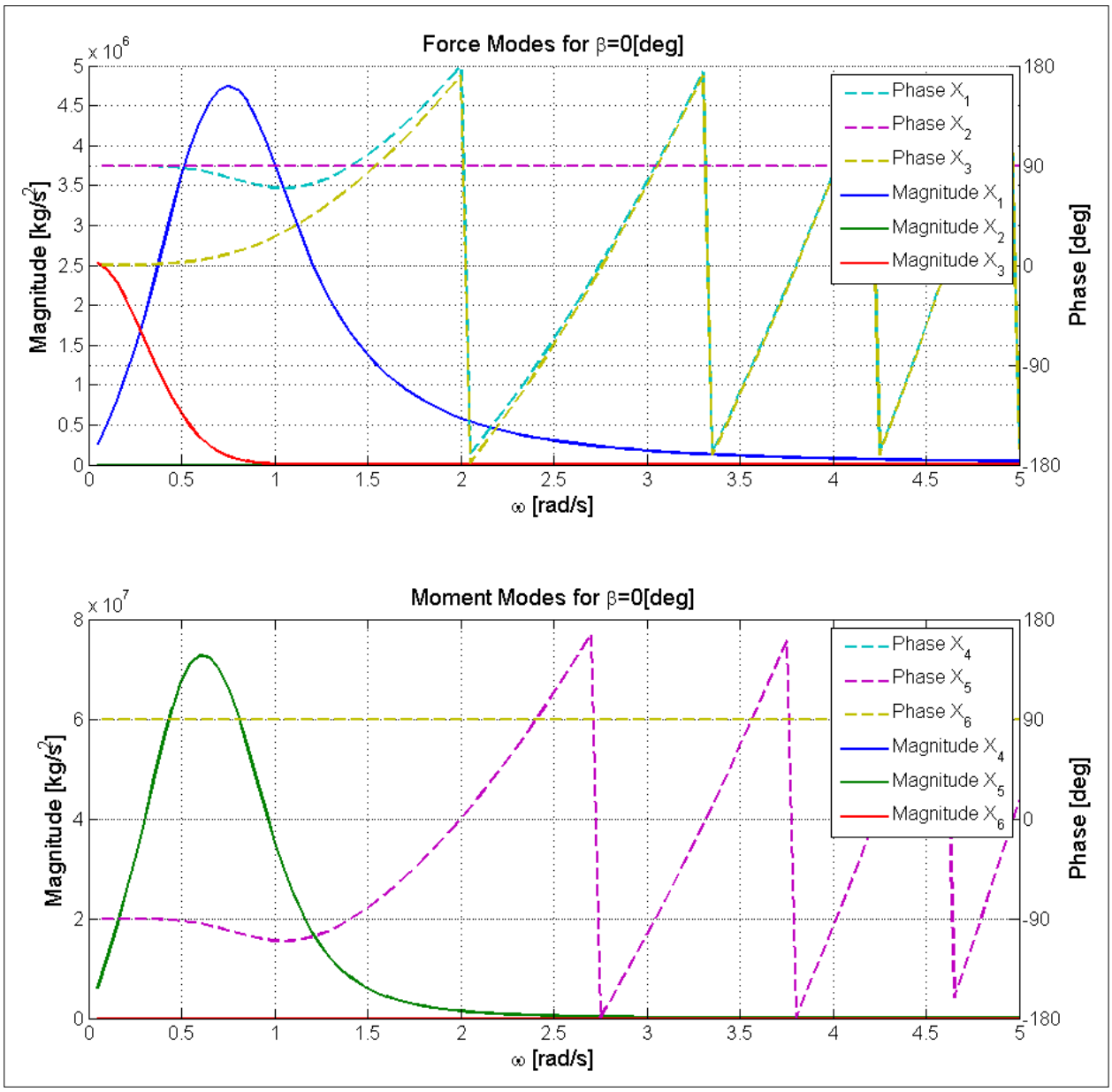

Figure 18. Tension leg platform hydrodynamic excitation force coefficients for β = 0° incident-wave direction

3.2.3 Tower Mode Shapes with ADAMS

To obtain valid simulation results, the correct tower mode shapes for the TLP design must be implemented into the FAST model. For the modal elements in FAST, the selected mode shapes have a great influence on the final results. The multi-body code ADAMS (MSC Software) is used for this purpose. First, the ADAMS input files are created using FAST. To calculate viable mode shapes, ADAMS linearizes the multi-body representation of the wind turbine. The linearization in ADAMS cannot be performed for accelerations, which are not independent states. Therefore the added mass cannot be included via HydroDyn. To account for added-mass effects, the actual mass of the platform is augmented to obtain a similar response. Due to numerical issues, ADAMS also cannot linearize the model with the quasi-static mooring system,

therefore the mooring system is linearized about the zero initial position and hardcoded into FAST's HydroCalc module (also used within ADAMS).

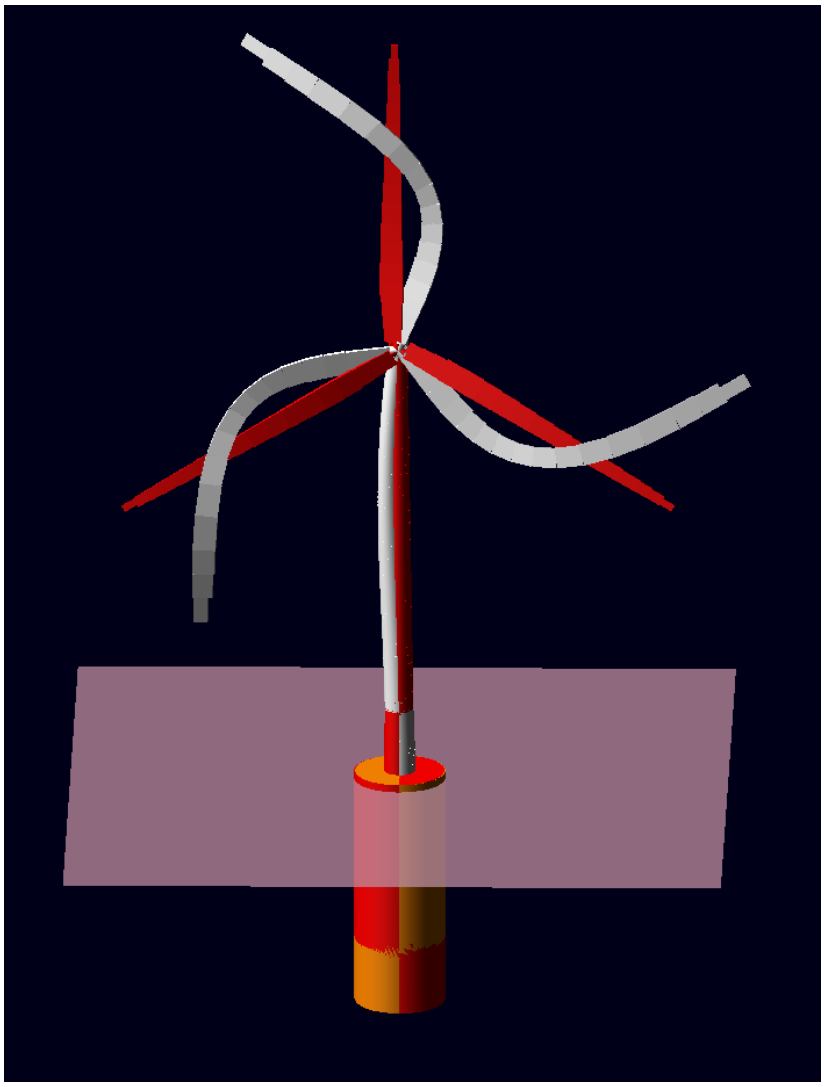

Figure 19. ADAMS visualization of second side-to-side tower bending mode

After performing these modifications to the original model, the tower mode shapes are calculated in ADAMS. The full model has more than 900 degrees of freedom and the same number of mode shapes therefore, by using the visualization in ADAMS, the correct first and second fore-aft and side-to-side tower mode shapes are identified. Figure 19 shows the ADAMS visualization of the second side-to-side tower bending mode. Here, the red depicts the undisplaced system. Possible ambiguities were discarded by also running an ADAMS simulation with rigid blades, where the tower modes are much easier to identify, and thus double-checking the natural frequencies for the identified tower modes. Because ADAMS only provides the x and y values and slopes of the mode shapes, a tool developed at NREL is used to obtain the 5 parameters needed by FAST, representing coefficients of a sixth-order polynomial of the mode shape. A normalized projection method is used for this calculation, and the coefficients then are put into FAST. To check the validity of the mode shapes, FAST is linearized and the eigenfrequencies of important modes are

compared to the ADAMS results. In the present study, results from both simulations were in good agreement. Additionally, the ratios between the first and second fore-aft and, respectively, side-to-side tower modes were checked. Large ratios were calculated; that is, the first and second modes are well separated. When all steps described above are completed, all data to create the FAST input files are available and the model in FAST can be assembled.

3.3 Design Evaluation

After completion of the TLP#1 model in FAST, the results predicted by Tracy [31] were attempted to be reproduced. A simulation was run with the FAST model under MIT's environmental conditions. These are:

- 11 m/s hub-height wind speed,
- 10-m significant wave height, and
- a wave peak spectral period of T_p = 17.64 sec.

These results showed a significant deviation compared to the predictions from Tracy [31]. Results differed both from the predicted steady-state and dynamic properties. In FAST, the line tensions, surge, and pitch offsets were considerably greater; the RMS values for surge, heave, and pitch were increased; and the line tension on the leeward line dropped to zero. The most significant deviation was the greatly increased pitch motion. Figure 20 shows that the RAO in pitch from the FAST calculation has increased five times compared to the MIT calculation. Due to this significantly increased pitch motion, the leeward mooring line went slack numerous times during a 10-min simulation, which in practice would mean the destruction of the mooring line and the failure of the TLP.

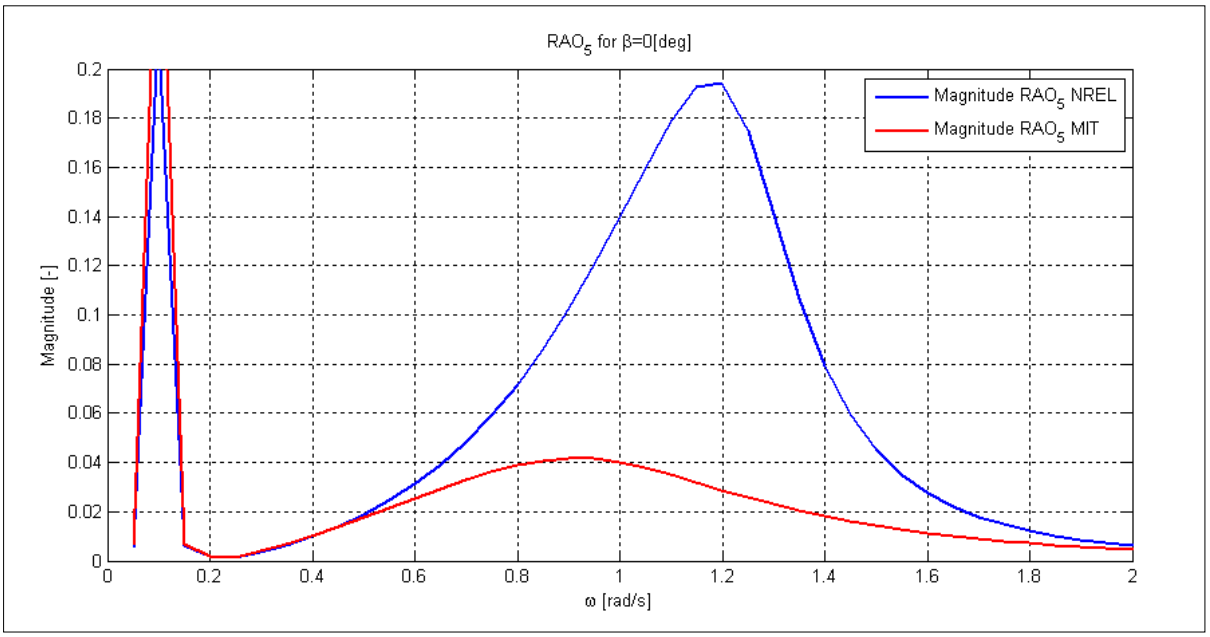

Figure 20. Tension leg platform pitch RAOs MIT TLP#1 from FAST and MIT

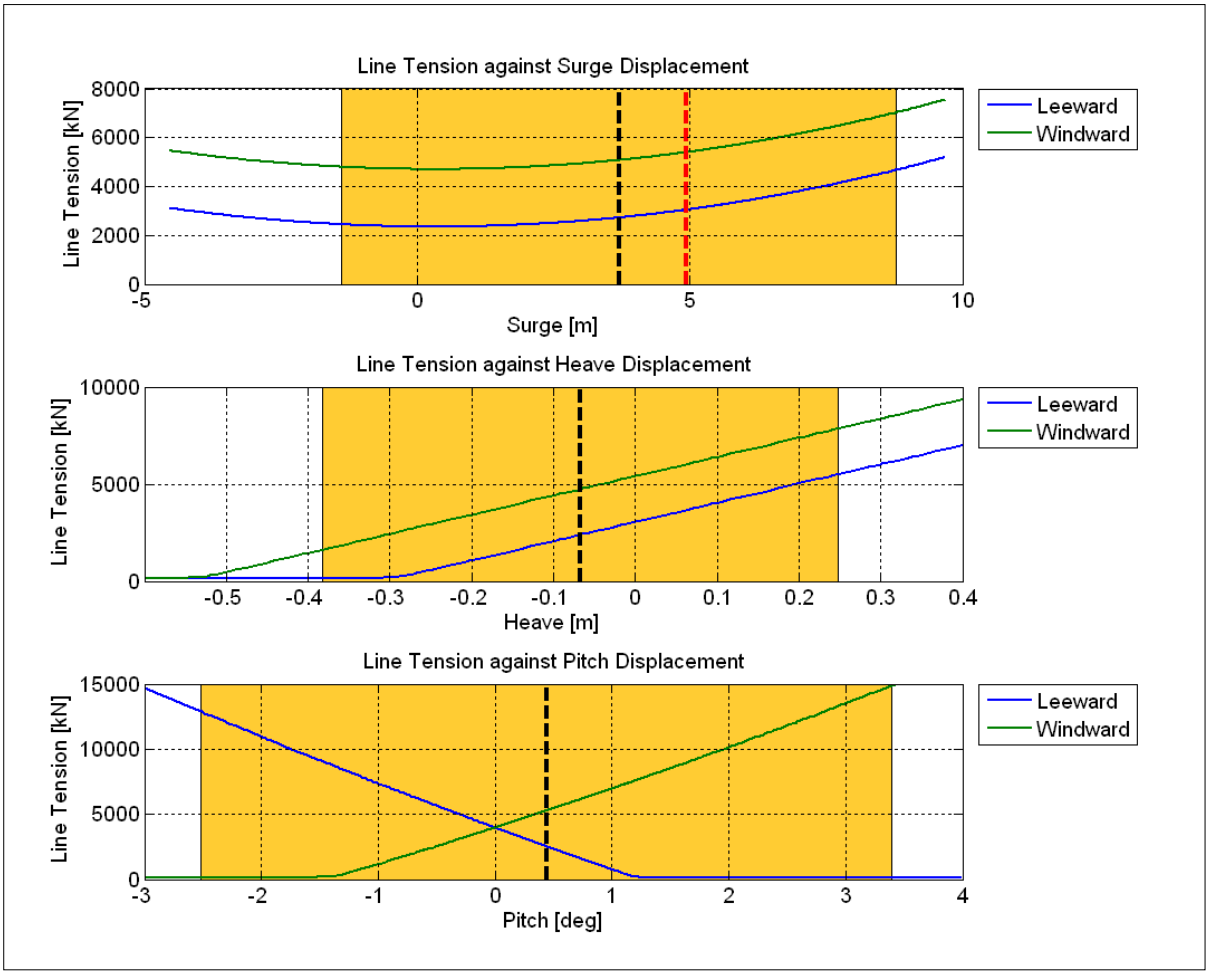

Figure 21. Tension leg platform line tensions

Various possible causes have been investigated to determine the reason for the great differences in the model. First, FAST's quasi-static mooring system was investigated but, as Figure 21 illustrates, the linearity assumption used by MIT in its frequency-domain calculation is considered valid over the range of possible platform displacements. The yellow highlighted ranges in the graphs represent the range of motion in surge, heave, and pitch of the TLP in the MIT 10-m reference sea state.

Next, the mass, stiffness, and damping matrices were compared. A meticulous analysis process was followed and ultimately an error in Tracy's calculation of the platform's mass matrix was identified as the cause of the lesser amount of pitch motion in MIT's results. By changing the mass matrix to imitate Tracy's error and re-running a frequency-domain analysis in WAMIT, the same pitch RAO as in Tracy's calculation was obtained. That result further proved that the design optimization in Tracy's thesis was flawed. After much deliberation, this fact was confirmed by MIT as well. Because the original optimization study from Tracy was flawed, Tracy's TLP#1 design cannot be considered an optimal design. Nevertheless, because it was impossible to quickly redo Tracy's extensive optimization study, it was decided that the existing sub-optimal TLP#1 design would be used as a basis for design where the concept would be modified to arrive at a viable design.

3.4 Modification of the TLP#1 and Final Redesign

Various possible modifications of the original design to overcome the design's limitations and resolve the increased pitch motion were assessed. These included changing the platform's inertias by changing ballast or its geometry, altering the stiffness of the tower and blades, or increasing the mooring lines stiffness. Eventually, a change in the fairlead location—where the mooring lines are attached to the platform—was found to be the most straightforward solution. This solution was favorable because, in the modeling process, the spokes are assumed to be massless. Except that the restoring in pitch is increased considerably, the extension of the spokes does not change the hydrostatic and hydrodynamic properties of the platform and also does not affect the NREL 5-MW baseline turbine properties. Regarding the input files for the FAST model, only the fairlead and anchor locations and the tower mode shapes are affected by this change and require recalculation in ADAMS.

In a parametric study, the necessary extension of the spokes length to satisfy the $[(F_{static}) - (3\,\sigma_{dynamic\ leeward\ and\ line\ tension})] > 0$ kN condition was identified as 23 m (increased from originally 18 m). This value also matches a formula found in Demirbilek [7] to estimate the optimum position for the fairlead connections. The equation states that the radius of the fairleads, that is, the distance from the center of the platform to the connection point of the mooring line, should be equal to or greater than the system's radius of gyration R_{gyr}.

$$r_{Fairleads} \geq R_{gyr} = \sqrt{\frac{I_{yy,sys\&a/m}}{m_{sys\&a/m}}} \tag{26}$$

Here $I_{yy,ss\&a/m}$ represents the turbine plus platform mass moment of inertia in pitch (including inertia from added mass) around the system's center of gravity and $m_{system\ \&\ added\text{-}mass}$ is the total system mass plus the added mass in pitch. After choosing a length of 23 m for the new spokes, new tower mode shapes were calculated and the modified FAST model assembled. Note that the basic TLP#1 design before the modification was not optimal due to the flawed optimization process, and that the extension of the spokes further changed the design. Therefore, no definite statement can be made on the quality and degree of optimization of the investigated TLP. Conversations with Sungho Lee from MIT, however, indicated that the modified TLP#1 still is a viable design. He also pointed out that the critical spokes length would be approximately 30 m.

To verify the capabilities of the new design, a time-domain simulation with MIT's reference conditions was conducted. Confirming the parametric study, the lines stayed taut in this design. To analyze the pitch motion, the platform's RAOs were calculated. These show a maximum in the pitch RAO exactly at the 1P rated wind-speed rotor frequency (illustrated in Figure 22) of $12\text{rpm} \approx 0.2\ \text{Hz} \approx 1.2\ \frac{rad}{s}$. In normal operation load cases, if the turbine spins at rated rotor speed, this could pose severe resonance problems.

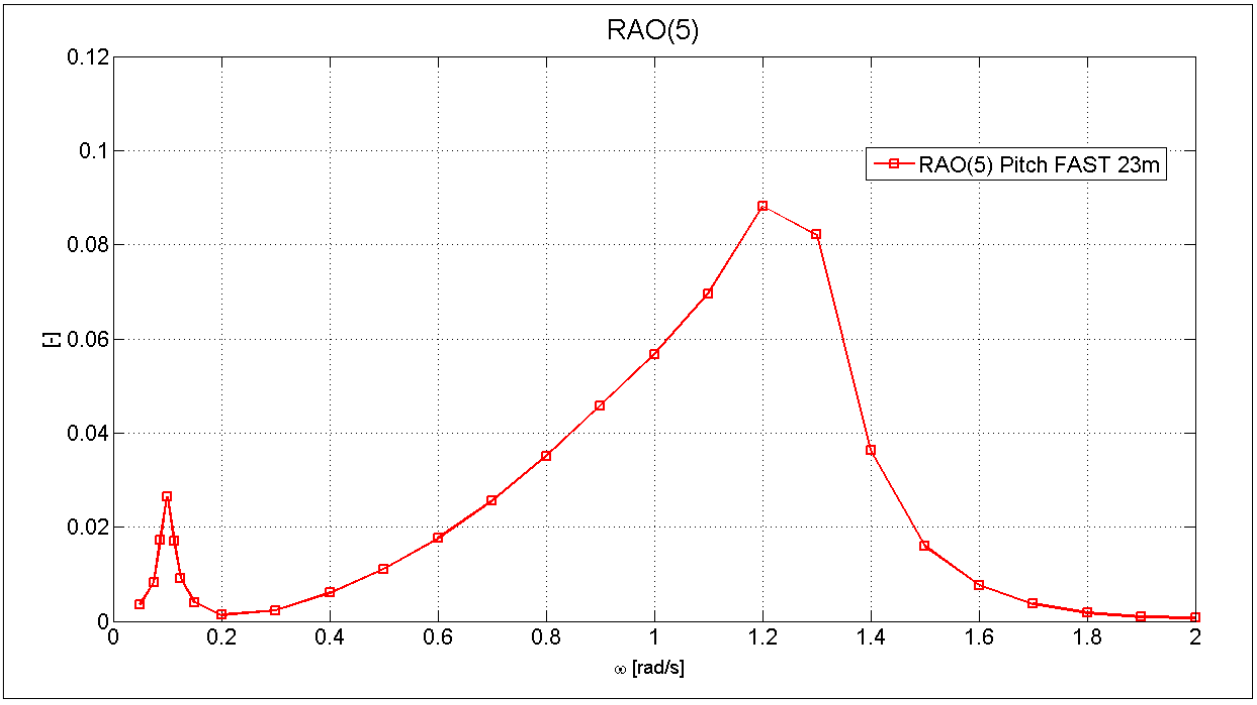

Figure 22. Tension leg platform (23-m spokes) pitch RAO resonance

To resolve that problem, the spokes were extended to 27 m—which still is within a reasonable range. Using the extended spokes, the RAO in pitch showed no coincidence with the 1P rotor frequency After confirming the non-existence of resonance problems, the TLP with 27-m spokes length was selected as the final model for the present TLP study. An illustration of the selected TLP is provided in Figure 23.

Using the final model, a linearization in FAST with a subsequent eigenanalysis was performed to obtain important natural frequencies. These are presented in Table 6 and the TLP's Campbell diagram is shown in Figure 24.

Table 6. Natural Frequencies of Redesigned (Final) TLP#1

Mode	Natural Frequency [Hz]	Mode	Natural Frequency [Hz]
Platform surge	0.0165	Platform roll	0.2229
Platform sway	0.0165	Platform pitch	0.2211
Platform heave	0.4375	Platform yaw	0.0972
1st Tower S-S	0.5745	1st Tower F-A	0.6311
2nd Tower S-S	3.1491	2nd Tower F-A	3.0578

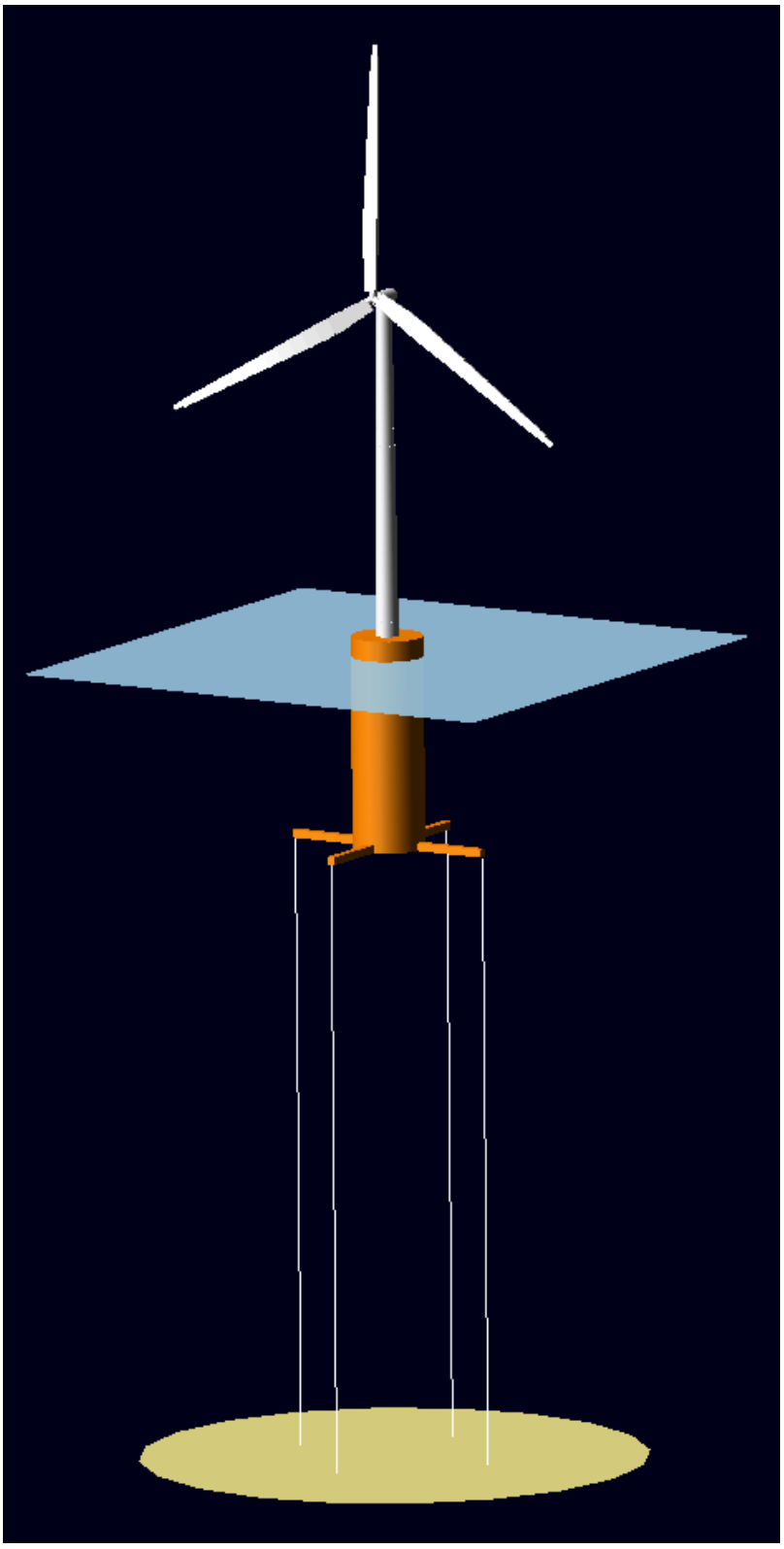

Figure 23. Tension leg platform with 27-m spokes (MIT/NREL TLP)

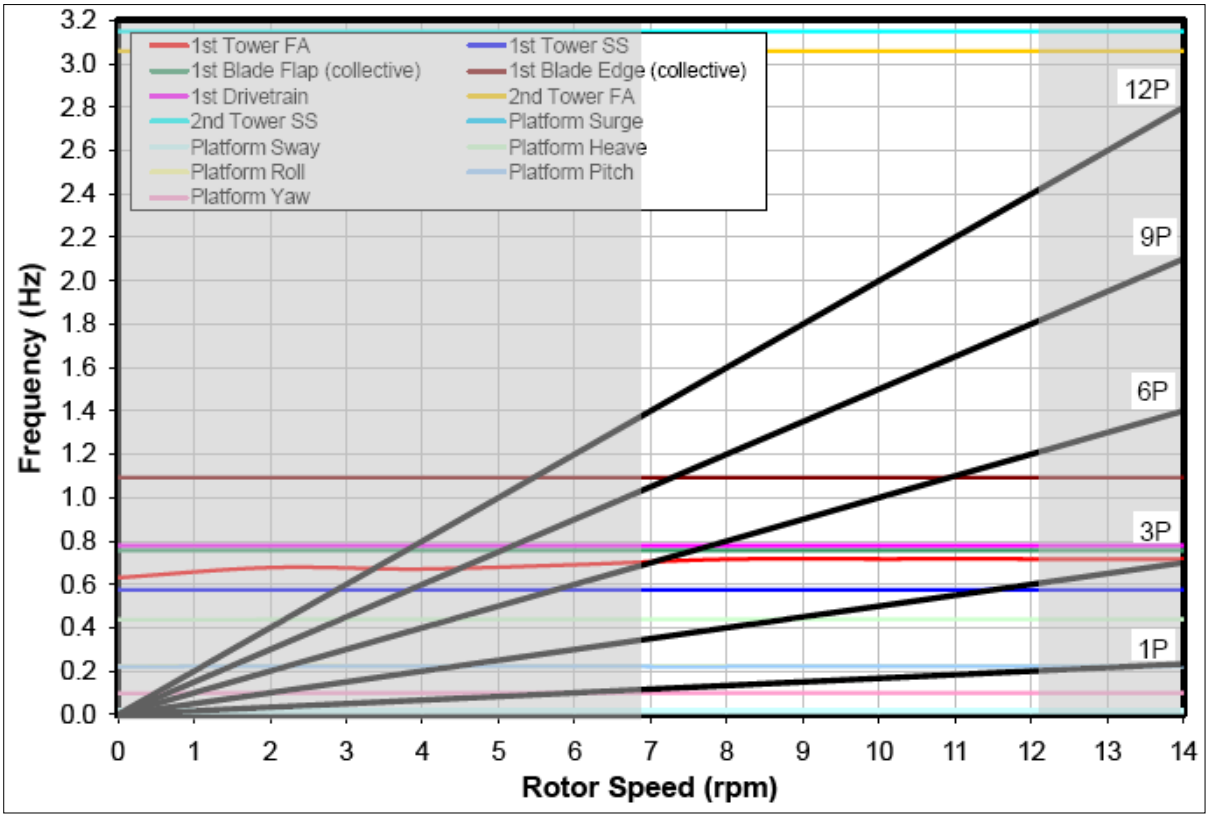

Figure 24. Campbell diagram of final redesigned TLP#1 with 27-m spokes; MIT/NREL TLP

3.5 Model Verification—Frequency Domain Versus Time Domain

To verify the results from the FAST model, a comparison with a frequency-domain solution was conducted. The commercial hydrodynamics code WAMIT has the capability of producing frequency-domain results if the non-hydrodynamic mass, damping, and stiffness matrices of the complete system (i.e., the turbine, the platform) are provided directly as inputs.

In WAMIT, the frequency-domain model calculates only the 6-DOF platform; the tower, blades, and remainder of the turbine are considered rigid and are represented by mass, stiffness, and damping matrices. To run WAMIT, these input matrices were obtained by linearizing a modified FAST model. In this model only the platform's 6 DOF are activated. The control system is turned off, no waves are present, and the rotor is spinning at 12.1 rpm at a constant wind hub-height wind speed of 11 m/s with no shear.

WAMIT automatically calculates the added-mass matrix. To obtain the WAMIT mass-matrix input, the infinite-frequency limit added-mass matrix is subtracted from the linearized FAST mass matrix. WAMIT also includes the hydrostatic restoring matrix by default; therefore the stiffness matrix from the FAST linearization also must be corrected for that factor. It also is important to exclude the gravity restoring terms in WAMIT. The simplest solution is to set the center of gravity position in WAMIT to zero. Using these inputs, WAMIT can calculate the response amplitude operators (RAO) for the 6 platform DOFs (ζ). The PDFs are computed based on these RAOs.

A response amplitude operator represents the non-dimensional response of a system to a unit-amplitude periodic incident wave at a given direction. It basically is the transfer function between the wave amplitude and the platform displacements, depending on the wave frequency and direction. A custom-programmed MATLAB script is used to compute probability density functions from the RAOs. This is done by first calculating the standard deviation as shown in Eq.27.

$$\begin{aligned}\sigma_\xi^2 &= \int_0^\infty (RAO_\xi(\omega))^2 S(\omega) d\omega, \quad for\ \xi = 1,2,3 \\ \sigma_\xi^2 &= \int_0^\infty (RAO_\xi(\omega))^2 S(\omega) rd\omega, \quad for\ \xi = 4,5,6\end{aligned} \tag{27}$$

Here, $S(\omega)$ represents the Pierson-Moskowitz wave spectrum with H_s = 10 m and T_p = 17.64 sec Assuming a normal, Gaussian probability density function and using the mean displacements (μ_ζ) from the previous FAST calculation, the PDFs are obtained as shown in Eq. 28.

$$PDF_\xi(x) = \frac{1}{\sigma_\xi \sqrt{2\pi}} \cdot e^{-[\frac{x-\mu_\xi}{2\sigma_\xi^2}]} . \tag{28}$$

These frequency-domain results are compared with the RAOs and PDFs calculated with FAST in the time domain. In FAST the RAOs are obtained simply by running numerous simulations with periodic, 1-m amplitude waves at different wave periods. After the transient effects have disappeared, the amplitudes of the platform's constant-amplitude surge, sway, heave, roll, pitch, and yaw displacement oscillations are recorded for each selected wave period. The resulting amplitudes at different wave periods are the RAOs for each platform DOF.

The PDFs are computed within MCrunch [4] using the outputs of aggregate standard deviations (σ_ξ^2) and mean displacements (μ_ζ) of 6 FAST simulations with all DOFs enabled, turbulent 11 m/s wind, stochastic waves, and an active control system.

Figure 25 presents four different RAO calculations. The black lines represent a FAST time-domain simulation with the inputs described above (i.e., a model with every possible DOF). This result is compared to the red lines, a WAMIT frequency-domain calculation. Additionally, to illustrate the previously described error, the RAOs from Tracy's flawed calculation are represented by the green lines. The most evident differences are that the FAST RAO values have higher maxima and the peaks are shifted towards smaller frequencies as compared to the WAMIT results.

To imitate the frequency-domain approach in FAST, and thus verify the model by the comparison to the frequency-domain results, the turbine also is simulated as a completely rigid structure. This approach results in RAOs represented by the blue curves. These FAST-generated RAOs resemble the WAMIT RAOs almost perfectly. Hence, the agreement of the RAOs constitutes a code-by-code verification of the FAST model with the commercial WAMIT code.

The differences between the FAST model and the WAMIT model were determined to be due to the turbine flexibility. The couplings between platform motions and the flexible tower and

blades—which mostly are not captured in a typical frequency-domain approach—have a significant influence on the results. Particularly the shift of the peaks to smaller frequencies in the time domain could cause problems in a design process that relies on frequency-domain simulations. A design which has no resonance problems in the frequency domain because all RAO maxima are outside the resonance zone could fail in the time domain. This is because down-shifting to smaller frequencies could move these maxima into the critical resonance frequency ranges and cause severe resonance issues. In further simulations not included here, the tower DOFs were identified to have the most significant impact on the shift for this TLP design.

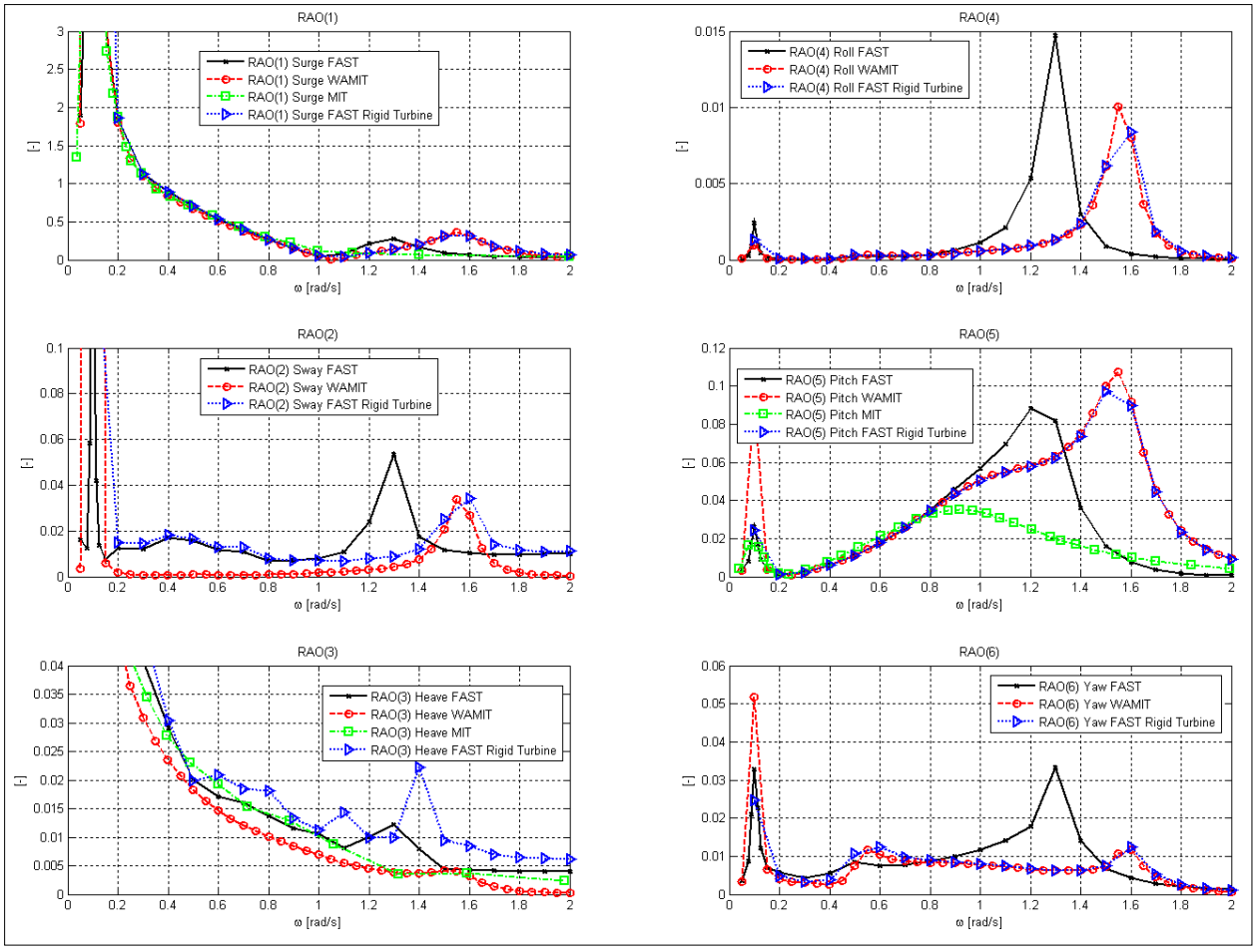

Figure 25. Tension leg platform RAOs for 23-m spokes

After identifying the source of the discrepancies, the RAOs for the two different spokes lengths were compared. Figure 26 shows the results from the fully flexible FAST model and the WAMIT model. Again, the shift to smaller frequencies and the higher maxima can be observed. The figure shows that the further increase in the TLP's spokes length results in reduced RAOs, therefore the platform is less susceptible to excessive motions, especially in pitch.

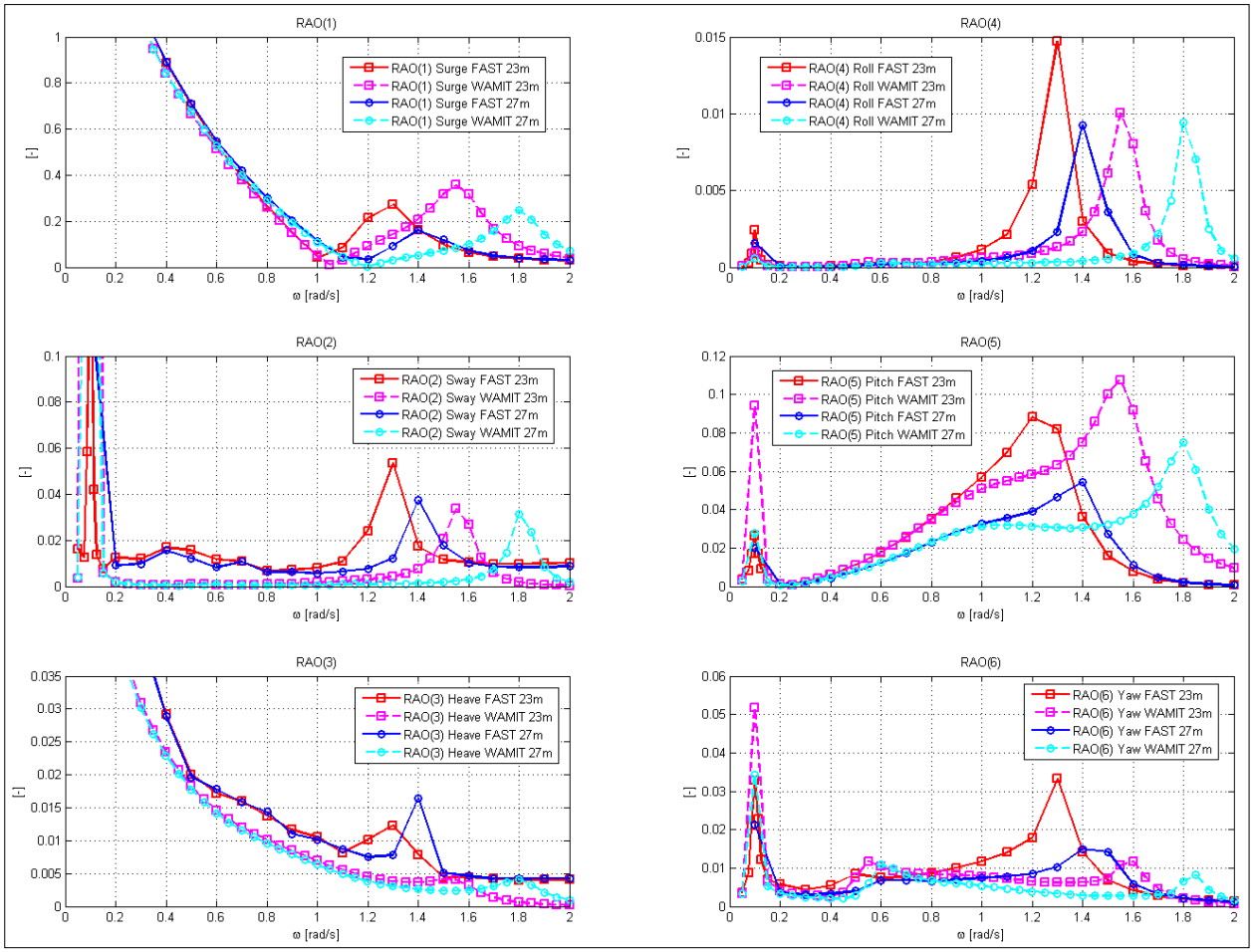

Figure 26. Tension leg platform RAOs for 23-m and 27-m spokes

In addition to the deviations in the RAOs, the PDFs also show significant differences between time-domain and frequency-domain simulations. Figure 27 presents the PDF results from the fully flexible FAST model and the WAMIT model. In surge, heave, and pitch the time-domain and frequency-domain results are similar. The PDFs have the same means and approximately the same standard deviation. In contrast, the PDFs for the platform's sway, roll, and yaw motion differ considerably. The WAMIT solutions have a much smaller standard deviation and therefore have highly increased peak PDF values, but the means remain the same. In this simulation, waves are proceeding in downwind direction along the turbine's surge direction (x-axis). The frequency-domain model is based on a linearized 6-DOF floating-turbine model, so the sway, roll, and yaw modes are not excited by the incoming wind and waves. Except the rotor gyroscopic effects, most couplings between the platform and the turbine are not captured in the frequency domain. The PDFs therefore show a very small standard deviation around the mean.

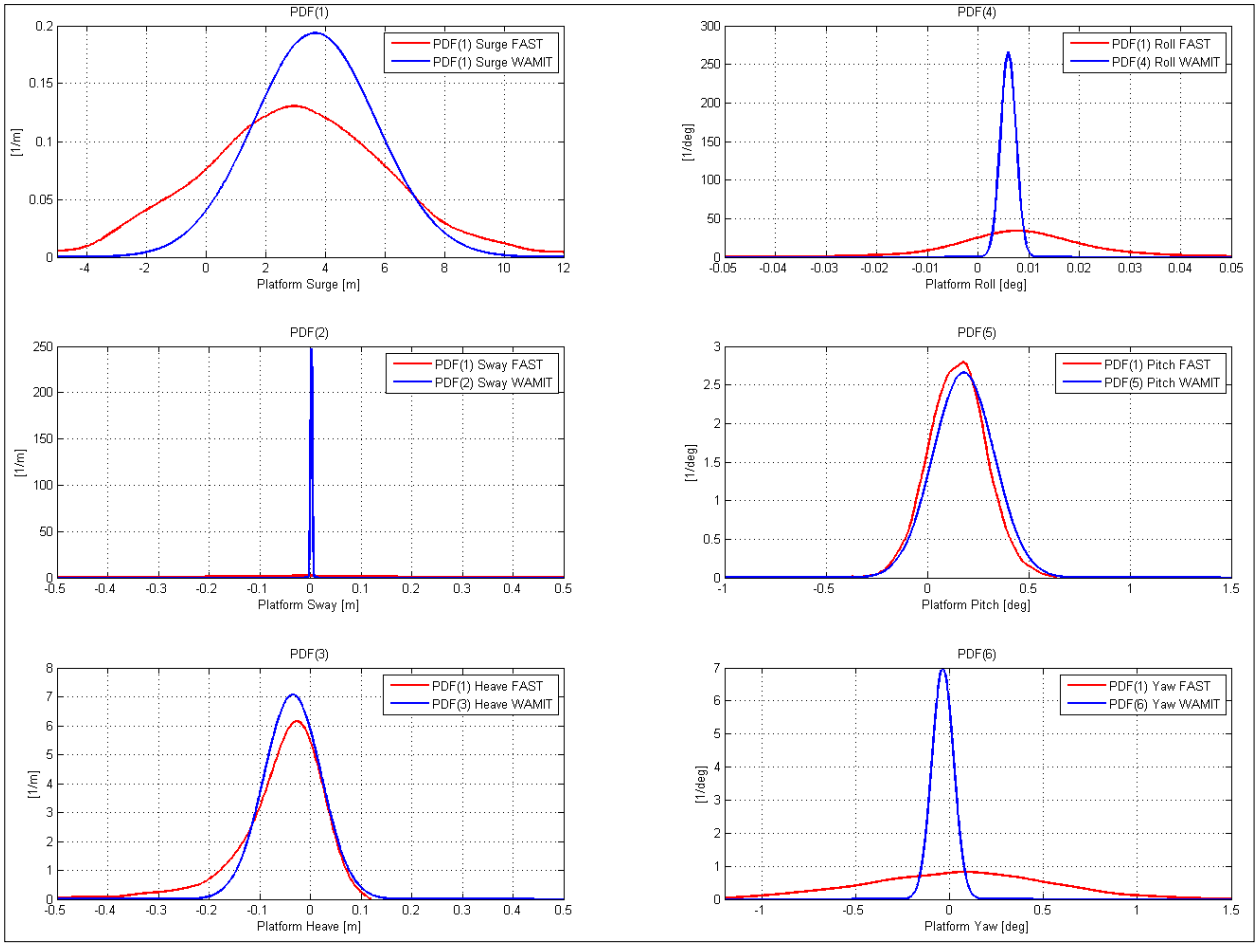

Figure 27. Tension leg platform PDFs for 23-m and 27-m spokes

3.6 Conclusion

Frequency-domain results for RAOs and PDFs were obtained with WAMIT, which has the capability to produce RAOs. To compare the results with the time domain, FAST was used to also calculate RAOs. Using the RAO results, PDFs were calculated for both frequency domain and time domain and compared to each other. These comparisons showed significant but explainable differences between the frequency-domain and time-domain simulation results. The most interesting result from the RAO comparison is that the maximum values in the time domain of the curves generally were shifted towards lower frequencies. That could mean that a model performing well in the frequency domain could run into critical resonance issues in the time domain. The PDFs showed that, in general, the standard deviations of the frequency-domain results were much smaller (and the peaks higher) because nonlinearities were neglected. In future frequency-domain design processes, these findings should be considered carefully. It is suggested that at least one tower fore-aft DOF should be added to the frequency-domain model to account for the errors.

4 Loads Analysis of Tension Leg Platform

Using the final FAST TLP model, multiple simulations of selected design load cases from the IEC 61400-3 standard [8] were defined and run. The steps performed in the study to complete the analysis are listed below.

- Ran series of time-domain simulations with the TLP model and analyzed the loads on the turbine
- Identified critical design load cases
- Investigated critical design load cases
- Analyzed statistics, extreme event tables, and fatigue loads
- Identified and analyzed instabilities
- Compared results to land-based system

4.1 Design Load Cases

The IEC 61400-3 standard prescribes running numerous design load cases to verify the structural integrity of an offshore wind turbine design. The results from each DLC are combined and analyzed to determine the extreme (ultimate) and fatigue loads expected over the lifetime of the turbine. Loads on each primary component of the turbine including the blades, tower, nacelle, drivetrain, and mooring system are examined. The DLCs in the IEC standard cover design-driving situations such as normal operation, start-up and shut-down events, and parked and idling states, combined with various sea and wind conditions and possible fault scenarios. Overall, the standard describes eight different design situations with sub-DLCs in each category dealing with ultimate or fatigue loads and covering different wind and wave conditions.

Only a subset of these DLCs is selected for the loads analysis of the TLP. First, DLCs 8.x, which define transport, assembly, maintenance, and repair situations are discarded because they are not considered in this study. The baseline control system routine does not include logic for start-up and shutdown events, so DLCs 3.x, 4.x—and 5.x, defining start-up, normal shutdown, and emergency shutdown situations—also are omitted. For fatigue analysis, only DLC 1.2 is selected. As described in more detail in Section 4.3, DLC 1.1 and DLC 1.2 are equivalent within this report's loads analysis. The remaining DLCs simulated in the present study are:

- Power Production: 1.1 (1.2), 1.3, 1.4, 1.5, 1.6a;
- Power Production and Fault: 2.1, 2.3;
- Parked: 6.1a, 6.2a, 6.3a; and
- Parked and Fault: 7.1a.

The standard defines the minimum length of each simulation used in each DLC and also requires performance of more than one simulation for each pair of turbulent wind and stochastic wave conditions. To reduce the number of simulations, wind and wave random seeds are combined. Instead of running *n* different wave seeds for each wind condition and vice versa—thus resulting

in n^2 simulations—only n seeds for each pair of wind and wave conditions are used, reducing the numbers of simulations to n.

For the loads analysis of the TLP the selected load cases are divided into three groups. The first group represents normal operation results from DLCs 1.1, 1.3, 1.4, and 1.5. The wind turbine is in normal operation in a normal sea state with varying wind conditions at or below rated wind speed. The second group represents the previous DLCs 1.1, 1.3, 1.4, and 1.5, and includes the normal operation DLC in an extreme sea state 1.6a, DLC 2.3, and DLC 6.1a. The latter two consider faults in normal operation and extreme 1-year or 50-year events with the turbine idling, but still generate no instabilities. The last group consists of DLCs in which the model failed or violated simulation constraints due to instabilities, or the results were unreasonable. This group consisted of DLCs 2.1, 6.2a, 6.3a, and 7.1a. For this group, no extreme event results are presented but each identified instability is discussed in detail. Results from groups one and two are compared to the land-based NREL 5-MW baseline wind turbine to correlate the performances, identify the major differences, and draw conclusions on the viability of the investigated TLP design. Overall, more than 2,000 single simulations—ranging from 60 sec to 3,600 sec simulation time—were performed and generated more than 100 GB of data.

Table 7 shows details on wind and wave conditions and the applied partial safety factors for each DLC. Table 8 presents the definitions of the abbreviations of the utilized wind and wave models. Note that the expected wave height $H_s = E[H_s \mid V_{Hub}]$ in Table 7 at a wind speed $[V_{Hub}]$ also determines the range of the associated peak spectral wave periods (T_p). Here, for each expected wave height (H_s), a set of three peak spectral wave periods (T_p) is used uniformly distributed over the associated wave period range. For further information on the DLC definitions refer to IEC 61400-3 [8] and Jonkman [18].

Table 7. Selected IEC 61400-3 Design Load Cases

DLC	Wind Conditions		Wave Conditions			Events	PSF
	Model	Wind Speed	Model	Wave Height	Direction		
1.x Power Production							
1.1	NTM	$V_{in} < V_{Hub} < V_{Out}$	NSS	$H_s = E[H_s \mid V_{Hub}]$	$\beta = 0°$	Normal operation	$1.25 \cdot 1.2$
1.3	ETM	$V_{in} < V_{Hub} < V_{Out}$	NSS	$H_s = E[H_s \mid V_{Hub}]$	$\beta = 0°$	Normal operation	1.35
1.4	ECD	$V_{Hub} = V_r \pm 2\frac{m}{s}$	NSS	$H_s = E[H_s \mid V_{Hub}]$	$\beta = 0°$	Normal operation	1.35
1.5	EWS	$V_{in} < V_{Hub} < V_{Out}$	NSS	$H_s = E[H_s \mid V_{Hub}]$	$\beta = 0°$	Normal operation	1.35
1.6a	NTM	$V_{in} < V_{Hub} < V_{Out}$	ESS	$H_s = 1.09 \cdot H_{s50}$	$\beta = 0°$	Normal operation	1.35
2.x Power production plus occurrence of fault							
2.1	NTM	$V_{in} < V_{Hub} < V_{Out}$	NSS	$H_s = E[H_s \mid V_{Hub}]$	$\beta = 0°$	Pitch runaway	1.35
2.3	EOG	$V_{Hub} = V_r \pm 2\frac{m}{s}, V_{Out}$	NSS	$H_s = E[H_s \mid V_{Hub}]$	$\beta = 0°$	Loss of load	1.1
6.x Parked (standing still or idling)							
6.1a	EWM	$V_{Hub} = 0.95 \cdot V_{50}$	ESS	$H_s = 1.09 \cdot H_{s50}$	$\beta = 0°, \pm 30°$	Yaw = 0°, ± 8°	1.35
6.2a	EWM	$V_{Hub} = 0.95 \cdot V_{50}$	ESS	$H_s = 1.09 \cdot H_{s50}$	$\beta = 0°, \pm 30°$	-180° < Yaw < 180°	1.1
6.3a	EWM	$V_{Hub} = 0.95 \cdot V_1$	ESS	$H_s = 1.09 \cdot H_{s1}$	$\beta = 0°, \pm 30°$	Yaw = 0°, ± 20°	1.35
7.x Parked and fault condition							
7.1a	EWM	$V_{Hub} = 0.95 \cdot V_1$	ESS	$H_s = 1.09 \cdot H_{s1}$	$\beta = 0°, \pm 30°$	Yaw = 0°, ± 8° 1 seized blade	1.1

Table 8. Design Load Case Abbreviations

Abbreviation	Definition
ECD	Extreme coherent gust with direction change
EOG	Extreme operating gust
ESS	Extreme sea state
ETM	Extreme turbulence model
EWM	Turbulent extreme wind model
EWS	Extreme wind shear
NSS	Normal sea state
NTM	Normal turbulence model
V_{Hub}	Hub-height wind speed averaged over simulation time
$V_{1,50}$	1-year, 50-year extreme wind speed over 10min
$H_{s,1,50}$	1-year, 50-year extreme significant wave height, based on a 3-hour reference period
$E[H_s \mid V_{Hub}]$	Expected significant wave height at V_{Hub}

4.2 Ultimate Loads and Deflections in Normal Operation

This section focuses on the dynamic response—the time series' statistics and the extreme events of the TLP in normal operation mode when the turbine is operating in a normal sea state with varying wind conditions at or below rated wind speed. For this group—composed of DLCs 1.1, 1.3, 1.4, and 1.5—all simulations yielded reasonable results and no simulation failed. The TLP statistics and extreme loads and deflections are compared to results of the equivalent land-based turbine in normal operation. This set was grouped for consistency with the ITI Barge anlysis of Jonkman [18].

4.2.1 Dynamic Response of Tension Leg Platform

To characterize the dynamic response of the wind turbine in normal operation, statistical data from the first group of DLCs was analyzed. Figure 28 shows the minimum, mean, and maximum values from each simulation in DLC 1.1 for eight important output parameters. The partial safety factors are not applied to these values. The dots and the lines represent the mean values, the maximum values are represented by upward-pointing triangles, and the minimum values are indicated using downward-pointing triangles. Each graph—except the first for platform pitch—contains data from the land-based system (displayed in green) and data from the offshore TLP system (displayed in blue). Both systems use the exact same controller, therefore the values for generator power, rotor speed, and rotor torque differ only very slightly.

The rotor speed mean values increase linearly with mean hub-height wind speed from cut-in: (3.0 m/s) to just below rated wind speed: (11.4 m/s). This increase keeps the tip-speed ratio constant, and ensures that the blades operate at the optimal lift-to-drag coefficient and that the system maintains optimal wind power conversion efficiency. Above rated speed, the rotor speed is held constant with active pitch control. Similarly, the generator power and the rotor torque increase below rated wind speed and maintain a constant value above rated wind speed.

The out-of-plane tip deflection and the root bending moment of blade 1 show an increase below rated wind speed and a decrease above the rated operating point. This behavior is characteristic of any active-pitch-to-feather controlled wind turbine, because the thrust reaches maximum at rated wind speed and drops due to active blade pitch action above rated wind speed. Therefore the maximum force on the blades is reached at the turbine's rated operating point.

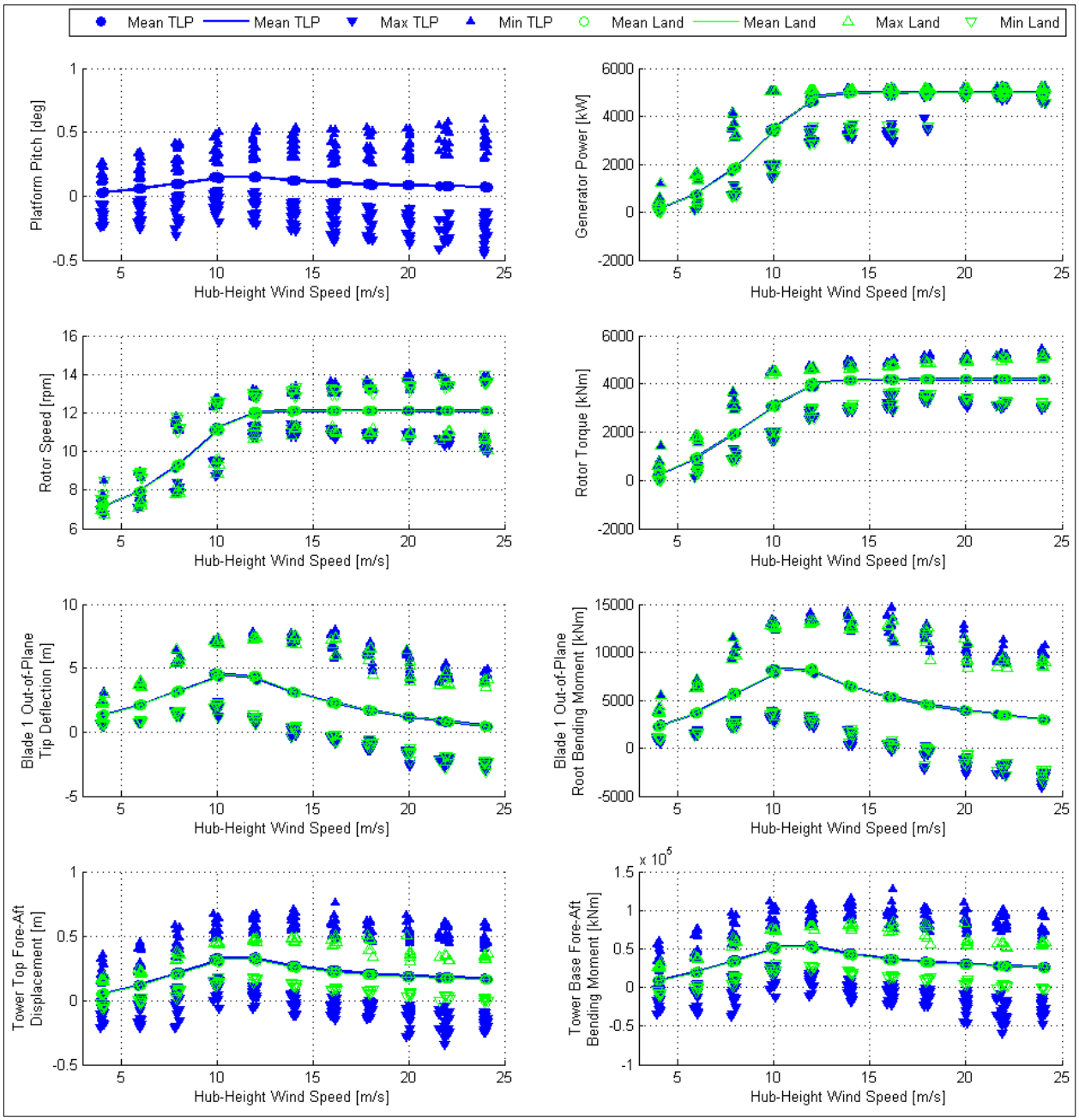

Figure 28. Statistics from DLC 1.1 simulations

The figures show that the differences between the TLP and the land-based turbine again are small, with a slightly greater tip deflection and root bending moment for the offshore system. These excursions increase with greater wind speeds, because a greater wind speed is reflected in

greater wave amplitudes and, therefore, increased surge and pitch motion of the TLP. Increased excursions in pitch with increasing wave height are shown in the upper-left graph in Figure 28. Because the pitch amplitude never exceeds 1 degree, even at the highest wind speed, the deviation between land and TLP systems is relatively small. This also is valid for the tower-top fore-aft displacements and bending moments, where an increasing deviation between the onshore and offshore system is shown. Compared to the blades, the tower's fore-aft motions are responding more sensitively to the increased surge and pitch motion of the offshore system because of the inverted-pendulum effect. This effect originates from the comparatively high inertia at the tower top and its great distance to the system's pivot point near the bottom of the platform. At the greatest wind speed, the excursions for the land-based tower fore-aft displacement and bending moment roughly are doubled for the TLP, as compared with the mere 10% increase in the blade deflection and bending moment.

Overall, the differences between the TLP and the land-based machine are moderate. The main effect derived from the statistics to be considered in a design process are the increased stresses on the tower, which might need to be strengthened to withstand the increased loads. Design load case 1.3 is not shown here but exhibits very similar behavior. For DLCs 1.4 and 1.5, the excursions become much greater because these DLCs dominate most of the extreme loads in normal operation. More detail on these DLCs is given in the following section.

4.2.2 Extreme Events

Table 9. Extreme Events for the Blade 1 Root Moments—Tension Leg Platform

Parameter	Type	File	RootMxc1 [kN·m]	RootMyc1 [kN·m]	RootMzc1 [kN·m]	Time [s]
RootMxc1	Min	DLC1.1_0187_Sea_24.0V0_05.5Hs_12.7Tp_S03.out	-7.23E3	-1.30E3	-1.54E2	5.94E2
RootMxc1	Max	DLC1.3_0183_Sea_24.0V0_05.5Hs_18.3Tp_S01.out	1.15E4	1.18E4	-9.19E1	5.66E2
RootMyc1	Min	DLC1.4_0099_Sea_ECD-R+20_02.7Hs_16.4Tp_S03.out	2.15E3	-9.55E3	-1.86E2	6.92E1
RootMyc1	Max	DLC1.4_0028_Sea_ECD+R_02.4Hs_09.2Tp_S04.out	7.64E2	2.63E4	9.98E1	7.88E1
RootMzc1	Min	DLC1.4_0037_Sea_ECD+R+20_02.7Hs_08.9Tp_S01.out	-1.26E3	-6.44E3	-3.57E2	8.13E1
RootMzc1	Max	DLC1.3_0112_Sea_16.0V0_03.4Hs_10.1Tp_S02.out	-2.21E3	1.97E4	2.07E2	1.14E2

Table 10. Extreme Events for the Tower-Base Moments—Tension Leg Platform

Parameter	Type	File	TwrBsMxt [kN·m]	TwrBsMyt [kN·m]	TwrBsMzt [kN·m]	Time [s]
TwrBsMxt	Min	DLC1.3_0187_Sea_24.0V0_05.5Hs_12.7Tp_S03.out	-4.16E4	2.17E4	-7.16E3	2.80E2
TwrBsMxt	Max	DLC1.1_0190_Sea_24.0V0_05.5Hs_12.7Tp_S04.out	5.11E4	1.55E4	-2.57E3	6.04E2
TwrBsMyt	Min	DLC1.3_0169_Sea_22.0V0_04.7Hs_11.0Tp_S03.out	3.09E3	-9.73E4	-2.18E3	8.16E1
TwrBsMyt	Max	DLC1.1_0124_Sea_16.0V0_03.4Hs_10.1Tp_S06.out	4.61E3	1.91E5	6.74E2	9.10E1
TwrBsMzt	Min	DLC1.3_0189_Sea_24.0V0_05.5Hs_18.3Tp_S03.out	1.27E4	-2.72E3	-1.39E4	2.77E2
TwrBsMzt	Max	DLC1.4_0081_Sea_ECD-R_02.4Hs_17.6Tp_S03.out	-2.84E3	1.28E5	1.28E4	7.78E1

The ultimate loads on the turbine were assessed by analyzing the Crunch-generated extreme event tables. Table 9 and Table 10 show two exemplary extreme event tables for the TLP, Table 9 for the root moments in blade 1 and Table 10 for the tower-base moments. Overall, 32 extreme

event tables have been generated for the floating platform, displaying all significant loads on the turbine, platform, and mooring system. These can be found in Appendix A.1. Each table's first columns contain a group of similar output parameters, representing certain internal loads such as blade or tower moments, mooring line tensions, and nacelle accelerations. The second and third columns give information on the type (minimum or maximum) and the specific load case filename for the extreme event. The filenames list the DLC, the simulation number, the land or sea basis, the hub-height wind speed, the significant wave height and peak spectral wave period, and the random seed identifier. The final columns show the minimum and maximum magnitudes of the extreme loads (the shaded values on the diagonal) with the last column containing the exact simulation time at which the particular extreme event occurred. All extreme loads presented in the extreme event tables are weighted with their associated PSFs according to Table 7.

Note that the loads presented in the extreme event tablesare recorded at the connections of the multi-body representations of the particular elements. They do not provide exact data on detailed stress distributions and possible stress peak values in the actual structural element; obtaining this data requires additional finite element analysis. The coordinate systems used in the extreme event tables are according to FAST's internal conventions, which are found in FAST's user manual [19], and for the platform and mooring system described in Jonkman [18]. The examination of the extreme event tables for normal operation DLCs shows that no particular load case is dominating the loads. No single DLC simulation produces more than 15 minima or maxima in the output parameters, which means there cannot be one single design-driving load case simulation identified. Therefore particular loads, which are considered most important and design driving, are analyzed in more detail (rather than examining each of the 92 distinct simulations which caused minimum or maximum values). The output parameter names and definitions are listed below.

- "WindVxi" represents the instantaneous wind speed component in x-direction
- "WaveElev" represents the instantaneous wave elevation relative to the still water level (SWL)
- "BldPitch3'' represents the instantaneous pitch angle of blade 3
- "Azimuth" represents the instantaneous rotor azimuth angle of blade 1, clockwise positively from the positive z-direction when looking downwind
- "RotSpeed" represents the instantaneous rotational speed of the rotor
- "OoPDefl3" represents the instantaneous out-of-plane deflection of blade 3
- "PtfmRoll, PtfmPitch, PtfmYaw" represent the instantaneous roll, yaw, and pitch angles of the platform
- "PtfmSurge, PtfmSway, PtfmHeave" represent the instantaneous surge, sway, and heave displacements of the platform
- "RootMMxy3" represents the instantaneous combined root bending moment of blade 3 around the blade's x-axis and y-axis
- "Anch1Ten" represents the instantaneous line tension at the leeward anchor 1

All simulations in normal operation mode use the NSS wave model, therefore the simulated wave conditions for each DLC are essentially equal. The highest wave peak and, respectively, lowest wave trough values recorded occurred in DLC 1.5 with approximately ±5 m, that is a possible maximum of 10 m absolute wave height.

Wind speed, the other significant environmental parameter for an offshore wind turbine, reaches its instantaneous maximum during an extreme turbulence in DLC 1.3 with 38 m/s in downwind x-direction. As described in the previous section, due to active pitch control (pitching between $0° \leq \theta_p \leq 29.6°$) the excursions in generator torque and power and rotor speed above the rated values are relatively small, with 5.34 MW as maximum generator power, 4.8 kNm torque and a maximum rotor speed of 14.6 m/s. These maximum excursions occur in DLC 1.3 and 1.4 simulations, and do not trigger any other significant extreme loads.

One design-driving parameter for a wind turbine during normal operation is the out-of-plane maximum blade deflection and the associated minimum tower clearance and maximum blade root moment. The maximum blade deflections for each blade occur solely in DLC 1.4 after extreme coherent gusts with direction changes. Figure 29 shows time series results from the DLC 1.4 simulations 88 and 106.

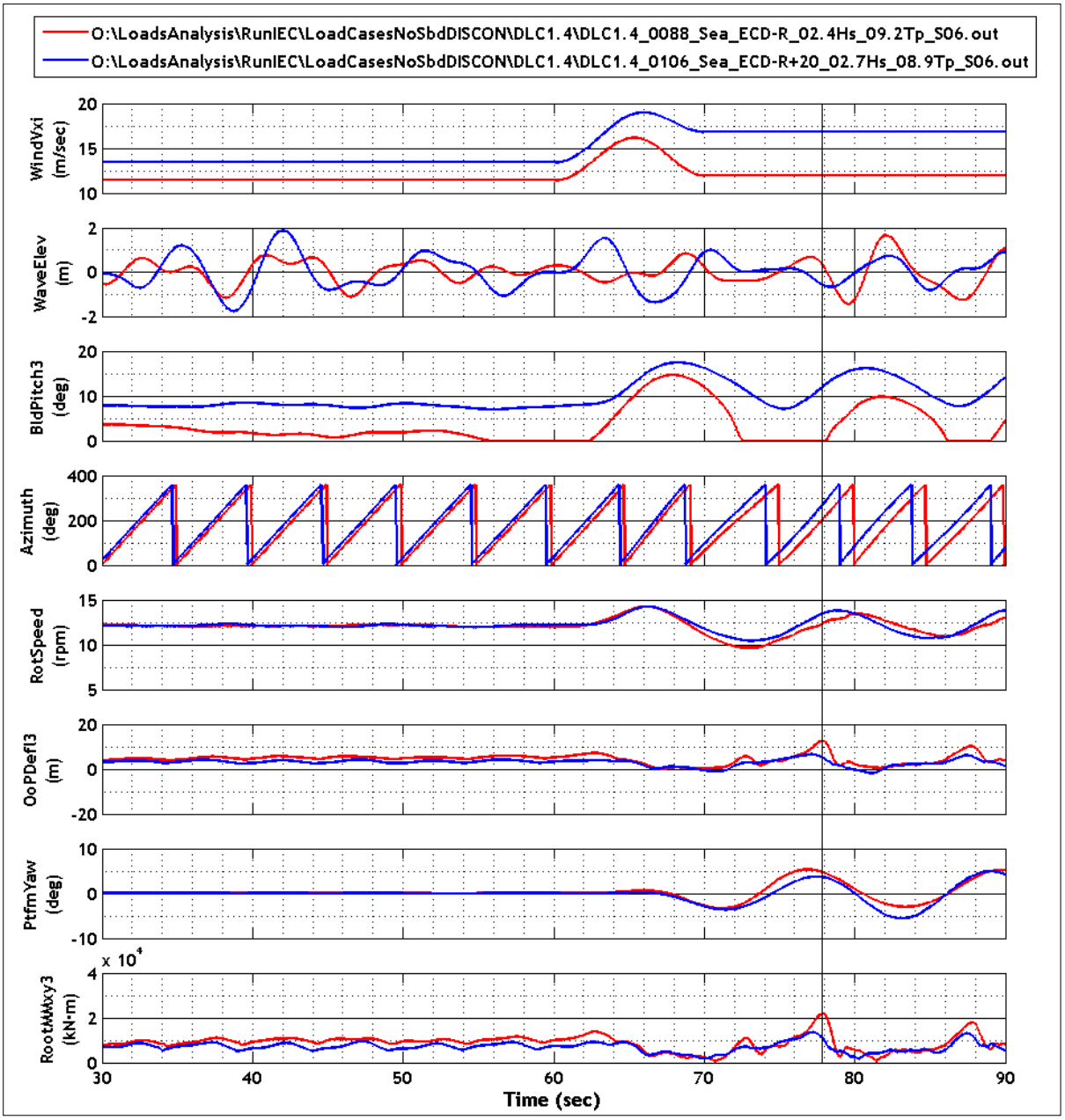

Figure 29. Histories from TLP DLC 1.4 simulations 88 and 106

The maximum blade deflection appears for blade 3 in simulation 88 at a time of 78 sec. This point in time is highlighted by the vertical solid line. Simulation 106 is plotted to illustrate why, compared to simulation 88, the 2 m/s higher constant wind speed and gust speed in simulation 106 does not yield the highest deflection as initially could be suspected.

Understanding this behavior requires looking at the blade pitch angle and the azimuth. For simulation 88, at the instant when the maximum deflection of 12.4 m is reached the pitch angle is 0° and the azimuth is 220°. That means blade 3 is facing flat into the wind at a azimuth position $\Omega = 220° - 120° = 100°$ measured clockwise from the rotor top. At the same time, the wind direction has changed 54° to the left (when looking downwind) and the turbine has yawed 5°. The highest lift coefficient on the blade's airfoil then is reached because it is not pitched, and at

an azimuth position of about 90°, where the resultant velocity vector on the airfoil reaches its maximum. This maximum in the blade's lift generates the maximum deflection. In contrast, the pitch of blade 3 in simulation 106 never drops to zero, therefore it more than compensates for the increased lift due to the greater wind speed.

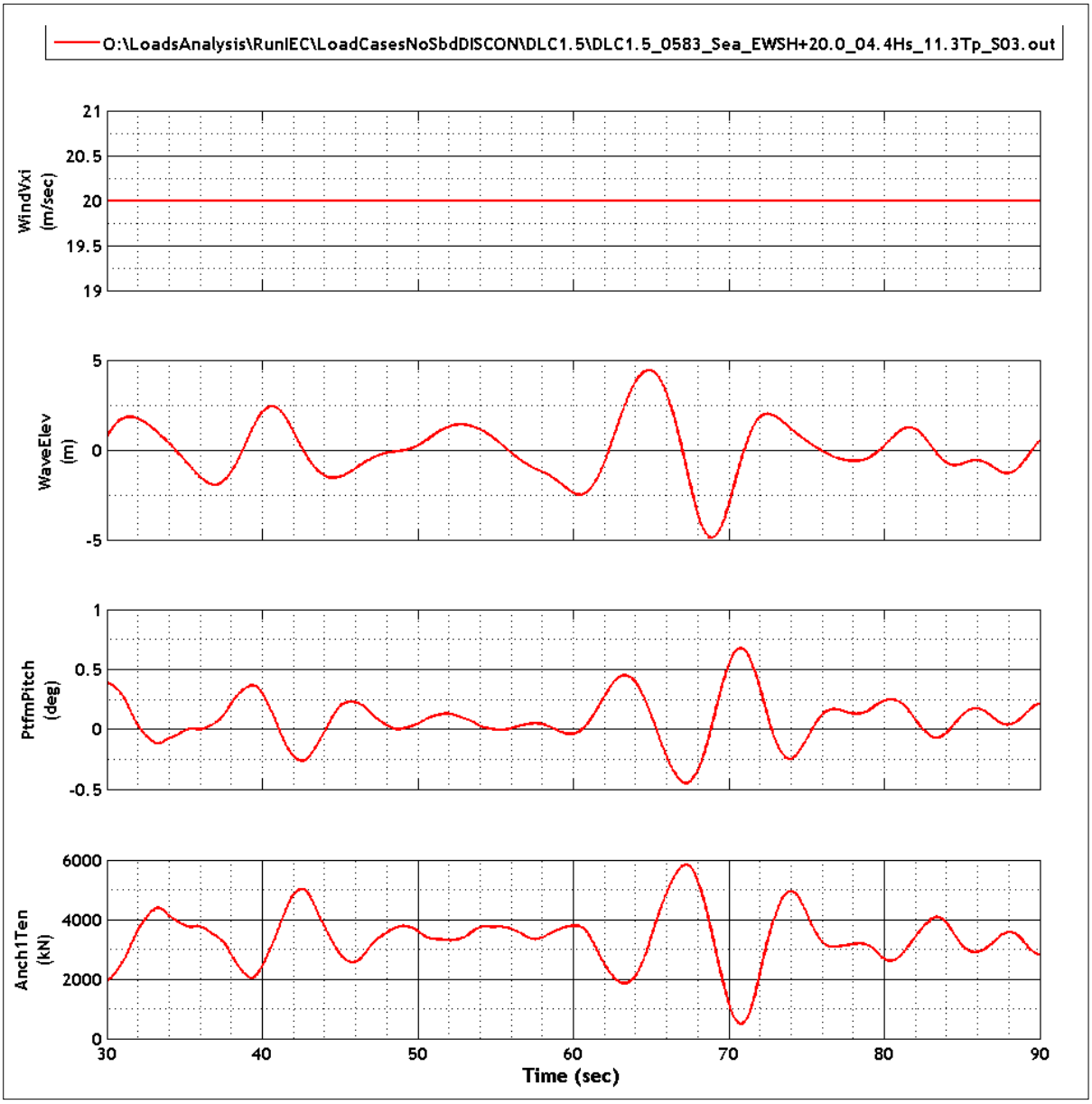

Figure 30. Time histories from TLP DLC 1.5 simulation 583

In summary, the maximum blade deflection and blade root moment are only triggered by the wind gust; the effect of the waves is negligible for the TLP. That result is coherent with the onshore turbine but can be different for other floating concepts, where the pitch motion due to incident-waves can dominate the extreme event for blade deflection. Design load case 1.4 also dominates most maxima for sway, yaw and roll displacements, forces, and moments because of the extreme gust with a direction change. Simulation 774 of DLC 1.5 has maximum platform

surge displacement which causes a minimum in heave, because the platform acts like a four-bar-linkage (parallelogram); therefore a displacement in surge is associated with a decrease in heave. The maximum tower-base bending moment occurs in DLC 1.1, where a blade pitch angle of 0° at rated wind speed results in a great thrust load on the rotor and a maximum bending moment at the tower base. Maxima in fore-aft top displacement and nacelle acceleration occur in DLC 1.3 simulations with high turbulence.

The most important criteria for avoiding failure of a TLP is that the mooring line tensions never drop to zero. When one or more lines go slack and then suddenly regain tension, the instant peak stresses on these lines, the anchors, and the fairleads are extensive and the lines are prone to snap. As explained in a previous section, the pitch motion of the TLP is most critical for the line tensions, with the leeward line tension being the most susceptible to going slack. Figure 30 shows DLC 1.5 simulation 583, in which—beginning at a time of 60 sec and lasting until 72 sec into the simulation—a considerably large wave (9 m crest to trough) hits the TLP. At 2 sec after the peak of the wave has passed the TLP, the pitch displacement reaches a local minimum of -0.48°. Following that event, the TLP pitches back in the other direction, and 2 sec after the trough of the large wave (–4.89 m, a global minimum for all normal operation DLCs) has passed the platform, it pitches to its maximum displacement of 0.68°. This large pitch motion causes the leeward line tension to drop to 646 kN, the minimum line tension value for all normal operation simulations. This result proves that the TLP design is viable in normal operation.

The complete extreme event tables for the TLP in normal operation are presented in Appendix A. The following section compares selected extreme events from the TLP to the land-based system's extreme events.

4.2.3 Ultimate Load Ratios of Tension Leg Platform

Figure 31 compares various output parameter extremes from the TLP and the land-based turbine. The bar charts present the ratios of the TLP extreme loads divided by the land-based extreme loads. A ratio of 1, for example, implies that the loads are unchanged compared to the land based system, and a ratio that is greater or less than 1 indicates that the loads have increased or decreased. These ratios provide a basis to estimate the impact on structural loads of placing a wind turbine on a floating TLP in an offshore environment. Based on this data, necessary changes to the land-based turbine design, such as strengthening of the tower base, can be estimated. With these results a detailed cost analysis is possible, but is out of the scope of this work.

Frequently throughout this work, ratio charts equivalent to the chart in Figure 31 are presented. Therefore a short description of the various parameters from the FAST User Guide [19] will be given here. For convenience some previously described parameters will be repeated:

Generator Output Parameters

- "GenPwr" represents the instantaneous electrical generator power
- "GenTq" represents the instantaneous electrical generator torque
- "GenSpeed" represents the instantaneous angular speed of the HSS and generator
- "RotSpeed" represents the instantaneous rotor azimuth angular speed

Rotor and Low Speed Shaft Output Parameters

- "RotThrust" represents the instantaneous rotor thrust force
- "LSSGagFMyz" represents the instantaneous total rotating LSS shear force (this is constant along the shaft)
- "RotTorq" represents the instantaneous rotor torque (this is constant along the shaft and is equivalent to the LSS torque)
- "LSSGagMMyz" represents the instantaneous total rotating LSS bending moment at the shaft tip

Blade Root Forces and Moments Output Parameters

- "RootFMxy1" represents the instantaneous Blade 1 total shear force at the blade root
- "RootFzc1" represents the instantaneous Blade 1 axial force at the blade root
- "RootMMxy1" represents the instantaneous Blade 1 total bending moment at the blade root
- "RootMzc1" represents the instantaneous Blade 1 pitching moment at the blade root

Blade Tip and Tower Top Deflections Output Parameters

- "OoPDefl1" represents the instantaneous Blade 1 out-of-plane tip deflection (relative to the pitch axis)
- "IPDefl1" represents the instantaneous Blade 1 in-plane tip deflection (relative to the pitch axis)
- "TTDspFA" represents the instantaneous Tower-top / yaw bearing fore-aft (translational) deflection (relative to the undeflected position)
- "TTDspSS" represents the instantaneous Tower-top / yaw bearing side-to-side (translational) deflection (relative to the undeflected position)

Tower Base Forces and Moments Output Parameters

- "TwrBsFMxy" represents the instantaneous total tower base shear force
- "TwrBsFzt" represents the instantaneous tower base axial force
- "TwrBsMMxy" represents the instantaneous total tower base bending moment
- "TwrBsMzt" represents the instantaneous tower base torsional moment

Yaw Bearing Forces and Moments Output Parameters

- "YawBrFMxy" represents the instantaneous total non-rotating (with nacelle) tower-top / yaw bearing shear force
- "YawBrFzp" represents the instantaneous tower-top / yaw bearing axial force

- "YawBrMMxy" represents the instantaneous total nonrotating tower-top / yaw bearing bending moment
- „YawBrMzp" represents the instantaneous tower-top / yaw bearing yaw moment

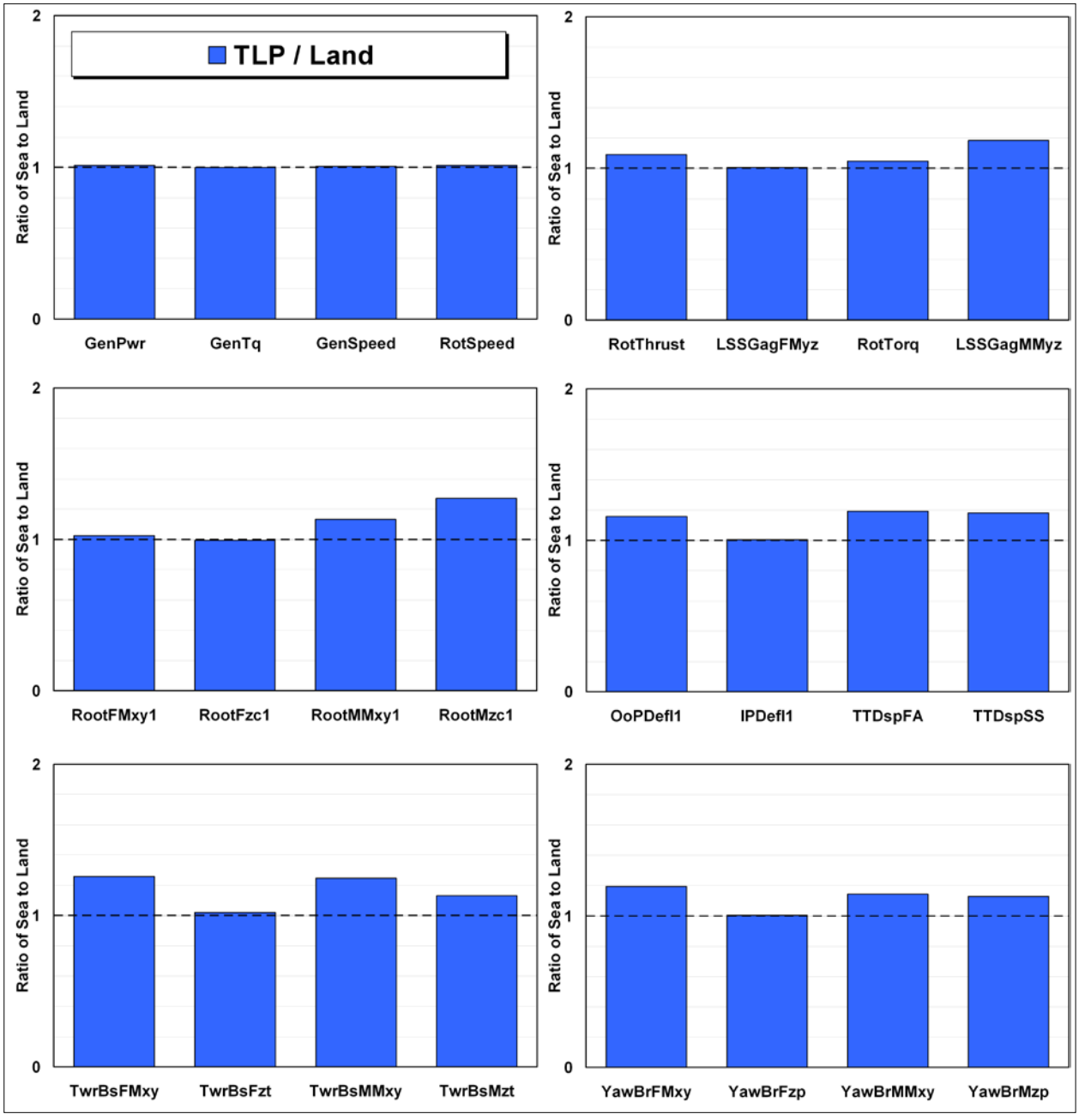

Figure 31. Ratios of TLP to land-based loads from normal operation DLCs

The chart in the upper-left corner of Figure 31 presents ratios of the generator's properties: Generator power, generator torque, generator speed, and rotor speed. The TLP ratios are close to unity because the variable-speed active pitch control system is identical to the onshore control

system. Increased surge and pitch motions generating oscillations in wind inflow nevertheless cause slight excursions in rotor and generator speed. Therefore ratios are not exactly 1, but are a negligible 1% greater. The wind inflow oscillations (and rotor inertia effects) also cause the rotor thrust and torque to be 5% to 10% greater than for the land-based machine, as illustrated in the upper-right chart of Figure 31. This also leads to increased moments in the low-speed shaft. The chart in the middle-left presents ratios of blade 1 root forces and moments. Platform pitch, roll, and yaw motions resulting in changed inflow increase the combined flap and edgewise blade-root bending moment by 13%, and the moment in twist around the blade's local z-axis is increased up to 27%. The chart in the middle-right position presents ratios for the out-of-plane and in-plane deflections of blade 1 and ratios of the tower top fore-aft and side-to-side displacements. Although the blade in-plane deflection is inreased by only a mere 0.4%, the out-of-plane blade deflection increases by 16%, primarily caused by platform pitch motions. The tower top is displaced 18% and 19% more than on the land-based system, again because of the wave-induced platform motions. The same effect is responsible for the greater than 1 ratios in the two charts at the bottom of Figure 31; tower-base forces and moments are increased by up to 25% and yaw bearing forces and moments by up to 20%. Here, greater platform heave motion caused the increased forces and moments in the turbine's loads in global z-direction.

Further assessment is required to fully evaluate and explain the implications of these calculated (maximal) 20% to 25% increased blade and tower loads. Partial safety factors for floating offshore wind turbine components, which are not yet standardized, will be significant as will fatigue-life calculations. As a first estimate, these numbers show the increases in turbine loads for this particular TLP design to be only moderate, therefore modified existing onshore turbines can be used instead of new wind turbines specifically designed for floating purposes.

4.3 Fatigue Loads

4.3.1 Fatigue Loads Analysis Overview

The design of most wind turbine components is not governed by ultimate loads but by fatigue loads. The rotation of the rotor, aerodynamic turbulence, and partial gusts cause up to 10^9 load alternations [20] in the typical 20-year lifetime of a turbine. Due to additional hydrodynamic loads, this number is presumably even greater for floating turbines. Because of the importance of fatigue loads and due to inconsistencies among different commonly used fatigue load calculation schemes, an overview of the method used in this report is given here.

The fatigue calculations performed in this analysis are according to Annex G of the IEC-61400-1 design standard [9], including modifications from the offshore IEC-61400-3 design standard to incorporate fatigue from waves. The guidelines given in the standards have been modified to be applicable to the simulation data of the present study. Design standard IEC-61400-3 originally demanded that, in addition to the normal operation DLC 1.1, an additional normal operation fatigue DLC 1.2 be simulated. The only major difference between DLC 1.1 and 1.2 is that, in addition to simulations at the expected significant wave height and associated wave peak, spectral periods at every considered wind speed in DLC 1.1, a wider range of possible wave heights and wave periods should be considered in DLC 1.2. The standard states that the selected number and resolution of the normal sea states must be sufficient to account for fatigue damage. Significant wave height, peak spectral period, and wave direction for each normal sea state at considered wind speeds should be based on the long-term joint probability distribution of metocean parameters.

In terms of the fatigue calculation, this means that the data not only must be binned regarding wind speed and load mean but also regarding significant wave height and peak spectral period. For the basic study presented in this report, this three-dimensional approach has been simplified to one dimension. For each wind speed, only the associated expected wave height and its median peak spectral period is used in the fatigue calculation.

For simulations at the exemplary wind speed 4 m/s with an expected wave height of 1.6 m, only the simulations at the median peak spectral period of 12.7 sec are used, disregarding the upper and lower periods of 8.9 sec and 16.4 sec. This data can be extracted from DLC 1.1, therefore no additional load case simulations for DLC 1.2 were performed in FAST. Both DLCs are equivalent and only the post-processing and the PSFs used are different.

4.3.2 Fatigue Loads Calculation Scheme

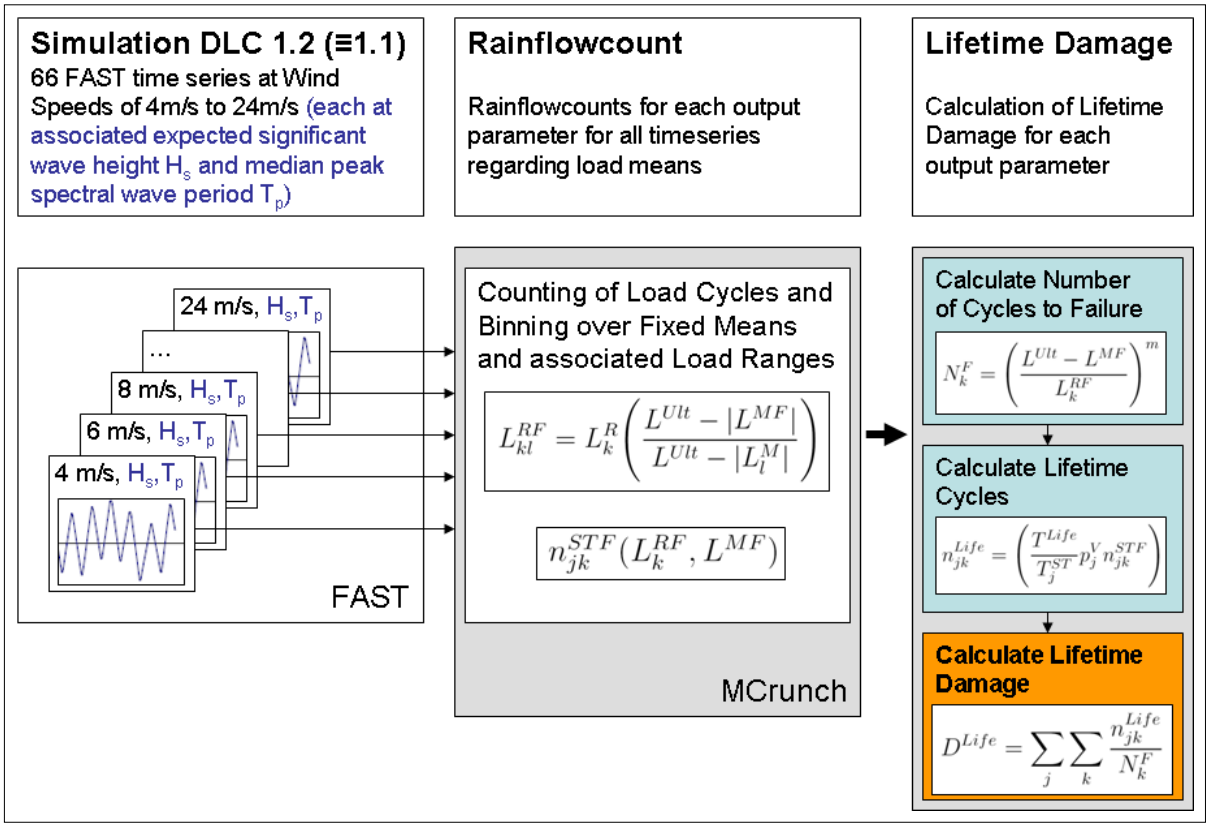

Figure 32. Fatigue calculation scheme

Figure 32 illustrates the procedure performed for this fatigue calculation. First the time series of DLC 1.1 FAST simulations at different wind speeds at the associated expected significant wave height are selected, only regarding the simulations with the median peak spectral period for each expected wave height. That means that, from the original 198 DLC 1.1 simulations, only one third (66 simulations) is utilized in the DLC 1.2 fatigue analysis. The 66 simulations represent each of the 11 wind speed bins which are equally distributed over the range of from 4 m/s to 24 m/s. Every wind speed is simulated with 6 different seeds, which results in 6 ⋅ 11 = 66

simulations. For the fatigue analysis, the load means of the cycles cannot be neglected and therefore all load ranges L_k^R are transformed to load ranges L_{kl}^{RF} at a fixed mean [26].

$$L_{kl}^{RF} = L_k^R \left(\frac{L^{Ult} - |L^{MF}|}{L^{Ult} - |L_l^M|}\right) \; with \, |L^{MF}| << L^{Ult} \tag{29}$$

L^{Ult} and $L^M{}_l$ represent the ultimate load and the l-th load mean bin. The fixed load mean L^{MF} is calculated as the mean load at each output parameter of all time series, with the means weighted according to the Rayleigh probability at the associated wind speed. With these fixed means, for all time series for each fatigue-relevant output parameter the numbers of short-term (ST) load cycles $n_{jk}^{STF}(L_k^{RF}, L^{MF})$ at each wind speed bin *j* and load range bin *k* at a fixed load mean are obtained using the rainflow counting algorithm according to the ASTM standard [2]. Then the lifetime cycles of the output parameters can be calculated as shown in Eq. 30.

$$n_{jk}^{Life} = \left(\frac{T^{Life}}{T_j^{ST}} p_j^V n_{jk}^{STF}\right) \tag{30}$$

Here, T^{Life} represents the total design lifetime (20 years in the present study), T_j^{ST} is the time of a single 10-min simulation at wind speed *j*, and p_j^V is the Rayleigh probability at wind speed *j*. The final result—the total lifetime damage (D^{Life}) of each output parameter—is computed as shown in Eq. 31.

$$D^{Life} = \sum_j \sum_k \frac{n_{jk}^{Life}}{N_k^F} \tag{31}$$

With N_k^F representing the number of cycles to failure (Eq. 32). Here the factor 0.5 is used to convert $L^{RF}{}_k$, representing a load range (peak-to-peak), to a load amplitude.

$$N_k^F = \left(\frac{L^{Ult} - |L^{MF}|}{0.5 \cdot L_k^{RF}}\right)^m \tag{32}$$

A lifetime damage $D^{Life} = 1$ means that the component likely will experience fatigue failure at a design lifetime of 20 years. Values that are less than unity indicate a component lifetime shorter than the system's planned lifetime.

Figure 33 presents the number of lifetime cycles n_{jk}^{Life} at the $j-th$ wind speed bin versus the $k-th$ load range L_{kl}^{RF} at fixed mean, exemplary for the OC3-Hywind's blade root bending moment range along the x-axis. Each of the 66 simulations is represented by one curve. Additionally, the upper red line represents the total number of lifetime cycles to failure N_k^F. The color of the lifetime cycles curves represent the wind speeds; low wind speeds are shown in blue, medium speeds in green and yellow, and high wind speeds in red. Characteristic for the presented in-plane blade root bending moment is the peak approximately 7,000 kNm, which is

the load range due to the in-plane moment caused by the blade weight of 17,740 kg, acting on the blade CM location at 20.274 m.

$$M_x = \pm 17,740kg \cdot 9.81\frac{m}{s^2} \cdot 20.274m = \pm 3,563kNm$$

At greater wind speeds and associated greater rotor speeds, this peak is less pronounced and more spread out because of the increasing influence of the centrifugal forces (and because the wind speed probability p_j^v is smaller at higher wind speeds). These types of diagrams were created for all important fatigue output parameters for all concepts, and were used to confirm the validity of the fatigue calculations.

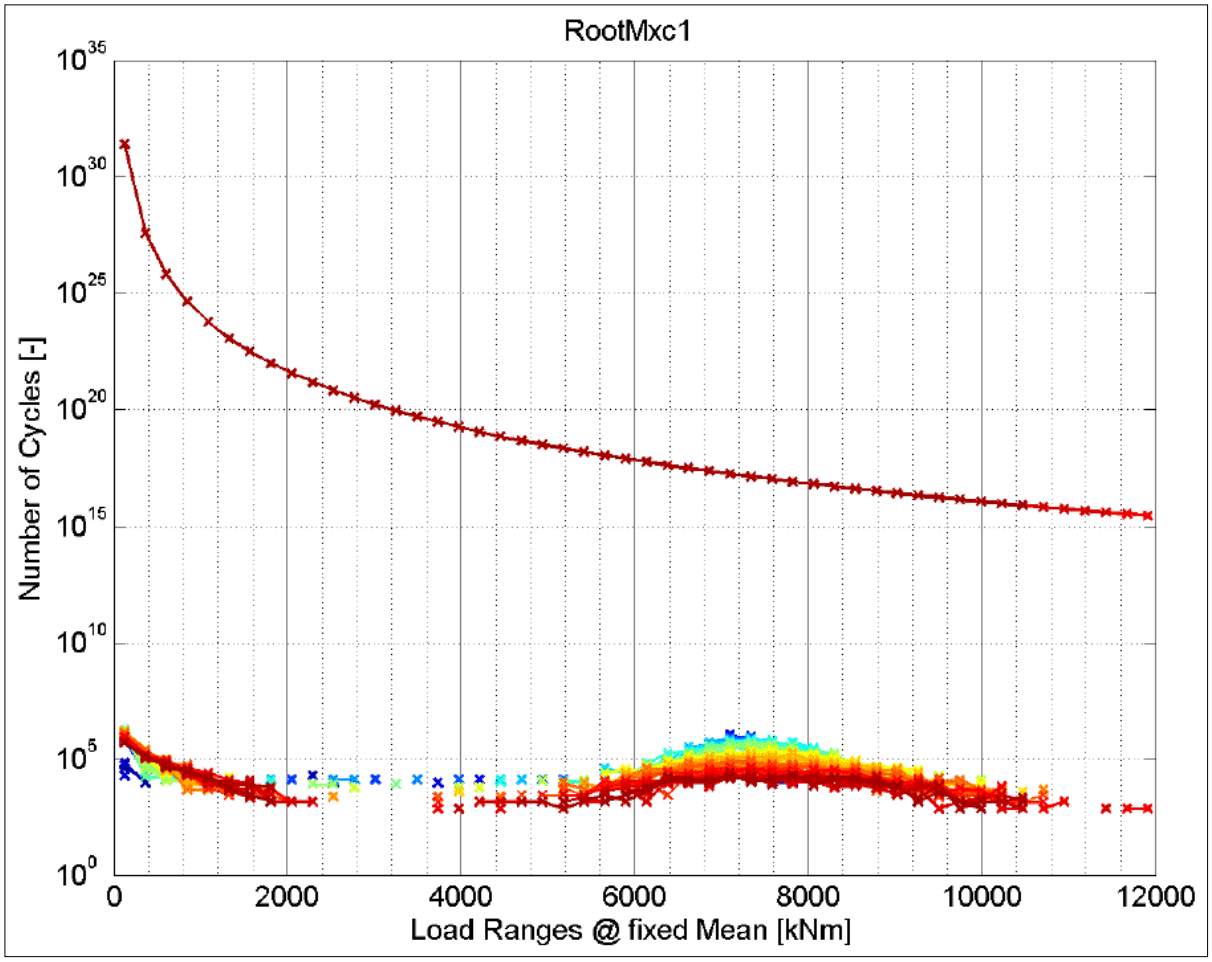

Figure 33. Lifetime cycles for each simulation and lifetime cycles to failure versus load ranges at fixed mean for the OC3-Hywind blade root bending moment load range along the x-axis

In addition to lifetime damages (D^{Life}) often damage equivalent loads (DEL) are used to characterize fatigue loads for wind turbines. A DEL essentially is the constant load applied over the lifetime of the turbine which causes the same accumulated damage as caused by the stochastic loads from the DLC simulations over the turbine's lifetime. The DEL, rendered using

the lifetime damage from Eq. 31, is as shown in Eq. 33, with the number of equivalent lifetime cycles determined as shown in Eq. 34.

$$DEL^{Life} = 2(L^{Ult} - |L^{MF}|)\left(\frac{D^{Life}}{\sum_j n_j^{Life,eq}}\right)^{\frac{1}{m}} \tag{33}$$

$$n_j^{Life,eq} = \left(\frac{T^{Life}}{T_j^{ST}} p_j^V n_j^{ST,eq}\right), \tag{34}$$

Here, $n_j^{ST,eq}$ (=600 in the presented calculation) is the number of DEL cycle counts in the $j-th$ wind speed bin over the short-term, single simulation time T_j^{ST} (=600s in the presented calculation). For design purposes, the DEL provides different information than the lifetime damage value and therefore often is preferred as a measurement for fatigue loads. The scheme presented here has been implemented into the post-processor MCrunch which was used in the subsequent analysis.

4.3.3 Ultimate Strength and S/N Curve Slopes

The selected output parameters are bending moments at the tower root, the blade root, the tower top yaw bearing, and the shaft. Following suggestions from Sutherland [30] the load range bin size for each parameter of DLC 1.2 was chosen such that at least 50 bins were within the maximum occurring load range. No data on the component ultimate strength (L^{Ult}) of the components of NREL's 5-MW baseline turbine is available; therefore, it is assumed that the component's ultimate strength can be obtained by multiplying the extreme loads of the land-based turbine (with safety factors included) occurring in the normal operation DLCs 1.1, 1.3, 1.4, and 1.5 with a so-called ultimate load factor (ULF). The other uncertain factor in the fatigue analysis is the S/N (stress/number of cycles to failure) curve slope *m,* a material-dependent factor. Commonly, values of $m = 3$ for steel and $m = 10$ for composite materials are chosen. In more-detailed fatigue analyses, however, segmented S/N curves with different slopes for different load ranges are used. These segmented curves approximate the material's real behavior more accurately. At the time the present analysis was performed this option was not supported by the post-processor MCrunch, therefore a range of S/N slopes was chosen.

A parametric study for all concepts was conducted to analyze the effect of various *m* and ULF. Figure 34 shows this comparison of various *m* and ULF values for DELs of tower base fore-aft bending moment. Here *m* was varied from $m = 3, 4, 5$ for the steel components of the tower and LSS and $m = 8, 10, 12$ for the composite blades. The ULF variation comprised ULF = 1.25, 2.5, 5, 10, 20. Note that for the ITI Energy barge the ULF of 1.25 and 2.5 resulted in failure of the fatigue calculation because the land-based system's ultimate loads with these factors were less than the actual maximum loads from the ITI barge time series. Therefore results for these two lower ULFs have been excluded. The parametric study shows that the particular ULF selected has only a minor effect for low ULFs and approaches an asymptotic DEL value for ULFs greater than 10. In contrast, the different *m* slopes have an effect which is not negligible. The same behavior could be identified in diagrams for all investigated output parameters and for lifetime damages as well. After a review of these results and discussions with fatigue analysis experts,

ULF = 20 has been chosen for all components, because the results change only slightly for different factors. By using ULF = 20, the problems with the ITI Energy barge for low ULFs also are resolved. As the S/N slope *m* has a much larger effect and no segmented S/N curve could be implemented, lifetime damage and DEL ratios for a range of *m* values is presented. Summarizing, the final factors chosen for the S/N curve slopes *m* and the ULF for the four investigated turbine parameters are presented in Table 11.

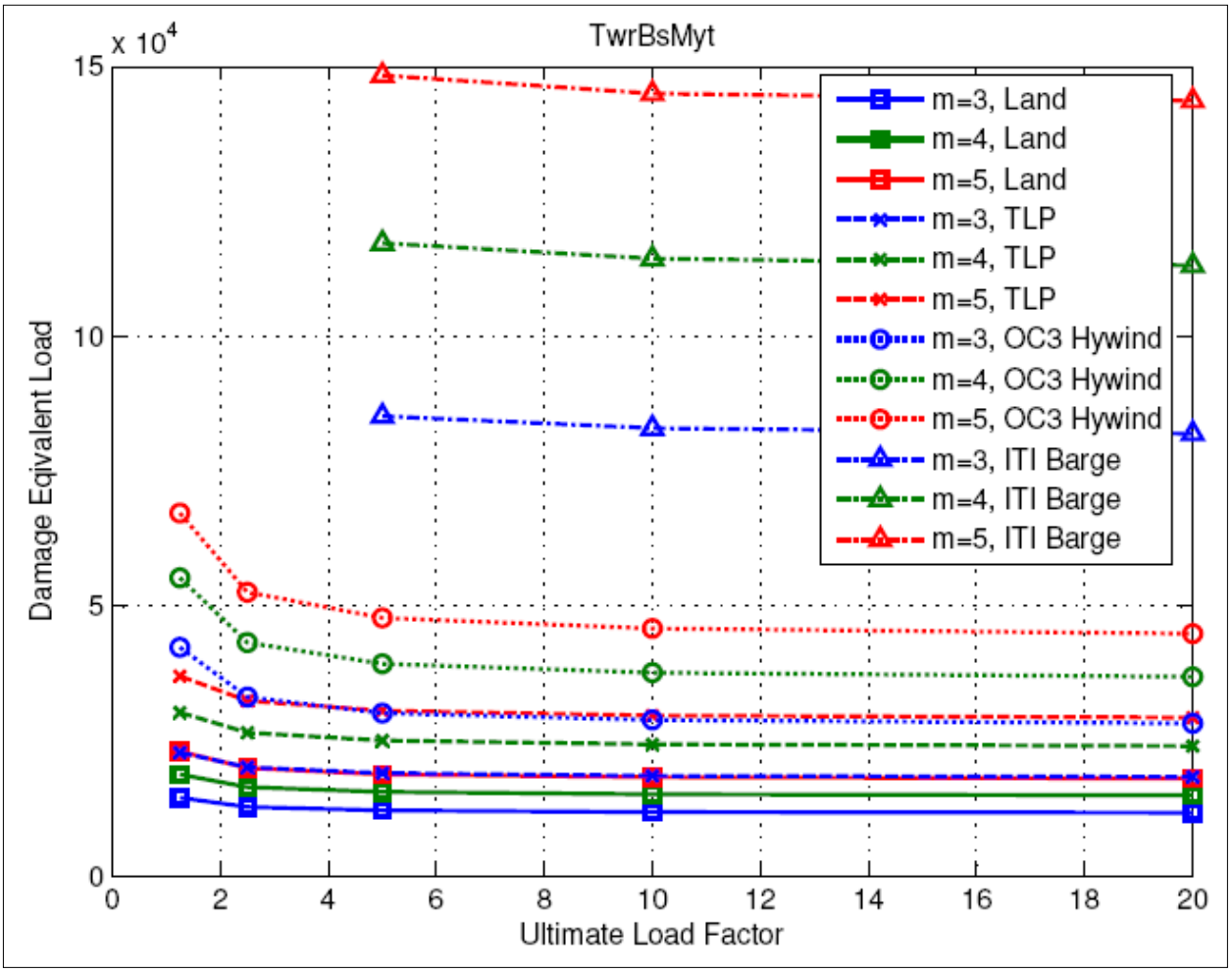

Figure 34. Comparison of various *m* and ULF values for DELs of tower base fore-aft bending moment

Table 11. Ultimate Load Factors and S/N Slopes

Component	Ultimate Load Factor (ULF)	S/N Slopes (m)
Tower base	20	3, 4, 5
Tower top yaw bearing	20	3, 4, 5
Blades	20	8, 10, 12
Low-speed shaft	20	3, 4, 5

4.3.4 Fatigue Load Ratios of Tension Leg Platform for Design Load Case 1.2

Figure 35 presents the fatigue lifetime ratios for the tension leg platform floating wind-turbine concept. The ratios represent the quotient of the lifetimes of the TLP and the land-based system's lifetimes, with a ratio of 1 representing the exact same lifetime as the land-based machine. A value of less than 1 means that the lifetime of the floating system is less than for the land-based system and vice versa. The y-axis of the charts is logarithmic to display the up to one order of magnitude lower lifetime ratios. Each diagram shows three ratios for each investigated S/N slope value *m*. Ratios and not absolute values are presented, therefore no definite increasing or decreasing of lifetimes for increasing *m* values can be identified, whereas the absolute lifetimes increase with increasing *m* for all concepts and components.

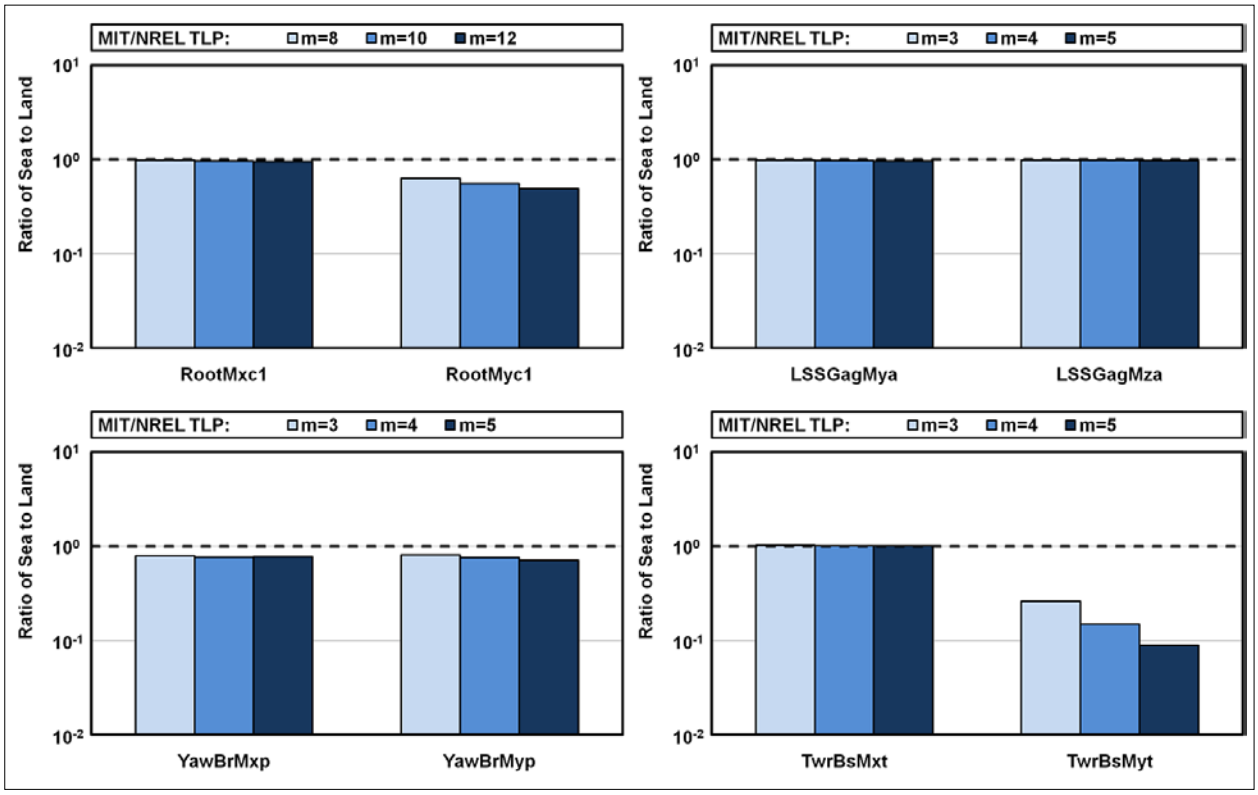

Figure 35. Ratios of fatigue lifetimes to land-based turbine from DLC 1.2

The upper-left chart shown in Figure 35 presents the lifetime ratios for the blade 1 edgewise and flap-wise root bending moments, RootMxc1 and RootMyc1. The edgewise moment ratios drop by maximal 6% and the flap-wise ratios by 52%, and the ratios decrease with increasing *m*. These decreased lifetimes are due to the slightly increased loads on the blade root compared to the land-based turbine. The flap-wise moment ratios are more decreased than the edgewise ratios because the greater pitch motion of the TLP influences particularly the flap-wise blade root moments

In the upper-right diagram shown in Figure 35, the lifetime ratios for the low-speed shaft bending moments are displayed. Only slightly decreased ratios are identified, with the TLP showing almost the same fatigue lifetimes as the land-based system, only a decrease of 4% is

calculated. This equality is due to the fact that both the TLP and the land-based turbine use the same control system.

The lower-left chart in Figure 35 presents ratios for the tower-top yaw bearing bending moments with the TLP showing moderately decreased ratios with a minimum of 0.71. Here, again, the increased pitch motion mainly is responsible for the shorter lifetimes.

In the lower-right chart in Figure 35, the ratios for the two tower base bending moments around the x-axis and y-axis are presented. Here, the greatest decreases occur for the fore-aft moment, with ratios as low as 0.09. The increased pitch motion once again is the driving mechanism because it has its greatest effect on the tower base bending moment due to the large tower-top mass and long moment arm. This difference of close to one order of magnitude between the TLP and the land-based turbine has great influence on future tower design. A significant increase in tower base strength is necessary to equal the lifetime of the land-based system. Alternatively, advanced control strategies might achieve load reductions to increase the TLP tower's lifetime.

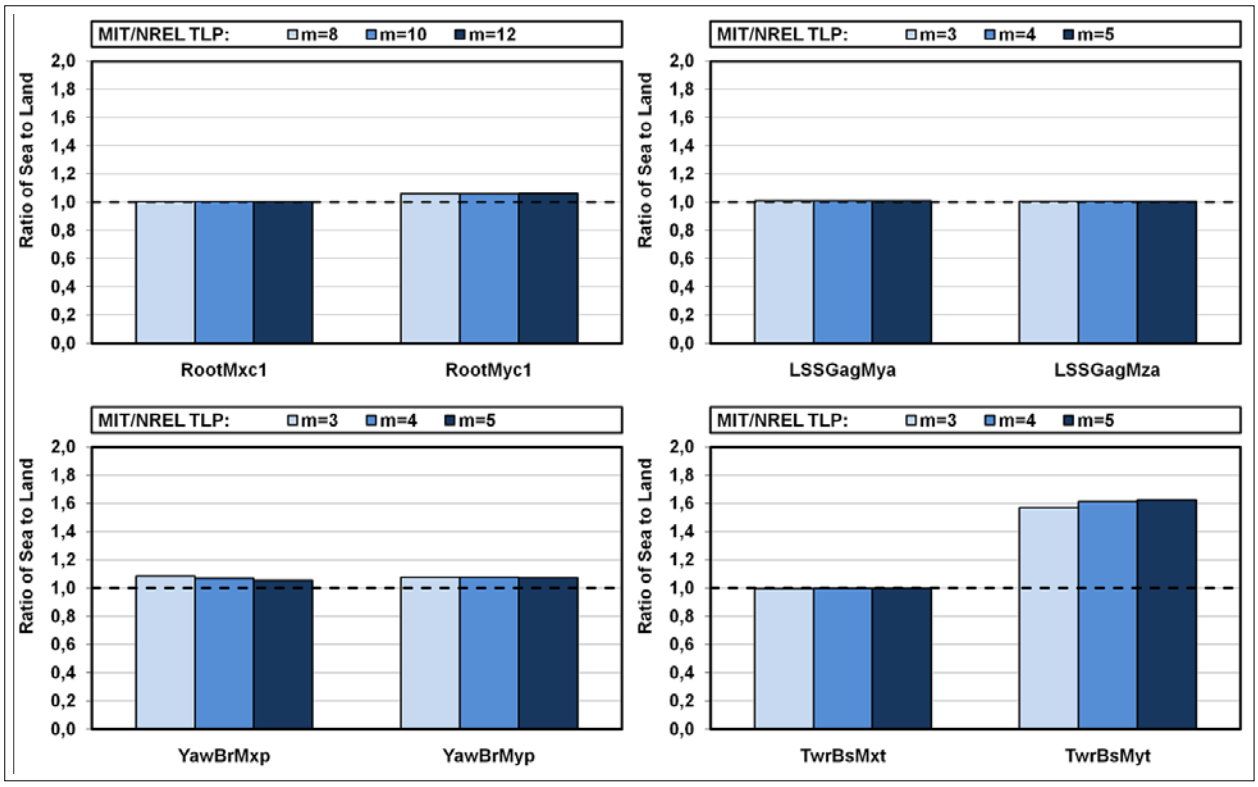

Figure 36. Ratios of tension leg platform fatigue DELs to land-based turbine from DLC 1.2

Figure 36 presents the DEL ratios for the TLP. The ratios represent the quotient of the DELs of the floating turbine and the land-based system's DELs, with a ratio of one representing the exact same DEL as the land-based machine. Ratios greater than one represent a higher DEL, which—in contrast to the lifetimes—means the floating machine's lifetime is lower than the land-based. The DEL ratios show essentially the same behavior as the lifetime ratios described previously, with the tower base fore-aft moment yielding the greatest DEL ratios—up to 60%—and therefore the shortest lifetimes.

4.4 Extreme Sea State, Fault, and Parked DLCs

The previous section analyzed normal operation DLCs 1.1, 1.3, 1.4, and 1.5, which all were operating in a normal sea state and without fault conditions. The loads analysis for the remaining DLCs in extreme sea states and with fault events is subdivided into two sections. The first section focuses on an extended loads analysis, adding the DLCs 1.6a, 2.3, and 6.1a to the normal operation DLCs analyzed in Section 2. The second section presents DLCs 2.1, 6.2a, 6.3a, and 7.1a, where instabilities occurred, simulation restrictions were violated, or the system failed. The results from these DLCs must be viewed cautiously and cannot simply be included in the regular loads analysis.

4.4.1 Loads Analysis of Tension Leg Platform, Extended Design Load Cases

In addition to the normal operation load cases. additional DLCs 1.6a, 2.3, and 6.1a are included in the extreme event tables. DLC 1.6a is a normal-operation load case with NTM wind but in a severe sea state. DLC 2.3 simulates the occurence of the loss of the grid during power production and an immediate shutdown of the turbine. Last, DLC 6.1a combines extreme wind and wave conditions with the turbine in a parked position and a yaw misalignment of up to ±8°. The extreme sea states in DLC 1.6a and 6.1a cause significantly greater extreme loads on the system, but DLC 2.3 does not contribute to any considerable extreme events.

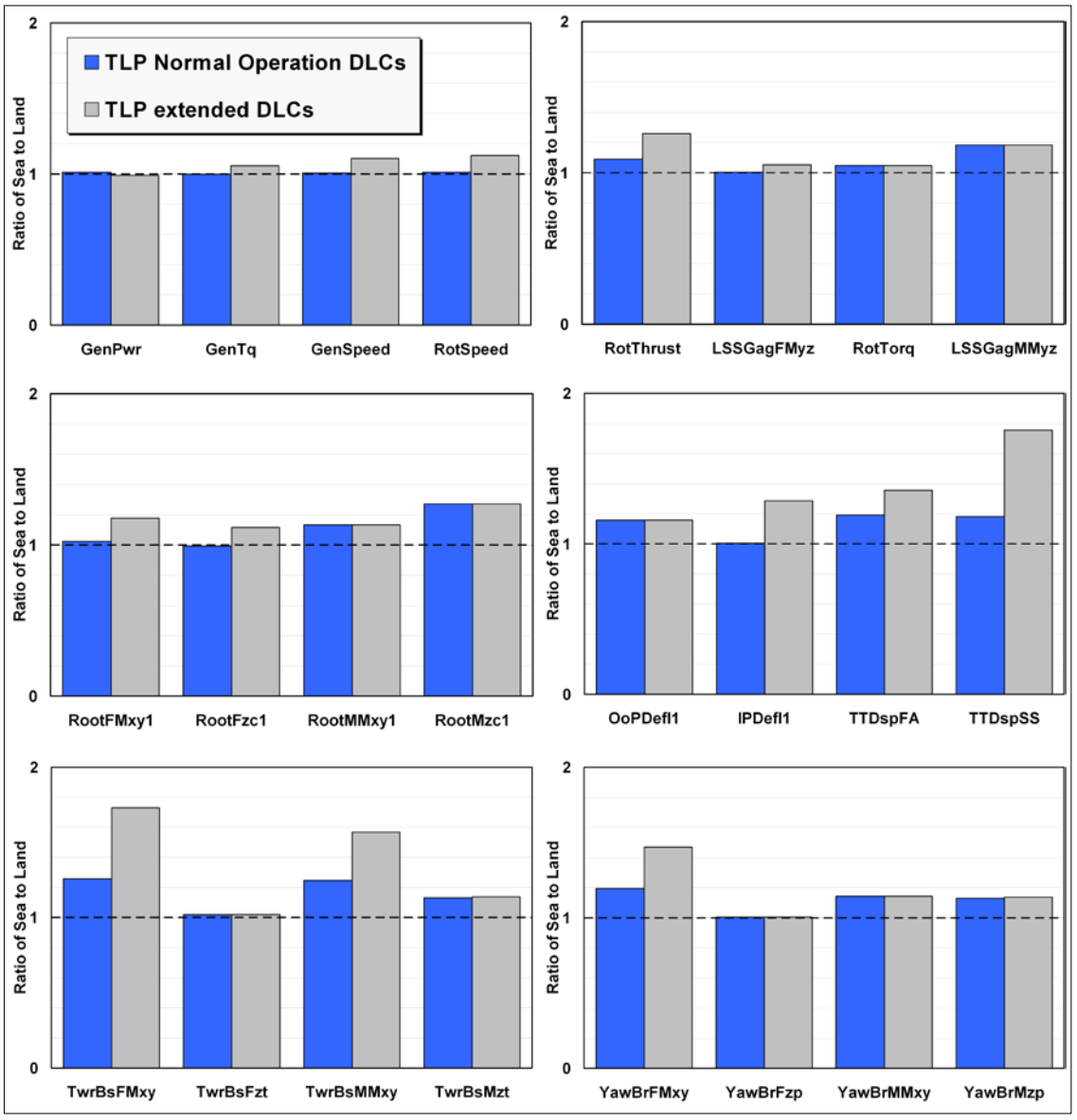

Figure 37. Tension leg platform to land ratios from extended DLCs

Figure 37 presents the ratios of the extreme loads on the TLP divided by the extreme loads on the land-based system for the same group of parameters previously discussed in Figure 31. Both the extreme load ratios for the TLP in normal operation and for the TLP in the described extended DLCs are depicted. Here, the extreme loads for the TLP in extended DLCs are divided by the appropriate extreme loads of the land-based system, including DLCs 1.6a, 2.3, and 6.1a. Compared to the TLP in normal operation, the addition of the 3 DLCs results in higher ratios for most output parameters. The upper two charts show that the excursions in rotor speed and therefore in generator torque have increased because of more extreme motions of the platform, especially in pitch, yaw, and roll. Generator power drops below 1 because the land-based system achieves a greater maximum power output due to lesser tower-top motions. In the middle charts, the overall blade 1 root bending and twisting moments remain the same as well as the out-of-plane blade 1 displacement. In-plane, the blade displacement is increased by 29% and the tower

fore-aft and side-to-side displacements also are increased by 17% and 57%, respectively. These considerably increased tower-top displacement are caused solely by the platform's increased pitch and roll motions. The bottom two charts show that the tower base bending moment is 32% greater and the tower base twisting moment and the yaw bearing moments remain unchanged.

Basically, all charts illustrate that under extreme environmental conditions—especially high-incident waves—the TLP increasingly behaves differently than the land-based turbine. Its roll, pitch, and yaw displacements and the associated accelerations increase much more than for the land-based turbine—which only is affected by extreme winds and not waves. Therefore the ratios for the TLP do not remain constant but increase unproportionally when adding the extreme DLCs. Regarding ultimate loads which mainly occur in extreme DLCs, the TLP experiences more than 50% increased ultimate loads on some components as compared to the land-based system.

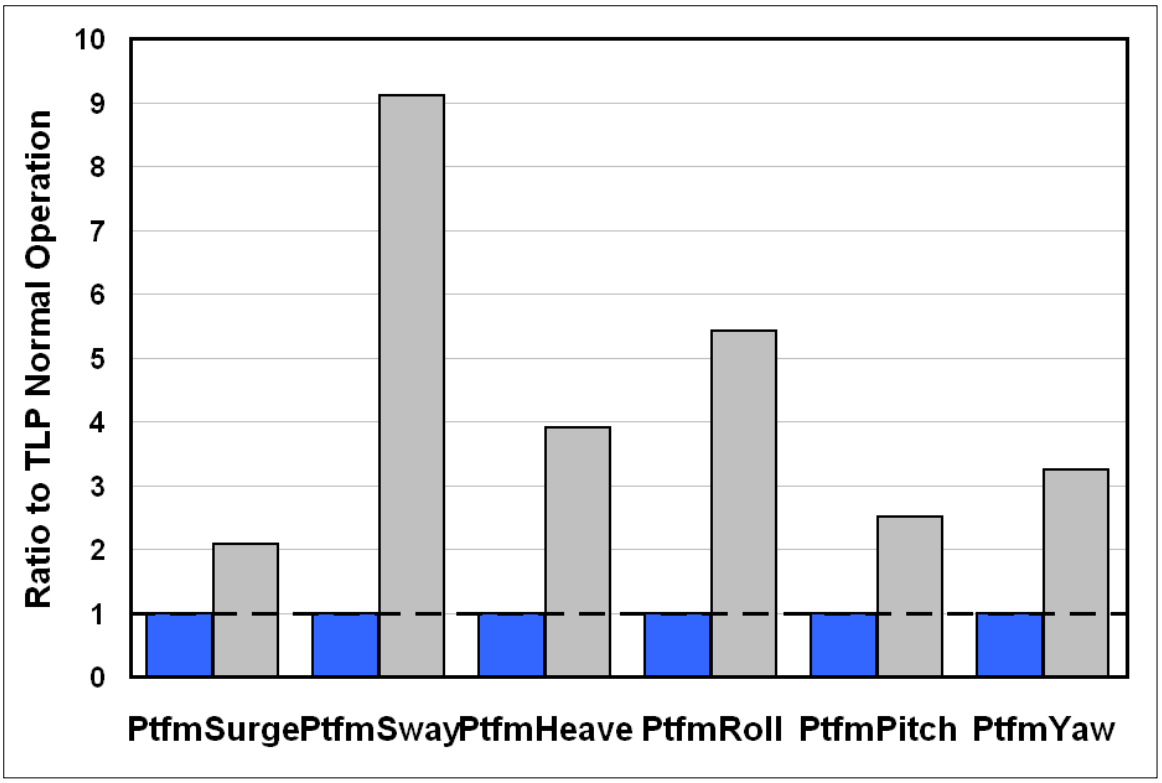

Figure 38. Platform displacement ratios

The ratios of platform displacements of the TLP in extended DLCs in Figure 38 provide further information on the platform motions. The diagram is obtained by dividing the extreme platform displacements of the TLP in normal and extended DLCs by the displacements of the TLP in normal operation. It illustrates and quantifies the impact of severe wind and wave conditions on the 6 platform DOFs. Most prominently, the sway displacement is more than 9 times greater due to the yaw misalignment in DLC 6.1a. Here, the aerodynamic forces and the misaligned rotor in the direction of sway are greatly increased.

Roll motion increased more than five times, which affirms that the increased tower side-to-side motion discussed above is caused by large roll displacements. Pitch and yaw also are significantly increased—by the factors 2.5 and 3.2—and surge is more than two times greater than in normal operation DLCs. Associated with this greater surge displacement is heave, which also increased almost four times. These ratios quantify the great impact of high waves and extreme winds on platform motions.

Maximum and minimum surge, heave, and pitch displacements occur in DLC 1.6a. The turbine in this load case still is in power production (i.e., a high thrust force is acting on the rotor and pushing the turbine downwind). Because of the stiffness of the mooring lines, a displacement in surge is accompanied by a decrease in heave (i.e. an increase of the absolute value in heave). High rotor thrust also adds to the pitch motion. Each of these motions is further increased by the severe sea state with 50-year waves of H_s = 15 m. Figure 39 shows a section of the time history of DLC 1.6a simulation 0017, when the extreme event in pitch occurs. Conditions in this DLC are a hub-height turbulent wind speed of 8 m/s and 50-year waves with a significant wave height of H_s = 15 m at a peak spectral period of T_p = 19.2 sec.

From 2,550 sec to 2,555 sec, a very large wave is hitting the TLP. The wave has a total height from crest to trough of more than 25 m and a period of 10 sec. With the beginning of the wave the platform pitches slightly negative before pitching back in positive direction and one second after the lowest point of the wave has passed the platform, the pitch reaches its maximum of 1.69°. The platform's heave motion first follows the wave trough but its high excess buoyancy lifts it back in positive heave direction before the lowest point of the wave is passing. The mooring lines go slack at this point, as the plot of the leeward anchor tension illustrates. Here a failure of the TLP (i.e. ripping of the leeward mooring lines) is likely. After the extreme wave has passed, the line tension increases again, followed by a slowly decaying oscillation in heave, as well as in pitch. During the extreme event and the excessive pitch motion, the rotor thrust first increases, but then drops below zero for a short time. This fluctuation in rotor thrust further increases the platform motions, thereby causing more extreme pitch displacements than those in DLC 6.1a, which has equally severe wave conditions. The time series demonstrates that the fluctuation in wind speed has a minor effect and that the extreme event in pitch and heave is dominated by the large incident wave. This conclusion can be transferred to most extreme events occurring in DLCs 1.6a and 6.1a, for which the waves always are the driving factor for the particular output parameter's extreme event.

The other minimum and maximum platform displacements in sway, roll, and yaw are recorded in DLC 6.1a and, as described above, are due to the yaw misalignment combined with the extreme sea state. Platform yaw stability is discussed further in the following section.

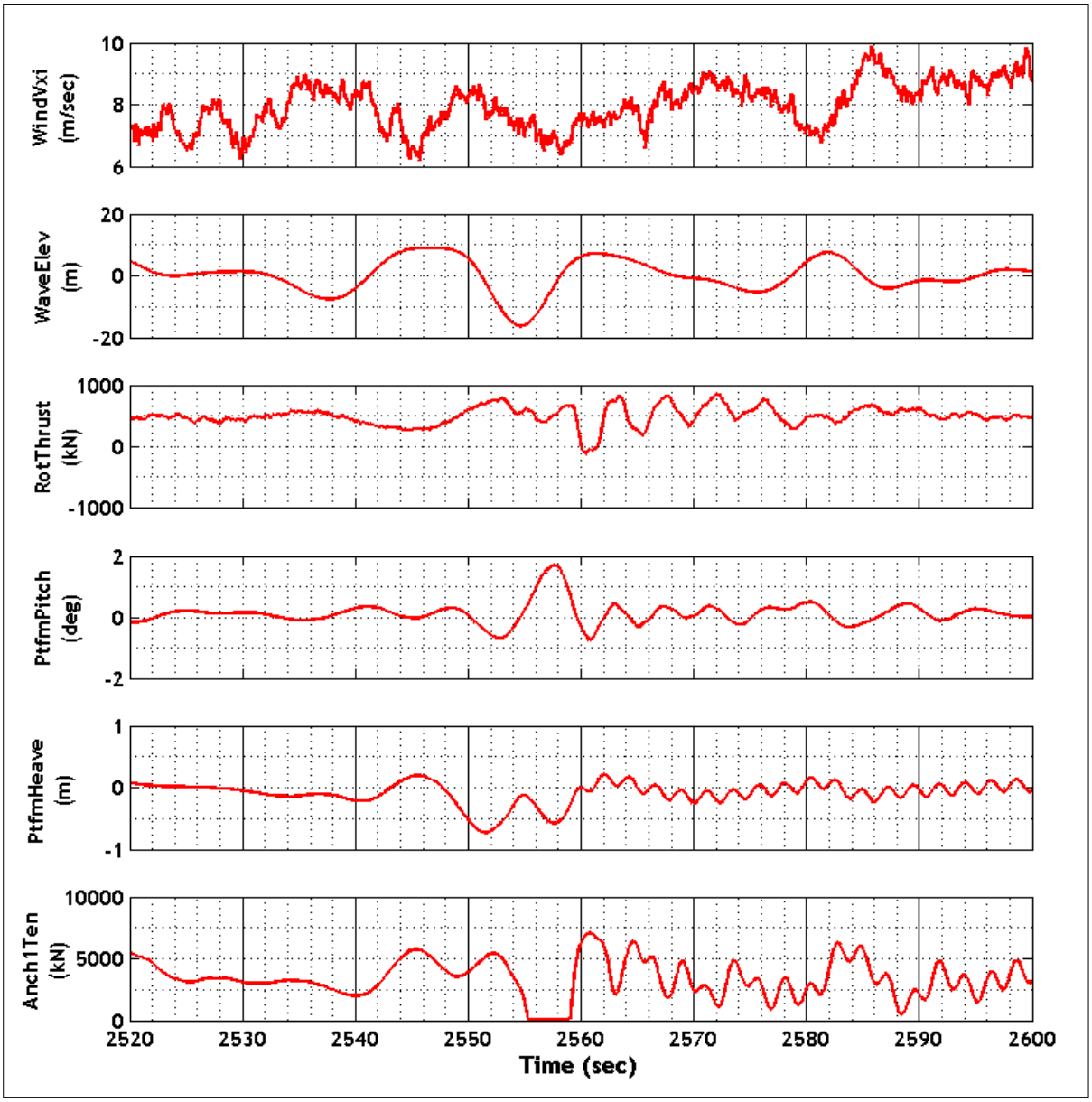

Figure 39. Time histories from DLC 1.6a simulation 0017

4.4.2 Platform Yaw Instability in Design Load Cases 2.1 and 7.1a

When analyzing DLC 2.1 a platform yaw instability was discovered—the same instability that Jonkman [18] discovered for the barge. The instability occurs when the rotor is idling and one blade is seized flat into the wind at a pitch angle of $\theta = 0°$ and the other two blades are fully feathered at $\theta = 90°$. This fault event with one seized blade also occurs in DLC 7.1a and results in the same yaw instability as discovered in DLC 2.1. In DLC 7.1a, the TLP is operating in an extreme sea state with extreme winds compared to normal wave and winds in DLC 2.1, therefore the yaw instability is more severe in DLC 7.1a. In DLC 7.1a, extreme platform yaw displacements are reached—resulting in extreme loads on the platform and possible knotting of the mooring lines. For those extreme rotational displacements the limits of the validity of FAST's theory are significantly exceeded, therefore no quantitative values are presented here.

The yaw instability, which is oscillating at the platform yaw natural frequency of 0.0972 Hz, is caused by a coupling of the platform yaw with the azimuthal motion of the seized blade. Compared with the barge the instability is more severe for the TLP. This confirms Jonkman's prediction that the instability would be more pronounced for a TLP design because it is more compliant to platform yaw motions and because smaller moment arms are available. Jonkman suggested several methods to prevent this yaw instability, including installment of damping plates, so-called crowfoots, applying the high-speed shaft brake or reducing the pitch angle of the feathered blades to generate a low persistent torque producing a slow rotor rotation.

In a simplified simulation, with no waves, a constant wind speed of 25 m/s, and no yaw misalignment, the effect of applying the shaft brake is demonstrated. Figure 40 presents the time histories for platform yaw from these two simulations, one without applying the brake and the other with high-speed shaft brake deployment at a simulation time of 200 sec. Up to 200 sec, both simulations show the same increased yaw oscillations. As soon as the brake is applied and the coupling between the azimuthal motions of the seized blade with the platform yaw motion is prevented, the yaw oscillation ceases to increase and shows a slight decrease. Compared to the barge, this decrease is much smaller due to the increased compliance of the TLP in yaw. HydroDyn does not account for drag from vortex shedding, flow separation, skin friction, and drag from the spokes, therefore the yaw instability most likely will be less severe in reality because all of these effects can add to more damping in platform yaw. Note that there is the possibility that the vortices generated at the spokes might lead to regions of lower pressure which also could—contrary to the statement above—lead to less damping. Further research on the damping of the platforms therefore is needed, especially regarding the influence of the spokes.

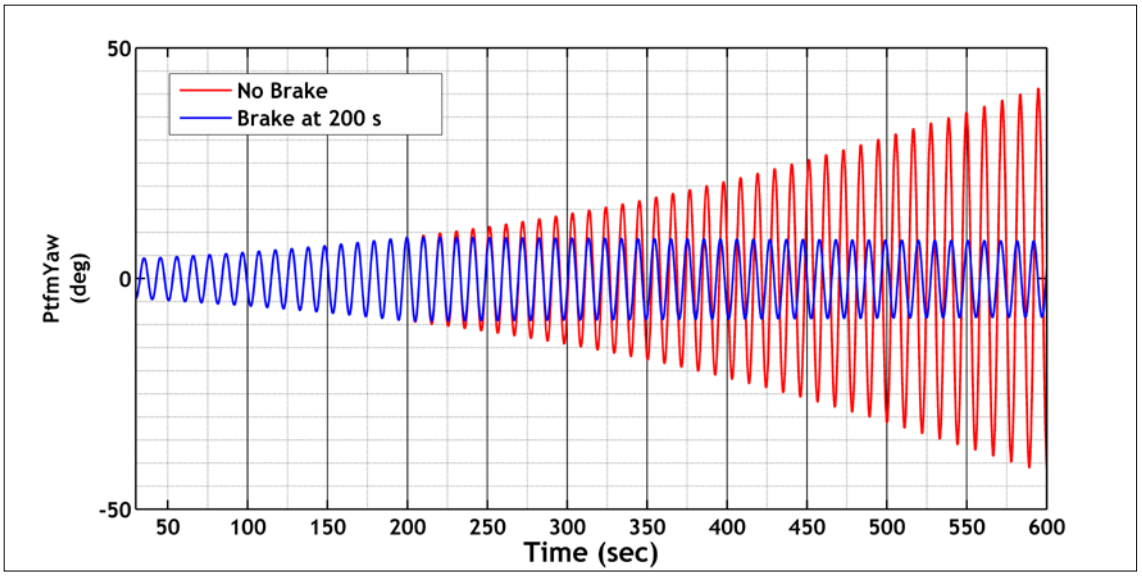

Figure 40. Time history for yaw instability with one seized blade

4.4.3 Combined Tower, Blade, and Platform Instability in Design Load Case 6.2

When trying to identify the existence of the tower side-to-side instability in the TLP model in DLC 6.2a, which Jonkman [18] discovered for the land-based turbine, an instability was identified, caused by the same effects, but affecting additional modes. In design load case 6.2a, the rotor idles and all blades are fully feathered at a pitch angle of 90° and nacelle yaw

misalignments range from –180° < Yaw < +180°. The turbine in this DLC floats in an extreme sea and 50-year wind speed conditions are present (*c.f.* Table 7).

Jonkman [18] describes a tower side-to-side instability in this DLC for the land-based NREL 5-MW baseline turbine. This instability occurs when the turbine is idling with all blades fully feathered, but only at certain rotor azimuth angles and at a misalignment of the nacelle with the mean wind direction of 20° to 40°. Jonkman's analysis shows that this instability does not occur with the barge model in still water, because the barge compliance and wave radiation damping helps prevent the side-to-side tower instability. The TLP uses taut lines and has less compliance than the barge, therefore an instability similar to the tower side-to-side instability of the land-based system is expected.

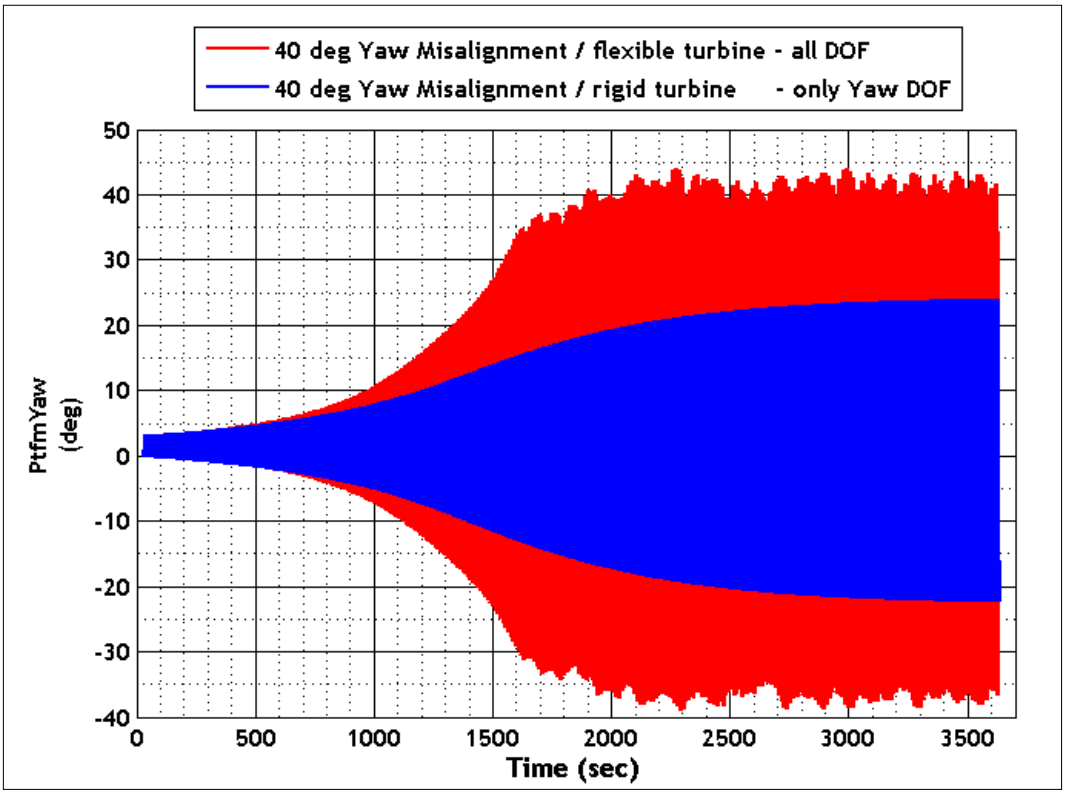

Figure 41. Yaw instability

It is difficult to analyze the yaw instability in a severe sea state, therefore a simpler test case was created in which the instability could be investigated isolated without the disturbing influences from random waves. The turbine floats in still water with a constant wind speed of 50 m/s, and the nacelle has a yaw misalignment between –180° < Yaw < 180°. Figure 41 presents the platform yaw angle of two simulations under these conditions, one with a fully flexible model, in which all DOFs are activated, and the other with only the platform's yaw DOF active. The platform yaw is oscillating exactly at the platform's natural frequency in yaw of 0.097 Hz with the oscillation increasing with simulation time. Clearly, the yaw instability is less severe in the 1-DOF case but still is present and is violating FASTs small-angle approximation, which is valid up to about 22°.

The instability occurs in still water, at constant wind, and only at certain yaw misalignments, it therefore is triggered by aero-structural effects. To further investigate the instability, the platform DOF's damping ratios are computed for the full range of possible yaw misalignments ranging from –180° to +180°. Figure 42 shows the TLP platform's damping ratios for these yaw misalignments. Negative damping in yaw occurs at yaw misalignments between 27° < Yaw < 46° and –68° < Yaw < –29°, and 135° < Yaw < +145°.

Thus far, only the instability in platform yaw has been discussed because it is most severe. The negative damping-ratio plots for other DOFs also show negative values. In roll, negative damping ratios are found at yaw misalignments between –59° < Yaw < –47°, 22° < Yaw < 38°, and between 166° < Yaw < 169°. Simulations not presented here showed, that in addition to a 1-DOF platform pitch model (cf. Figure 41), a single 1-DOF model in roll also leads to negative damping. Damping ratio charts for all 21 DOFs of the FAST TLP model are presented in Appendix B.1. These charts show additional negative damping ratios in flap-wise and edgewise blade modes and in tower side-to-side and fore-aft modes.

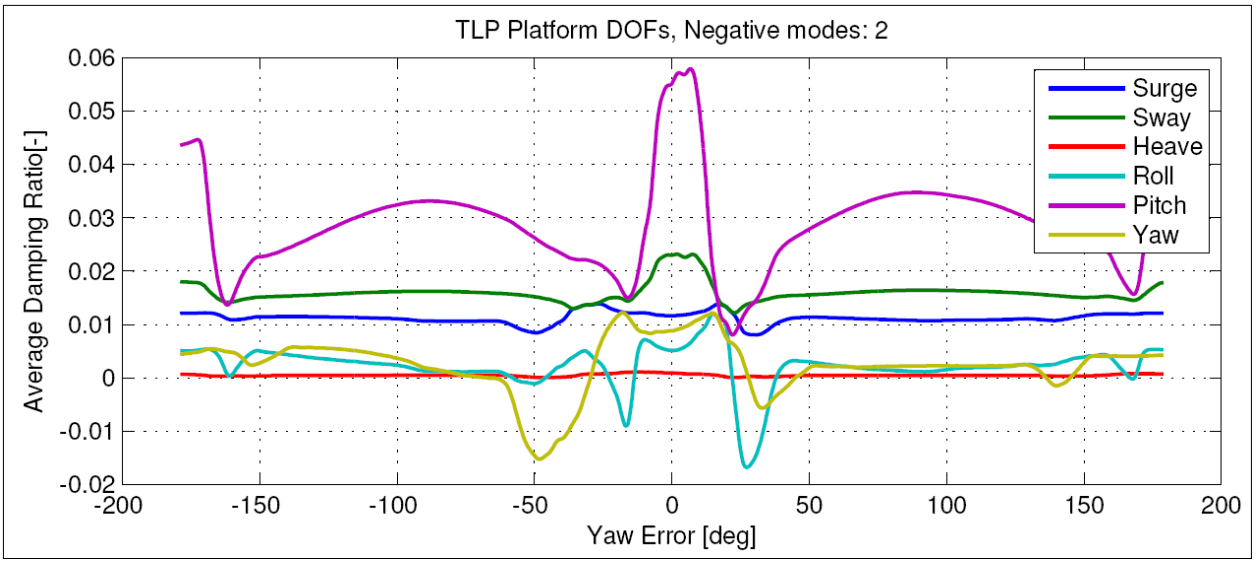

Figure 42. Damping ratios for tension leg platform degrees of freedom at different yaw misalignments

To further investigate the cause of the instability the aerodynamics at each blade for 1-DOF models are examined. Appendix B.3 contains a section of the time series of the angle of attack α and the lift coefficient c_l at two positions on blade 1 for a yaw misalignment of 40° in a 1-DOF platform yaw model. These diagrams have been created for all three blades at different yaw misalignments for all 1-DOF models where negative damping ratios were found. So far, the author has reached no conclusion on the cause of the aerodynamic instability but it will be further investigated and published as soon as the cause is identified.

4.4.4 Surge Instability

In addition to the severe instabilities described in previous sections, a less-severe instability in surge relating to the active pitch-control system has been identified. The TLP in still water with a constant wind that is less than cut-out tends to limit cycle-surge oscillations. For a case at rated

wind speed V_{Hub} = 11.5 m/s and active pitch control (shown in Figure 43), the TLP oscillates in surge from –1 m < Surge < 8 m. This oscillation of 9 m occurs at the platform's natural surge frequency of 0.0165 Hz, which is out of the main wave-energy spectrum. The time series show that the surge oscillation excites the other 5 platform degrees of freedom by couplings with the mooring system to oscillations at the surge natural frequency, illustrated for pitch and heave in Figure 43.

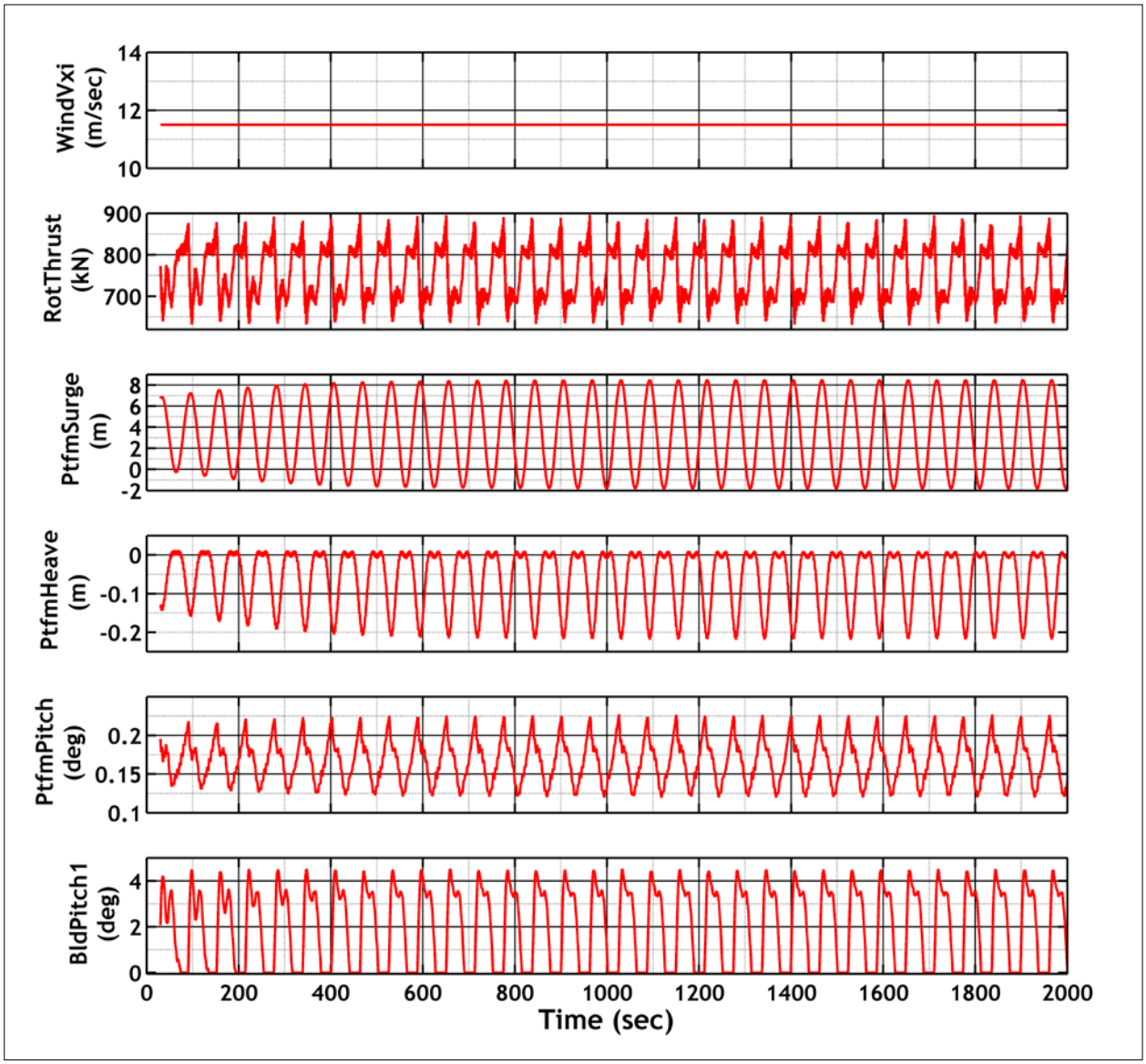

Figure 43. Time histories of platform displacements during surge instability

Causing the surge oscillation is the variation in rotor thrust which, in turn, is caused by the varying blade pitch. The wind speed is slightly greater than rated in this particular case, so the surge and pitch motions cause the controller to command pitch angles to maintain constant power. Simply stated, this blade pitch sustains the surge oscillation because it decreases thrust when the surge is maximal and increases thrust when the platform reaches its minimum surge

displacement, thereby further increasing surge in each period until the limit-cycle amplitude is reached. To verify that assumption, a more-detailed investigation considering a 1-DOF rigid body platform surge equation of motion was conducted (Eq. 35).

$$\underbrace{(I_{Mass} + A_{Radiation})}_{M_x}\ddot{x} + \underbrace{(B_{Radiation} + B_{Viscous} + \frac{\partial T}{\partial V})}_{C_x}\dot{x} + \underbrace{(C_{Lines})}_{K_x}x = T_0 \tag{35}$$

With a damping ratio of:

$$\xi_x = \frac{C_x}{2\sqrt{K_x M_x}}. \tag{36}$$

Here, x denotes the translational platform displacement in surge, $\dot{x}$ the velocity, and $\ddot{x}$ the translational acceleration. The surge mass of the turbine and the platform is I_{Mass}; $A_{Radiation}$ and $B_{Radiation}$ are the added mass and the damping associated with hydrodynamic radiation at the surge natural frequency, $B_{Viscous}$ represents the linearized damping due to hydrodynamic viscous drag, and C_{Lines} is the linearized restoring from the mooring system. The rotor thrust at a reference linearization point is $T_{0,}$ and the thrust sensitivity to wind speed is ∂T/∂V. All values can be obtained from a FAST linearization and WAMIT results, except for ∂T/∂V. For the thrust sensitivity to wind speed, two methods described by Jonkman [18] can be used. One refers to a ideal closed-loop blade pitch control system in which the slope ∂T/∂V of the steady-state thrust versus the wind-speed response is computed with a simple central difference approximation using steady-state FAST simulation results: $(T_{n+1}-T_{n-1})/(V_{n+1}-V_{n-1})$.

The other method is performed by perturbating the wind speed at each operating point (wind speed, rotor speed, pitch angle) and calculating the sensitivity in thrust by using FAST's linearization with a 1-DOF surge model. This method refers to an open-loop system, because the blade pitch angle is not varied with the imposed wind-speed perturbations. The results provided in Figure 44 show that the damping ratio for the ideal closed-loop system drops to less than zero at approximately 11.2 m/s, reaches its minimum of –2% at about 12. m/s, and increases until the ratio becomes positive again, at approximately 17 m/s.

For the open-loop system, the ratio stays well above zero (1% to 3.5%) over the full range of frequencies. The real system's control system responds to rotor-speed error and not to variations in wind speed (as is the case in the ideal closed-loop approach), therefore the damping ratio falls somewhere between the bounds imposed by the open-loop and ideal closed-loop results. The active blade pitch affecting the rotor thrust eventually yields negative surge damping ratios for short periods, and this leads to the oscillation in platform surge.

Jonkman [18] discovered a similar instability in the barge pitch motion, which also was caused by negative damping ratios in pitch. Due to the significantly greater stiffness of the TLP in pitch, for this design the control system–induced instability mainly affects surge, which leads to the described oscillations in the platform DOF at the surge natural frequency. In fact, the instability will happen on any DOF affecting fore-aft motion that has a natural frequency less than the blade-pitch-control natural frequency [21].

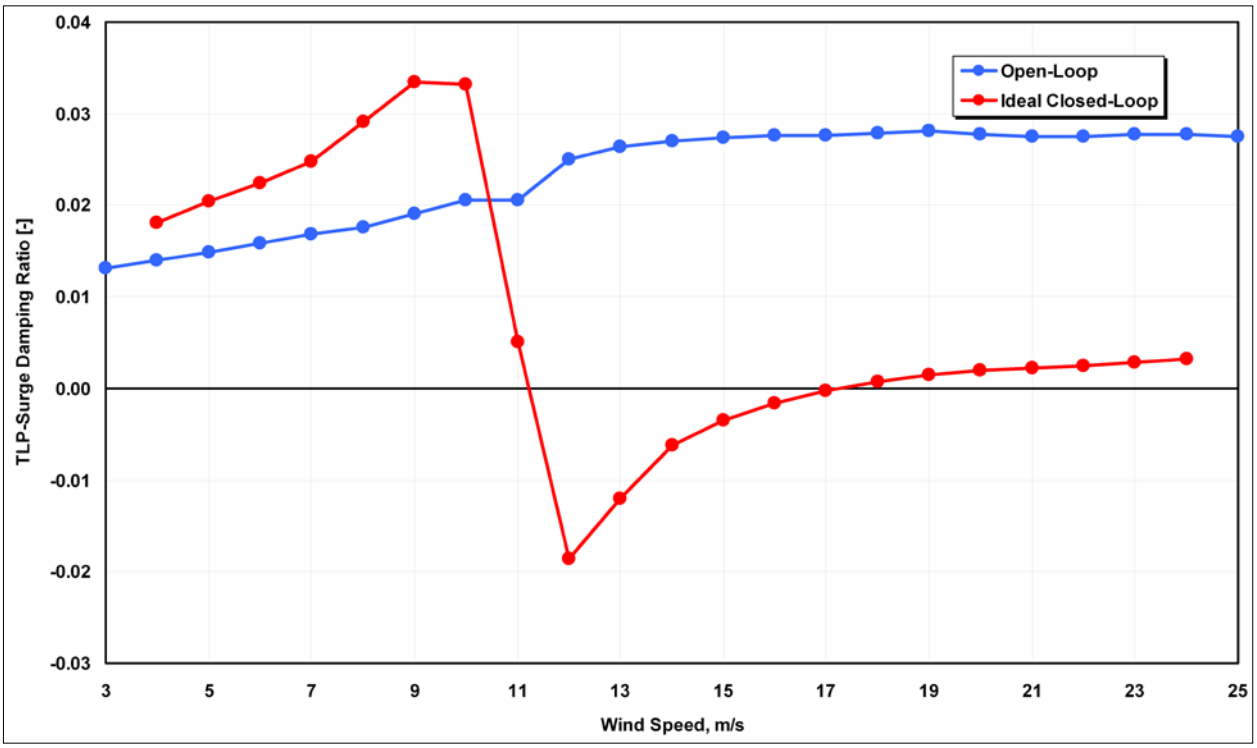

Figure 44. Tension leg platform surge damping ratios

Several methods for improving the pitch damping for the barge system by modifying the control system have been suggested and described in detail by Jonkman [18]. These concepts also are applicable to improving the TLP's surge damping. In brief, the possible modifications include: adding a second blade-pitch control loop through platform translational acceleration feedback; and changing from variable-blade pitch-to-feather speed control to variable-blade pitch-to-stall speed control regulation. Detuning the gains in the variable blade-pitch-to-feather rotor-speed controller also could improve the damping, but this is rather difficult to implement due to the TLP's already very low surge natural frequency. Despite these possible improvements, these methods have not been applied or further investigated in the present study because the slow surge instability is not considered critical for the loads on the TLP.

5 Comparison of TLP, Barge, Spar Buoy, and Land-Based Systems

This section focuses on the comparison of TLP, ITI Energy barge, OC3-Hywind, and land-based systems. It first provides a short description of the ITI Energy barge and the OC3-Hywind spar buoy designs. Following the analysis procedure used for the TLP is a discussion of the ratios between each concept and the land-based system, for both extreme and fatigue loads. The last section summarizes the results and identifies and discusses positive and negative features of each concept.

5.1 ITI Energy Barge

This section compares loads for various output parameters from the ITI Energy barge, the tension leg platform, the OC3-Hywind, and the land-based turbine, therefore a brief summary of

the ITI Energy barge design is provided here. This design is stabilized simply by the buoyancy effect of its large water-plane area and the resulting great restoring moments when the platform is displaced in heave, pitch, and roll. The shallow draft and square shape of the support platform enable easy, inexpensive onshore assembly of the system.

The barge is ballasted with seawater to achieve a reasonable draft to avoid excessive wave slamming. In the center of the barge, an oscillating water column wave-power device is installed to produce additional electric power. It is not possible to model that complex device in FAST, therefore a square moon pool located at the center of the platform covered by a fixed plate just below the free surface is modeled. As Figure 45 illustrates, the barge has a catenary mooring system consisting of 8 lines total, 2 at each corner of the rectangular platform. The basic properties of the barge are provided in the Table 12. To avoid control-system induced negative damping, the controller's natural response frequency for the ITI Energy barge system is reduced. The next section—on the OC3-Hywind concept—discusses this issue in more detail. The major instability identified by Jonkman is a platform yaw instability in DLCs 2.1 and 7.1, which is the same instability described for the TLP in Section 4.2. Jonkman describes the susceptibility of the barge to excessive platform motions in extreme waves, mainly pronounced in the platform's pitch DOF. Further information and additional references on the ITI Energy barge design are provided by Jonkman [18].

Table 12. Properties of ITI Energy Barge System

Static Properties	Value
Size (W x L x H)	40 m x 40 m x 10 m
Moon pool (W x L x H)	10 m x 10 m x 3.99 m
Draft	4 m
Freeboard	6 m
Platform mass	5,452,330 kg
Center of mass location below SWL	0.281768 m
Water depth	150 m
Total displacement	6,000 m^3
Unstreched mooring-line length	473.3 m
Radius to anchors from centerline	386.9 m
Line diameter	0.0809 m
Line mass per unit length	130.4 $\frac{kg}{m}$
Line extensional stiffness	589,000,000 N

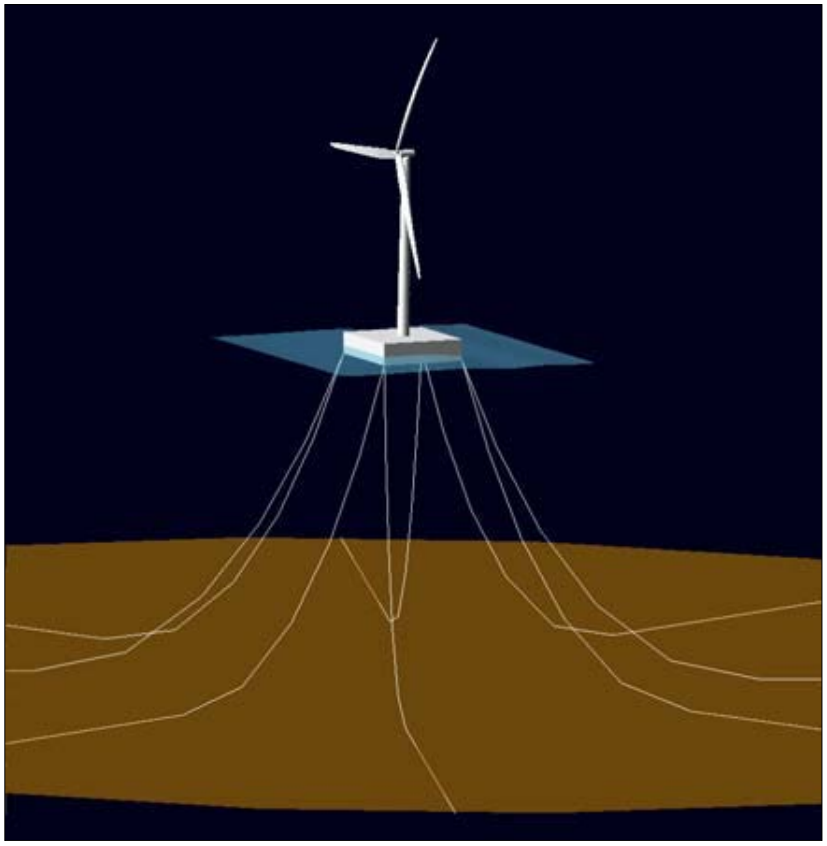

Figure 45. ADAMS visualization of ITI Energy barge design

Table 13. Natural Frequencies of ITI Energy Barge System

Mode	Natural Frequency [Hz]	Mode	Natural Frequency [Hz]
Platform surge	0.0076	Platform roll	0.0854
Platform sway	0.0076	Platform pitch	0.0849
Platform heave	0.1283	Platform yaw	0.0198
1st Tower S-S	0.5375	1st Tower F-A	0.5282
2nd Tower S-S	3.0458	2nd Tower F-A	2.9760

5.2 OC3-Hywind Spar Buoy

5.2.1 Design Description

Completing the comparison of the three major floating wind turbine concepts is the analysis of a ballast-stabilized spar buoy concept. The design originates from a model used in Phase IV of the IEA Annex XXIII Offshore Code Comparison Collaboration (OC3) described in an OC3 paper by Jonkman [17]. The so-called OC3-Hywind design is based on StatoilHydro's Hywind concept and features a deeply drafted, slender spar buoy with three catenary mooring lines, each 120° apart (as illustrated in Figure 46).

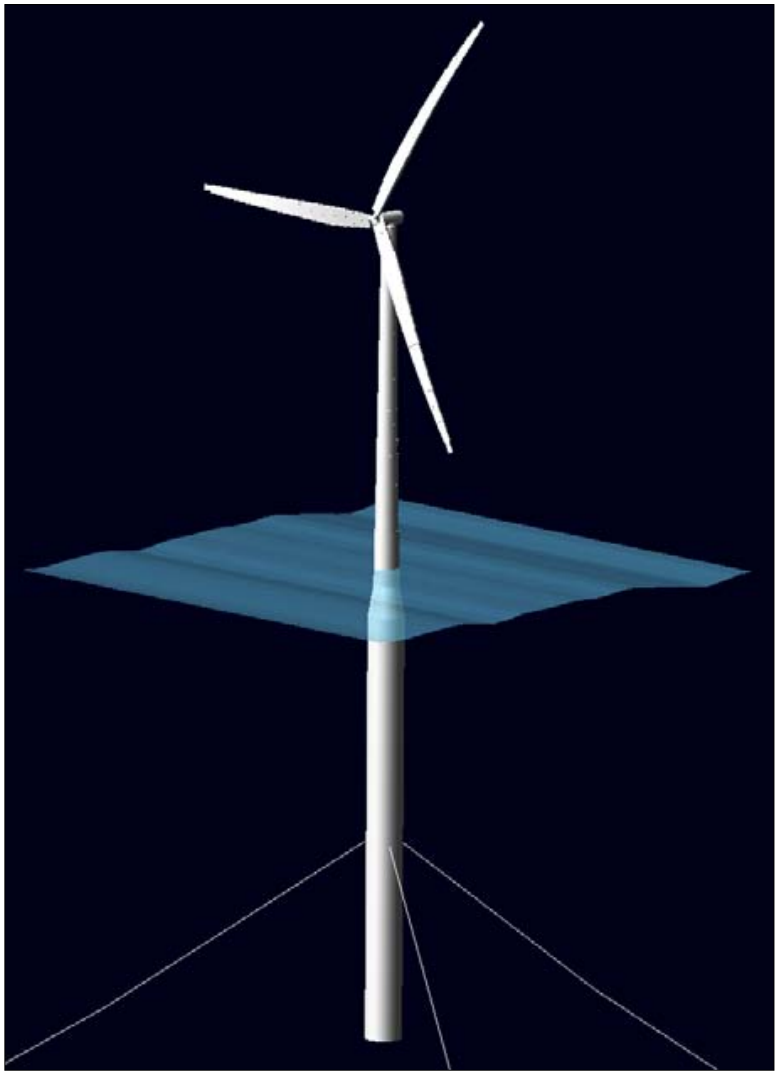

Figure 46. OC3-Hywind design

The NREL 5-MW baseline wind turbine atop of the spar buoy incorporates slightly changed tower properties because the tower is cantilevered 10 m above mean sea level to the top of the floating platform. That decreases the tower length to 77.6 m, as compared to a tower length of 87.6 m for the TLP (measuring up from MSL). Nevertheless, the effective tower height remains the same and the hub elevation of 90 m above MSL is consistent with the land-based and TLP system. To be consistent in the analysis and comparison of the other three concepts, for this analysis all tower base moments and forces were extrapolated 10 m down to the MSL, which is where the tower base loads measurements also begin. The draft of the platform is 120 m and the buoy consists of two cylindrical regions connected by a tapered conical region. Detailed platform properties are summarized in Table 14.

Table 14. Properties of OC3-Hywind System

Static Properties	Value
Total draft	120 m
Elevation to platform top	10 m
Depth to top of taper below SWL	4 m
Depth to bottom of taper below SWL	12 m
Platform diameter above taper	6.5 m
Platform diameter below taper	9.4 m
Platform mass	7,466,330 kg
Center of mass location below SWL	89.9155 m
Water depth	320 m
Total displacement	8,029.21 m^3
Unstreched mooring-line length	902.2 m
Radius to anchors from centerline	853.87 m
Line diameter	0.09 m
Line extensional stiffness	384,243,000 N
Line mass per unit length	77.7066 $\frac{kg}{m}$

Additionally the original baseline controller used with the land-based and TLP system is modified for the OC3-Hywind system. In blade pitch-to-feather controlled systems, steady-state rotor thrust is reduced with increasing wind speed above rated. This effect, according to Hansen et al. [14], introduces negative damping in the Hywind system, because the baseline controller frequency of 0.095 Hz is higher than the platform's natural frequency in pitch of 0.034 Hz. Therefore, the controller's natural response frequency for the OC3-Hywind System is reduced to 0.032 Hz. Natural frequencies of the platform for selected DOF are presented in Table 15. The control law of region 3 (*c.f.* Section 3.1) is changed from a constant generator power to a constant generator torque control region, set to 43,093.55 Nm. The modification helps to reduce rotor-speed excursions, which are amplified by the reduced gains in the blade pitch controller. A negative effect of this change, however, is increased generator overloading when power increases with rotor speed excursions greater than rated speeds. A more-detailed description of the OC3-Hywind system is provided by Jonkman [17].

Table 15. Natural Frequencies of OC3-Hywind System

Mode	Natural Frequency [Hz]	Mode	Natural Frequency [Hz]
Platform surge	0.0080	Platform roll	0.0342
Platform sway	0.0080	Platform pitch	0.0343
Platform heave	0.0324	Platform yaw	0.1210
1st Tower S-S	0.4573	1st Tower F-A	0.4732
2nd Tower S-S	4.2584	2nd Tower F-A	3.7512

5.2.2 Instabilities

For the OC3-Hywind design, the same set of DLCs described in Section 4.1 were simulated. For the DLC simulations database for the OC3-Hywind, the same loads analysis as for the TLP design was performed. The analysis, however, is not as extensively presented in this work, because the focus of the present work is the TLP and the comparison of the three different floating concepts.

Out of all DLC simulations for the OC3-Hywind, DLCs 6.1, 6.2, and 7.1 failed to finish the simulations. These failing FAST simulations did not occur for the TLP, for which all simulations were completed without errors. Characteristic for these failed simulations is the quick build-up of a severe instability at a certain simulation time. This ultimately causes the platform translational displacements to become great enough to be out of the limits of the simulated turbulent wind field, with a grid height of 179.980 m and a grid width of 254.090 m. At that point the FAST simulations stop and generate error messages.

To eliminate the possibility of a numeric instability in FAST causing the simulations to crash, additional ADAMS simulations for selected failing runs were performed. These ADAMS results confirm the instabilities—and the simulations in ADAMS crash earlier due to ADAMS' inability to solve the equations of motion within the given tolerance for the extreme displacements. An increase in the ADAMS tolerance to very high—and therefore inaccurate—values of up to 0.2 [-] only slightly increases the simulation time before the simulation fails. Figure 47 illustrates for the platform yaw a time series of such a failed simulation from DLC 6.2, with both the FAST and ADAMS results included. The time series for most of the other output paramters are very similar. The series all show the sudden increases in the output parameters over the time of one or two periods, which then cause FAST and ADAMS to abort the simulation.

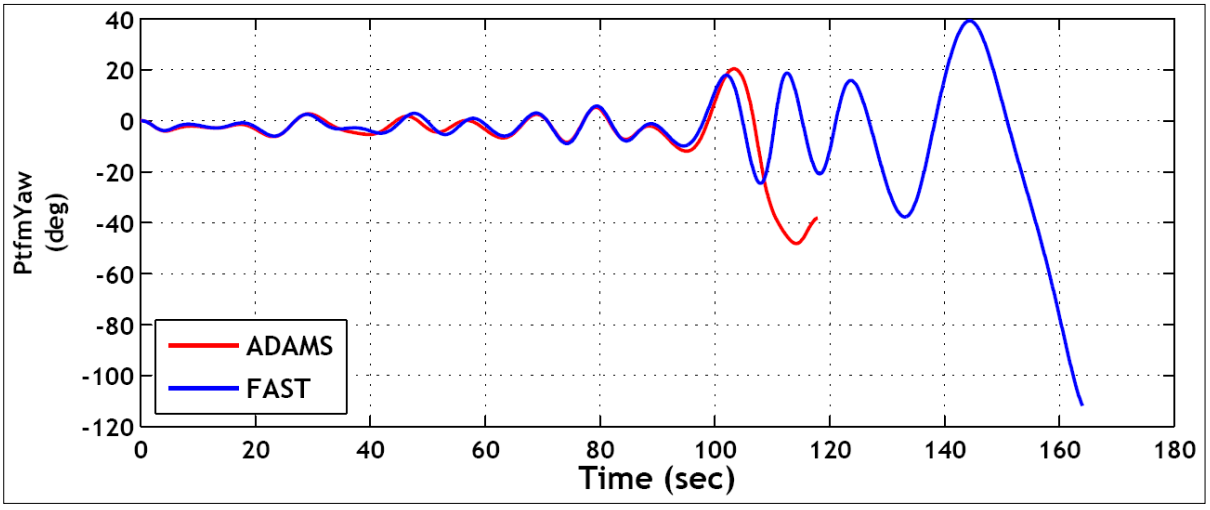

Figure 47. Time history of platform yaw of failed OC3-Hywind FAST/ADAMS DLC 6.2 simulation

This behavior occurs because the system encounters a severe instability at the beginning of the increase, which then triggers the presented extreme response. For DLCs 6.1 and 6.2, the instability described in Section 4.4.3 for the TLP is triggered.

For this case—in which the turbine's blades are fully feathered—the damping ratios for a case with constant 50 m/s wind speed and no waves for different yaw misalignments have been investigated in the same way as was done for the TLP. The resulting charts are presented in Appendix B. These charts show negative ratios for the blade and tower modes. Contrary to the TLP example, there is no negative damping in the platform DOFs. This difference is due to the fact that the OC3-Hywind model has increased yaw damping artificially. This additional damping has been added to match free-decay responses supplied by StatoilHydro and has been discussed by Jonkman [17]. The magnitude of this addition is great enough that the OC3-Hywind model maintains positive damping ratios for all platform DOFs—especially in yaw and roll—which are negative for the TLP. For the failing simulations in DLC 7.1, no extensive study was conducted for this report because this particular instability already is described in detail by Jonkman [18].

The surge instability found for the TLP (described in Section 4.4.4) cannot be identified for the OC3-Hywind. This mainly can be attributed to the changes in the control system, with the reduced gains and the changed region 3 control law. Appendix A.2 contains the complete extreme event tables for the normal operation DLCs 1.1 to 1.5.

5.3 Floating Wind Turbines Stability Triangle

The two concepts described above and the TLP concept achieve static stability by different means. The introduction discussed the classifications made based on how the concepts achieve static stability: (1) The barge concept, represented by the ITI Energy barge, achieves restoring from buoyancy via waterplane area moment; (2) the spar buoy, represented by the OC3-Hywind concept, is statically stable because restoring primarily is provided by ballast; and (3) for the tension leg platform, here represented by the MIT/NREL TLP, restoring mainly is provided by the mooring system. The static restoring coefficient in pitch C_{55} is used to quantify this classification. For each concept, the restoring moments due to:

- hydrostatics (buoyancy) $C_{55}^{Buoyancy}$,
- weight (ballast) $C_{55}^{Ballast}$, and
- the mooring system $C_{55}^{Mooring}$

are determined. These moments each then are normalized by the total restoring in pitch $C_{55}^{Total} = C_{55}^{Buoyancy} + C_{55}^{Ballast} + C_{55}^{Mooring}$ and plotted in a so-called ternary plot.

The ternary plot, ternary graph, triangle plot, simplex plot, and de Finetti diagram each is a barycentric plot of three variables which sum to a constant, in this case chosen to be unity or 100%. Such plots graphically depict the ratios of the three variables as positions in an equilateral triangle. These plots typically are used in petrology, mineralogy, metallurgy, and other physical sciences to show the compositions of systems composed of three species. They also provide a valuable tool used to graphically show how a specific floating wind turbine concept achieves static stability.

In the floating wind turbine design space ternary plot, for each concept the proportions of the three variables buoyancy, ballast, and mooring sum to one (100%). The three proportions cannot

vary independently, thereofore it is possible to graph the intersection of all three variables in only two dimensions. Each base—or side of the triangle—represents a proportion of 0 (0%), with the point of the triangle opposite that base representing a proportion of 1 (100%). As a proportion increases from 0, the point representing that sample moves from the base to the opposite point of the triangle.

Table 16. Stability Triangle—Non-Dimensional Pitch Restoring

Concept	$C_{55}^{Buoyancy}$	$C_{55}^{Ballast}$	$C_{55}^{Mooring}$
MIT/NREL tension leg platform	-0.12550	0.13019	0.99530
OC3-Hywind spar buoy	-3.37374	4.16379	0.20995
ITI Energy barge	1.24362	-0.25974	0.01612

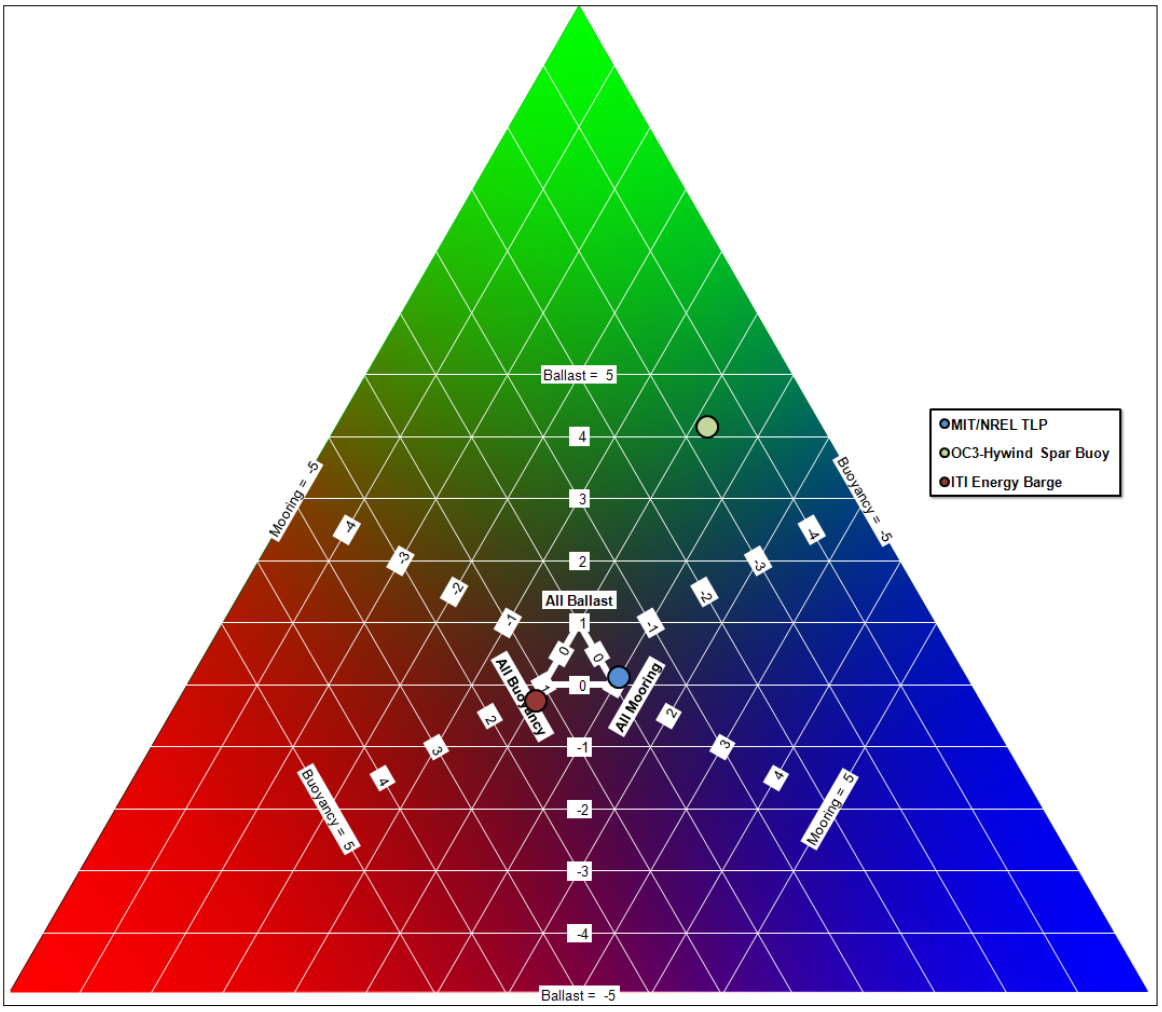

Figure 48. Floating wind turbines stability triangle (ternary plot)

The ternary plot for the concepts investigated in this project is shown in Figure 48. Important points and lines of the triangle are annotated to make the plot more easily readable. The underlying data, normalized to unity, is presented in Table 16. The TLP and ITI Energy barge

concept appear very close to the associated, previously predicted corners of the triangle. The TLP is located close to the mooring = 1 corner, and most of the static restoring (99.5%) for the TLP is provided by the mooring system. The contributions from buoyancy and ballast restoring—±13% of the total restoring—cancel each other out.

Restoring for the ITI Energy barge primarily (+1.24) is provided by the water-plane area effect from buoyancy of the platform, therefore the barge is located in the proximity of the left corner of the triangle representing buoyancy = 1. The excess buoyancy of 24% is similar to the TLP canceled out by the –26% negative restoring from weight. The mooring-line restoring contribution for the barge concept is negligible at 1.6%.

At first glance, the OC3-Hywind concept appears at an odd location—far away from the upper corner of the triangle, where restoring by ballast equal to 1. However, the location far from the core triangle illustrates the different restoring contributions very well. The positive restoring from ballast of 416% of the total restoring is counteracted by -337% of negative restoring originating from hydrostatic buoyancy. That is, without ballast the spar statically would be extremely unstable. The ballast provides enough restoring to more than compensate for this effect. In contrast to the slack catenary barge moorings, the slack catenary mooring lines of the OC3-Hywind contribute with 21% positive restoring to the spar's static stability.

The locations of the different concepts on the stability triangle illustrate the different restoring contributions for each concept graphically. The positions in the ternary plot, however, do not provide a basis for determining the quality of the specific design. That is, the TLP—which is positioned almost perfectly in the mooring = 1 corner of the triangle—is not an optimized design. For example, the absolute value of the ballast restoring for the TLP is much greater as compared to the ITI Energy barge. A TLP design with much less ballast probably could be designed and would be placed at almost the exact same position as the MIT/NREL TLP, but would have a much more economic design. This example illustrates that no statements on design quality can be derived from concept's the position in the stability triangle.

5.4 Ultimate Load Ratios in Normal Operation

Figure 49 compares various output parameter extreme loads from the TLP, barge, and OC3-Hywind to the land-based turbine in normal operation DLCs 1.1, 1.3, 1.4, and 1.5. An analogue to the TLP analysis, the bar charts present the ratios of the floating designs extreme loads divided by the land-based extreme loads. A ratio of 1, for example, implies that the loads are unchanged as compared to the land-based system, and a ratio that is greater or less than 1 indicates that the loads have increased or decreased. These ratios enable estimation of the differences between the three floating platform concepts and the effects on structural loads. Based on this data, substantiated statements on advantages and disadvantages of the concepts can be made. Also, using these results would enable performance of a preliminary cost analysis, however this is out of the scope of this work.

The chart in the upper-left corner of Figure 49 provides ratios of the generator's properties of generator power, generator torque, generator speed, and rotor speed. The TLP ratios are close to unity, because the variable-speed active pitch control system is identical to that of the onshore control system. The ITI Energy barge controller's gains are reduced and the OC3-Hywind has both reduced gains and a changed region 3 control law. This results in large excursions in

generator power, with the barge generator power ratio being 13% greater and the OC3-Hywind ratio being 38% greater than the land-based system. The changed region 3 control law also is responsible for the OC3-Hywind generator torque ratio of les than 1. Increased pitch motions of the platforms generate oscillations in wind inflow and add towards excursions in rotor and generator speed. The barge design is most susceptible to pitch motions in waves, therefore it shows the highest ratios (+36%) for these two parameters, and the OC3-Hywind also displays a ratio 22% greater than 1. The TLP basically is behaving like the land-based system for these parameters.

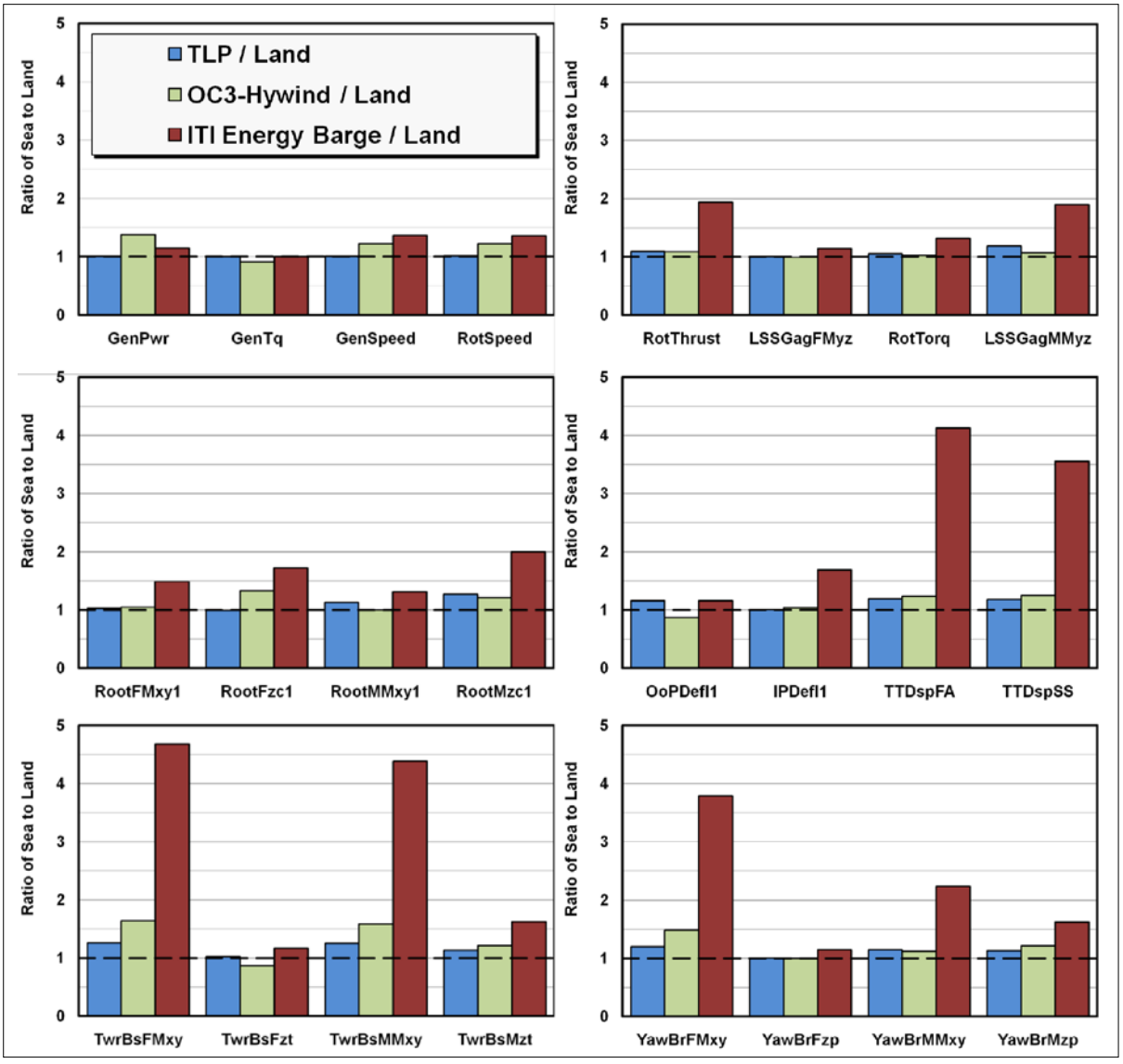

Figure 49. Ratios of TLP, barge, and Hywind concepts to land-based loads for normal operation DLCs

The wind inflow oscillations due to platform motions also cause the rotor thrust illustrated in the upper-right chart in Figure 49 to show the same behavior. This also leads to increased moments

in the low-speed shaft. For all parameters in the upper-right chart the barge shows the greatest ratios. Interestingly, the low-speed shaft moment for the OC3-Hywind is lower than for the TLP. The extreme event causing the maximum LSS moment for the TLP occurs in DLC 1.4 during an extreme coherent gust with direction change and the maximum for the OC3-Hywind occurs in DLC 1.3, featuring the extreme turbulence model. Overall, for the OC3-Hywind, approximately 50% fewer extreme events are caused by DLC 1.4 than for the TLP. As previously mentioned, the OC3-Hywind has increased damping and stiffness in platform yaw. An analysis of time series for both systems of the DLC 1.4 simulation, which causes the maximum for the TLP, was performed. The time series are provided in Appendix C. Following the extreme gust with direction change, the TLP platform yaws up to a maximum of 5°; the OC3-Hywind remains much more stable and yaws less than 2°. This peak in platform yaw applies a large force in y-direction on the shaft, and causes the peak of the total low-speed shaft moment for the TLP, which is is the sum of the LSS moments in y-axis and z-axis directions.

The chart in the middle-left position in Figure 49 presents ratios of blade 1 root forces and moments. Extreme platform pitch, roll, and yaw motions of the barge increase the combined flap-wise and edgewise blade root bending moment by 31%, and the moment in twist around the blade's local z-axis is increased up to 100%. Again, the OC3-Hywind shows lower ratios for the moments than for the TLP. Similar to the LSS moment, the maximum for the TLP is caused by the extreme gust in DLC 1.4 and the OC3-Hywind's maximum occurs in DLC 1.3. The time series provided in Appendix C illustrates that the TLP's increased yaw is the driving event for the maximum blade root moment. Additionally, the TLP's control system has 0° pitch angle at the time that the extreme event occurs. The OC3-Hywind has a pitch angle of about 9° during the same period, thus decreasing the lift coefficient and the force on the blade.

The same conclusion applies for the out-of-plane deflection presented in the chart in the middle-right position in Figure 49, which also presents ratios for the in-plane deflections of blade 1 and ratios of the tower-top fore-aft and side-to-side displacements. Again, the extreme motions of the ITI barge cause the highest ratios for all parameters. The tower-top fore-aft and side-to-side displacements especially are affected, and are 313% and 255% greater for the barge than for the land-based system. For the tower displacements, which occur in DLC 1.3, the OC3-Hywind yields higher ratios than the TLP, because the spar buoy's roll and pitch motions are greater. The time series in Appendix C illustrates this effect of increased platform motions on the tower-top displacements.

The same effect is responsible for the OC3-Hywind's higher moment ratios in the bottom-left chart in Figure 49, where tower base forces and moments are displayed. The barge again dominates these forces and moments ratios, which exceed the factor 4 for the combined total base force and moment in x-direction and y-direction. Note that the tower base force in z-direction for the OC3-Hywind is less than 1 because the tower in FAST has an offset of 10 m, as described in Section 5.2.1. The moments are unaffected by that offset. The bottom-left chart in Figure 29 displays the nacelle yaw bearing forces and moments, which are dominated by the barge. The spar buoy has similar or slightly increased ratios as compared to the TLP.

Further assessment is needed to fully understand and evaluate the implications of these calculated increased blade and tower loads. Clearly, the barge's tower and blades must be strengthened to sustain the (up to four times) greater moments and forces. The generally slightly

higher ratios for the OC3-Hywind compared to the TLP certainly affect the turbine cost in favor of the TLP, but final results only can be provided by a thorough and detailed cost assessment (particularly the cost of the platform itself and its installation).

Figure 50 presents the ratios of platform displacements for the three concepts, which provide good insight into the difference in the concept's platform motions. The diagram is obtained by normalizing the extreme platform displacements of the TLP, barge, and spar in normal DLCs by the displacements of the TLP in normal operation. The TLP has been chosen as reference because in most DOFs it yields the lowest maximum platform displacements. The ITI barge yields the greatest ratios by far, particularly in pitch and roll; they are more than 20 times greater than the reference TLP ratios. The spar also has 8 and 11.5 times greater ratios for roll and pitch than the TLP. The slack catenary mooring system for the barge and the OC3-Hywind permit greater motions in surge and sway than does the TLP's mooring system. This also affects the heave, for which the high-tension mooring of the TLP prevents greater heave motions, especially in positive z-direction. Only in yaw is the spar's ratio lower than the TLP's. This a direct effect of the significantly increased platform yaw damping and stiffness of the OC3-Hywind.

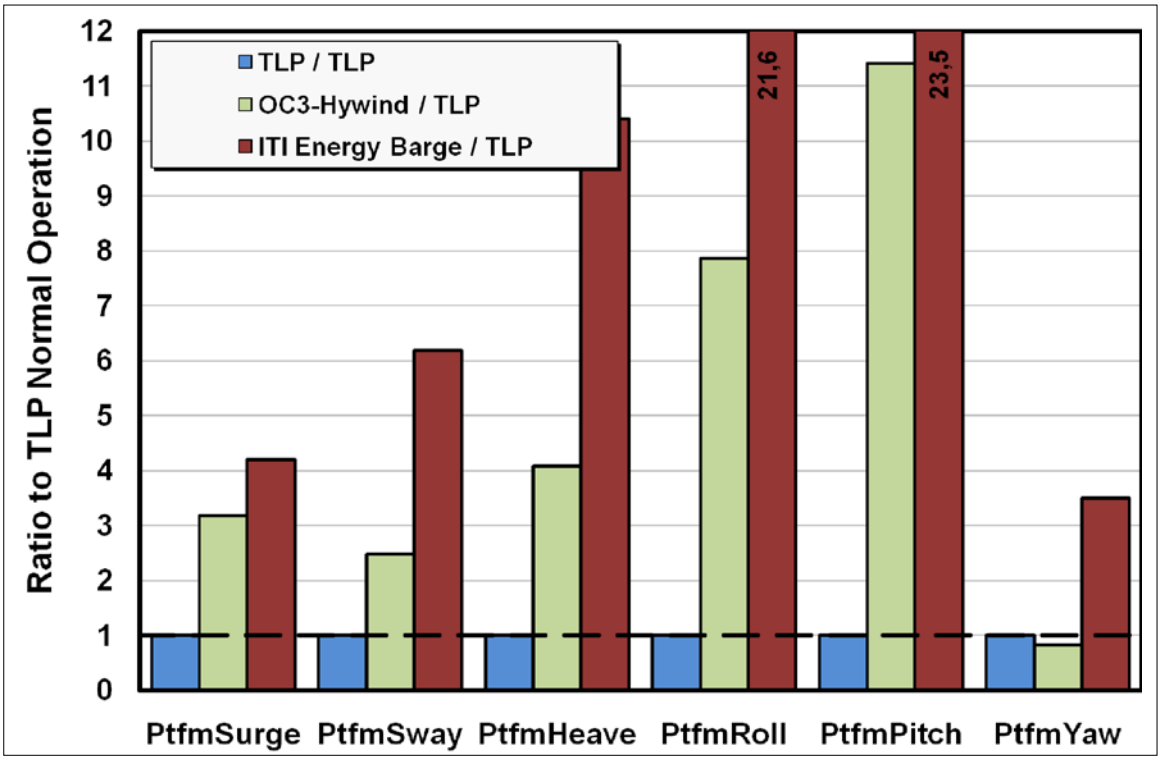

Figure 50. Ratios of tension leg platform, barge, and Hywind concepts displacements to tension leg platform from normal operation DLCs

5.5 Fatigue Load Ratios for Design Load Case 1.2

Figure 51 presents the comparison of the fatigue lifetime ratios for the three investigated floating wind turbine concepts. Comparable to those of the TLP, the ratios represent the quotient of the lifetimes of the floating turbines and the land-based system's lifetimes, with a ratio of one

representing the exact same lifetime as the land-based machine. A value of less than one means that the lifetime of the particular floating system is significantly less than for the land-based system, and vice-versa. The y-axis of the charts is logarithmic because particular lifetimes, especially for the barge, are several orders of magnitude less than for the land-based system. For each concept, three ratios for each investigated S/N slope value *m* are displayed. Because ratios and not absolute values are presented, no definite increasing or decreasing of lifetimes for increasing *m* values can be identified, whereas the absolute lifetimes increase with increasing *m* values for all concepts and components.

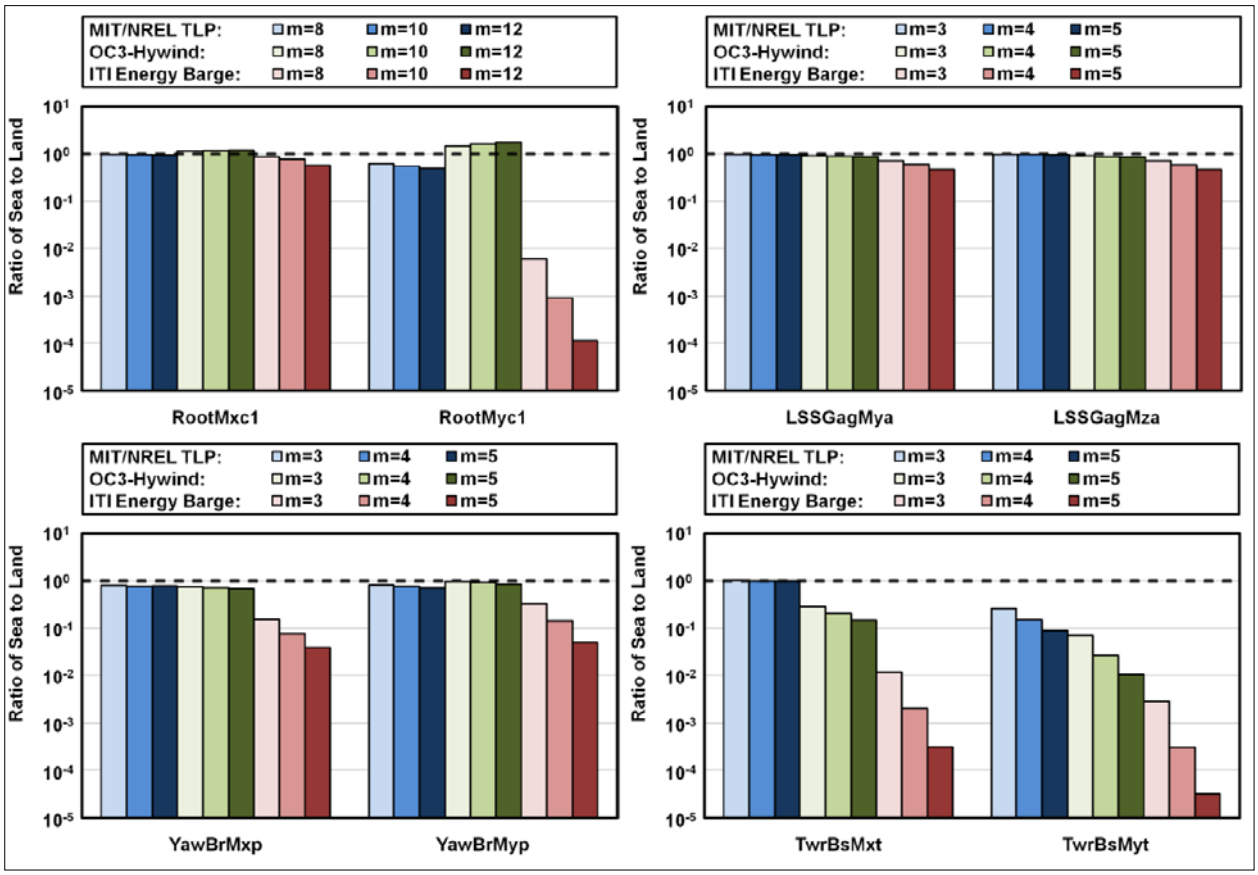

Figure 51. Ratios of tension leg platform, OC3-Hywind, and ITI Energy barge fatigue lifetimes to land-based turbine from normal operation DLCs

The upper-left chart in Figure 51 presents the lifetime ratios for the blade 1 edgewise and flap-wise root bending moments. For the TLP the lifetimes drop by maximal 52%. The barge shows very low lifetime ratios which means that the barge's blades fail within a very short time period of normal operation. The OC3-Hywind surprisingly shows increased lifetime ratios for the blade roots compared to the land-based system. This result is explained by the changed control system region 3, which takes ultimate and fatigue loads off the blades but increases rotor speed excursions and therefore decreases the lifetime of the shaft.

In the upper-right diagram in Figure 51, the lifetime ratios for the low-speed shaft bending moments are displayed. For all concepts only slightly decreased ratios are identified, with the

barge accounting for the lowest lifetime ratios. The TLP shows almost the same fatigue lifetimes as the land-based system, and the OC3-Hywind ratios also are close to those of the land-based system.

The lower-left chart in Figure 51 presents ratios for the tower-top yaw bearing bending moments. The effect from the changed OC3-Hywind control system seen at the blade root ratios also can be seen for the tower-top yaw bearing moment in pitch (i.e., around the y-axis). The OC3-Hywind controller decreases the thrust forces on the rotor in region 3 of the control law, therefore the ratios are greater than for the TLP and only slightly less than the land-based system's ratios. Nevertheless, the TLP also shows only slightly decreased ratios with a minimum of 0.71. Again, the barge provides the lowest ratios by more than one order.

The lower-right chart in Figure 51 presents the ratios for the two tower base bending moments around the x-axis and y-axis. Especially in the bending moment in pitch around the y-axis, the differences between the concepts are great. Although the TLP already has ratios as low as 0.09, the OC3 Hywind shows significantly lower ratios of 0.01. The ITI Energy barge—due to the excessive platform pitch motion—has a very low ratio which would mean failure after a considerably short time in normal operation. The difference of close to one order of magnitude between the TLP and the OC3-Hywind, however, already has great influence on the tower design for the two concepts. A significant increase in tower base strength is necessary for the spar-buoy to achieve a lifetime equal to the lifetime of the TLP. For the barge, a strategy to decrease the fatigue loads instead of strengthening the tower base probably is the better option.

Figure 52 presents the DEL ratios for all three floating concepts. The ratios represent the quotient of the damage equivalent loads of the floating turbines and the land-based system's DELs, with a ratio of 1 representing the exact same lifetime as the land-based machine. Ratios greater than one represent a higher DEL, which means that the floating machine's lifetime is less than that of the land-based turbine. Simply stated, the DEL ratios show essentially the same behavior as the lifetime ratios described previously. Of all concepts, the ITI Energy barge has the greates ratios and therefore the worst fatigue lifetime, and the differences between the TLP and the OC3-Hywind are not significant, except for the tower base bending moments. Here, the TLP DEL ratios are 0.5 to 1.5 less than the OC3-Hywind ratios.

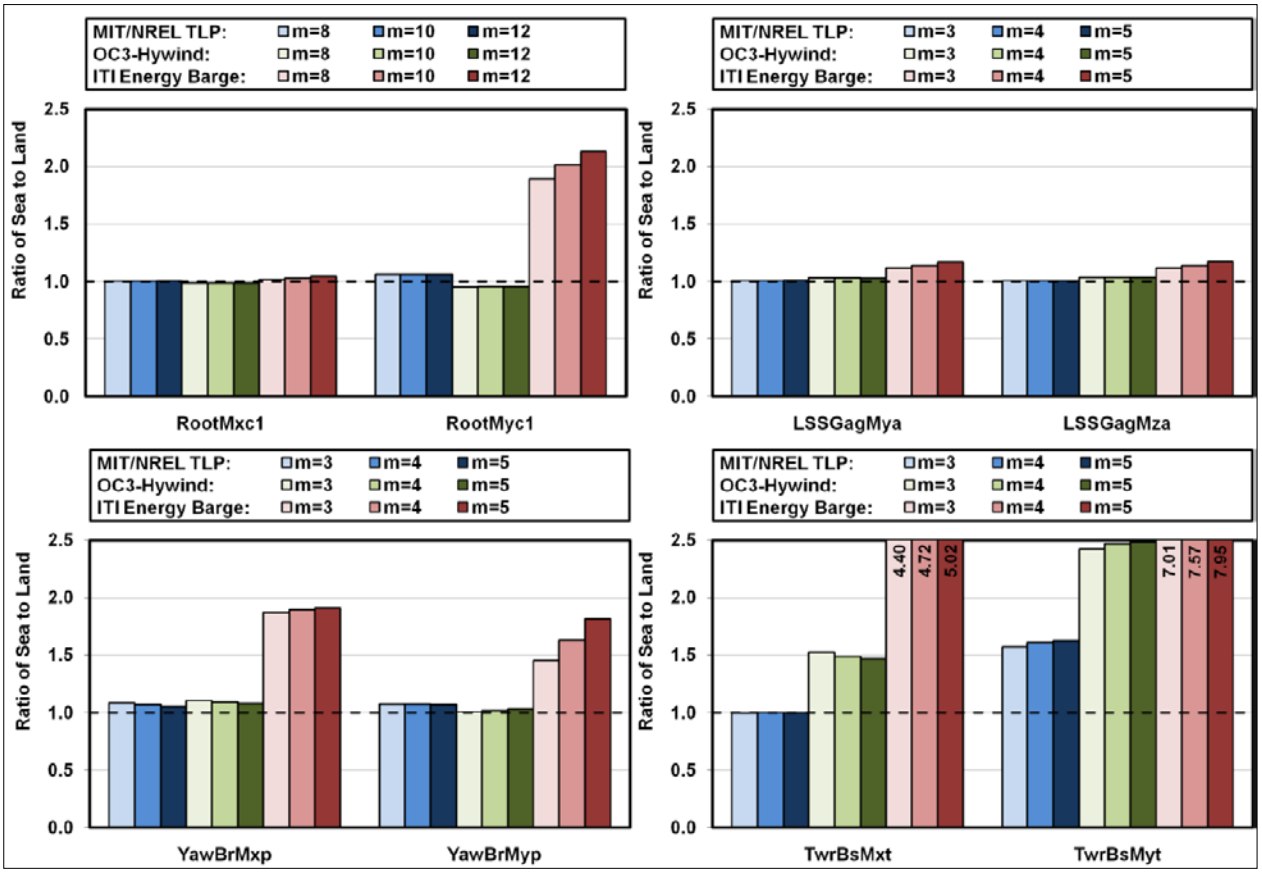

Figure 52. Ratios of tension leg platform, OC3-Hywind, and ITI Energy barge fatigue DELs to land-based turbine from normal operation DLCs

5.6 Comparison

Based on the analysis described in this section, the three basic floating wind turbine concepts—represented by the MIT/NREL TLP#1, the ITI Energy barge, and the OC3-Hywind spar buoy—are compared to each other. Because the TLP design investigated in this study is not a "pure" TLP, but rather a hybrid between a TLP and a spar buoy, hybrid features are difficult to identify. Nevertheless some general statements on each concept can be made.

5.6.1 ITI Energy Barge

The ITI Energy barge primarily has the advantage that the platform design is easy to manufacture and install. It consists mainly of inexpensive off-the-shelf flat steel panels and can be assembled in almost any coastal facility due to the shallow draft. The slack catenary mooring system allows for a simple inexpensive anchoring system. The stability analysis also showed fewer instabilities for the barge than for the other two concepts.

In harsh contrast to these advantages are the results from the ultimate and fatigue load comparisons. Here, the barge is by far the concept with the highest ultimate loads and lowest fatigue lifetimes. These high loads mainly are caused by the barge's extreme motions and accelerations in high waves, which means that the barge design is affected greatly by extreme seas. Nakim [38] showed that using a control system with individual blade pitching on the floating barge wind turbine system, significant reduction in platform pitching motion could be achieved without affecting power regulation in the above rated wind speed region. Economic

cost analysis must show to what extent the savings due to the simple design are outweighed by the need for a strengthened turbine. Particularly for sites that have less-severe sea states, such as the Great Lakes, an improved barge design could provide the most cost-effective choice.

5.6.2 OC3-Hywind Spar Buoy

Of the three concepts investigated, the OC3-Hywind is the only system which is close to a real system, Statoil Hydro's Hywind concept, which actually is being tested full-scale in the North Sea in 2009. The OC3-Hywind model is not completely identical to the real Hywind design and also lacks certain details, which (most likely) make the real design superior to the investigated OC3 model. Nevertheless, compared to the other two floating concepts investigated, the OC3-Hywind design is supposed to be quite optimized. The analysis of the ultimate and (especially) the fatigue ratios however indicate that the concept, although experiencing significantly less loads than the ITI Energy barge, meets a strong challenge posed by the investigated TLP design. The fatigue ratios—which differ up to one order from the TLP—indicate a great need for improvements in the tower strength or the control system. Additionally, the spar buoy has the disadvantage that it is very deep drafted and could require deep-water harbors for manufacturing and assembly. The amount of ballast needed also adds to total costs. Compared to the TLP, the design has the advantage of a simpler anchoring system, due to the slack catenary mooring and the slender cylindrical body, which results in a small cross-section at MSL, it also has advantages regarding drag forces. The spar's natural frequencies also are very well placed out of the energy-rich wave spectra. Further iterations, economic design analysis, and experimental data will help to clarify the pros and cons of the spar concept, particularly as compared to the TLP.

5.6.3 MIT/NREL Tension Leg Platform

The investigated tension leg platform showed the best ratios for ultimate and fatigue loads of all investigated concepts. It is the floating concept closest to the land-based system and therefore requires the least effort for strengthening the turbine, which saves costs. A disadvantage of all TLP designs is the expensive tension leg mooring system and expensive anchors needed. This particular TLP also has the disadvantage of a large amount of ballast and a very high volume of the platform—the largest of all three concepts. The big cross-section at mean sea level also poses a significant obstacle for incident-waves and adds to drag. The long spokes are a source of failure; to build them with the necessary strength requires additional costly material and manufacturing work. Installation also is the most difficult of the three designs because the design is fairly deep drafted, the tension leg anchors are difficult to install, and without adding additional ballast the design is quite unstable without a mooring system (which makes the towing-out process challenging). Nevertheless, the TLP design yields the lowest ultimate and fatigue loads for all other concepts. The great potential for optimization of the TLP adds to its advantages, especially regarding a possible decrease of the amount of ballast required, or development of alternative installation and anchoring methods. The present study only provides initial information on the loads for, and stability of, each concept. A thorough cost analysis, improvements in the control system, further design optimization, and analysis of more concepts can lead to a conclusion on the optimal concept.

6 Summary and Conclusion

Three primary concepts for floating platforms exist for offshore wind turbines, classified in terms of how the concepts achieve basic static stability in pitch and roll. The first is a shallow-drafted barge that achieves restoring via water-plane area moment. The second is a deep-drafted spar buoy that achieves restoring from its ballast. The third is a tension leg platform, for which restoring mainly is provided by the mooring system.

First, the analysis of a 5-MW wind turbine on a floating offshore tension leg platform in the fully coupled time-domain aero-hydro-servo-elastic design code FAST with AeroDyn and HydroDyn was performed. This code has the capability of simulating time-domain hydrodynamic effects from linear hydrostatic restoring; added-mass and damping contributions from linear radiation, including free-surface memory effects; incident-wave excitation from linear diffraction; and nonlinear viscous drag, including sea-current loading. The code also includes a nonlinear quasi-static mooring line module. These models are of higher fidelity than most of the models that have been used to analyze floating turbines in the past, and which have neglected important hydrodynamic and mooring system effects. The TLP design was modified from a MIT design derived from a parametric linear frequency-domain optimization process. The modifications were needed to eliminate flaws in the original design.

The model has been verified and compared to frequency-domain calculations in terms of response amplitude operators and probability density functions. Significant differences between the higher-fidelity time-domain model and lower-fidelity frequency-domain model have been found and explained. For instance, a shift of the platform-pitch RAO maxima to lower frequencies is observed as a result of the tower bending in the time-domain model. These differences have important implications to the required design process for floating offshore turbine systems.

An extensive loads and stability analysis for ultimate and fatigue loads according to the procedures of the IEC 61400-3 offshore wind turbine design standard was performed with the verified TLP model. Response statistics, extreme event tables, fatigue lifetimes, and selected time histories of design-driving extreme events were analyzed and presented in this report. For normal operation cases, the loads for the wind turbine on the TLP are compared to those of an equivalent land-based turbine. The ultimate loads for the TLP turbine are increased up to 25% for the tower and more than 20% for the blades. The stability analysis identified a severe aerodynamic instability in the platform pitch, platform roll, and tower and blade bending modes for a TLP wind turbine that is idling in high winds at certain yaw misalignments with all blades fully feathered at 90º. Also identified is a platform yaw instability occurring when the TLP turbine is idling in high winds with one blade seized at 0º pitch (and the other two blades at 90º). Furthermore, a minor surge instability for the turbine operating at rated wind speed is presented.

These TLP results are compared to two other basic floating platform concepts. A quantitative comparison of the responses of each concept is presented. To make this comparison, three additional models of the NREL 5-MW wind turbine were analyzed: One model for the turbine supported on land and two models for the turbine supported offshore independently on the ITI Energy barge and the OC3-Hywind spar-buoy. Using the MIT/NREL tension leg platform, models representing the three primary floating platform concepts were analyzed. A com-

prehensive loads and stability analysis according to the procedures of the IEC 61400-3 offshore wind turbine design standard then was performed for each of the three additional models.

The calculations again used NREL's fully coupled time-domain aero-hydro-servo-elastic design code FAST with AeroDyn and HydroDyn. The exact same environmental conditions and loads analysis process as for the TLP were used on all three models to facilitate a direct, equal comparison. The concepts are compared based on the statistics, extreme event tables, and fatigue lifetime calculations. Common and individual instabilities for each system are described and analyzed. The comparison indicates that all floating wind turbines show increased loads on turbine components as compared to the land-based system. The investigated barge design is very susceptible to significant roll and pitch motions and, consequently, has the greatest turbine loads by far among the concepts. The spar-buoy platform motions in roll and pitch are greater than for the TLP, but for yaw the spar-buoy is more stable than the TLP. This yields generally greater blade and tower loads for the spar buoy than for the TLP, except for loads affected primarily by platform yaw. In addition to the quantitative comparison of the different floating system concepts, a qualitative assessment of each concept regarding the technical and economic considerations of the mooring system and platform was presented, including the influence of manufacturing, installation, maintenance, and decommissioning. The results of the present analysis can help resolve the fundamental design trade-offs between the floating system concepts.

To arrive at a technically and economically feasible concept, further work in various research areas is required. First the FAST with AeroDyn and HydroDyn design code could need further enhancements. In FAST, the modal representation of the tower could be extended by a torsional DOF, and the blades representation could be extended by including mass and elastic offsets, torsion DOFs, and coupled mode-shape properties. The linear first-order hydrodynamic module HydroDyn could be improved by adding second-order effects, loading from vortex induced vibration and sea ice, and replacing the quasi-static mooring system with a fully coupled dynamic module. A validation of the code against experimental data also should be performed in the near future.

Besides improvements in the code, additional conceptual studies adding to the results provided in this report are necessary to improve the knowledge on floating wind turbine concepts. The loads-analysis process performed in the present study should be applied to further designs. Design iterations with the presented systems also are an option to arrive at an improved concept. As a special interest, in addition to the hybrid MIT/NREL TLP investigated here a pure TLP design without ballast and with less draft should be analyzed to finally cover all three basic concepts and draw further conclusions on the advantages and disadvantages of each. Promising alternative turbine configurations such as downwind rotors, two-bladed rotors, and higher than 5-MW rated systems with larger blades will give additional insight into the primary question of how the optimum floating wind turbine should be designed. In the broader perspective, a study on grid costs for the electrical power transmission from offshore floating wind parks to large coastal metropolitan areas could be helpful to determine the impact of probable greater floating wind turbine costs compared against cheaper onshore turbines located farther away from large coastal metropolitan areas.

Based on the results and designs from the present study, it would be of great interest to investigate sophisticated controllers for the analyzed concepts to estimate the load reductions

made possible by improved control systems. Controller improvements also should be considered for eliminating the described instabilities. Regarding instabilities, more research into the driving causes and possible resolutions also is necessary. The ultimate and fatigue loads analysis results could be utilized to perform a conceptual economic study on each design to draw more substantiated conclusions on which design is providing the most cost-effective choice. Besides examining loads, this economic study also should focus more specifically on influences from manufacturing, installation, anchoring, and decommissioning and examine costs and complexities of different methods thereof.

When these engineering challenges are addressed and economically feasible offshore floating wind turbine designs are developed, these systems will diversify the wind energy portfolio further and will be capable of providing a significant source of indigenous, nonpolluting, inexhaustible, renewable, green energy for the world.

7 References

[1] Anderson, J. D. *Fundamentals of Aerodynamics.* 4th edition. McGraw-Hill International Editions, 2003.

[2] ASTM. "E 1049-85; Standard Practices for Cycle Counting in Fatigue Analysis." ASTM International, 1985 (reapproved 2005).

[3] Bulder, B. et al. "Study to Feasibility of and Boundary Conditions for Floating Offshore Wind Turbines." ECN, MARIN, TNO, TUD, MSC, Lagerway the Windmaster: 2002.

[4] Buhl, M. L. *MCrunch User's Guide.* NREL/TP-500-43139. Golden, CO: National Renewable Energy Laboratory, 2008.

[5] Burton, T.; Sharpe, D.; Jenkins, N.; Bossanyi, E. *Wind Energy Handbook*. New York: Wiley, 2001.

[6] Cummins, W. *The Impulse Response Function and Ship Motions*. Schiffstechnik, Vol. 9, 1962.

[7] Demirbilek, Z., ed. *Tension Leg Platform—A State of the Art Review*. New York: ASCE, 1989.

[8] International Electrotechnical Commission. IEC 61400-3 Ed.1. *Wind Turbines—Part 3: Design Requirements for Offshore Wind Turbines*. International Electrotechnical Commission (IEC), 2009.

[9] International Electrotechnical Commission. IEC 61400-1 Ed.3. *Wind Turbines—Part 1: Design Requirements.* International Electrotechnical Commission (IEC), 2005.

[10] European Wind Energy Association (EWEA). "Offshore Statistics 2008." EWEA, 2008.

[11] Faltinsen, O. M. *Sea Loads on Ships and Offshore Structures*. Cambridge University Press, 1999.

[12] Gasch, R.; Twele, J. *Windkraftanlagen: Grundlagen, Entwurf, Planung und Betrieb.* Teubner Verlag, 2007.

[13] Gudmestad, O. *Basics of Offshore Petroleum Engineering and Development of Marine Facilities—with Emphasis on the Arctic Offshore*. Moscow, St. Petersburg, Trondheim: Stavanger, 1998.

[14] Hansen, M.; Hansen, A.; Larsen, T.; Oye, T.; Sorensen, S.; Fuglsang, R. *Control Design for a Pitch-Regulated, Variable-Speed Wind Turbine*. Riso National Laboratory for Sustainable Energy at the Technical University of Denmark, 2005.

[15] Henderson, A.; Patel, M. "On the Modelling of a Floating Offshore Wind Turbine." *Wind Energy*, Vol. 6, No. 1, 2003.

[16] Jonkman, B.; Buhl Jr., M. L. *TurbSim User's Guide for Version 1.40.* Golden, CO: National Renewable Energy Laboratory, September 2008.

[17] Jonkman, J. *Definition of the Floating System for Phase IV of OC3.* OC3, unpublished internal report, 2009.

[18] Jonkman, J. *Dynamics Modeling and Loads Analysis of an Offshore Floating Wind Turbine*. NREL/TP-500-41958. Golden, CO: National Renewable Energy Laboratory, November 2007.

[19] Jonkman, J.; Buhl, M. *FAST User's Guide.* NREL/TP-500-38230. Golden, CO: National Renewable Energy Laboratory, October 2005.

[20] Kühn, M.; Fischer, T. "Entwurf von Windenergieanlagen 1." Universität Stuttgart lecture script, 2001.

[21] Larson, T. J.; Hanson, T. D. "A Method to Avoid Negative Damped Low Frequent Tower Vibrations for a Floating, Pitch Controlled Wind Turbine." *Journal of Physics*, Conference Series 75, 2007.

[22] Lee, C.; Newman, J. *WAMIT User Manual.* Chestnut Hill, MA: WAMIT Inc. 2006.

[23] Lee, K. H. *Responses of Floating Wind Turbines to Wind and Wave Excitation.* MSc Thesis. University of Michigan, 2005.

[24] Manjock, A. *Evaluation Report—Design Codes FAST and ADAMS for Load Calculations of Onshore Wind Turbines.* Germanischer Lloyd WindEnergie GmbH, 2005.

[25] Manwell, J.; McGowan, J.; Rogers, A. *Wind Energy Explained*. New York: Wiley, 2002.

[26] Moriarty, P.; Holley, P. "Using Probabilistic Models in Wind Turbine Design." *Ninth International Conference on Applications of Statistics and Probability in Civil Engineering (ICASP9), Proceedings, 2003*.

[27] Newman, J. N. *Marine Hydrodynamics*. Cambridge, MA: The MIT Press, 1977.

[28] Nielsen, F. G.; Hanson, T. D.; Skaare, B. *Integrated Dynamic Analysis of Floating Offshore Wind Turbines*. Bergen, Norway: Hydro Oil and Energy, 2007.

[29] Oglivie, T. F. "Recent Progress Toward the Understanding and Prediction of Ship Motions." *Proceedings, Fifth Symposium on Naval Hydrodynamics, Bergen, Norway, 1964*.

[30] Sutherland, H. *On the Fatigue Analysis of Wind Turbines.* Albuquerque, NM: Sandia National Laboratories, 1999.

[31] Tracy, C. *Parametric Design of Floating Wind Turbines.* M.S. Thesis. MIT, 2007.

[32] Vijfhuizen, W. *Design of a Wind and Wave Power Barge.* M.S. Dissertation. Glasgow, Scotland: Universities of Glasgow and Strathclyde, Department of Naval Architecture and Mechanical Engineering, 2006.

[33] Wayman, E.; Sclavounos, P.; Butterfield, S.; Jonkman, J.; Musial, W. "Coupled Dynamic Modeling of Floating Wind Turbine Systems." *Offshore Technology Conference 2006, May 1–4, 2006, Houston, Texas.*

[34] Wayman, E. *Coupled Dynamics and Economic Analysis of Floating Wind Turbine Systems*. M.S. Thesis. MIT, 2006.

[35] Withee, J. *Fully Coupled Dynamic Analysis of a Floating Wind Turbine System.* Ph.D. Dissertation. MIT, 2004.

[36] World Wind Energy Association (WWEA). *World Wind Energy Report 2008*. Germany: World Wind Energy Association WWEA, 2009.

[37] Zambrano, T.; MacCready, T.; Roddier, D.; Cermelli, C. "Design and Installation of a Tension Moored Wind Turbine." *Proceedings of the 26th International Conference on Offshore Mechanics and Arctic Engineering OMAE2007 June 10–15, 2007, San Diego, California*. 2007.

[38] Nakim, H.; Stol, K. "Control Methods for Reducing Platform Pitching Motion of Floating Wind Turbines." *European Offshore Wind 2009 Conference & Exhibition, September 14-16, 2009, Stockholm, Sweden* .

Appendix A. Extreme Event Tables

A.1. Tension Leg Platform Normal Operation Design Load Cases

Extreme events for Wind:

Parameter	Type	File	WindVxi (m/sec)	WindVyi (m/sec)	WindVzi (m/sec)	WaveElev (m)	Time (sec)
WindVxi	Minimum	DLC1.3_0007_Sea_04.0V0_01.6Hs_08.9Tp_S03.out	-1.97E+00	1.11E+00	5.67E-01	4.12E-01	1.65E+02
WindVxi	Maximum	DLC1.3_0107_Sea_24.0V0_05.5Hs_12.7Tp_S03.out	3.04E+01	9.40E-02	7.60E-01	-1.23E+00	3.23E+02
WindVyi	Minimum	DLC1.4_0001_Sea_ECD+R-20_02.0Hs_10.6Tp_S01.out	5.66E+00	-2.37E+01	0.00E+00	-1.61E-01	7.00E+01
WindVyi	Maximum	DLC1.4_0055_Sea_ECD-R-20_02.0Hs_10.6Tp_S01.out	5.66E+00	2.37E+01	0.00E+00	-5.59E-01	7.00E+01
WindVzi	Minimum	DLC1.3_0190_Sea_24.0V0_05.5Hs_12.7Tp_S04.out	2.02E+01	-3.44E+00	-6.42E+00	-7.00E-01	5.70E+02
WindVzi	Maximum	DLC1.3_0193_Sea_24.0V0_05.5Hs_12.7Tp_S05.out	2.74E+01	1.76E+00	5.67E+00	-3.34E-02	1.70E+02

Extreme events for Waves:

Parameter	Type	File	WaveElev (m)	WaveVxi (m/sec)	WaveVyi (m/sec)	WaveVzi (m/sec)	WaveAxi (m/sec^2)	WaveAyi (m/sec^2)	WaveAzi (m/sec^2)	WindVxi (m/sec)	Time (sec)
WaveElev	Minimum	DLC1.5_0503_Sea_EWSH+20.0_04.4Hs_11.3Tp_S03.out	-4.09E+00	-3.04E+00	0.00E+00	3.55E-01	5.55E-01	0.00E+00	3.39E+00	2.00E+01	6.90E+01
WaveElev	Maximum	DLC1.5_0745_Sea_EWSH-24.0_05.5Hs_12.7Tp_S03.out	5.06E+00	3.12E+00	0.00E+00	1.93E-01	2.06E-01	0.00E+00	-2.09E+00	2.40E+01	9.10E+01
WaveVxi	Minimum	DLC1.5_0503_Sea_EWSH+20.0_04.4Hs_11.3Tp_S03.out	-4.07E+00	-3.07E+00	0.00E+00	-5.02E-01	-2.88E-01	0.00E+00	3.44E+00	2.00E+01	6.88E+01
WaveVxi	Maximum	DLC1.5_0745_Sea_EWSH-24.0_05.5Hs_12.7Tp_S03.out	5.04E+00	3.13E+00	0.00E+00	-3.34E-01	-1.69E-01	0.00E+00	-2.11E+00	2.40E+01	9.13E+01
WaveVyi	Minimum	DLC1.1_0001_Sea_04.0V0_01.6Hs_08.9Tp_S01.out	3.19E-01	3.57E-01	0.00E+00	2.08E-01	1.47E-01	0.00E+00	-4.14E-01	2.13E+00	3.00E+01
WaveVyi	Maximum	DLC1.1_0001_Sea_04.0V0_01.6Hs_08.9Tp_S01.out	3.19E-01	3.57E-01	0.00E+00	2.08E-01	1.47E-01	0.00E+00	-4.14E-01	2.13E+00	3.00E+01
WaveVzi	Minimum	DLC1.5_0583_Sea_EWSH+20.0_04.4Hs_11.3Tp_S03.out	-9.74E-01	-6.09E-01	0.00E+00	-3.73E+00	-3.09E+00	0.00E+00	2.06E-01	2.00E+01	6.73E+01
WaveVzi	Maximum	DLC1.5_0503_Sea_EWSH+20.0_04.4Hs_11.3Tp_S03.out	-1.46E+00	-4.25E-01	0.00E+00	3.13E+00	2.89E+00	0.00E+00	-2.66E-01	2.00E+01	7.05E+01
WaveAxi	Minimum	DLC1.5_0583_Sea_EWSH+20.0_04.4Hs_11.3Tp_S03.out	-9.74E-01	-6.09E-01	0.00E+00	-3.73E+00	-3.09E+00	0.00E+00	2.06E-01	2.00E+01	6.73E+01
WaveAxi	Maximum	DLC1.1_0100_Sea_14.0V0_03.0Hs_08.7Tp_S04.out	3.43E-01	2.46E-01	0.00E+00	2.29E+00	3.17E+00	0.00E+00	-2.29E-01	1.43E+01	1.62E+02
WaveAyi	Minimum	DLC1.1_0001_Sea_04.0V0_01.6Hs_08.9Tp_S01.out	3.19E-01	3.57E-01	0.00E+00	2.08E-01	1.47E-01	0.00E+00	-4.14E-01	2.13E+00	3.00E+01
WaveAyi	Maximum	DLC1.1_0001_Sea_04.0V0_01.6Hs_08.9Tp_S01.out	3.19E-01	3.57E-01	0.00E+00	2.08E-01	1.47E-01	0.00E+00	-4.14E-01	2.13E+00	3.00E+01
WaveAzi	Minimum	DLC1.5_0409_Sea_EWSV+14.0_03.0Hs_00.7Tp_S05.out	2.62E+00	2.75E+00	0.00E+00	-1.91E-01	-2.29E-01	0.00E+00	-3.14E+00	1.40E+01	3.03E+01
WaveAzi	Maximum	DLC1.5_0583_Sea_EWSH+20.0_04.4Hs_11.3Tp_S03.out	-4.87E+00	-3.87E+00	0.00E+00	-5.02E-01	-2.88E-01	0.00E+00	3.44E+00	2.00E+01	6.88E+01

Extreme events for Drivetrain:

Parameter	Type	File	GenPwr (kW)	GenTq (kN-m)	HSShftTq (kN-m)	GenSpeed (rpm)	RotSpeed (rpm)	WaveElev (m)	WindVxi (m/sec)	Time (sec)
GenPwr	Minimum	DLC1.1_0008_Sea_04.0V0_01.6Hs_12.7Tp_S03.out	-8.53E-02	-1.29E-03	0.00E+00	6.72E+02	6.92E+00	2.74E-01	3.94E+00	2.42E+02
GenPwr	Maximum	DLC1.3_0107_Sea_24.0V0_05.5Hs_12.7Tp_S03.out	5.34E+03	4.64E+01	0.00E+00	1.17E+03	1.20E+01	-3.46E+00	2.16E+01	5.06E+02
GenTq	Minimum	DLC1.1_0008_Sea_04.0V0_01.6Hs_12.7Tp_S03.out	-8.53E-02	-1.29E-03	0.00E+00	6.72E+02	6.92E+00	2.74E-01	3.94E+00	2.42E+02
GenTq	Maximum	DLC1.3_0004_Sea_12.0V0_02.4Hs_17.6Tp_S04.out	4.94E+03	4.75E+01	0.00E+00	1.05E+03	1.09E+01	-1.51E+00	1.11E+01	3.40E+02
HSShftTq	Minimum	DLC1.1_0001_Sea_04.0V0_01.6Hs_08.9Tp_S01.out	7.47E+00	1.13E-01	0.00E+00	6.70E+02	6.91E+00	3.19E-01	2.13E+00	3.00E+01
HSShftTq	Maximum	DLC1.1_0001_Sea_04.0V0_01.6Hs_08.9Tp_S01.out	7.47E+00	1.13E-01	0.00E+00	6.70E+02	6.91E+00	3.19E-01	2.13E+00	3.00E+01
GenSpeed	Minimum	DLC1.3_0009_Sea_04.0V0_01.6Hs_16.4Tp_S03.out	0.00E+00	0.00E+00	0.00E+00	6.39E+02	6.59E+00	2.03E-01	1.51E+00	2.33E+02
GenSpeed	Maximum	DLC1.4_0099_Sea_ECD-R+20_02.7Hs_16.4Tp_S03.out	5.09E+03	3.65E+01	0.00E+00	1.41E+03	1.46E+01	-1.18E+00	1.89E+01	6.65E+01
RotSpeed	Minimum	DLC1.3_0009_Sea_04.0V0_01.6Hs_16.4Tp_S03.out	0.00E+00	0.00E+00	0.00E+00	6.39E+02	6.58E+00	-1.44E-01	2.81E+00	2.32E+02
RotSpeed	Maximum	DLC1.4_0099_Sea_ECD-R+20_02.7Hs_16.4Tp_S03.out	5.09E+03	3.65E+01	0.00E+00	1.41E+03	1.46E+01	-1.18E+00	1.89E+01	6.65E+01

Extreme events for Blade Pitch:

Parameter	Type	File	BldPitch1 (deg)	BldPitch2 (deg)	BldPitch3 (deg)	WaveElev (m)	WindVxi (m/sec)	Time (sec)
BldPitch1	Minimum	DLC1.3_0104_Sea_14.0V0_03.0Hs_12.0Tp_S05.out	-4.40E-02	-4.40E-02	-4.40E-02	5.07E-01	1.21E+01	9.20E+01
BldPitch1	Maximum	DLC1.3_0189_Sea_24.0V0_05.5Hs_15.5Tp_S03.out	2.96E+01	2.96E+01	2.96E+01	6.86E-01	3.33E+01	3.25E+02
BldPitch2	Minimum	DLC1.3_0104_Sea_14.0V0_03.0Hs_12.0Tp_S05.out	-4.40E-02	-4.40E-02	-4.40E-02	5.07E-01	1.21E+01	9.20E+01
BldPitch2	Maximum	DLC1.3_0189_Sea_24.0V0_05.5Hs_15.5Tp_S03.out	2.96E+01	2.96E+01	2.96E+01	6.86E-01	3.33E+01	3.25E+02
BldPitch3	Minimum	DLC1.3_0104_Sea_14.0V0_03.0Hs_12.0Tp_S05.out	-4.40E-02	-4.40E-02	-4.40E-02	5.07E-01	1.21E+01	9.20E+01
BldPitch3	Maximum	DLC1.3_0189_Sea_24.0V0_05.5Hs_15.5Tp_S03.out	2.96E+01	2.96E+01	2.96E+01	6.86E-01	3.33E+01	3.25E+02

Extreme events for Nacelle Yaw:

Parameter	Type	File	NacYaw (deg)	NacYawErr (deg)	WaveElev (m)	WindVxi (m/sec)	Time (sec)
NacYaw	Minimum	DLC1.3_0189_Sea_24.0V0_05.5Hs_18.3Tp_S03.out	-6.53E-02	5.49E+00	-7.36E-02	3.00E+01	2.77E+02
NacYaw	Maximum	DLC1.4_0081_Sea_ECD-R_02.4Hs_17.6Tp_S03.out	6.01E-02	5.82E+01	-7.08E-02	1.19E+01	7.78E+01
NacYawErr	Minimum	DLC1.3_0001_Sea_04.0V0_01.6Hs_08.9Tp_S01.out	-1.64E-03	-2.22E+02	2.45E-01	-8.09E-01	3.14E+01
NacYawErr	Maximum	DLC1.3_0004_Sea_04.0V0_01.6Hs_00.9Tp_S02.out	-5.14E-03	2.23E+02	-2.16E-01	-8.26E-01	3.22E+02

Extreme events for Blade 1 Defl:

Parameter	Type	File	OoPDefl1 (m)	IPDefl1 (m)	TwstDefl1 (deg)	WaveElev (m)	WindVxi (m/sec)	Time (sec)
OoPDefl1	Minimum	DLC1.3_0187_Sea_24.0V0_05.5Hs_12.7Tp_S03.out	-3.71E+00	1.59E+00	0.00E+00	9.29E-01	3.03E+01	2.78E+02
OoPDefl1	Maximum	DLC1.4_0028_Sea_ECD+R_02.4Hs_09.2Tp_S04.out	1.17E+01	-1.08E+00	0.00E+00	-1.27E+00	1.19E+01	7.88E+01
IPDefl1	Minimum	DLC1.3_0183_Sea_24.0V0_05.5Hs_10.3Tp_S01.out	3.65E+00	-2.49E+00	0.00E+00	-2.08E+00	2.60E+01	5.67E+02
IPDefl1	Maximum	DLC1.3_0190_Sea_24.0V0_05.5Hs_12.7Tp_S04.out	-3.48E+00	2.43E+00	0.00E+00	9.57E-01	2.90E+01	5.48E+02
TwstDefl1	Minimum	DLC1.1_0001_Sea_04.0V0_01.6Hs_00.9Tp_S01.out	1.00E+00	-9.51E-02	0.00E+00	3.19E-01	2.13E+00	3.00E+01
TwstDefl1	Maximum	DLC1.1_0001_Sea_04.0V0_01.6Hs_08.9Tp_S01.out	1.00E+00	-9.51E-02	0.00E+00	3.19E-01	2.13E+00	3.00E+01

Extreme events for Blade 2 Defl:

Parameter	Type	File	OoPDefl2 (m)	IPDefl2 (m)	TwstDefl2 (deg)	WaveElev (m)	WindVxi (m/sec)	Time (sec)
OoPDefl2	Minimum	DLC1.3_0169_Sea_22.0V0_04.7Hs_11.0Tp_S03.out	-4.32E+00	2.33E+00	0.00E+00	1.36E+00	2.33E+01	3.03E+02
OoPDefl2	Maximum	DLC1.4_0082_Sea_ECD-R_02.4Hs_09.2Tp_S04.out	1.18E+01	-1.95E+00	0.00E+00	-4.21E-01	1.19E+01	8.95E+01
IPDefl2	Minimum	DLC1.4_0085_Sea_ECD-R_02.4Hs_09.2Tp_S05.out	1.03E+01	-2.56E+00	0.00E+00	9.51E-01	1.19E+01	7.95E+01
IPDefl2	Maximum	DLC1.3_0184_Sea_24.0V0_05.5Hs_12.7Tp_S02.out	-3.53E+00	2.57E+00	0.00E+00	-2.99E+00	3.24E+01	3.13E+02
TwstDefl2	Minimum	DLC1.1_0001_Sea_04.0V0_01.6Hs_08.9Tp_S01.out	8.16E-01	3.60E-01	0.00E+00	3.19E-01	2.13E+00	3.00E+01
TwstDefl2	Maximum	DLC1.1_0001_Sea_04.0V0_01.6Hs_08.9Tp_S01.out	8.16E-01	3.60E-01	0.00E+00	3.19E-01	2.13E+00	3.00E+01

Extreme events for Blade 3 Defl:

Parameter	Type	File	OoPDefl3 (m)	IPDefl3 (m)	TwstDefl3 (deg)	WaveElev (m)	WindVxi (m/sec)	Time (sec)
OoPDefl3	Minimum	DLC1.3_0190_Sea_24.0V0_05.5Hs_12.7Tp_S04.out	-5.16E+00	2.98E+00	0.00E+00	1.48E+00	2.98E+01	5.50E+02
OoPDefl3	Maximum	DLC1.4_0088_Sea_ECD-R_02.4Hs_09.2Tp_S06.out	1.24E+01	-2.00E+00	0.00E+00	3.13E-01	1.19E+01	7.78E+01
IPDefl3	Minimum	DLC1.3_0181_Sea_24.0V0_05.5Hs_12.7Tp_S01.out	4.20E+00	-2.50E+00	0.00E+00	1.47E+00	2.00E+01	3.21E+02
IPDefl3	Maximum	DLC1.3_0190_Sea_24.0V0_05.5Hs_12.7Tp_S04.out	-5.09E+00	3.01E+00	0.00E+00	1.48E+00	3.02E+01	5.50E+02
TwstDefl3	Minimum	DLC1.1_0001_Sea_04.0V0_01.6Hs_00.9Tp_S01.out	1.12E+00	-4.69E-01	0.00E+00	3.19E-01	2.13E+00	3.00E+01
TwstDefl3	Maximum	DLC1.1_0001_Sea_04.0V0_01.6Hs_08.9Tp_S01.out	1.12E+00	-4.69E-01	0.00E+00	3.19E-01	2.13E+00	3.00E+01

Extreme events for Blade Clrnc:

Parameter	Type	File	BldClrnc1 (m)	BldClrnc2 (m)	BldClrnc3 (m)	Azimuth (deg)	WaveElev (m)	WindVxi (m/sec)	Time (sec)
BldClrnc1	Minimum	DLC1.4_0028_Sea_ECD+R_02.4Hs_09.2Tp_S04.out	-5.07E+00	5.36E+00	2.57E+00	2.64E+02	-1.27E+00	1.19E+01	7.88E+01
BldClrnc1	Maximum	DLC1.3_0187_Sea_24.0V0_05.5Hs_12.7Tp_S03.out	1.55E+01	1.24E+01	1.01E+01	7.46E+01	9.29E-01	3.03E+01	2.78E+02
BldClrnc2	Minimum	DLC1.4_0082_Sea_ECD-R_02.4Hs_09.2Tp_S04.out	1.62E+00	-5.19E+00	5.53E+00	3.23E+02	-4.21E-01	1.19E+01	8.95E+01
BldClrnc2	Maximum	DLC1.3_0169_Sea_22.0V0_04.7Hs_11.0Tp_S03.out	9.45E+00	1.63E+01	9.05E+00	1.09E+02	1.36E+00	2.33E+01	3.03E+02
BldClrnc3	Minimum	DLC1.4_0088_Sea_ECD-R_02.4Hs_09.2Tp_S06.out	5.96E+00	2.11E+00	-6.04E+00	2.01E+02	3.13E-01	1.19E+01	7.78E+01
BldClrnc3	Maximum	DLC1.3_0190_Sea_24.0V0_05.5Hs_12.7Tp_S04.out	9.99E+00	1.15E+01	1.75E+01	3.33E+02	1.48E+00	2.98E+01	5.50E+02

Extreme events for Nacelle Acc:

Parameter	Type	File	NclMUTAxs (m/sec^2)	NclMUTAys (m/sec^2)	NclMUTAzs (m/sec^2)	NclMUTAMag (m/sec^2)	WaveElev (m)	WindVxi (m/sec)	Time (sec)
NclMUTAxs	Minimum	DLC1.3_0163_Sea_22.0V0_04.7Hs_11.0Tp_S01.out	-2.12E+00	-1.14E-01	-4.45E-01	2.16E+00	1.74E+00	2.31E+01	5.41E+02
NclMUTAxs	Maximum	DLC1.3_0169_Sea_22.0V0_04.7Hs_11.0Tp_S03.out	2.13E+00	-1.31E-01	2.88E-01	2.16E+00	-1.16E+00	2.11E+01	8.15E+01
NclMUTAys	Minimum	DLC1.3_0196_Sea_24.0V0_05.5Hs_12.7Tp_S06.out	-9.11E-01	-1.05E+00	-3.04E-01	1.43E+00	2.91E+00	3.05E+01	2.75E+02
NclMUTAys	Maximum	DLC1.3_0196_Sea_24.0V0_05.5Hs_12.7Tp_S06.out	8.99E-01	9.95E-01	1.72E-01	1.26E+00	2.91E+00	2.52E+01	2.77E+02
NclMUTAzs	Minimum	DLC1.3_0195_Sea_24.0V0_05.5Hs_18.3Tp_S05.out	-9.49E-01	-2.08E-01	-5.75E-01	1.13E+00	1.35E+00	2.66E+01	3.95E+02
NclMUTAzs	Maximum	DLC1.3_0195_Sea_24.0V0_05.5Hs_18.3Tp_S05.out	1.13E+00	-2.53E-01	5.91E-01	1.29E+00	-1.59E+00	2.67E+01	3.33E+01
NclMUTAMag	Minimum	DLC1.1_0159_Sea_20.0V0_04.4Hs_16.9Tp_S05.out	-3.26E-04	-1.75E-02	3.17E-03	-7.02E-03	1.39E+00	1.98E+01	6.19E+02
NclMUTAMag	Maximum	DLC1.3_0163_Sea_22.0V0_04.7Hs_11.0Tp_S01.out	-2.12E+00	-1.14E-01	-4.45E-01	2.16E+00	1.74E+00	2.31E+01	5.41E+02

Extreme events for TwrTop Disp:

Parameter	Type	File	TTDspFA (m)	TTDspSS (m)	TTDspTwst (deg)	WaveElev (m)	WindVxi (m/sec)	Time (sec)
TTDspFA	Minimum	DLC1.3_0169_Sea_22.0V0_04.7Hs_11.0Tp_S03.out	-4.20E-01	-2.99E-02	0.00E+00	-1.10E+00	2.10E+01	8.16E+01
TTDspFA	Maximum	DLC1.3_0142_Sea_18.0V0_03.7Hs_10.1Tp_S06.out	7.88E-01	-6.29E-02	0.00E+00	-3.42E-01	1.60E+01	1.01E+02
TTDspSS	Minimum	DLC1.3_0190_Sea_24.0V0_05.5Hs_12.7Tp_S04.out	7.13E-02	-2.43E-01	0.00E+00	-2.03E+00	2.32E+01	6.04E+02
TTDspSS	Maximum	DLC1.3_0187_Sea_24.0V0_05.5Hs_12.7Tp_S03.out	6.89E-02	1.58E-01	0.00E+00	2.44E+00	2.96E+01	2.80E+02
TTDspTwst	Minimum	DLC1.1_0001_Sea_04.0V0_01.6Hs_08.9Tp_S01.out	7.03E-02	2.75E-04	0.00E+00	3.19E-01	2.13E+00	3.00E+01
TTDspTwst	Maximum	DLC1.1_0001_Sea_04.0V0_01.6Hs_08.9Tp_S01.out	7.03E-02	2.75E-04	0.00E+00	3.19E-01	2.13E+00	3.00E+01

Extreme events for Platform Dsp:

Parameter	Type	File	PtfmSurge (m)	PtfmSway (m)	PtfmHeave (m)	PtfmRoll (deg)	PtfmPitch (deg)	PtfmYaw (deg)	WaveElev (m)	WindVxi (m/sec)	Time (sec)
PtfmSurge	Minimum	DLC1.5_0781_Sea_EWSV-24.0_05.5Hs_12.7Tp_S03.out	-8.31E+00	-1.57E-01	-2.19E-01	1.52E-02	1.20E-01	-5.33E-01	2.37E-02	2.40E+01	4.63E+01
PtfmSurge	Maximum	DLC1.5_0774_Sea_EWSV+24.0_05.5Hs_18.3Tp_S06.out	1.12E+01	-1.55E-01	-2.85E-01	-5.69E-03	1.55E-01	-8.51E-02	-9.26E-01	2.40E+01	4.28E+01
PtfmSway	Minimum	DLC1.3_0192_Sea_24.0V0_05.5Hs_18.3Tp_S04.out	2.22E+00	-1.34E+00	-3.20E-02	7.13E-02	1.56E-01	1.42E+00	-7.14E-01	2.05E+01	5.32E+02
PtfmSway	Maximum	DLC1.3_0192_Sea_24.0V0_05.5Hs_10.3Tp_S04.out	3.00E+00	9.75E-01	-2.25E-02	-2.45E-02	-1.12E-01	-1.91E-01	9.95E-02	1.90E+01	5.00E+02
PtfmHeave	Minimum	DLC1.5_0774_Sea_EWSV+24.0_05.5Hs_18.3Tp_S06.out	1.11E+01	-1.53E-01	-4.57E-01	1.00E-02	1.58E-01	-8.05E-02	-1.10E+00	2.40E+01	4.35E+01
PtfmHeave	Maximum	DLC1.1_0109_Sea_24.0V0_05.5Hs_10.3Tp_S03.out	-4.88E-01	-1.13E-01	9.14E-02	1.33E-02	5.44E-02	-2.01E-01	4.22E+00	2.05E+01	8.12E+01
PtfmRoll	Minimum	DLC1.4_0102_Sea_ECD-R+20_02.7Hs_16.4Tp_S04.out	4.70E+00	6.00E-01	-8.94E-02	-2.20E-01	6.62E-02	-5.23E+00	-1.88E+00	1.69E+01	9.23E+01
PtfmRoll	Maximum	DLC1.4_0093_Sea_ECD-R+20_02.7Hs_16.4Tp_S01.out	5.70E+00	7.37E-01	-1.15E-01	2.10E-01	1.93E-01	5.68E+00	3.88E-01	1.68E+01	8.95E+01
PtfmPitch	Minimum	DLC1.3_0187_Sea_24.0V0_05.5Hs_12.7Tp_S03.out	1.95E+00	-4.15E-01	-2.37E-02	-1.87E-02	-4.54E-01	6.10E-01	-5.47E-01	2.39E+01	6.19E+02
PtfmPitch	Maximum	DLC1.5_0583_Sea_EWSH+20.0_04.4Hs_11.3Tp_S03.out	2.38E+00	-5.90E-02	-2.09E-02	-7.59E-03	6.76E-01	-1.12E+00	-6.75E-01	2.00E+01	7.08E+01
PtfmYaw	Minimum	DLC1.4_0092_Sea_ECD-R+20_02.7Hs_12.7Tp_S01.out	3.74E+00	6.42E-01	-6.52E-02	-2.13E-01	2.20E-02	-6.49E+00	-7.47E-02	1.68E+01	8.34E+01
PtfmYaw	Maximum	DLC1.4_0092_Sea_ECD-R+20_02.7Hs_12.7Tp_S01.out	5.24E+00	7.50E-01	-1.02E-01	2.00E-01	2.70E-01	6.04E+00	5.28E-01	1.68E+01	8.92E+01

Extreme events for Platform Acc:

Parameter	Type	File	PtfmTAxt (m/sec^2)	PtfmTAyt (m/sec^2)	PtfmTAzt (m/sec^2)	PtfmTAMag (m/sec^2)	WaveElev (m)	WindVxi (m/sec)	Time (sec)
PtfmTAxt	Minimum	DLC1.3_0196_Sea_24.0V0_05.5Hs_12.7Tp_S06.out	-1.16E+00	-2.22E-01	5.75E-02	1.18E+00	-1.35E+00	3.10E+01	2.70E+02
PtfmTAxt	Maximum	DLC1.3_0196_Sea_24.0V0_05.5Hs_12.7Tp_S06.out	1.31E+00	2.83E-01	-2.41E-02	1.34E+00	-1.46E+00	2.91E+01	2.74E+02
PtfmTAyt	Minimum	DLC1.3_0165_Sea_22.0V0_04.7Hs_15.7Tp_S01.out	2.60E-01	-4.04E-01	2.27E-02	4.79E-01	8.27E-01	1.83E+01	3.41E+02
PtfmTAyt	Maximum	DLC1.3_0165_Sea_22.0V0_04.7Hs_15.7Tp_S01.out	-8.14E-02	4.00E-01	-3.26E-02	4.07E-01	-2.51E-01	1.98E+01	3.37E+02
PtfmTAzt	Minimum	DLC1.5_0774_Sea_EWSV+24.0_05.5Hs_18.3Tp_S06.out	7.10E-02	-2.53E-02	-4.63E-01	4.88E-01	8.11E-01	2.40E+01	3.09E+01
PtfmTAzt	Maximum	DLC1.5_0774_Sea_EWSV+24.0_05.5Hs_10.3Tp_S06.out	-2.64E-01	-1.04E-02	4.97E-01	5.55E-01	-1.39E-01	2.40E+01	4.11E+01
PtfmTAMag	Minimum	DLC1.3_0051_Sea_08.0V0_01.8Hs_17.4Tp_S05.out	-1.03E-03	-1.00E-03	-7.39E-04	-9.58E-04	-3.84E-01	9.53E+00	3.75E+02
PtfmTAMag	Maximum	DLC1.3_0196_Sea_24.0V0_05.5Hs_12.7Tp_S06.out	1.31E+00	2.83E-01	-2.41E-02	1.34E+00	-1.46E+00	2.91E+01	2.74E+02

Extreme events for Blade 1 Root:

Parameter	Type	File	RootFxc1 (kN)	RootFyc1 (kN)	RootFzc1 (kN)	RootMxc1 (kN-m)	RootMyc1 (kN-m)	RootMzc1 (kN-m)	RootFmxy1 (kN)	RootMmxy1 (kN-m)	WaveElev (m)	WindVx1 (m/sec)	Time (sec)
RootFxc1	Minimum	DLC1.4_0039_Sea_ECD+R+20_02.7Hs_16.4Tp_S01.out	-2.65E+02	1.04E+02	1.11E+03	-1.63E+03	-7.06E+03	-3.29E+09	2.87E+02	7.25E+03	7.95E-02	1.68E+01	8.13E+01
RootFxc1	Maximum	DLC1.4_0024_Sea_ECD+R_02.4Hs_09.2Tp_S06.out	7.02E+02	9.43E+01	7.30E+02	7.51E+02	2.63E+04	7.96E+01	7.08E+02	2.63E+04	7.43E-01	1.19E+01	7.98E+01
RootFyc1	Minimum	DLC1.1_0192_Sea_24.0V0_05.5Hs_18.3Tp_S04.out	1.83E+02	-4.88E+02	8.92E+02	1.10E+04	3.18E+03	-1.13E+02	5.21E+02	1.14E+04	1.35E+00	2.72E+01	8.97E+01
RootFyc1	Maximum	DLC1.1_0198_Sea_24.0V0_05.5Hs_18.3Tp_S06.out	4.99E+01	2.80E+02	1.03E+03	-6.91E+03	-5.74E+02	-1.50E+02	2.84E+02	6.93E+03	1.36E-01	2.61E+01	6.14E+02
RootFzc1	Minimum	DLC1.3_0009_Sea_04.0V0_01.6Hs_16.4Tp_S03.out	3.23E+01	-2.43E+00	1.59E+01	4.52E+01	1.43E+03	-2.55E+01	3.24E+01	1.43E+03	-1.54E-01	2.27E+00	2.26E+02
RootFzc1	Maximum	DLC1.1_0193_Sea_24.0V0_05.5Hs_12.7Tp_S05.out	3.92E+01	-8.11E+00	1.48E+03	-6.99E+01	-7.88E+09	-1.50E+09	4.00E+01	7.91E+09	-1.60E+00	9.13E+01	1.07E+09
RootMxc1	Minimum	DLC1.1_0187_Sea_24.0V0_05.5Hs_12.7Tp_S03.out	4.27E+01	2.77E+02	9.32E+02	-7.23E+03	-1.30E+03	-1.54E+02	2.81E+02	7.34E+03	1.61E+00	2.53E+01	5.94E+02
RootMxc1	Maximum	DLC1.3_0183_Sea_24.0V0_05.5Hs_18.3Tp_S01.out	3.94E+02	-4.62E+02	9.21E+02	1.15E+04	1.18E+04	-9.19E+01	6.08E+02	1.64E+04	-2.10E+00	2.67E+01	5.66E+02
RootMyc1	Minimum	DLC1.4_0099_Sea_ECD-R+20_02.7Hs_16.4Tp_S03.out	-2.41E+02	-1.17E+02	7.26E+02	2.15E+03	-9.55E+03	-1.96E+02	2.68E+02	9.70E+03	-1.57E+00	1.70E+01	6.92E+01
RootMyc1	Maximum	DLC1.4_0028_Sea_ECD+R_02.4Hs_09.2Tp_S04.out	6.92E+02	9.57E+01	7.32E+02	7.64E+02	2.63E+04	9.98E+01	7.00E+02	2.64E+04	-1.27E+00	1.19E+01	7.88E+01
RootMzc1	Minimum	DLC1.4_0037_Sea_ECD+R+20_02.7Hs_08.9Tp_S01.out	-2.49E+02	9.00E+01	1.15E+03	-1.26E+03	-6.44E+03	-3.57E+02	2.67E+02	6.56E+03	3.17E-01	1.68E+01	8.13E+01
RootMzc1	Maximum	DLC1.3_0112_Sea_16.0V0_03.4Hs_10.1Tp_S02.out	5.66E+02	1.49E+02	7.72E+02	-2.21E+03	1.97E+04	2.07E+02	5.86E+02	1.98E+04	-1.04E+00	1.53E+01	1.14E+02
RootFMxy1	Minimum	DLC1.3_0196_Sea_24.0V0_05.5Hs_12.7Tp_S06.out	-4.59E-01	1.47E+00	1.05E+03	-3.17E+02	-1.96E+03	-1.05E+02	-0.25E-01	1.89E+02	-1.94E+00	2.32E+01	6.00E+02
RootFMxy1	Maximum	DLC1.4_0034_Sea_ECD+R_02.4Hs_09.2Tp_S06.out	7.02E+02	9.43E+01	7.30E+02	7.51E+02	2.63E+04	7.96E+01	7.08E+02	2.63E+04	7.43E-01	1.19E+01	7.98E+01
RootMMxy1	Minimum	DLC1.1_0166_Sea_22.0V0_04.7Hs_11.0Tp_S02.out	8.99E+01	-2.18E+01	1.16E+03	-3.37E+00	-1.13E+00	-1.11E+00	9.25E+01	3.75E-01	1.51E+00	2.71E+01	2.45E+02
RootMMxy1	Maximum	DLC1.4_0028_Sea_ECD+R_02.4Hs_09.2Tp_S04.out	6.92E+02	9.57E+01	7.32E+02	7.64E+02	2.63E+04	9.98E+01	7.00E+02	2.64E+04	-1.27E+00	1.19E+01	7.88E+01

Extreme events for Blade 2 Root:

Parameter	Type	File	RootFxc2 (kN)	RootFyc2 (kN)	RootFzc2 (kN)	RootMxc2 (kN-m)	RootMyc2 (kN-m)	RootMzc2 (kN-m)	RootFmxy2 (kN)	RootMmxy2 (kN-m)	WaveElev (m)	WindVx1 (m/sec)	Time (sec)
RootFxc2	Minimum	DLC1.4_0039_Sea_ECD+R+20_02.7Hs_12.7Tp_S01.out	-2.33E+02	1.09E+02	1.03E+03	-1.95E+03	-7.40E+02	-2.44E+02	2.57E+02	7.73E+03	4.00E-02	1.60E+01	6.97E+01
RootFxc2	Maximum	DLC1.4_0078_Sea_ECD-R_02.4Hs_17.6Tp_S01.out	6.88E+02	-3.50E+02	6.69E+02	9.30E+03	2.59E+04	-1.86E+02	7.72E+02	2.75E+04	2.67E-01	1.19E+01	8.93E+01
RootFyc2	Minimum	DLC1.1_0196_Sea_24.0V0_05.5Hs_12.7Tp_S06.out	2.47E+02	-5.12E+02	9.21E+02	1.09E+04	4.51E+03	-9.26E+01	5.69E+02	1.18E+04	1.51E-01	2.76E+01	5.94E+02
RootFyc2	Maximum	DLC1.1_0189_Sea_24.0V0_05.5Hs_18.3Tp_S03.out	2.90E+01	2.86E+02	9.56E+02	-9.22E+03	-1.40E+03	-1.40E+02	2.87E+02	7.40E+03	5.41E-01	2.53E+01	5.92E+02
RootFzc2	Minimum	DLC1.3_0009_Sea_04.0V0_01.6Hs_16.4Tp_S03.out	5.33E+01	-1.10E+01	1.67E+01	2.76E+02	2.31E+03	-1.42E+01	5.43E+01	2.33E+03	-9.64E-02	2.97E+00	2.32E+02
RootFzc2	Maximum	DLC1.1_0177_Sea_22.0V0_04.7Hs_15.7Tp_S05.out	1.96E+02	-0.13E+01	1.50E+03	1.50E+03	3.66E+03	-1.35E+02	2.11E+02	3.99E+03	-3.90E-01	2.52E+01	1.64E+02
RootMxc2	Minimum	DLC1.3_0188_Sea_24.0V0_05.5Hs_15.5Tp_S03.out	-1.45E+01	2.82E+02	8.82E+02	-7.41E+03	-2.97E+03	-1.50E+02	2.83E+02	7.95E+03	-1.25E-01	2.56E+01	5.92E+02
RootMxc2	Maximum	DLC1.1_0187_Sea_24.0V0_05.5Hs_12.7Tp_S03.out	4.49E+02	-4.82E+02	8.81E+02	1.11E+04	1.21E+04	-6.67E+01	6.59E+02	1.64E+04	1.92E-01	2.78E+01	5.99E+02
RootMyc2	Minimum	DLC1.3_0190_Sea_24.0V0_05.5Hs_12.7Tp_S04.out	-1.41E+02	9.17E+01	1.13E+03	-3.54E+03	-7.92E+03	-8.78E+01	1.68E+02	8.56E+03	1.87E+00	2.96E+01	5.51E+02
RootMyc2	Maximum	DLC1.4_0082_Sea_ECD-R_02.4Hs_09.2Tp_S04.out	6.80E+02	-3.63E+02	6.78E+02	9.88E+03	2.59E+04	-2.58E+02	7.71E+02	2.77E+04	-4.21E-01	1.19E+01	8.95E+01
RootMzc2	Minimum	DLC1.4_0039_Sea_ECD+R+20_02.7Hs_16.4Tp_S01.out	-8.93E+01	6.20E+01	1.26E+03	-9.20E+02	-2.27E+03	-3.68E+02	1.09E+02	2.45E+03	1.57E-02	1.68E+01	7.98E+01
RootMzc2	Maximum	DLC1.3_0120_Sea_16.0V0_03.4Hs_16.7Tp_S04.out	5.08E+02	1.71E+02	8.15E+02	-2.40E+03	1.83E+04	2.05E+02	5.36E+02	1.84E+04	2.91E-01	1.28E+01	2.46E+02
RootFMxy2	Minimum	DLC1.3_0197_Sea_24.0V0_05.5Hs_15.5Tp_S06.out	1.00E+00	4.51E-01	1.15E+03	-4.98E+01	-2.12E+03	-1.97E+09	-2.60E+00	9.19E+03	2.14E+00	9.62E+01	1.05E+09
RootFMxy2	Maximum	DLC1.4_0079_Sea_ECD-R_02.4Hs_17.6Tp_S02.out	6.79E+02	-3.84E+02	7.41E+02	1.02E+04	2.57E+04	-2.35E+02	7.79E+02	2.76E+04	7.95E-01	1.19E+01	8.95E+01
RootMMxy2	Minimum	DLC1.3_0178_Sea_22.0V0_04.7Hs_11.0Tp_S06.out	2.71E+01	5.85E+00	1.17E+03	4.10E+01	-1.05E+02	-1.22E+02	2.72E+01	-2.38E+01	2.29E+00	2.28E+01	2.34E+02
RootMMxy2	Maximum	DLC1.4_0082_Sea_ECD-R_02.4Hs_09.2Tp_S04.out	6.80E+02	-3.63E+02	6.78E+02	9.88E+03	2.59E+04	-2.58E+02	7.71E+02	2.77E+04	-4.21E-01	1.19E+01	8.95E+01

Extreme events for Blade 3 Root:

Parameter	Type	File	RootFxc3 (kN)	RootFyc3 (kN)	RootFzc3 (kN)	RootMxc3 (kN-m)	RootMyc3 (kN-m)	RootMzc3 (kN-m)	RootFmxy3 (kN)	RootMmxy3 (kN-m)	WaveElev (m)	WindVx1 (m/sec)	Time (sec)
RootFxc3	Minimum	DLC1.4_0033_Sea_ECD+R_02.4Hs_17.6Tp_S05.out	-2.21E+02	6.19E+01	1.15E+03	-6.66E+02	-5.51E+03	-3.38E+02	2.26E+02	5.57E+03	7.45E-01	1.31E+01	6.84E+01
RootFxc3	Maximum	DLC1.4_0088_Sea_ECD-R_02.4Hs_09.2Tp_S06.out	7.42E+02	-3.50E+02	6.55E+02	9.74E+03	2.78E+04	-2.83E+02	8.20E+02	2.94E+04	3.13E-01	1.19E+01	7.78E+01
RootFyc3	Minimum	DLC1.1_0181_Sea_24.0V0_05.5Hs_12.7Tp_S01.out	3.01E+02	-4.85E+02	9.33E+02	1.05E+04	7.04E+03	-8.37E+01	5.69E+02	1.26E+04	-1.85E+00	2.96E+01	2.45E+02
RootFyc3	Maximum	DLC1.1_0180_Sea_22.0V0_04.7Hs_15.7Tp_S06.out	1.51E+02	2.76E+02	1.07E+03	-6.21E+03	3.78E+03	-9.10E+01	3.15E+02	7.27E+03	-2.16E+00	1.70E+01	5.27E+02
RootFzc3	Minimum	DLC1.3_0009_Sea_04.0V0_01.6Hs_16.4Tp_S03.out	3.80E+01	-8.91E+00	1.70E+01	2.14E+02	1.79E+03	-2.22E+01	3.90E+01	1.80E+03	-1.48E-01	2.15E+00	2.29E+02
RootFzc3	Maximum	DLC1.1_0150_Sea_20.0V0_04.4Hs_16.9Tp_S02.out	1.92E+02	-6.88E+01	1.47E+03	1.20E+03	3.67E+03	-1.31E+02	1.95E+02	3.89E+03	-3.55E+00	2.28E+01	5.25E+02
RootMxc3	Minimum	DLC1.3_0187_Sea_24.0V0_05.5Hs_12.7Tp_S03.out	9.89E+01	2.64E+02	8.99E+02	-7.27E+03	4.65E+02	-1.52E+02	2.79E+02	7.29E+03	-1.90E+00	2.62E+01	5.91E+02
RootMxc3	Maximum	DLC1.1_0195_Sea_24.0V0_05.5Hs_18.3Tp_S05.out	3.13E+02	-4.73E+02	7.60E+02	1.12E+04	8.06E+03	-9.53E+01	5.65E+02	1.42E+04	-0.35E-01	2.67E+01	1.71E+02
RootMyc3	Minimum	DLC1.3_0191_Sea_24.0V0_05.5Hs_15.5Tp_S04.out	-2.07E+02	8.05E+01	1.17E+03	-3.40E+03	-1.04E+04	-6.44E+01	2.23E+02	1.09E+04	2.25E+00	2.91E+01	5.49E+02
RootMyc3	Maximum	DLC1.4_0088_Sea_ECD-R_02.4Hs_09.2Tp_S06.out	7.42E+02	-3.50E+02	6.55E+02	9.74E+03	2.78E+04	-2.83E+02	8.20E+02	2.94E+04	3.13E-01	1.19E+01	7.78E+01
RootMzc3	Minimum	DLC1.4_0023_Sea_ECD+R_02.4Hs_17.6Tp_S05.out	-2.21E+02	6.19E+01	1.15E+03	-6.66E+02	-5.51E+03	-3.38E+02	2.26E+02	5.57E+03	7.45E-01	1.31E+01	6.84E+01
RootMzc3	Maximum	DLC1.3_0143_Sea_18.0V0_02.7Hs_13.4Tp_S06.out	5.49E+02	1.69E+02	9.70E+02	-3.02E+03	1.96E+04	2.15E+02	5.72E+02	1.98E+04	-0.19E-02	1.51E+01	1.91E+02
RootFMxy3	Minimum	DLC1.3_0183_Sea_24.0V0_05.5Hs_18.3Tp_S01.out	-1.93E-02	-3.91E+01	1.05E+03	-6.45E+02	-2.67E+03	-8.02E+01	3.88E-01	2.75E+02	-9.34E-02	2.96E+01	6.84E+01
RootFMxy3	Maximum	DLC1.4_0088_Sea_ECD-R_02.4Hs_09.2Tp_S06.out	7.36E+02	-3.70E+02	6.96E+02	9.99E+03	2.74E+04	-2.60E+02	8.24E+02	2.92E+04	2.16E-01	1.19E+01	7.80E+01
RootMMxy3	Minimum	DLC1.1_0197_Sea_24.0V0_05.5Hs_15.5Tp_S06.out	5.51E+01	-1.55E+01	1.21E+02	4.68E-01	8.67E+00	-1.18E+02	5.71E+01	7.00E+00	-6.74E-01	2.05E+01	2.08E+02
RootMMxy3	Maximum	DLC1.4_0088_Sea_ECD-R_02.4Hs_09.2Tp_S06.out	7.42E+02	-3.50E+02	6.55E+02	9.74E+03	2.78E+04	-2.83E+02	8.20E+02	2.94E+04	3.13E-01	1.19E+01	7.78E+01

Extreme events for Blade 1 50%:

Parameter	Type	File	Spn1MLxb1 (kN-m)	Spn1MLyb1 (kN-m)	Spn1MLzb1 (kN-m)	Spn1MMxy1 (kN-m)	WaveKlev (m)	WindVxi (m/sec)	Time (sec)
Spn1MLxb1	Minimum	DLC1.1_0182_Sea_24.0V0_05.5Hs_15.5Tp_S01.out	-1.66E+03	3.59E+02	-6.32E+01	1.69E+03	3.03E-01	2.72E+01	8.33E+01
Spn1MLxb1	Maximum	DLC1.3_0196_Sea_24.0V0_05.5Hs_12.7Tp_S06.out	2.31E+03	-1.99E+03	-6.73E+01	2.90E+03	-6.31E-02	2.63E+01	2.64E+02
Spn1MLyb1	Minimum	DLC1.3_0190_Sea_24.0V0_05.5Hs_12.7Tp_S04.out	-2.57E+02	-2.87E+03	-1.10E+02	2.88E+03	9.05E-01	2.54E+01	5.48E+02
Spn1MLyb1	Maximum	DLC1.4_0028_Sea_ECD+R_02.4Hs_09.2Tp_S04.out	4.45E+01	7.41E+03	-7.04E+00	7.41E+03	-1.27E+00	1.19E+01	7.88E+01
Spn1MLzb1	Minimum	DLC1.4_0033_Sea_ECD+R_02.4Hs_17.6Tp_S05.out	-2.30E+01	4.93E+02	-2.01E+02	4.93E+02	1.20E+00	1.19E+01	8.22E+01
Spn1MLzb1	Maximum	DLC1.3_0114_Sea_16.0V0_03.4Hs_16.7Tp_S02.out	-1.03E+03	4.26E+03	6.23E+01	4.30E+03	-0.39E-01	1.32E+01	1.53E+02
Spn1MMxy1	Minimum	DLC1.3_0192_Sea_24.0V0_05.5Hs_15.5Tp_S01.out	1.20E+00	2.16E+00	-0.22E+01	-1.21E+00	-1.65E+00	2.64E+01	3.20E+02
Spn1MMxy1	Maximum	DLC1.4_0028_Sea_ECD+R_02.4Hs_09.2Tp_S04.out	4.45E+01	7.41E+03	-7.04E+00	7.41E+03	-1.27E+00	1.19E+01	7.88E+01

Extreme events for Blade 2 50%:

Parameter	Type	File	Spn1MLxb2 (kN-m)	Spn1MLyb2 (kN-m)	Spn1MLzb2 (kN-m)	Spn1MMxy2 (kN-m)	WaveKlev (m)	WindVxi (m/sec)	Time (sec)
Spn1MLxb2	Minimum	DLC1.1_0178_Sea_22.0V0_04.7Hs_11.0Tp_S04.out	-1.64E+03	1.81E+02	-1.99E+01	2.44E+03	7.50E-01	2.64E+01	6.22E+02
Spn1MLxb2	Maximum	DLC1.3_0197_Sea_24.0V0_05.5Hs_15.5Tp_S06.out	1.65E+03	-1.50E+03	-1.06E+02	2.29E+03	-1.32E+00	2.64E+01	2.62E+02
Spn1MLyb2	Minimum	DLC1.3_0169_Sea_22.0V0_04.7Hs_11.0Tp_S03.out	4.21E+02	-3.23E+03	-7.43E+01	3.25E+03	1.34E+00	2.41E+01	3.04E+02
Spn1MLyb2	Maximum	DLC1.4_0082_Sea_ECD-R_02.4Hs_09.2Tp_S04.out	1.31E+03	7.51E+03	-1.29E+02	7.64E+03	-4.16E-01	1.19E+01	8.94E+01
Spn1MLzb2	Minimum	DLC1.4_0033_Sea_ECD+R_02.4Hs_17.6Tp_S05.out	-3.74E+02	1.49E+02	-1.88E+02	1.53E+03	1.65E+00	1.19E+01	8.06E+01
Spn1MLzb2	Maximum	DLC1.3_0120_Sea_16.0V0_03.4Hs_16.7Tp_S04.out	-0.06E+02	4.80E+03	6.05E+01	4.97E+03	2.91E-01	1.20E+01	2.46E+02
Spn1MMxy2	Minimum	DLC1.5_0714_Sea_EWSV-22.0_04.7Hs_15.7Tp_S04.out	1.42E+00	3.95E+00	-9.23E+01	-1.79E+00	-2.22E+00	2.20E+01	5.04E+01
Spn1MMxy2	Maximum	DLC1.4_0082_Sea_ECD-R_02.4Hs_09.2Tp_S04.out	1.31E+03	7.51E+03	-1.29E+02	7.64E+03	-4.16E-01	1.19E+01	8.94E+01

Extreme events for Blade 3 50%:

Parameter	Type	File	Spn1MLxb3 (kN-m)	Spn1MLyb3 (kN-m)	Spn1MLzb3 (kN-m)	Spn1MMxy3 (kN-m)	WaveKlev (m)	WindVxi (m/sec)	Time (sec)
Spn1MLxb3	Minimum	DLC1.2_0196_Sea_24.0V0_05.5Hs_12.7Tp_S04.out	-1.70E+03	-7.38E+02	-9.06E+01	1.85E+03	2.55E+00	2.69E+01	4.81E+02
Spn1MLxb3	Maximum	DLC1.3_0109_Sea_24.0V0_05.5Hs_10.3Tp_S03.out	1.63E+03	-1.02E+03	-7.06E+01	1.91E+03	1.32E+00	3.01E+01	2.05E+02
Spn1MLyb3	Minimum	DLC1.3_0190_Sea_24.0V0_05.5Hs_12.7Tp_S04.out	7.47E+02	-3.94E+03	-7.72E+01	4.01E+03	1.40E+00	2.98E+01	5.50E+02
Spn1MLyb3	Maximum	DLC1.4_0082_Sea_ECD-R_02.4Hs_09.2Tp_S04.out	1.30E+03	7.87E+03	-1.32E+02	7.98E+03	2.57E-01	1.19E+01	7.78E+01
Spn1MLzb3	Minimum	DLC1.4_0099_Sea_ECD-R+20_02.7Hs_12.7Tp_S01.out	3.65E+02	-8.34E+02	-1.88E+02	9.11E+02	3.19E-02	1.48E+01	8.05E+01
Spn1MLzb3	Maximum	DLC1.3_0005_Sea_12.0V0_02.4Hs_09.2Tp_S05.out	-6.02E+02	4.36E+03	6.43E+01	4.43E+03	-2.63E-01	1.12E+01	3.47E+02
Spn1MMxy3	Minimum	DLC1.3_0161_Sea_20.0V0_04.4Hs_14.1Tp_S06.out	3.71E+00	1.55E+00	-8.52E+01	-3.89E+01	2.99E-01	2.37E+01	2.05E+02
Spn1MMxy3	Maximum	DLC1.4_0082_Sea_ECD-R_02.4Hs_09.2Tp_S04.out	1.30E+03	7.87E+03	-1.32E+02	7.98E+03	2.57E-01	1.19E+01	7.78E+01

Extreme events for LSS Main Br:

Parameter	Type	File	RotThrust (kN)	LSSGagFya (kN)	LSSGagFra (kN)	RotTorq (kN-m)	LSSGagMya (kN-m)	LSSGagMra (kN-m)	LSSGagFMyr (kN)	LSSGagMMyr (kN-m)	WaveElev (m)	WindVxi (m/sec)	Time (sec)
RotThrust	Minimum	DLC1.4_0021_Sea_ECD+R_02.4Hs_09.2Tp_S05.out	-1.43E+02	1.13E+03	-9.45E+02	4.31E+03	-3.09E+02	5.51E+03	1.46E+03	5.52E+03	6.17E-01	1.31E+01	6.83E+01
RotThrust	Maximum	DLC1.1_0111_Sea_16.0V0_02.4Hs_16.7Tp_S01.out	1.67E+03	-1.56E+03	-6.03E+02	6.03E+03	1.88E+03	7.57E+03	1.68E+03	7.81E+03	1.07E+00	1.33E+01	3.63E+01
LSSGagFya	Minimum	DLC1.1_0195_Sea_24.0V0_05.5Hs_18.3Tp_S05.out	3.33E+02	-1.01E+03	-4.88E+01	5.82E+03	5.10E+02	1.22E+03	1.81E+03	5.24E+03	-7.62E-01	2.65E+01	4.32E+02
LSSGagFya	Maximum	DLC1.1_0189_Sea_24.0V0_05.5Hs_10.3Tp_S03.out	2.53E+02	1.77E+03	-1.61E+02	6.16E+03	-5.27E+02	1.39E+03	1.70E+03	5.45E+03	2.42E+00	2.49E+01	5.94E+02
LSSGagFza	Minimum	DLC1.1_0169_Sea_22.0V0_04.7Hs_11.0Tp_S03.out	3.14E+02	-1.51E+02	-1.00E+03	5.76E+03	-5.93E+03	2.43E+03	1.01E+03	6.40E+03	-8.35E-02	2.53E+01	1.69E+02
LSSGagFza	Maximum	DLC1.1_0195_Sea_24.0V0_05.5Hs_18.3Tp_S05.out	4.56E+02	5.84E+01	1.78E+03	5.79E+03	-1.40E+03	-5.52E+03	1.79E+03	5.69E+03	-8.24E-01	2.63E+01	1.71E+02
RotTorq	Minimum	DLC1.3_0009_Sea_04.0V0_01.6Hs_08.9Tp_S03.out	8.10E+01	-1.16E+02	1.47E+03	-6.43E+01	4.65E+03	-3.36E+09	1.47E+03	4.64E+03	1.73E-01	9.90E-01	1.95E+02
RotTorq	Maximum	DLC1.1_0187_Sea_24.0V0_05.5Hs_12.7Tp_S03.out	9.56E+02	-1.33E+03	8.77E+02	8.22E+03	1.33E+03	4.11E+03	1.60E+03	4.32E+03	-3.81E-01	2.07E+01	3.49E+02
LSSGagMya	Minimum	DLC1.4_0099_Sea_ECD-R+20_02.7Hs_16.4Tp_S03.out	-9.33E+01	-7.46E+02	-1.27E+03	4.47E+03	-1.56E+04	2.23E+03	1.47E+03	1.57E+04	-1.57E+00	1.70E+01	6.92E+01
LSSGagMya	Maximum	DLC1.4_0033_Sea_ECD+R_02.4Hs_17.6Tp_S05.out	1.21E+03	8.97E+02	1.04E+03	5.80E+03	1.64E+04	-8.07E+03	1.37E+03	1.82E+04	5.94E-01	1.19E+01	7.80E+01
LSSGagMza	Minimum	DLC1.4_0092_Sea_ECD-R+20_02.7Hs_12.7Tp_S01.out	-3.07E+01	1.42E+03	-1.02E+02	4.77E+03	3.92E+03	-1.35E+04	1.42E+03	1.40E+04	-2.91E-01	1.60E+01	0.25E+01
LSSGagMza	Maximum	DLC1.4_0036_Sea_ECD+R_02.4Hs_17.6Tp_S06.out	1.17E+03	-1.24E+03	4.98E+02	4.22E+03	5.14E+02	1.61E+04	1.34E+03	1.41E+04	-7.35E-01	1.19E+01	7.47E+01
LSSGagFMyr	Minimum	DLC1.3_0185_Sea_24.0V0_05.5Hs_15.5Tp_S02.out	4.45E+02	-9.19E+02	-6.64E+02	5.72E+03	-2.90E+03	-5.72E+03	1.13E+03	6.41E+03	2.42E-01	2.98E+01	5.65E+02
LSSGagFMyr	Maximum	DLC1.1_0196_Sea_24.0V0_05.5Hs_12.7Tp_S06.out	3.95E+02	9.91E+02	-1.54E+03	6.77E+03	-7.25E+03	2.99E+03	1.84E+03	7.26E+03	1.43E-01	2.77E+01	5.94E+02
LSSGagMMyr	Minimum	DLC1.5_0626_Sea_EWSV+20.0_0.4Hs_14.1Tp_S05.out	6.62E+02	-1.33E+03	-5.97E+02	5.45E+03	-1.99E+01	8.70E+01	1.46E+03	-3.39E+01	+4.23E-01	2.00E+01	5.05E+01
LSSGagMMyr	Maximum	DLC1.4_0036_Sea_ECD+R_02.4Hs_17.6Tp_S06.out	1.22E+03	1.06E+03	8.10E+02	6.07E+03	1.60E+04	-9.40E+03	1.34E+03	1.84E+04	-9.15E-01	1.19E+01	7.83E+01

Extreme events for Yaw Bearing:

Parameter	Type	File	YawBrFxp (kN)	YawBrFyp (kN)	YawBrFzp (kN)	YawBrMxp (kN-m)	YawBrMyp (kN-m)	YawBrMzp (kN-m)	YawBrFMxy (kN)	YawBrMMxy (kN-m)	WaveElev (m)	WindVxi (m/sec)	Time (sec)
YawBrFxp	Minimum	DLC1.3_0169_Sea_22.0V0_04.7Hs_11.0Tp_S03.out	-8.56E+02	6.71E+01	-4.65E+03	4.45E+03	-3.44E+03	-2.56E+03	8.60E+02	5.63E+03	-1.16E+00	2.11E+01	8.15E+01
YawBrFxp	Maximum	DLC1.1_0124_Sea_16.0V0_03.4Hs_10.1Tp_S06.out	1.96E+03	2.02E+01	-5.27E+03	4.71E+03	9.27E+02	-2.33E+02	1.96E+03	4.81E+03	7.85E-02	1.10E+01	9.10E+01
YawBrFyp	Minimum	DLC1.3_0196_Sea_24.0V0_05.5Hs_12.7Tp_S06.out	2.61E+02	-4.75E+02	-4.69E+03	6.91E+03	4.71E+03	1.58E+03	5.43E+02	8.36E+03	3.59E-01	9.14E+01	6.20E+02
YawBrFyp	Maximum	DLC1.3_0187_Sea_24.0V0_05.5Hs_12.7Tp_S03.out	2.65E+02	4.97E+02	-4.49E+03	4.21E+03	-3.96E+03	-7.65E+03	5.63E+02	5.70E+03	2.46E+00	2.94E+01	2.00E+02
YawBrFzp	Minimum	DLC1.1_0195_Sea_24.0V0_05.5Hs_18.3Tp_S05.out	6.06E+02	7.71E+01	-5.44E+03	6.73E+03	-3.10E+03	1.42E+03	6.10E+02	7.41E+03	-5.87E-01	2.58E+01	4.08E+02
YawBrFzp	Maximum	DLC1.3_0189_Sea_24.0V0_05.5Hs_10.3Tp_S03.out	1.55E+02	-1.71E+02	-4.33E+03	4.09E+03	-2.29E+03	-1.19E+04	2.31E+02	4.69E+03	1.14E-01	3.01E+01	2.78E+02
YawBrMxp	Minimum	DLC1.3_0015_Sea_04.0V0_01.6Hs_16.4Tp_S05.out	1.92E+02	1.09E+01	-4.63E+03	-2.20E+02	-1.54E+03	-2.50E+03	1.92E+02	1.55E+03	-5.11E-01	5.77E-01	4.83E+02
YawBrMxp	Maximum	DLC1.1_0127_Sea_18.0V0_03.7Hs_10.1Tp_S01.out	5.09E+02	-2.76E+02	-5.25E+03	8.57E+03	3.70E+03	5.57E+03	5.79E+02	9.32E+03	-2.36E-01	1.85E+01	5.49E+02
YawBrMyp	Minimum	DLC1.4_0019_Sea_ECD+R_02.4Hs_09.2Tp_S01.out	9.33E+02	-1.32E+02	-4.62E+02	5.18E+03	-1.41E+04	-5.50E+03	9.42E+02	1.50E+04	-1.07E+00	1.19E+01	7.82E+01
YawBrMyp	Maximum	DLC1.4_0005_Sea_ECD-R_02.4Hs_09.2Tp_S05.out	1.42E+03	6.60E+01	-4.75E+03	6.10E+03	1.75E+04	4.40E+03	1.42E+03	1.85E+04	9.03E-01	1.19E+01	7.90E+01
YawBrMzp	Minimum	DLC1.3_0189_Sea_24.0V0_05.5Hs_18.3Tp_S03.out	-4.98E+00	-6.88E+00	-4.38E+02	4.14E+03	-2.64E+03	-1.39E+04	4.31E+00	4.91E+03	-7.36E-02	3.00E+01	2.77E+02
YawBrMzp	Maximum	DLC1.4_0081_Sea_ECD-R_02.4Hs_17.6Tp_S03.out	1.40E+03	1.15E+02	-4.95E+03	6.75E+03	7.85E+03	1.20E+04	1.40E+03	1.04E+04	-7.08E-02	1.19E+01	7.78E+01
YawBrFMxy	Minimum	DLC1.3_0176_Sea_22.0V0_04.7Hs_13.4Tp_S05.out	-1.59E+00	-2.63E+00	-4.59E+03	4.05E+03	-3.79E+01	-1.58E+03	-9.56E-09	4.05E+03	-6.17E-01	9.71E+01	5.67E+02
YawBrFMxy	Maximum	DLC1.1_0124_Sea_16.0V0_03.4Hs_10.1Tp_S06.out	1.96E+03	2.02E+01	-5.27E+03	4.71E+03	9.27E+02	-2.33E+02	1.96E+03	4.81E+03	7.85E-02	1.10E+01	9.10E+01
YawBrMMxy	Minimum	DLC1.3_0006_Sea_04.0V0_01.6Hs_16.4Tp_S02.out	9.16E+01	-2.03E+00	-4.64E+03	1.04E+01	-3.58E+00	-3.60E+02	9.16E+01	-4.10E+00	5.62E-01	1.11E+00	3.08E+02
YawBrMMxy	Maximum	DLC1.4_0005_Sea_ECD-R_02.4Hs_09.2Tp_S05.out	1.42E+03	6.60E+01	-4.75E+03	6.10E+03	1.75E+04	4.40E+03	1.42E+03	1.85E+04	9.03E-01	1.19E+01	7.90E+01

Extreme events for Tower Base:

Parameter	Type	File	TwrBsFxt (kN)	TwrBsFyt (kN)	TwrBsFzt (kN)	TwrBsMxt (kN-m)	TwrBsMyt (kN-m)	TwrBsMzt (kN-m)	TwrBsFMxy (kN)	TwrBsMMxy (kN-m)	WaveElev (m)	WindVxi (m/sec)	Time (sec)
TwrBsFxt	Minimum	DLC1.3_0169_Sea_22.0V0_04.7Hs_11.0Tp_S03.out	-1.19E+03	6.38E+00	-9.27E+03	3.09E+03	-9.33E+04	-2.18E+03	1.19E+03	9.74E+04	-1.10E+00	2.10E+01	8.16E+01
TwrBsFxt	Maximum	DLC1.1_0124_Sea_16.0V0_03.4Hs_10.1Tp_S06.out	2.28E+03	5.53E+00	-1.04E+04	4.61E+03	1.91E+05	6.74E+02	2.28E+03	1.91E+05	9.49E-02	1.14E+01	9.10E+01
TwrBsFyt	Minimum	DLC1.3_0190_Sea_24.0V0_05.5Hs_12.7Tp_S04.out	-9.30E+01	-5.33E+02	-9.10E+03	4.60E+04	1.24E+04	-1.90E+03	5.44E+02	4.04E+04	-1.34E+00	2.27E+01	5.95E+02
TwrBsFyt	Maximum	DLC1.3_0187_Sea_24.0V0_05.5Hs_12.7Tp_S03.out	3.65E+02	5.02E+02	-9.10E+02	-4.14E+04	2.09E+04	-6.83E+03	6.23E+02	4.62E+04	2.42E+00	2.95E+01	2.90E+02
TwrBsFzt	Minimum	DLC1.1_0195_Sea_24.0V0_05.5Hs_18.3Tp_S05.out	6.71E+02	4.28E+01	-1.07E+04	5.40E+02	5.20E+04	1.42E+03	6.73E+02	5.20E+04	-5.87E-01	2.58E+01	4.08E+02
TwrBsFzt	Maximum	DLC1.5_0774_Sea_EWSV+24.0_05.5Hs_18.3Tp_S06.out	2.18E+02	-1.95E+01	-8.78E+03	9.01E+03	9.27E+04	-5.04E+02	2.19E+02	2.45E+04	-9.49E-02	2.40E+01	4.91E+01
TwrBsMxt	Minimum	DLC1.3_0187_Sea_24.0V0_05.5Hs_12.7Tp_S03.out	3.72E+02	4.83E+02	-9.09E+03	-4.14E+04	2.17E+04	-7.16E+03	6.09E+02	4.69E+04	2.46E+00	2.96E+01	2.80E+02
TwrBsMxt	Maximum	DLC1.1_0190_Sea_24.0V0_05.5Hs_12.7Tp_S04.out	1.02E+02	-4.88E+02	-1.02E+04	5.11E+04	1.55E+04	-2.57E+02	4.99E+02	5.34E+04	-2.03E+00	2.34E+01	6.94E+02
TwrBsMyt	Minimum	DLC1.3_0169_Sea_22.0V0_04.7Hs_11.0Tp_S03.out	-1.19E+03	6.38E+00	-9.27E+03	3.09E+03	-9.33E+04	-2.18E+03	1.19E+03	9.74E+04	-1.10E+00	2.10E+01	8.16E+01
TwrBsMyt	Maximum	DLC1.1_0124_Sea_16.0V0_03.4Hs_10.1Tp_S06.out	2.28E+03	5.53E+00	-1.04E+04	4.61E+03	1.91E+05	6.74E+02	2.28E+03	1.91E+05	9.49E-02	1.14E+01	9.10E+01
TwrBsMzt	Minimum	DLC1.3_0189_Sea_24.0V0_05.5Hs_18.3Tp_S03.out	1.39E+01	-1.88E+02	-8.94E+03	1.27E+04	-2.72E+03	-1.39E+04	1.89E+02	1.30E+04	-7.36E-02	3.00E+01	2.77E+02
TwrBsMzt	Maximum	DLC1.4_0081_Sea_ECD-R_02.4Hs_17.6Tp_S03.out	1.31E+03	1.19E+02	-9.64E+03	-2.84E+03	1.98E+05	1.20E+04	1.32E+03	1.28E+05	-7.08E-02	1.19E+01	7.78E+01
TwrBsFMxy	Minimum	DLC1.3_0164_Sea_22.0V0_04.7Hs_13.4Tp_S01.out	-9.31E-01	2.68E+00	-1.03E+04	8.71E+03	2.59E+03	1.67E+03	-5.06E+00	9.09E+03	-7.00E-01	9.87E+01	2.62E+02
TwrBsFMxy	Maximum	DLC1.1_0124_Sea_16.0V0_03.4Hs_10.1Tp_S06.out	2.28E+03	5.53E+00	-1.04E+04	4.61E+03	1.91E+05	6.74E+02	2.28E+03	1.91E+05	9.49E-02	1.14E+01	9.10E+01
TwrBsMMxy	Minimum	DLC1.3_0161_Sea_20.0V0_04.4Hs_14.1Tp_S06.out	-1.25E+02	9.84E+01	-9.35E+03	1.79E+02	1.05E+02	1.85E+03	1.60E+02	-4.59E+01	9.82E-02	2.37E+01	3.45E+02
TwrBsMMxy	Maximum	DLC1.1_0124_Sea_16.0V0_03.4Hs_10.1Tp_S06.out	2.28E+03	5.53E+00	-1.04E+04	4.61E+03	1.91E+05	6.74E+02	2.28E+03	1.91E+05	9.49E-02	1.14E+01	9.10E+01

Extreme events for Tower 50%:

Parameter	Type	File	TwDtTlMxt (kN-m)	TwDtTlMyt (kN-m)	TwDtTlMzt (kN-m)	TwDtTlMMxy (kN-m)	WaveElev (m)	WindVxi (m/sec)	Time (sec)
TwDtTlMLxt	Minimum	DLC1.3_0187_Sea_24.0V0_05.5Hs_12.7Tp_S03.out	-1.99E+04	0.54E+03	-7.65E+03	2.16E+04	2.46E+00	2.94E+01	2.00E+02
TwDtTlMLxt	Maximum	DLC1.3_0190_Sea_24.0V0_05.5Hs_12.7Tp_S04.out	2.99E+04	8.55E+03	-2.78E+03	3.11E+04	-2.03E+00	2.27E+01	6.04E+02
TwDtTlMLyt	Minimum	DLC1.3_0169_Sea_22.0V0_04.7Hs_11.0Tp_S03.out	1.94E+03	-4.90E+04	-2.56E+02	4.91E+04	-1.16E+00	2.11E+01	8.15E+01
TwDtTlMLyt	Maximum	DLC1.1_0124_Sea_16.0V0_03.4Hs_10.1Tp_S06.out	5.33E+03	9.71E+04	8.37E+02	9.73E+04	9.53E-02	1.15E+01	9.10E+01
TwDtTlMLzt	Minimum	DLC1.3_0189_Sea_24.0V0_05.5Hs_18.3Tp_S03.out	6.41E+03	-3.23E+03	-1.39E+04	7.17E+03	-7.36E-02	3.00E+01	2.77E+02
TwDtTlMLzt	Maximum	DLC1.4_0081_Sea_ECD-R_02.4Hs_17.6Tp_S03.out	1.74E+03	7.16E+04	1.20E+04	7.16E+04	-7.08E-02	1.19E+01	7.78E+01
TwDtTlMMxy	Minimum	DLC1.5_0067_Sea_EWSV-04.0_01.6Hs_08.9Tp_S05.out	-2.34E-01	-7.44E+00	-2.51E+02	7.42E+00	-1.44E-01	4.00E+00	6.35E+01
TwDtTlMMxy	Maximum	DLC1.1_0124_Sea_16.0V0_03.4Hs_10.1Tp_S06.out	5.33E+03	9.71E+04	8.37E+02	9.73E+04	9.53E-02	1.15E+01	9.10E+01

Extreme events for Line 1:

Parameter	Type	File	Anch1Ten (kN)	Anch1Ang (deg)	Fair1Ten (kN)	Fair1Ang (deg)	WaveElev (m)	WindVxi (m/sec)	Time (sec)
Anch1Ten	Minimum	DLC1.5_0583_Sea_EWSH+20.0_0.4Hs_11.3Tp_S03.out	6.46E+02	8.92E+01	8.53E+02	8.94E+01	-6.75E-01	2.00E+01	7.08E+01
Anch1Ten	Maximum	DLC1.3_0196_Sea_24.0V0_05.5Hs_12.7Tp_S06.out	9.00E+03	8.93E+01	9.23E+03	8.93E+01	1.34E+00	2.47E+01	2.70E+02
Anch1Ang	Minimum	DLC1.5_0774_Sea_EWSV+24.0_05.5Hs_18.3Tp_S06.out	3.18E+03	8.57E+01	3.39E+03	8.60E+01	-1.10E+00	2.40E+01	4.35E+01
Anch1Ang	Maximum	DLC1.1_0001_Sea_04.0V0_01.6Hs_08.9Tp_S01.out	5.31E+03	9.00E+01	5.54E+03	9.00E+01	-9.19E-01	3.95E+00	1.39E+02
Fair1Ten	Minimum	DLC1.5_0583_Sea_EWSH+20.0_0.4Hs_11.3Tp_S03.out	6.46E+02	8.92E+01	8.53E+02	8.94E+01	-6.75E-01	2.00E+01	7.08E+01
Fair1Ten	Maximum	DLC1.1_0196_Sea_24.0V0_05.5Hs_12.7Tp_S06.out	9.00E+03	8.93E+01	9.23E+03	8.93E+01	1.34E+00	2.47E+01	2.70E+02

Extreme events for Line 2:

Parameter	Type	File	Anch2Ten (kN)	Anch2Ang (deg)	Fair2Ten (kN)	Fair2Ang (deg)	WaveElev (m)	WindVxi (m/sec)	Time (sec)
Anch2Ten	Minimum	DLC1.3_0189_Sea_24.0V0_05.5Hs_10.3Tp_S03.out	3.95E+03	8.87E+01	4.15E+03	8.88E+01	-2.68E+00	2.74E+01	2.54E+02
Anch2Ten	Maximum	DLC1.3_0192_Sea_24.0V0_05.5Hs_18.3Tp_S04.out	7.08E+03	8.93E+01	7.31E+03	8.93E+01	3.89E+00	2.84E+01	5.50E+02
Anch2Ang	Minimum	DLC1.5_0774_Sea_EWSV+24.0_05.5Hs_18.3Tp_S06.out	4.39E+03	8.57E+01	4.60E+03	8.59E+01	-1.05E+00	2.40E+01	4.33E+01
Anch2Ang	Maximum	DLC1.1_0001_Sea_04.0V0_01.6Hs_08.9Tp_S01.out	5.53E+03	9.00E+01	5.76E+03	9.00E+01	1.46E-01	2.92E+00	6.40E+01
Fair2Ten	Minimum	DLC1.3_0189_Sea_24.0V0_05.5Hs_18.3Tp_S03.out	3.95E+03	8.87E+01	4.15E+03	8.88E+01	-2.68E+00	2.74E+01	2.54E+02
Fair2Ten	Maximum	DLC1.1_0192_Sea_24.0V0_05.5Hs_18.3Tp_S04.out	7.08E+03	8.93E+01	7.31E+03	8.93E+01	3.89E+00	2.84E+01	5.50E+02

Extreme events for Line 3:

Parameter	Type	File	Anch3Ten (kN)	Anch3Ang (deg)	Fair3Ten (kN)	Fair3Ang (deg)	WaveElev (m)	WindVxi (m/sec)	Time (sec)
Anch3Ten	Minimum	DLC1.3_0187_Sea_24.0V0_05.5Hs_12.7Tp_S03.out	2.07E+03	8.90E+01	2.28E+03	8.91E+01	-4.14E-01	2.44E+01	6.18E+02
Anch3Ten	Maximum	DLC1.1_0187_Sea_24.0V0_05.5Hs_12.7Tp_S03.out	9.94E+03	8.91E+01	1.02E+04	8.91E+01	-1.68E-03	2.78E+01	4.32E+02
Anch3Ang	Minimum	DLC1.5_0774_Sea_EWSV+24.0_05.5Hs_18.3Tp_S06.out	5.45E+03	8.58E+01	5.66E+03	8.59E+01	-1.03E+00	2.40E+01	4.31E+01
Anch3Ang	Maximum	DLC1.1_0001_Sea_04.0V0_01.6Hs_08.9Tp_S01.out	5.70E+03	9.00E+01	5.93E+03	9.00E+01	-9.19E-01	3.95E+00	1.39E+02
Fair3Ten	Minimum	DLC1.3_0187_Sea_24.0V0_05.5Hs_12.7Tp_S03.out	2.07E+03	8.90E+01	2.28E+03	8.91E+01	-4.14E-01	2.44E+01	6.18E+02
Fair3Ten	Maximum	DLC1.1_0187_Sea_24.0V0_05.5Hs_12.7Tp_S03.out	9.94E+03	8.91E+01	1.02E+04	8.91E+01	-1.68E-03	2.78E+01	4.32E+02

Extreme events for Line 4:

Parameter	Type	File	Anch4Ten (kN)	Anch4Ang (deg)	Fair4Ten (kN)	Fair4Ang (deg)	WaveElev (m)	WindVxi (m/sec)	Time (sec)
Anch4Ten	Minimum	DLC1.3_0195_Sea_24.0V0_05.5Hs_18.3Tp_S05.out	3.80E+03	8.96E+01	4.00E+03	8.97E+01	-4.14E+00	2.59E+01	2.32E+02
Anch4Ten	Maximum	DLC1.1_0189_Sea_24.0V0_05.5Hs_18.3Tp_S03.out	7.05E+03	8.91E+01	7.28E+03	8.91E+01	4.65E+00	2.43E+01	2.46E+02
Anch4Ang	Minimum	DLC1.5_0774_Sea_EWSV+24.0_05.5Hs_18.3Tp_S06.out	4.12E+03	8.58E+01	4.33E+03	8.60E+01	-1.08E+00	2.40E+01	4.34E+01
Anch4Ang	Maximum	DLC1.1_0001_Sea_04.0V0_01.6Hs_08.9Tp_S01.out	5.70E+03	9.00E+01	5.93E+03	9.00E+01	-2.81E-01	3.03E+00	6.72E+01
Fair4Ten	Minimum	DLC1.3_0195_Sea_24.0V0_05.5Hs_18.3Tp_S05.out	3.80E+03	8.96E+01	4.00E+03	8.97E+01	-4.14E+00	2.59E+01	2.32E+02
Fair4Ten	Maximum	DLC1.1_0189_Sea_24.0V0_05.5Hs_18.3Tp_S03.out	7.05E+03	8.91E+01	7.28E+03	8.91E+01	4.65E+00	2.43E+01	2.46E+02

Extreme events for Line 5:

Parameter	Type	File	Anch5Ten (kN)	Anch5Ang (deg)	Fair5Ten (kN)	Fair5Ang (deg)	WaveElev (m)	WindVxi (m/sec)	Time (sec)
Anch5Ten	Minimum	DLC1.5_0583_Sea_EWSH+20.0_04.4Hs_11.3Tp_S03.out	6.46E+02	8.92E+01	8.53E+02	8.94E+01	-6.75E-01	2.00E+01	7.08E+01
Anch5Ten	Maximum	DLC1.1_0196_Sea_24.0V0_05.5Hs_12.7Tp_S06.out	9.00E+03	8.93E+01	9.23E+03	8.93E+01	1.34E+00	2.47E+01	2.78E+02
Anch5Ang	Minimum	DLC1.5_0774_Sea_EWSV+24.0_05.5Hs_18.3Tp_S06.out	3.18E+03	8.57E+01	3.39E+03	8.60E+01	-1.10E+00	2.40E+01	4.35E+01
Anch5Ang	Maximum	DLC1.1_0001_Sea_04.0V0_01.6Hs_08.9Tp_S01.out	5.31E+03	9.00E+01	5.54E+03	9.00E+01	-9.19E-01	3.95E+00	1.39E+02
Fair5Ten	Minimum	DLC1.5_0583_Sea_EWSH+20.0_04.4Hs_11.3Tp_S03.out	6.46E+02	8.92E+01	8.53E+02	8.94E+01	-6.75E-01	2.00E+01	7.08E+01
Fair5Ten	Maximum	DLC1.1_0196_Sea_24.0V0_05.5Hs_12.7Tp_S06.out	9.00E+03	8.93E+01	9.23E+03	8.93E+01	1.34E+00	2.47E+01	2.78E+02

Extreme events for Line 6:

Parameter	Type	File	Anch6Ten (kN)	Anch6Ang (deg)	Fair6Ten (kN)	Fair6Ang (deg)	WaveElev (m)	WindVxi (m/sec)	Time (sec)
Anch6Ten	Minimum	DLC1.3_0189_Sea_24.0V0_05.5Hs_18.3Tp_S03.out	3.95E+03	8.87E+01	4.15E+03	8.88E+01	-2.68E+00	2.74E+01	2.54E+02
Anch6Ten	Maximum	DLC1.1_0192_Sea_24.0V0_05.5Hs_18.3Tp_S04.out	7.08E+03	8.93E+01	7.31E+03	8.93E+01	3.89E+00	2.84E+01	5.50E+02
Anch6Ang	Minimum	DLC1.5_0774_Sea_EWSV+24.0_05.5Hs_18.3Tp_S06.out	4.39E+03	8.57E+01	4.60E+03	8.59E+01	-1.05E+00	2.40E+01	4.33E+01
Anch6Ang	Maximum	DLC1.1_0001_Sea_04.0V0_01.6Hs_08.9Tp_S01.out	5.53E+03	9.00E+01	5.76E+03	9.00E+01	1.66E-01	2.92E+00	6.40E+01
Fair6Ten	Minimum	DLC1.3_0189_Sea_24.0V0_05.5Hs_18.3Tp_S03.out	3.95E+03	8.87E+01	4.15E+03	8.88E+01	-2.68E+00	2.74E+01	2.54E+02
Fair6Ten	Maximum	DLC1.1_0192_Sea_24.0V0_05.5Hs_18.3Tp_S04.out	7.08E+03	8.93E+01	7.31E+03	8.93E+01	3.89E+00	2.84E+01	5.50E+02

Extreme events for Line 7:

Parameter	Type	File	Anch7Ten (kN)	Anch7Ang (deg)	Fair7Ten (kN)	Fair7Ang (deg)	WaveElev (m)	WindVxi (m/sec)	Time (sec)
Anch7Ten	Minimum	DLC1.3_0187_Sea_24.0V0_05.5Hs_12.7Tp_S03.out	2.07E+03	8.90E+01	2.28E+03	8.91E+01	-4.14E-01	2.44E+01	6.18E+02
Anch7Ten	Maximum	DLC1.1_0187_Sea_24.0V0_05.5Hs_12.7Tp_S03.out	9.94E+03	8.91E+01	1.02E+04	8.91E+01	-1.68E-03	2.78E+01	4.32E+02
Anch7Ang	Minimum	DLC1.5_0774_Sea_EWSV+24.0_05.5Hs_18.3Tp_S06.out	5.45E+03	8.58E+01	5.66E+03	8.59E+01	-1.03E+00	2.40E+01	4.31E+01
Anch7Ang	Maximum	DLC1.1_0001_Sea_04.0V0_01.6Hs_08.9Tp_S01.out	5.70E+03	9.00E+01	5.93E+03	9.00E+01	-9.19E-01	3.95E+00	1.39E+02
Fair7Ten	Minimum	DLC1.3_0187_Sea_24.0V0_05.5Hs_12.7Tp_S03.out	2.07E+03	8.90E+01	2.28E+03	8.91E+01	-4.14E-01	2.44E+01	6.18E+02
Fair7Ten	Maximum	DLC1.1_0187_Sea_24.0V0_05.5Hs_12.7Tp_S03.out	9.94E+03	8.91E+01	1.02E+04	8.91E+01	-1.68E-03	2.78E+01	4.32E+02

Extreme events for Line 8:

Parameter	Type	File	Anch8Ten (kN)	Anch8Ang (deg)	Fair8Ten (kN)	Fair8Ang (deg)	WaveElev (m)	WindVxi (m/sec)	Time (sec)
Anch8Ten	Minimum	DLC1.3_0195_Sea_24.0V0_05.5Hs_18.3Tp_S05.out	3.80E+03	8.96E+01	4.00E+03	8.97E+01	-4.14E+00	2.59E+01	2.32E+02
Anch8Ten	Maximum	DLC1.1_0189_Sea_24.0V0_05.5Hs_18.3Tp_S03.out	7.05E+03	8.91E+01	7.28E+03	8.91E+01	4.65E+00	2.43E+01	2.46E+02
Anch8Ang	Minimum	DLC1.5_0774_Sea_EWSV+24.0_05.5Hs_18.3Tp_S06.out	4.12E+03	8.58E+01	4.33E+03	8.60E+01	-1.08E+00	2.40E+01	4.34E+01
Anch8Ang	Maximum	DLC1.1_0001_Sea_04.0V0_01.6Hs_08.9Tp_S01.out	5.70E+03	9.00E+01	5.93E+03	9.00E+01	-2.81E-01	3.03E+00	6.72E+01
Fair8Ten	Minimum	DLC1.3_0195_Sea_24.0V0_05.5Hs_18.3Tp_S05.out	3.80E+03	8.96E+01	4.00E+03	8.97E+01	-4.14E+00	2.59E+01	2.32E+02
Fair8Ten	Maximum	DLC1.1_0189_Sea_24.0V0_05.5Hs_18.3Tp_S03.out	7.05E+03	8.91E+01	7.28E+03	8.91E+01	4.65E+00	2.43E+01	2.46E+02

Extreme events for Rotor Perf:

Parameter	Type	File	RotCp (-)	RotCt (-)	RotCq (-)	TipSpdRat (-)	WaveElev (m)	WindVxi (m/sec)	Time (sec)
RotCp	Minimum	DLC1.3_0004_Sea_04.0V0_01.6Hs_08.9Tp_S02.out	-7.44E+10	2.39E+05	9.57E+02	-3.48E+04	-3.66E-01	-9.26E-03	3.58E+02
RotCp	Maximum	DLC1.3_0004_Sea_04.0V0_01.6Hs_08.9Tp_S02.out	5.95E+11	6.08E+08	2.41E+06	2.46E+05	-3.67E-01	1.86E-04	3.58E+02
RotCt	Minimum	DLC1.3_0013_Sea_04.0V0_01.6Hs_08.9Tp_S05.out	2.19E+08	-5.26E+05	-4.93E+03	-2.63E+03	2.14E-02	-1.08E-02	4.90E+02
RotCt	Maximum	DLC1.3_0005_Sea_04.0V0_01.6Hs_12.7Tp_S02.out	4.84E+11	6.24E+08	1.96E+06	2.46E+05	-2.51E-01	1.86E-04	3.58E+02
RotCq	Minimum	DLC1.3_0009_Sea_04.0V0_01.6Hs_16.4Tp_S03.out	5.03E+09	6.55E+07	-5.95E+04	-8.45E+04	-1.64E-01	5.90E-03	1.61E+02
RotCq	Maximum	DLC1.3_0004_Sea_04.0V0_01.6Hs_08.9Tp_S02.out	5.95E+11	6.08E+08	2.41E+06	2.46E+05	-3.67E-01	1.86E-04	3.58E+02

A.2. OC3-Hywind Normal Operation Design Load Cases

Extreme events for Wind:

Parameter	Type	File	WindVxi (m/sec)	WindVyi (m/sec)	WindVzi (m/sec)	WaveElev (m)	Time (sec)
WindVxi	Minimum	DLC1.3_0007_Sea_04.0V0_01.6Hs_09.9Tp_S03.out	-1.97E+00	1.11E+00	5.67E-01	4.12E-01	1.65E+02
WindVxi	Maximum	DLC1.3_0107_Sea_24.0V0_05.5Hs_12.7Tp_S03.out	3.04E+01	9.40E-02	7.60E-01	-1.23E+00	3.23E+02
WindVyi	Minimum	DLC1.4_0001_Sea_ECD+R-20_02.0Hs_10.6Tp_S01.out	5.66E+00	-2.37E+01	0.00E+00	-1.61E-01	7.00E+01
WindVyi	Maximum	DLC1.4_0055_Sea_ECD-R-20_02.0Hs_10.6Tp_S01.out	5.66E+00	2.37E+01	0.00E+00	-5.59E-01	7.00E+01
WindVzi	Minimum	DLC1.3_0190_Sea_24.0V0_05.5Hs_12.7Tp_S04.out	2.02E+01	-3.44E+00	-6.43E+00	-7.00E-01	5.70E+02
WindVzi	Maximum	DLC1.2_0193_Sea_24.0V0_05.5Hs_12.7Tp_S05.out	2.74E+01	1.78E+00	5.67E+00	-2.34E-02	1.70E+02

Extreme events for Waves:

Parameter	Type	File	WaveElev (m)	WaveVxi (m/sec)	WaveVyi (m/sec)	WaveVzi (m/sec)	WaveAxi (m/sec^2)	WaveAyi (m/sec^2)	WaveAzi (m/sec^2)	WindVxi (m/sec)	Time (sec)
WaveElev	Minimum	DLC1.5_0582_Sea_EWSH+20.0_04.4Hs_11.3Tp_S02.out	-4.89E+00	-2.82E+00	0.00E+00	2.55E-01	5.54E-01	0.00E+00	2.28E+00	2.00E+01	6.90E+01
WaveElev	Maximum	DLC1.5_0745_Sea_EWSH-24.0_05.5Hs_12.7Tp_S02.out	5.06E+00	3.12E+00	0.00E+00	1.92E-01	2.06E-01	0.00E+00	-2.09E+00	2.40E+01	8.10E+01
WaveVxi	Minimum	DLC1.5_0583_Sea_EWSH+20.0_04.4Hs_11.3Tp_S03.out	-4.87E+00	-3.87E+00	0.00E+00	-5.02E-01	-2.88E-01	0.00E+00	3.43E+00	2.00E+01	6.88E+01
WaveVxi	Maximum	DLC1.5_0745_Sea_EWSH-24.0_05.5Hs_12.7Tp_S03.out	5.04E+00	3.12E+00	0.00E+00	-3.34E-01	-1.69E-01	0.00E+00	-2.11E+00	2.40E+01	8.13E+01
WaveVyi	Minimum	DLC1.1_0001_Sea_04.0V0_01.6Hs_08.9Tp_S01.out	3.19E-01	3.57E-01	0.00E+00	2.08E-01	1.47E-01	0.00E+00	-4.13E-01	2.13E+00	3.00E+01
WaveVyi	Maximum	DLC1.1_0001_Sea_04.0V0_01.6Hs_08.9Tp_S01.out	3.19E-01	3.57E-01	0.00E+00	2.08E-01	1.47E-01	0.00E+00	-4.13E-01	2.13E+00	3.00E+01
WaveVzi	Minimum	DLC1.5_0583_Sea_EWSH+20.0_04.4Hs_11.3Tp_S03.out	-9.74E-01	-6.09E-01	0.00E+00	-3.73E+00	-3.09E+00	0.00E+00	2.07E-01	2.00E+01	6.73E+01
WaveVzi	Maximum	DLC1.5_0583_Sea_EWSH+20.0_04.4Hs_11.3Tp_S03.out	-1.46E+00	-4.26E-01	0.00E+00	3.13E+00	2.88E+00	0.00E+00	-2.64E-01	2.00E+01	7.05E+01
WaveAxi	Minimum	DLC1.5_0583_Sea_EWSH+20.0_04.4Hs_11.3Tp_S03.out	-9.74E-01	-6.09E-01	0.00E+00	-3.73E+00	-3.09E+00	0.00E+00	2.07E-01	2.00E+01	6.73E+01
WaveAxi	Maximum	DLC1.1_0100_Sea_14.0V0_03.0Hs_09.7Tp_S04.out	3.43E-01	2.46E-01	0.00E+00	2.29E+00	3.17E+00	0.00E+00	-2.26E-01	1.43E+01	1.62E+02
WaveAyi	Minimum	DLC1.1_0001_Sea_04.0V0_01.6Hs_08.9Tp_S01.out	3.19E-01	3.57E-01	0.00E+00	2.08E-01	1.47E-01	0.00E+00	-4.13E-01	2.13E+00	3.00E+01
WaveAyi	Maximum	DLC1.1_0001_Sea_04.0V0_01.6Hs_08.9Tp_S01.out	3.19E-01	3.57E-01	0.00E+00	2.08E-01	1.47E-01	0.00E+00	-4.13E-01	2.13E+00	3.00E+01
WaveAzi	Minimum	DLC1.5_0409_Sea_EWSV+14.0_03.0Hs_08.0Tp_S05.out	2.62E+00	2.74E+00	0.00E+00	-1.90E-01	-2.28E-01	0.00E+00	-3.13E+00	1.40E+01	3.83E+01
WaveAzi	Maximum	DLC1.5_0583_Sea_EWSH+20.0_04.4Hs_11.3Tp_S03.out	-4.87E+00	-3.87E+00	0.00E+00	-5.02E-01	-2.88E-01	0.00E+00	3.43E+00	2.00E+01	6.88E+01

Extreme events for Drivetrain:

Parameter	Type	File	GenPwr (kW)	GenTq (kN-m)	HSSBrTq (kN-m)	GenSpeed (rpm)	RotSpeed (rpm)	WaveElev (m)	WindVxi (m/sec)	Time (sec)
GenPwr	Minimum	DLC1.3_0012_Sea_04.0V0_01.6Hs_16.4Tp_S04.out	-8.27E-02	-1.24E-03	0.00E+00	6.72E+02	6.93E+00	-5.96E-01	2.34E+00	1.25E+02
GenPwr	Maximum	DLC1.3_0165_Sea_22.0V0_04.7Hs_15.7Tp_S01.out	7.27E+03	4.31E+01	0.00E+00	1.71E+03	1.76E+01	-1.03E+00	2.86E+01	1.94E+02
GenTq	Minimum	DLC1.3_0012_Sea_04.0V0_01.6Hs_16.4Tp_S04.out	-0.27E-02	-1.24E-03	0.00E+00	6.72E+02	6.93E+00	-5.96E-01	2.34E+00	1.25E+02
GenTq	Maximum	DLC1.1_0050_Sea_10.0V0_02.2Hs_09.2Tp_S02.out	4.20E+03	4.32E+01	0.00E+00	9.93E+02	1.01E+01	-0.51E-02	1.21E+01	5.00E+02
HSSBrTq	Minimum	DLC1.1_0001_Sea_04.0V0_01.6Hs_08.9Tp_S01.out	1.06E+01	2.80E-01	0.00E+00	6.72E+02	6.93E+00	3.19E-01	2.13E+00	3.00E+01
HSSBrTq	Maximum	DLC1.1_0001_Sea_04.0V0_01.6Hs_08.9Tp_S01.out	1.86E+01	2.80E-01	0.00E+00	6.72E+02	6.93E+00	3.19E-01	2.13E+00	3.00E+01
GenSpeed	Minimum	DLC1.3_0001_Sea_04.0V0_01.6Hs_08.9Tp_S01.out	0.00E+00	0.00E+00	0.00E+00	6.45E+02	6.65E+00	2.27E-01	1.25E+00	4.30E+01
GenSpeed	Maximum	DLC1.3_0165_Sea_22.0V0_04.7Hs_15.7Tp_S01.out	7.27E+03	4.31E+01	0.00E+00	1.71E+03	1.76E+01	-1.03E+00	2.86E+01	1.94E+02
RotSpeed	Minimum	DLC1.3_0001_Sea_04.0V0_01.6Hs_08.9Tp_S01.out	0.00E+00	0.00E+00	0.00E+00	6.45E+02	6.65E+00	2.25E-01	7.76E-01	4.29E+01
RotSpeed	Maximum	DLC1.3_0165_Sea_22.0V0_04.7Hs_15.7Tp_S01.out	7.27E+03	4.31E+01	0.00E+00	1.71E+03	1.76E+01	-9.92E-01	2.85E+01	1.94E+02

Extreme events for Blade Pitch:

Parameter	Type	File	BldPitch1 (deg)	BldPitch2 (deg)	BldPitch3 (deg)	WaveElev (m)	WindVxi (m/sec)	Time (sec)
BldPitch1	Minimum	DLC1.3_0104_Sea_14.0V0_03.0Hs_12.0Tp_S05.out	-9.27E-03	-9.27E-03	-9.27E-03	-8.37E-01	1.30E+01	3.42E+02
BldPitch1	Maximum	DLC1.3_0185_Sea_24.0V0_05.5Hs_15.5Tp_S02.out	2.66E+01	2.66E+01	2.66E+01	-2.24E+00	2.68E+01	3.14E+02
BldPitch2	Minimum	DLC1.3_0104_Sea_14.0V0_03.0Hs_12.0Tp_S05.out	-9.27E-03	-9.27E-03	-9.27E-03	-8.37E-01	1.30E+01	3.42E+02
BldPitch2	Maximum	DLC1.3_0185_Sea_24.0V0_05.5Hs_15.5Tp_S02.out	2.66E+01	2.66E+01	2.66E+01	-2.24E+00	2.68E+01	3.14E+02
BldPitch3	Minimum	DLC1.3_0104_Sea_14.0V0_03.0Hs_12.0Tp_S05.out	-9.27E-03	-9.27E-03	-9.27E-03	-0.37E-01	1.30E+01	3.42E+02
BldPitch3	Maximum	DLC1.3_0185_Sea_24.0V0_05.5Hs_15.5Tp_S02.out	2.66E+01	2.66E+01	2.66E+01	-2.24E+00	2.68E+01	3.14E+02

Extreme events for Nacelle Yaw:

Parameter	Type	File	NacYaw (deg)	NacYawErr (deg)	WaveElev (m)	WindVxi (m/sec)	Time (sec)
NacYaw	Minimum	DLC1.3_0187_Sea_24.0V0_05.5Hs_12.7Tp_S03.out	-6.99E-02	-1.03E+00	-1.48E+00	2.57E+01	2.84E+02
NacYaw	Maximum	DLC1.4_0062_Sea_ECD-R-20_02.0Hs_14.8Tp_S03.out	5.59E-02	7.39E+01	-4.67E-01	5.66E+00	7.55E+01
NacYawErr	Minimum	DLC1.3_0001_Sea_04.0V0_01.6Hs_08.9Tp_S01.out	-1.34E-03	-2.22E+02	2.45E-01	-8.08E-01	3.14E+01
NacYawErr	Maximum	DLC1.3_0004_Sea_04.0V0_01.6Hs_08.9Tp_S02.out	-2.20E-03	2.23E+02	-2.16E-01	-8.26E-01	3.22E+02

Extreme events for Blade 1 Defl:

Parameter	Type	File	CoPDefl1 (m)	IPDefl1 (m)	TwstDefl1 (deg)	WaveElev (m)	WindVxi (m/sec)	Time (sec)
CoPDefl1	Minimum	DLC1.3_0181_Sea_24.0V0_05.5Hs_12.7Tp_S01.out	-3.57E+00	1.91E+00	0.00E+00	1.17E+00	2.67E+01	5.76E+02
CoPDefl1	Maximum	DLC1.4_0003_Sea_ECD+R-20_02.0Hs_19.0Tp_S01.out	8.77E+00	-6.10E-01	0.00E+00	-4.02E-01	5.66E+00	7.29E+01
IPDefl1	Minimum	DLC1.3_0181_Sea_24.0V0_05.5Hs_12.7Tp_S01.out	4.25E+00	-2.57E+00	0.00E+00	-3.21E+00	2.95E+01	5.65E+02
IPDefl1	Maximum	DLC1.3_0183_Sea_24.0V0_05.5Hs_19.3Tp_S01.out	-3.42E+00	2.38E+00	0.00E+00	1.25E+00	3.28E+01	2.48E+02
TwstDefl1	Minimum	DLC1.1_0001_Sea_04.0V0_01.6Hs_08.9Tp_S01.out	1.02E+00	-9.91E-02	0.00E+00	3.19E-01	2.13E+00	3.00E+01
TwstDefl1	Maximum	DLC1.1_0001_Sea_04.0V0_01.6Hs_08.9Tp_S01.out	1.02E+00	-9.91E-02	0.00E+00	3.19E-01	2.13E+00	3.00E+01

Extreme events for Blade 2 Defl:

Parameter	Type	File	CoPDefl2 (m)	IPDefl2 (m)	TwstDefl2 (deg)	WaveElev (m)	WindVxi (m/sec)	Time (sec)
CoPDefl2	Minimum	DLC1.3_0181_Sea_24.0V0_05.5Hs_12.7Tp_S01.out	-2.62E+00	2.15E+00	0.00E+00	4.53E-01	2.81E+01	5.75E+02
CoPDefl2	Maximum	DLC1.2_0119_Sea_16.0V0_02.4Hs_10.1Tp_S04.out	8.92E+00	-1.80E+00	0.00E+00	-2.97E-02	1.45E+01	5.00E+01
IPDefl2	Minimum	DLC1.3_0189_Sea_24.0V0_05.5Hs_18.3Tp_S03.out	3.97E+00	-2.36E+00	0.00E+00	1.06E-01	2.93E+01	6.00E+02
IPDefl2	Maximum	DLC1.3_0183_Sea_24.0V0_05.5Hs_18.3Tp_S01.out	-3.02E+00	2.27E+00	0.00E+00	3.07E+00	3.10E+01	2.51E+02
TwstDefl2	Minimum	DLC1.1_0001_Sea_04.0V0_01.6Hs_08.9Tp_S01.out	6.65E-01	3.73E-01	0.00E+00	3.19E-01	2.13E+00	3.00E+01
TwstDefl2	Maximum	DLC1.1_0001_Sea_04.0V0_01.6Hs_08.9Tp_S01.out	6.65E-01	3.73E-01	0.00E+00	3.19E-01	2.13E+00	3.00E+01

Extreme events for Blade 3 Defl:

Parameter	Type	File	CoPDefl3 (m)	IPDefl3 (m)	TwstDefl3 (deg)	WaveElev (m)	WindVxi (m/sec)	Time (sec)
CoPDefl3	Minimum	DLC1.3_0190_Sea_24.0V0_05.5Hs_12.7Tp_S04.out	-4.37E+00	2.30E+00	0.00E+00	1.49E+00	3.00E+01	5.50E+02
CoPDefl3	Maximum	DLC1.4_0065_Sea_ECD-R-20_02.0Hs_14.8Tp_S04.out	8.83E+00	-1.59E+00	0.00E+00	-7.54E-01	1.11E+01	6.67E+01
IPDefl3	Minimum	DLC1.3_0182_Sea_24.0V0_05.5Hs_15.5Tp_S01.out	4.15E+00	-2.71E+00	0.00E+00	-2.58E+00	2.81E+01	5.67E+02
IPDefl3	Maximum	DLC1.3_0190_Sea_24.0V0_05.5Hs_12.7Tp_S04.out	-4.30E+00	2.34E+00	0.00E+00	1.48E+00	2.98E+01	5.50E+02
TwstDefl3	Minimum	DLC1.1_0001_Sea_04.0V0_01.6Hs_08.9Tp_S01.out	1.01E+00	-4.59E-01	0.00E+00	3.19E-01	2.13E+00	3.00E+01
TwstDefl3	Maximum	DLC1.1_0001_Sea_04.0V0_01.6Hs_08.9Tp_S01.out	1.01E+00	-4.59E-01	0.00E+00	3.19E-01	2.13E+00	3.00E+01

Extreme events for Blade Clrnc:

Parameter	Type	File	BldClrnc1 (m)	BldClrnc2 (m)	BldClrnc3 (m)	Azimuth (deg)	WaveElev (m)	WindVel (m/sec)	Time (sec)
BldClrnc1	Minimum	DLC1.4_0003_Sea_ECD+R-20_02.0Hz_19.0Tp_S01.out	-1.18E+00	6.06E+00	0.94E+00	2.65E+02	-4.02E-02	5.66E+00	7.29E+01
BldClrnc1	Maximum	DLC1.3_0181_Sea_24.0V0_05.5Hz_12.7Tp_S01.out	1.53E+01	9.77E+00	1.00E+01	2.14E+02	1.17E+00	2.67E+01	5.76E+02
BldClrnc2	Minimum	DLC1.3_0118_Sea_16.0V0_02.4Hz_10.1Tp_S04.out	4.19E+00	-1.39E+00	5.78E+00	1.88E+01	-2.07E-02	1.45E+01	5.00E+01
BldClrnc2	Maximum	DLC1.3_0181_Sea_24.0V0_05.5Hz_12.7Tp_S01.out	9.10E+00	1.54E+01	7.48E+00	1.01E+02	4.53E-01	2.01E+01	5.75E+02
BldClrnc3	Minimum	DLC1.4_0065_Sea_ECD-R-20_02.0Hz_14.0Tp_S04.out	5.57E+00	4.22E+00	-1.26E+00	2.02E+02	-7.54E-01	1.11E+01	6.67E+01
BldClrnc3	Maximum	DLC1.3_0190_Sea_24.0V0_05.5Hz_12.7Tp_S04.out	9.18E+00	1.13E+01	1.64E+01	3.34E+02	1.49E+00	3.00E+01	5.50E+02

Extreme events for Nacelle Acc:

Parameter	Type	File	NclMUTAxs (m/sec^2)	NclMUTAys (m/sec^2)	NclMUTAzs (m/sec^2)	NclMUTAMag (m/sec^2)	WaveElev (m)	WindVel (m/sec)	Time (sec)
NclMUTAxs	Minimum	DLC1.3_0181_Sea_24.0V0_05.5Hz_12.7Tp_S01.out	-2.68E+00	4.04E-01	-4.69E-01	2.75E+00	-3.20E-02	2.65E+01	6.42E+01
NclMUTAxs	Maximum	DLC1.3_0101_Sea_14.0V0_02.0Hz_12.0Tp_S04.out	2.62E+00	-3.36E-01	4.34E-01	2.67E+00	3.15E-01	1.37E+01	6.29E+02
NclMUTAys	Minimum	DLC1.3_0181_Sea_24.0V0_05.5Hz_12.7Tp_S01.out	4.95E-01	-1.11E+00	1.72E-01	1.29E+00	3.21E-01	1.51E+01	4.00E+02
NclMUTAys	Maximum	DLC1.3_0163_Sea_22.0V0_04.7Hz_11.0Tp_S01.out	9.77E-02	1.26E+00	3.18E-03	1.27E+00	-2.80E-01	1.90E+01	3.01E+02
NclMUTAzs	Minimum	DLC1.3_0183_Sea_24.0V0_05.5Hz_18.3Tp_S01.out	-1.89E+00	1.15E-01	-4.67E-01	2.01E+00	6.27E-01	2.75E+01	8.31E+01
NclMUTAzs	Maximum	DLC1.3_0191_Sea_24.0V0_05.5Hz_15.5Tp_S04.out	1.88E+00	-2.67E-01	6.36E-01	2.00E+00	-3.41E-01	2.29E+01	1.67E+02
NclMUTAMag	Minimum	DLC1.3_0152_Sea_20.0V0_04.4Hz_14.1Tp_S03.out	-1.23E-04	-1.33E-02	5.36E-03	-1.04E-02	-5.15E-01	2.02E+01	6.01E+02
NclMUTAMag	Maximum	DLC1.3_0181_Sea_24.0V0_05.5Hz_12.7Tp_S01.out	-2.68E+00	4.04E-01	-4.69E-01	2.75E+00	-3.20E-01	2.65E+01	6.42E+01

Extreme events for TwrTop Disp:

Parameter	Type	File	TTDspFA (m)	TTDspSS (m)	TTDspTwst (deg)	WaveElev (m)	WindVel (m/sec)	Time (sec)
TTDspFA	Minimum	DLC1.3_0181_Sea_24.0V0_05.5Hz_12.7Tp_S01.out	-3.64E-01	-1.07E-01	0.00E+00	1.31E+00	2.36E+01	5.58E+02
TTDspFA	Maximum	DLC1.3_0098_Sea_14.0V0_02.0Hz_12.0Tp_S02.out	9.14E-01	-8.20E-02	0.00E+00	-2.75E-01	1.99E+01	5.97E+01
TTDspSS	Minimum	DLC1.3_0163_Sea_22.0V0_04.7Hz_11.0Tp_S01.out	1.02E-01	-2.57E-01	0.00E+00	-3.71E-01	2.00E+01	3.01E+02
TTDspSS	Maximum	DLC1.3_0195_Sea_24.0V0_05.5Hz_18.3Tp_S05.out	2.70E-01	1.36E-01	0.00E+00	-2.99E-03	2.02E+01	5.07E+02
TTDspTwst	Minimum	DLC1.1_0001_Sea_04.0V0_01.6Hz_08.9Tp_S01.out	-2.61E-02	1.02E-03	0.00E+00	3.19E-01	2.13E+00	3.00E+01
TTDspTwst	Maximum	DLC1.1_0001_Sea_04.0V0_01.6Hz_08.9Tp_S01.out	-2.61E-02	1.02E-03	0.00E+00	3.19E-01	2.13E+00	3.00E+01

Extreme events for Platform Dsp:

Parameter	Type	File	PtfmSurge (m)	PtfmSway (m)	PtfmHeave (m)	PtfmRoll (deg)	PtfmPitch (deg)	PtfmYaw (deg)	WaveElev (m)	WindVel (m/sec)	Time (sec)
PtfmSurge	Minimum	DLC1.5_0774_Sea_EWEV+24.0_05.5Hz_18.3Tp_S06.out	-4.51E+00	-3.31E-01	-4.48E-01	-1.36E-01	3.35E-01	-2.42E-01	6.26E-01	2.49E+01	3.04E+02
PtfmSurge	Maximum	DLC1.4_0023_Sea_ECD+R_02.4Hz_17.6Tp_S05.out	3.56E+01	-3.47E-01	-1.63E+00	1.23E-01	6.68E+00	-2.12E+00	1.20E-01	1.22E+01	6.93E+01
PtfmSway	Minimum	DLC1.3_0177_Sea_22.0V0_04.7Hz_15.7Tp_S05.out	7.17E+00	-3.33E+00	1.22E+01	5.83E-01	5.96E-01	-5.07E-01	2.43E-01	1.36E+01	5.83E+02
PtfmSway	Maximum	DLC1.3_0189_Sea_24.0V0_05.5Hz_18.3Tp_S03.out	8.43E+00	3.15E+00	4.52E-01	-8.47E-01	1.94E+00	-2.75E+00	5.10E-01	2.67E+01	3.14E+02
PtfmHeave	Minimum	DLC1.4_0087_Sea_ECD-R_02.4Hz_17.6Tp_S05.out	3.43E+01	-3.54E-02	-1.67E+00	1.96E-01	5.92E+00	2.25E+00	-3.72E-01	1.21E+01	6.95E+01
PtfmHeave	Maximum	DLC1.3_0186_Sea_24.0V0_05.5Hz_18.3Tp_S02.out	9.55E+00	-1.21E+00	1.20E+00	2.66E-01	1.88E+00	1.09E+00	1.74E+00	3.00E+01	3.05E+02
PtfmRoll	Minimum	DLC1.3_0086_Sea_12.0V0_02.4Hz_13.4Tp_S05.out	1.96E+01	6.49E-01	1.14E-01	-1.39E+00	4.41E+00	-2.95E+00	5.60E-01	1.48E+01	4.03E+02
PtfmRoll	Maximum	DLC1.3_0198_Sea_24.0V0_05.5Hz_18.3Tp_S06.out	7.52E+00	-1.55E+00	2.15E-01	1.73E+00	9.57E-01	-1.72E+00	1.64E-01	3.00E+01	5.64E+02
PtfmPitch	Minimum	DLC1.3_0121_Sea_16.0V0_03.4Hz_10.1Tp_S05.out	1.41E+01	-7.33E-01	-4.07E-01	2.53E-01	-1.00E+00	0.13E-01	-5.05E-01	1.50E+01	4.72E+02
PtfmPitch	Maximum	DLC1.3_0132_Sea_18.0V0_03.7Hz_16.7Tp_S02.out	1.91E+01	-6.24E-01	-8.48E-01	1.71E-01	7.72E+00	-9.69E-01	-8.11E-01	1.66E+01	6.15E+02
PtfmYaw	Minimum	DLC1.3_0189_Sea_24.0V0_05.5Hz_18.3Tp_S03.out	5.88E+00	7.24E-01	-1.63E-01	-9.15E-01	1.41E+00	-5.42E+00	-1.76E+00	2.73E+01	2.76E+02
PtfmYaw	Maximum	DLC1.4_0091_Sea_ECD-R-20_02.0Hz_14.0Tp_S06.out	2.64E+01	-4.15E-02	-1.14E+00	2.84E-01	4.96E+00	4.38E+00	-9.62E-01	5.66E+00	7.10E+01

Extreme events for Platform Acc:

Parameter	Type	File	PtfmTAxt (m/sec^2)	PtfmTAyt (m/sec^2)	PtfmTAzt (m/sec^2)	PtfmTAMag (m/sec^2)	WaveElev (m)	WindVel (m/sec)	Time (sec)
PtfmTAxt	Minimum	DLC1.3_0190_Sea_24.0V0_05.5Hz_12.7Tp_S04.out	-9.88E-01	-5.91E-03	-3.29E-02	9.88E-01	1.06E+00	2.11E+01	5.00E+02
PtfmTAxt	Maximum	DLC1.3_0181_Sea_24.0V0_05.5Hz_12.7Tp_S01.out	1.02E+00	4.34E-02	-4.11E-04	1.02E+00	-9.67E-01	2.45E+01	5.57E+02
PtfmTAyt	Minimum	DLC1.3_0195_Sea_24.0V0_05.5Hz_18.3Tp_S05.out	-1.40E-01	-3.48E-01	-2.53E-02	3.83E-01	2.96E-01	2.45E+01	5.06E+02
PtfmTAyt	Maximum	DLC1.3_0183_Sea_24.0V0_05.5Hz_18.3Tp_S01.out	9.13E-02	3.71E-01	2.98E-02	3.82E-01	-2.08E+00	1.70E+01	4.10E+02
PtfmTAzt	Minimum	DLC1.5_0745_Sea_EWSH-24.0_05.5Hz_12.7Tp_S03.out	-8.51E-02	-3.43E-03	-1.82E-01	2.01E-01	5.05E+00	2.40E+01	8.11E+01
PtfmTAzt	Maximum	DLC1.3_0163_Sea_22.0V0_04.7Hz_11.0Tp_S01.out	1.96E-01	9.66E-03	1.46E-01	2.45E-01	-4.13E+00	2.12E+01	2.38E+02
PtfmTAMag	Minimum	DLC1.3_0130_Sea_10.0V0_03.7Hz_16.7Tp_S04.out	-1.30E-03	2.22E-03	0.93E-04	-3.11E-04	-1.95E-01	2.00E+01	5.07E+02
PtfmTAMag	Maximum	DLC1.3_0181_Sea_24.0V0_05.5Hz_12.7Tp_S01.out	1.02E+00	4.34E-02	-4.11E-04	1.02E+00	-9.67E-01	2.45E+01	5.57E+02

Extreme events for Blade 1 Root:

Parameter	Type	File	RootFxc1 (kN)	RootFyc1 (kN)	RootFzc1 (kN)	RootMxc1 (kN-m)	RootMyc1 (kN-m)	RootMzc1 (kN-m)	RootMxa1 (kN)	RootMya1 (kN-m)	WaveElev (m)	WindVel (m/sec)	Time (sec)
RootFxc1	Minimum	DLC1.3_0182_Sea_24.0V0_05.5Hz_15.5Tp_S01.out	-1.08E+02	-2.04E+01	1.17E+03	-1.22E+02	-6.86E+03	-4.68E+01	1.09E+02	6.86E+03	-3.84E-01	2.18E+01	3.57E+02
RootFyc1	Maximum	DLC1.3_0110_Sea_16.0V0_02.4Hz_10.1Tp_S04.out	6.33E+02	-3.44E+02	1.04E+03	9.97E+03	2.15E+04	-1.25E+02	7.19E+02	2.33E+04	2.86E-04	1.25E+01	5.12E+01
RootFyc1	Minimum	DLC1.3_0183_Sea_24.0V0_05.5Hz_18.3Tp_S01.out	2.97E+02	-4.91E+02	1.19E+03	9.79E+03	6.40E+03	-1.17E+02	5.74E+02	1.17E+04	-1.85E+00	3.14E+01	2.66E+02
RootFyc1	Maximum	DLC1.3_0151_Sea_20.0V0_04.4Hz_11.3Tp_S03.out	9.02E+01	2.84E+02	9.57E+02	-7.21E+03	1.38E+03	-1.15E+02	2.98E+02	7.34E+03	4.32E-01	1.99E+01	5.84E+02
RootFzc1	Minimum	DLC1.3_0126_Sea_16.0V0_02.4Hz_16.7Tp_S06.out	1.76E+02	-1.88E+00	1.21E+01	2.22E+02	6.62E+02	1.38E+01	1.76E+02	6.62E+02	4.09E-01	1.07E+01	6.20E+02
RootFzc1	Maximum	DLC1.3_0164_Sea_22.0V0_04.7Hz_13.4Tp_S01.out	2.41E+02	-3.35E+01	1.90E+03	2.33E+02	5.13E+03	-1.45E+02	2.42E+02	5.13E+03	-1.19E+00	2.74E+01	1.07E+02
RootMxc1	Minimum	DLC1.1_0187_Sea_24.0V0_05.5Hz_12.7Tp_S03.out	8.38E+01	2.79E+02	9.69E+02	-7.38E+03	1.92E+01	-1.45E+02	2.92E+02	7.38E+03	2.09E-01	2.72E+01	5.99E+02
RootMxc1	Maximum	DLC1.1_0181_Sea_24.0V0_05.5Hz_12.7Tp_S01.out	4.14E+02	-4.71E+02	9.76E+02	1.11E+04	1.20E+04	-6.39E+01	6.27E+02	1.64E+04	-3.39E+00	2.78E+01	5.66E+02
RootMyc1	Minimum	DLC1.3_0189_Sea_24.0V0_05.5Hz_15.5Tp_S01.out	-1.04E+02	1.98E+01	1.15E+03	-7.00E+02	-6.94E+03	-4.90E+01	1.06E+02	6.96E+03	-3.37E-01	2.17E+01	3.57E+02
RootMyc1	Minimum	DLC1.3_0118_Sea_16.0V0_03.4Hz_10.1Tp_S04.out	6.33E+02	-3.44E+02	1.04E+03	9.97E+03	2.15E+04	-1.25E+02	7.19E+02	2.33E+04	2.86E-04	1.25E+01	5.12E+01
RootMzc1	Minimum	DLC1.4_0096_Sea_ECD-R+20_02.7Hz_16.4Tp_S02.out	6.11E+01	-6.98E+01	1.27E+03	1.66E+03	1.40E+03	-3.40E+02	9.28E+01	2.17E+03	1.26E-01	1.72E+01	6.98E+01
RootMzc1	Maximum	DLC1.3_0076_Sea_12.0V0_02.4Hz_09.2Tp_S02.out	4.97E+02	1.15E+02	7.05E+02	-1.69E+03	1.74E+04	1.80E+02	5.10E+02	1.75E+04	-8.52E-01	1.43E+01	5.51E+02
RootFMxy1	Minimum	DLC1.3_0195_Sea_24.0V0_05.5Hz_18.3Tp_S05.out	8.25E-01	4.86E-01	1.50E+03	-1.12E+03	-3.07E+03	-1.27E+02	6.66E-01	3.27E+03	-5.51E-01	2.85E+01	1.48E+02
RootFMxy1	Maximum	DLC1.3_0118_Sea_16.0V0_03.4Hz_10.1Tp_S04.out	6.28E+02	-3.54E+02	1.03E+03	9.14E+03	2.14E+04	-1.13E+02	7.22E+02	2.33E+04	-5.45E-04	1.27E+01	5.11E+01
RootMMxy1	Minimum	DLC1.1_0169_Sea_22.0V0_04.7Hz_15.7Tp_S02.out	1.55E+02	-7.95E+01	1.42E+03	1.17E+01	5.52E+01	-3.42E+01	1.74E+02	-2.15E+01	3.66E-01	2.66E+01	5.40E+02
RootMMxy1	Maximum	DLC1.3_0118_Sea_16.0V0_03.4Hz_10.1Tp_S04.out	6.33E+02	-3.44E+02	1.04E+03	9.97E+03	2.15E+04	-1.25E+02	7.19E+02	2.33E+04	2.86E-04	1.25E+01	5.12E+01

Extreme events for Blade 2 Root:

Parameter	Type	File	RootFxc2 (kN)	RootFyc2 (kN)	RootFzc2 (kN)	RootMxc2 (kN-m)	RootMyc2 (kN-m)	RootMzc2 (kN-m)	RootFMxy2 (kN)	RootMMxy2 (kN-m)	WaveElev (m)	WindVel (m/sec)	Time (sec)
RootFxc2	Minimum	DLC1.3_0182_Sea_24.0V0_05.5Hz_15.5Tp_S01.out	-1.31E+02	8.56E+01	1.05E+03	-3.04E+03	-6.26E+03	-8.70E+01	1.56E+02	6.95E+03	-7.41E-02	2.14E+01	2.64E+02
RootFxc2	Maximum	DLC1.3_0119_Sea_16.0V0_03.4Hz_10.1Tp_S04.out	6.22E+02	-3.18E+02	9.68E+02	9.14E+03	2.15E+04	-9.45E+01	6.99E+02	2.30E+04	-4.47E-03	1.90E+01	4.97E+01
RootFyc2	Minimum	DLC1.1_0187_Sea_24.0V0_05.5Hz_12.7Tp_S03.out	4.37E+02	-4.65E+02	8.57E+02	1.07E+04	1.21E+04	-8.23E+01	6.38E+02	1.61E+04	7.66E-02	2.77E+01	6.00E+02
RootFyc2	Maximum	DLC1.3_0188_Sea_24.0V0_05.5Hz_15.5Tp_S03.out	-5.64E+01	2.83E+02	9.29E+02	-7.22E+03	-4.14E+03	-1.51E+02	2.88E+02	8.31E+03	6.18E-01	2.32E+01	5.93E+02
RootFzc2	Minimum	DLC1.3_0126_Sea_16.0V0_03.4Hz_16.7Tp_S06.out	2.43E+02	-9.27E+01	1.63E+01	2.91E+03	8.54E+03	-9.69E+00	2.60E+02	9.02E+03	-6.17E-01	1.26E+01	6.17E+02
RootFzc2	Maximum	DLC1.3_0126_Sea_16.0V0_03.4Hz_16.7Tp_S06.out	2.69E+02	-9.14E+01	1.99E+03	2.61E+03	6.95E+03	-1.50E+02	2.83E+02	7.34E+03	-2.05E+00	1.90E+01	1.24E+02
RootMxc2	Minimum	DLC1.3_0188_Sea_24.0V0_05.5Hz_15.5Tp_S03.out	-5.64E+01	2.83E+02	9.29E+02	-7.22E+03	-4.14E+03	-1.51E+02	2.88E+02	8.31E+03	6.18E-01	2.32E+01	5.93E+02
RootMxc2	Maximum	DLC1.1_0188_Sea_24.0V0_05.5Hz_15.5Tp_S03.out	4.58E+02	-4.64E+02	7.86E+02	1.09E+04	1.31E+04	-6.60E+01	6.50E+02	1.71E+04	2.97E-01	2.72E+01	6.00E+02
RootMyc2	Minimum	DLC1.3_0187_Sea_24.0V0_05.5Hz_12.7Tp_S02.out	-1.02E+02	-1.32E+02	1.15E+02	2.19E+02	-6.51E+02	-7.07E+01	1.67E+02	6.85E+02	-9.48E-01	2.41E+01	4.98E+02
RootMyc2	Maximum	DLC1.3_0110_Sea_16.0V0_03.4Hz_10.1Tp_S04.out	6.10E+02	-3.13E+02	9.70E+02	9.09E+03	2.16E+04	-1.05E+02	6.92E+02	2.30E+04	-9.24E-03	1.22E+01	4.90E+01
RootMzc2	Minimum	DLC1.4_0099_Sea_ECD-R+20_02.7Hz_16.4Tp_S03.out	3.69E+01	-4.52E+01	1.15E+03	1.25E+03	8.80E+02	-3.38E+02	5.84E+01	1.53E+03	-7.45E-01	1.68E+01	7.13E+01
RootMzc2	Maximum	DLC1.3_0119_Sea_16.0V0_03.4Hz_13.4Tp_S04.out	5.01E+02	1.27E+02	8.96E+02	-1.70E+03	1.72E+04	1.90E+02	5.17E+02	1.73E+04	-1.12E+00	1.10E+01	2.69E+02
RootFMxy2	Minimum	DLC1.3_0195_Sea_24.0V0_05.5Hz_18.3Tp_S05.out	-1.69E+00	3.27E+00	1.40E+03	-7.34E+02	-2.40E+03	-3.80E+01	-3.40E+00	2.51E+03	-3.00E+00	2.99E+01	6.11E+02
RootFMxy2	Maximum	DLC1.3_0069_Sea_10.0V0_02.2Hz_17.6Tp_S05.out	6.21E+02	-3.23E+02	7.16E+02	7.79E+03	2.05E+04	-5.39E+01	7.01E+02	2.18E+04	1.65E-01	1.42E+01	5.96E+01
RootMMxy2	Minimum	DLC1.3_0165_Sea_22.0V0_04.7Hz_15.7Tp_S01.out	6.72E+01	-2.47E+01	9.61E+02	-4.86E+01	-3.11E+01	-4.34E+01	7.16E+01	-7.15E+00	6.34E-01	2.14E+01	2.75E+02
RootMMxy2	Maximum	DLC1.3_0118_Sea_16.0V0_03.4Hz_10.1Tp_S04.out	6.10E+02	-3.13E+02	9.70E+02	9.09E+03	2.16E+04	-1.05E+02	6.92E+02	2.30E+04	-9.24E-03	1.22E+01	4.90E+01

Extreme events for Blade 3 Root:

Parameter	Type	File	RootFxc3 (kN)	RootFyc3 (kN)	RootFzc3 (kN)	RootMxc3 (kN-m)	RootMyc3 (kN-m)	RootMzc3 (kN-m)	RootFxa3 (kN)	RootMxa3 (kN-m)	WaveElev (m)	WindVel (m/sec)	Time (sec)
RootFxc3	Minimum	DLC1.3_0192_Sea_24.0V0_05.SHs_18.3Tp_S04.out	-1.35E+02	1.04E+02	1.20E+03	-2.94E+03	-7.03E+02	-1.25E+02	1.71E+02	7.63E+03	+8.72E-01	2.55E+01	5.62E+02
RootFxc3	Maximum	DLC1.3_0177_Sea_22.0V0_04.7Hs_15.7Tp_S05.out	6.25E+00	-1.57E+02	1.48E+03	3.98E+03	1.69E+04	5.55E+01	6.44E+02	1.74E+04	-1.22E+00	3.02E+01	6.30E+02
RootFyc3	Minimum	DLC1.1_0181_Sea_24.0V0_05.SHs_12.7Tp_S01.out	3.74E+02	-4.79E+02	9.89E+02	1.13E+04	1.11E+04	-1.08E+02	6.10E+02	1.58E+04	-2.76E+00	2.58E+01	5.67E+02
RootFyc3	Maximum	DLC1.1_0172_Sea_22.0V0_04.7Hs_11.0Tp_S04.out	8.13E+01	2.70E+02	9.84E+02	-6.56E+03	2.64E+02	-1.44E+02	2.83E+02	6.57E+03	6.11E-01	2.43E+01	5.40E+02
RootFzc3	Minimum	DLC1.3_0001_Sea_04.0V0_01.6Hs_08.9Tp_S01.out	4.40E+01	-1.40E+01	2.17E+01	2.92E+02	1.73E+03	-2.87E+01	4.61E+01	1.76E+03	-2.98E-01	2.11E+00	4.68E+01
RootFzc3	Maximum	DLC1.3_0165_Sea_22.0V0_04.7Hs_15.7Tp_S01.out	1.11E+02	-2.23E+01	1.97E+03	-5.53E+02	4.86E+02	-1.33E+02	1.10E+02	7.26E+02	-1.51E+00	2.71E+01	1.95E+02
RootMxc3	Minimum	DLC1.3_0187_Sea_24.0V0_05.SHs_12.7Tp_S03.out	1.34E+02	2.62E+02	9.60E+02	-6.99E+03	1.70E+03	-1.39E+02	2.94E+02	7.19E+03	-3.01E-01	2.66E+01	6.01E+02
RootMxc3	Maximum	DLC1.1_0183_Sea_24.0V0_05.SHs_18.3Tp_S01.out	3.84E+02	-4.77E+02	9.41E+02	1.14E+04	1.13E+04	-1.16E+02	6.12E+02	1.60E+04	-1.86E+00	2.64E+01	5.67E+02
RootMyc3	Minimum	DLC1.3_0192_Sea_24.0V0_05.SHs_18.3Tp_S04.out	-1.26E+02	6.32E+01	1.20E+03	-1.95E+03	-7.11E+03	-1.31E+02	1.41E+02	7.31E+03	-9.61E-01	2.60E+01	5.62E+02
RootMyc3	Maximum	DLC1.1_0105_Sea_14.0V0_03.0Hs_15.3Tp_S05.out	6.15E+00	-3.17E+02	7.94E+02	7.54E+03	2.17E+04	-4.45E+01	6.91E+02	2.30E+04	-4.69E-01	1.30E+01	1.99E+02
RootMzc3	Minimum	DLC1.4_0092_Sea_ECD-R+20_02.7Hs_12.7Tp_S01.out	1.96E+01	-4.51E+01	1.21E+03	1.23E+03	3.12E+02	-3.53E+02	4.91E+01	1.26E+03	-2.03E-02	1.68E+01	7.00E+01
RootMzc3	Maximum	DLC1.3_0124_Sea_16.0V0_03.4Hs_10.1Tp_S06.out	5.06E+02	1.86E+02	9.67E+02	-3.14E+03	1.74E+04	1.91E+02	5.40E+02	1.77E+04	-9.19E-01	2.04E+01	5.65E+01
RootFMxy3	Minimum	DLC1.3_0102_Sea_24.0V0_05.SHs_15.5Tp_S01.out	-3.71E+00	-1.95E-01	9.33E+02	-5.05E+02	-1.92E+03	-5.54E+01	-1.20E-01	1.97E+03	1.33E+00	2.67E+01	5.80E+02
RootFMxy3	Maximum	DLC1.3_0088_Sea_12.0V0_02.4Hs_09.2Tp_S06.out	6.17E+02	-3.96E+02	8.09E+02	9.76E+03	2.06E+04	-8.95E+01	7.34E+02	2.28E+04	-8.51E-01	1.32E+01	1.08E+02
RootMMxy3	Minimum	DLC1.3_0188_Sea_24.0V0_05.SHs_15.5Tp_S03.out	8.76E+01	-2.00E+01	1.26E+03	-1.06E+01	2.03E+01	-6.27E+01	8.99E+01	9.51E+00	1.19E+00	2.51E+01	4.05E+02
RootMMxy3	Maximum	DLC1.3_0088_Sea_12.0V0_02.4Hs_09.2Tp_S06.out	6.21E+02	-3.90E+02	8.15E+02	9.72E+03	2.08E+04	-1.01E+02	7.32E+02	2.30E+04	-4.95E-01	1.31E+01	1.08E+02

Extreme events for Blade 1 50%:

Parameter	Type	File	Spn1MLxb1 (kN-m)	Spn1MLyb1 (kN-m)	Spn1MLzb1 (kN-m)	Spn1MMxy1 (kN-m)	WaveElev (m)	WindVel (m/sec)	Time (sec)
Spn1MLxb1	Minimum	DLC1.1_0184_Sea_24.0V0_05.SHs_12.7Tp_S02.out	-1.71E+03	3.38E+02	-7.30E+01	1.74E+02	-1.64E+00	2.49E+01	5.72E+02
Spn1MLxb1	Maximum	DLC1.3_0196_Sea_24.0V0_05.SHs_12.7Tp_S06.out	1.72E+03	-8.25E+02	-1.24E+02	1.90E+03	3.00E+00	3.07E+01	2.75E+02
Spn1MLyb1	Minimum	DLC1.1_0181_Sea_24.0V0_05.SHs_12.7Tp_S01.out	4.38E+01	-2.88E+03	-1.20E+02	2.89E+03	1.95E+00	3.17E+01	2.49E+02
Spn1MLyb1	Maximum	DLC1.4_0003_Sea_ECD+R-20_02.0Hs_19.0Tp_S01.out	-2.48E+02	5.71E+03	1.79E+01	5.72E+03	-4.02E-01	5.66E+00	7.29E+01
Spn1MLzb1	Minimum	DLC1.1_0163_Sea_22.0V0_04.7Hs_11.0Tp_S01.out	2.47E+09	-9.46E+09	-2.34E+09	3.41E+09	-9.76E-01	2.89E+01	1.97E+09
Spn1MLzb1	Maximum	DLC1.3_0175_Sea_22.0V0_04.7Hs_11.0Tp_S05.out	-2.78E+02	2.22E+03	7.16E+01	2.24E+03	-1.59E+00	1.98E+01	4.75E+02
Spn1MMxy1	Minimum	DLC1.1_0174_Sea_22.0V0_04.7Hs_15.7Tp_S04.out	-8.93E-01	1.11E+00	-4.66E+01	-1.69E+01	8.28E-01	2.42E+01	3.62E+02
Spn1MMxy1	Maximum	DLC1.4_0003_Sea_ECD+R-20_02.0Hs_19.0Tp_S01.out	-2.48E+02	5.71E+03	1.79E+01	5.72E+03	-4.02E-01	5.66E+00	7.29E+01

Extreme events for Blade 2 50%:

Parameter	Type	File	Spn1MLxb2 (kN-m)	Spn1MLyb2 (kN-m)	Spn1MLzb2 (kN-m)	Spn1MMxy2 (kN-m)	WaveElev (m)	WindVel (m/sec)	Time (sec)
Spn1MLxb2	Minimum	DLC1.1_0149_Sea_20.0V0_04.4Hs_14.1Tp_S02.out	-1.63E+03	2.01E+03	1.83E+00	2.58E+03	-2.70E+00	2.21E+01	5.24E+02
Spn1MLxb2	Maximum	DLC1.3_0184_Sea_24.0V0_05.SHs_18.3Tp_S02.out	1.76E+03	-1.36E+03	-1.03E+02	9.22E+03	5.43E-01	2.80E+01	5.77E+02
Spn1MLyb2	Minimum	DLC1.3_0181_Sea_24.0V0_05.SHs_12.7Tp_S01.out	6.26E+01	-2.87E+03	-1.03E+02	2.87E+03	4.53E-01	2.81E+01	5.75E+02
Spn1MLyb2	Maximum	DLC1.3_0118_Sea_16.0V0_03.4Hs_10.1Tp_S04.out	6.86E+02	5.87E+03	-2.20E+01	5.91E+03	-1.61E-02	1.46E+01	4.99E+01
Spn1MLzb2	Minimum	DLC1.3_0165_Sea_22.0V0_04.7Hs_15.7Tp_S01.out	-4.03E+01	-7.97E+02	-2.30E+02	7.97E+02	-1.66E+00	2.74E+01	1.96E+02
Spn1MLzb2	Maximum	DLC1.3_0161_Sea_20.0V0_04.4Hs_14.1Tp_S06.out	-2.12E+02	2.67E+03	8.39E+01	2.68E+03	-3.10E-01	2.03E+01	6.20E+02
Spn1MMxy2	Minimum	DLC1.3_0142_Sea_18.0V0_03.7Hs_10.1Tp_S06.out	1.44E-01	-3.33E-01	-7.46E+01	-1.67E+01	1.18E-01	2.51E+01	4.59E+02
Spn1MMxy2	Maximum	DLC1.3_0118_Sea_16.0V0_03.4Hs_10.1Tp_S04.out	6.86E+02	5.87E+03	-2.20E+01	5.91E+03	-1.61E-02	1.46E+01	4.99E+01

Extreme events for Blade 3 50%:

Parameter	Type	File	Spn1MLxb3 (kN-m)	Spn1MLyb3 (kN-m)	Spn1MLzb3 (kN-m)	Spn1MMxy3 (kN-m)	WaveElev (m)	WindVel (m/sec)	Time (sec)
Spn1MLxb3	Minimum	DLC1.1_0196_Sea_24.0V0_05.SHs_12.7Tp_S06.out	-1.72E+03	9.22E+02	-6.94E+01	1.95E+03	-1.51E+00	2.98E+01	2.70E+02
Spn1MLxb3	Maximum	DLC1.3_0184_Sea_24.0V0_05.SHs_18.3Tp_S02.out	1.86E+03	-1.67E+03	-8.08E+01	2.49E+03	1.94E-01	2.65E+01	5.75E+02
Spn1MLyb3	Minimum	DLC1.3_0190_Sea_24.0V0_05.SHs_12.7Tp_S04.out	4.74E+02	-3.35E+03	-1.04E+02	3.36E+03	1.49E+00	3.00E+01	5.50E+02
Spn1MLyb3	Maximum	DLC1.4_0065_Sea_ECD-R-20_02.0Hs_14.8Tp_S04.out	9.40E+02	5.74E+03	-7.69E+01	5.82E+03	-7.54E-01	1.11E+01	6.67E+01
Spn1MLzb3	Minimum	DLC1.3_0165_Sea_22.0V0_04.7Hs_15.7Tp_S01.out	-1.99E+09	-8.21E+09	-2.53E+09	8.40E+09	-1.53E+00	2.72E+01	1.95E+09
Spn1MLzb3	Maximum	DLC1.3_0105_Sea_14.0V0_03.0Hs_15.3Tp_S05.out	-9.45E+02	3.31E+03	5.73E+01	3.46E+03	6.59E-03	6.61E+00	3.25E+02
Spn1MMxy3	Minimum	DLC1.3_0184_Sea_24.0V0_05.SHs_12.7Tp_S02.out	-4.29E+00	-6.81E+00	-1.16E+02	-7.68E-01	3.50E-01	2.75E+01	5.52E+02
Spn1MMxy3	Maximum	DLC1.4_0065_Sea_ECD-R-20_02.0Hs_14.8Tp_S04.out	9.40E+02	5.73E+03	-7.75E+01	5.82E+03	-7.53E-01	1.10E+01	6.66E+01

Extreme events for LSS Main Br:

Parameter	Type	File	RotThrust (kN)	LSSGagFya (kN)	LSSGagFza (kN)	RotTorq (kN-m)	LSSGagMya (kN-m)	LSSGagMza (kN-m)	LSSGagFMys (kN)	LSSGagMMys (kN-m)	WaveElev (m)	WindVel (m/sec)	Time (sec)
RotThrust	Minimum	DLC1.3_0196_Sea_24.0V0_05.SHs_12.7Tp_S06.out	-1.14E+03	-1.30E+03	-4.39E+02	3.79E+03	-2.29E+03	-1.15E+03	1.37E+03	2.57E+03	1.95E+00	2.92E+01	2.75E+02
RotThrust	Maximum	DLC1.1_0099_Sea_14.0V0_03.0Hs_12.0Tp_S03.out	1.66E+03	-1.27E+03	9.22E+02	6.42E+03	4.07E+03	2.16E+03	1.57E+03	4.61E+03	-1.41E+00	1.43E+01	5.36E+01
LSSGagFya	Minimum	DLC1.1_0186_Sea_24.0V0_05.SHs_18.3Tp_S02.out	6.63E+02	-1.76E+03	-1.66E+02	6.66E+03	3.45E+03	5.34E+03	1.77E+03	6.36E+03	6.67E-01	2.56E+01	3.85E+02
LSSGagFya	Maximum	DLC1.1_0101_Sea_24.0V0_05.SHs_12.7Tp_S01.out	5.09E+02	1.76E+03	9.45E+00	6.26E+03	2.33E+02	2.83E+02	1.77E+03	3.60E+02	-1.49E+00	3.04E+01	3.49E+02
LSSGagFza	Minimum	DLC1.1_0191_Sea_24.0V0_05.SHs_15.5Tp_S04.out	4.20E+02	8.55E+01	-1.76E+03	5.99E+03	7.20E+02	3.18E+03	1.76E+03	3.27E+03	-1.36E+00	2.91E+01	8.59E+01
LSSGagFza	Maximum	DLC1.1_0176_Sea_22.0V0_04.7Hs_13.4Tp_S05.out	5.81E+02	2.79E+01	1.78E+02	5.94E+03	-2.02E+03	-6.39E+03	1.78E+03	6.70E+03	-1.79E+00	2.14E+01	5.53E+02
RotTorq	Minimum	DLC1.3_0008_Sea_04.0V0_01.4Hs_12.7Tp_S03.out	9.18E+01	-1.15E+09	1.45E+02	-7.15E+01	4.79E+03	-3.18E+09	1.46E+03	4.80E+03	1.64E-01	9.01E-01	1.95E+02
RotTorq	Maximum	DLC1.1_0193_Sea_24.0V0_05.SHs_12.7Tp_S05.out	1.07E+03	-1.69E+03	-2.57E+01	8.04E+03	2.59E+03	-1.48E+03	1.69E+03	2.98E+03	-3.04E+00	2.46E+01	2.31E+02
LSSGagMya	Minimum	DLC1.3_0187_Sea_24.0V0_05.SHs_12.7Tp_S03.out	7.74E+02	-1.18E+03	-7.26E+02	6.31E+03	-1.41E+04	5.04E+03	1.39E+03	1.51E+04	-8.64E-01	2.80E+01	2.75E+02
LSSGagMya	Maximum	DLC1.3_0175_Sea_22.0V0_04.7Hs_11.0Tp_S05.out	9.16E+02	3.11E+02	1.34E+03	6.53E+03	1.60E+04	3.80E+03	1.38E+03	1.65E+04	-8.92E-02	2.60E+01	6.20E+02
LSSGagMza	Minimum	DLC1.3_0177_Sea_22.0V0_04.7Hs_15.7Tp_S05.out	8.73E+02	1.08E+03	-1.01E+03	6.09E+03	-6.03E+03	-1.54E+04	1.46E+03	1.65E+04	-1.22E+00	3.06E+01	6.29E+02
LSSGagMza	Maximum	DLC1.3_0187_Sea_24.0V0_05.SHs_12.7Tp_S02.out	3.69E+02	-5.75E+02	1.16E+02	5.98E+02	-1.74E+03	1.46E+04	1.29E+03	1.47E+04	-1.40E+00	2.61E+01	2.84E+02
LSSGagMYz	Minimum	DLC1.3_0185_Sea_24.0V0_05.SHs_15.5Tp_S02.out	4.72E+02	3.17E+02	-1.05E+02	5.40E+02	3.52E+02	-6.59E+02	1.09E+02	7.47E+02	-1.88E+00	2.52E+01	5.72E+02
LSSGagMYz	Maximum	DLC1.1_0189_Sea_24.0V0_05.SHs_18.3Tp_S03.out	5.07E+02	-1.74E+03	5.34E+02	6.59E+03	4.35E+03	-1.41E+03	1.82E+03	4.50E+03	-4.13E+00	1.94E+01	8.87E+01
LSSGagMMyz	Minimum	DLC1.5_0742_Sea_EWSH-24.0_05.SHs_12.7Tp_S02.out	2.80E+02	2.16E+02	1.38E+03	4.97E+03	-1.26E+02	-3.02E+00	1.39E+03	-5.53E+01	1.43E-01	2.40E+01	3.73E+01
LSSGagMMyz	Maximum	DLC1.3_0177_Sea_22.0V0_04.7Hs_15.7Tp_S05.out	9.04E+02	9.76E+02	-1.12E+03	6.02E+03	-6.96E+03	-1.52E+04	1.40E+03	1.60E+04	-1.22E+00	3.02E+01	6.30E+02

Extreme events for Yaw Bearing:

Parameter	Type	File	YawBrFxp (kN)	YawBrFyp (kN)	YawBrFzp (kN)	YawBrMxp (kN-m)	YawBrMyp (kN-m)	YawBrMzp (kN-m)	YawBrFMxy (kN)	YawBrMMxy (kN-m)	WaveElev (m)	WindVel (m/sec)	Time (sec)
YawBrFxp	Minimum	DLC1.3_0181_Sea_24.0V0_05.SHs_12.7Tp_S01.out	-9.49E+02	-1.86E+02	-4.64E+02	6.22E+03	-3.33E+03	6.53E+02	9.68E+02	7.06E+03	1.31E+00	2.38E+01	5.58E+02
YawBrFxp	Maximum	DLC1.1_0104_Sea_14.0V0_02.0Hs_12.0Tp_S05.out	2.43E+03	-8.58E+01	-5.16E+02	4.64E+03	4.26E+03	-1.64E+03	2.43E+03	6.37E+03	-5.95E-01	9.47E+00	1.16E+02
YawBrFyp	Minimum	DLC1.1_0179_Sea_22.0V0_04.7Hs_11.0Tp_S06.out	1.02E+03	-6.58E+02	-5.22E+03	8.37E+03	8.66E+03	1.70E+03	1.21E+03	1.20E+04	6.61E-02	1.94E+01	5.29E+02
YawBrFyp	Maximum	DLC1.3_0195_Sea_24.0V0_05.SHs_18.3Tp_S05.out	7.97E+02	5.31E+02	-4.56E+03	4.15E+03	2.00E+03	-5.32E+03	9.57E+02	4.60E+03	6.63E-01	2.58E+01	5.05E+02
YawBrFzp	Minimum	DLC1.1_0190_Sea_24.0V0_05.SHs_12.7Tp_S04.out	1.61E+02	5.99E+01	-5.41E+03	7.14E+03	-2.72E+02	4.06E+03	1.91E+03	7.15E+03	-3.97E+00	2.50E+01	2.97E+02
YawBrFzp	Maximum	DLC1.3_0187_Sea_24.0V0_05.SHs_12.7Tp_S03.out	1.52E+02	1.42E+02	-4.38E+03	4.61E+03	2.99E+03	-8.72E+03	2.03E+02	5.50E+03	2.78E+00	2.72E+01	3.14E+02
YawBrMxp	Minimum	DLC1.3_0013_Sea_04.0V0_01.6Hs_08.9Tp_S05.out	2.06E+02	1.12E+00	-4.64E+03	-1.73E+02	-6.70E+02	-2.47E+03	2.06E+02	6.92E+02	-6.11E-02	1.15E-02	4.82E+02
YawBrMxp	Maximum	DLC1.1_0193_Sea_24.0V0_05.SHs_12.7Tp_S05.out	1.38E+03	-3.05E+02	-5.32E+02	8.80E+03	4.82E+02	2.12E+03	1.41E+03	9.99E+02	-3.09E+00	2.49E+01	2.31E+02
YawBrMyp	Minimum	DLC1.3_0189_Sea_24.0V0_05.SHs_15.5Tp_S03.out	6.30E+02	-1.11E+02	-4.74E+03	5.95E+03	-1.33E+04	-1.99E+03	6.40E+02	1.45E+04	-8.02E-01	2.26E+01	6.06E+02
YawBrMyp	Maximum	DLC1.3_0192_Sea_24.0V0_05.SHs_18.3Tp_S04.out	1.00E+03	-8.09E+01	-4.41E+03	6.19E+03	1.70E+04	-4.26E+03	1.01E+03	1.81E+04	3.20E+00	3.12E+01	5.52E+02
YawBrMzp	Minimum	DLC1.3_0167_Sea_22.0V0_04.7Hs_13.4Tp_S02.out	5.48E+02	-5.14E+01	-4.51E+03	5.03E+03	-1.48E+03	-1.49E+04	5.50E+02	5.24E+03	1.01E+00	2.75E+01	4.65E+02
YawBrMzp	Maximum	DLC1.4_0062_Sea_ECD-R-20_02.0Hs_14.8Tp_S03.out	1.30E+03	-2.98E+01	-4.74E+03	4.75E+03	1.72E+02	1.19E+04	1.30E+03	4.75E+03	-4.67E-01	5.66E+00	7.55E+01
YawBrFMxy	Minimum	DLC1.3_0185_Sea_24.0V0_05.SHs_15.5Tp_S02.out	-1.92E+00	-9.15E-01	-4.61E+03	4.06E+03	5.46E+03	9.15E+02	-2.09E+00	7.31E+03	-1.56E+00	1.02E+01	5.05E+02
YawBrFMxy	Maximum	DLC1.1_0104_Sea_14.0V0_02.0Hs_12.0Tp_S05.out	2.43E+03	-8.59E+01	-5.16E+02	4.64E+03	4.26E+03	-1.64E+03	2.43E+03	6.37E+03	-5.95E-01	9.47E+00	1.16E+02
YawBrMMxy	Minimum	DLC1.3_0013_Sea_04.0V0_01.6Hs_08.9Tp_S05.out	1.52E+02	4.05E-01	-4.65E+03	-1.13E+00	2.23E+00	-7.75E+02	1.52E+02	1.29E+00	-4.03E-01	7.77E-01	4.83E+02
YawBrMMxy	Maximum	DLC1.3_0192_Sea_24.0V0_05.SHs_18.3Tp_S04.out	1.00E+03	-8.09E+01	-4.41E+03	6.19E+03	1.70E+04	-4.26E+03	1.01E+03	1.81E+04	3.20E+00	3.12E+01	5.52E+02

Extreme events for Tower Base:

Parameter	Type	File	TwrBsFxt (kN)	TwrBsFyt (kN)	TwrBsFzt (kN)	TwrBsMxt10 (kN-m)	TwrBsMyt10 (kN-m)	TwrBsMzt (kN-m)	TwrBsFMxy (kN)	TwrBsMMxy1 (kN-m)	WaveElev (m)	WindVxi (m/sec)	Time (sec)
TwrBsFxt	Minimum	DLC1.3_0181_Sea_24.0V0_05.5Hs_12.7Tp_S01.out	-1.38E+03	-2.23E+02	-7.92E+03	2.39E+04	-1.09E+05	1.09E+03	1.40E+03	1.11E+05	1.45E+00	2.42E+01	5.58E+02
TwrBsFxt	Maximum	DLC1.3_0098_Sea_14.0V0_03.0Hs_12.0Tp_S03.out	2.95E+03	-1.94E+02	-7.98E+03	1.95E+04	2.41E+05	7.10E+02	2.96E+03	2.42E+05	-2.15E-01	1.27E+01	5.21E+01
TwrBsFyt	Minimum	DLC1.3_0163_Sea_22.0V0_04.7Hs_11.0Tp_S01.out	1.45E+02	-6.74E+02	-8.02E+03	6.64E+04	2.23E+04	-1.02E+03	6.87E+02	7.03E+04	-3.71E-01	2.00E+01	3.01E+02
TwrBsFyt	Maximum	DLC1.1_0198_Sea_24.0V0_05.5Hs_18.1Tp_S06.out	4.92E+02	5.84E+02	-8.80E+03	-4.15E+04	3.42E+04	-2.18E+03	7.42E+02	5.27E+04	-1.62E-01	2.97E+01	5.48E+02
TwrBsFzt	Minimum	DLC1.1_0190_Sea_24.0V0_05.5Hs_12.7Tp_S04.out	-7.73E+01	3.68E+01	-9.12E+03	3.12E+03	1.54E+03	4.06E+02	8.63E+01	3.48E+03	-3.97E+00	2.50E+01	2.97E+02
TwrBsFzt	Maximum	DLC1.3_0187_Sea_24.0V0_05.5Hs_12.7Tp_S02.out	2.82E+02	2.78E+02	-7.65E+03	-1.55E+04	2.05E+04	-8.72E+02	2.95E+02	2.57E+04	2.78E+00	2.72E+01	2.14E+02
TwrBsMxt10	Minimum	DLC1.3_0195_Sea_24.0V0_05.5Hs_10.3Tp_S05.out	1.02E+03	5.03E+02	-7.07E+02	-4.56E+04	8.71E+04	-4.70E+03	1.17E+03	9.03E+04	6.95E-01	2.60E+01	5.05E+02
TwrBsMxt10	Maximum	DLC1.1_0170_Sea_22.0V0_04.7Hs_11.0Tp_S06.out	7.76E+02	-6.61E+02	-8.90E+03	6.01E+04	8.04E+04	1.03E+03	1.02E+03	1.12E+05	9.96E-02	1.03E+01	5.29E+02
TwrBsMyt10	Minimum	DLC1.3_0181_Sea_24.0V0_05.5Hs_12.7Tp_S01.out	-1.38E+03	-2.23E+02	-7.92E+03	2.39E+04	-1.09E+05	1.09E+03	1.40E+03	1.11E+05	1.45E+00	2.42E+01	5.58E+02
TwrBsMyt10	Maximum	DLC1.3_0098_Sea_14.0V0_03.0Hs_12.0Tp_S03.out	2.95E+03	-1.94E+02	-7.98E+03	1.95E+04	2.41E+05	7.10E+02	2.96E+03	2.42E+05	-2.15E-01	1.27E+01	5.21E+01
TwrBsMzt	Minimum	DLC1.3_0167_Sea_22.0V0_04.7Hs_13.4Tp_S02.out	7.38E+02	1.49E+01	-7.80E+03	6.37E+03	5.48E+04	-1.40E+04	7.38E+02	5.51E+04	1.01E+00	2.75E+01	4.65E+02
TwrBsMzt	Maximum	DLC1.4_0062_Sea_ECD-R-20_02.0Hs_14.0Tp_S03.out	1.49E+03	-4.51E+01	-8.05E+03	9.59E+03	1.25E+05	1.19E+04	1.49E+03	1.25E+05	-4.67E-01	5.66E+00	7.55E+01
TwrBsMMxy	Minimum	DLC1.3_0168_Sea_22.0V0_04.7Hs_15.7Tp_S02.out	5.39E+00	2.11E+00	-7.93E+03	7.05E+03	-8.95E+02	-5.84E+03	-4.71E+00	7.90E+03	-1.74E+00	2.11E+01	5.59E+02
TwrBsFMxy	Maximum	DLC1.3_0098_Sea_14.0V0_03.0Hs_12.0Tp_S03.out	2.95E+03	-1.94E+02	-7.98E+03	1.95E+04	2.41E+05	7.10E+02	2.96E+03	2.42E+05	-2.15E-01	1.27E+01	5.21E+01
TwrBsMMxy1	Minimum	DLC1.3_0189_Sea_24.0V0_05.5Hs_18.3Tp_S03.out	-9.68E+01	3.94E+01	-7.87E+03	6.75E-01	2.92E+02	-2.48E+03	1.05E+02	-8.05E+01	4.99E-01	3.05E+01	3.38E+02
TwrBsMMxy1	Maximum	DLC1.3_0098_Sea_14.0V0_03.0Hs_12.0Tp_S03.out	2.95E+03	-1.94E+02	-7.98E+03	1.95E+04	2.41E+05	7.10E+02	2.96E+03	2.42E+05	-2.15E-01	1.27E+01	5.21E+01

Extreme events for Tower 50%:

Parameter	Type	File	TwHt1MLxt (kN-m)	TwHt1MLyt (kN-m)	TwHt1MLzt (kN-m)	TwHt1MMxy (kN-m)	WaveElev (m)	WindVxi (m/sec)	Time (sec)
TwHt1MLxt	Minimum	DLC1.3_0195_Sea_24.0V0_05.5Hs_10.3Tp_S05.out	-1.06E+04	3.73E+04	-4.14E+03	4.14E+04	5.22E-03	1.95E+01	5.07E+02
TwHt1MLxt	Maximum	DLC1.1_0170_Sea_22.0V0_04.7Hs_11.0Tp_S06.out	3.63E+04	4.99E+04	1.52E+03	6.17E+04	9.62E-02	1.92E+01	5.29E+02
TwHt1MLyt	Minimum	DLC1.3_0181_Sea_24.0V0_05.5Hs_12.7Tp_S01.out	1.43E+04	-4.73E+04	6.52E+02	4.96E+04	1.31E+00	2.38E+01	5.58E+02
TwHt1MLyt	Maximum	DLC1.1_0104_Sea_14.0V0_03.0Hs_12.0Tp_S05.out	8.04E+03	1.09E+05	-1.68E+03	1.09E+05	-5.41E-01	9.43E+00	1.16E+02
TwHt1MLzt	Minimum	DLC1.3_0167_Sea_22.0V0_04.7Hs_13.4Tp_S02.out	6.63E+03	2.21E+04	-1.48E+04	2.31E+04	1.01E+00	2.75E+01	4.65E+02
TwHt1MLzt	Maximum	DLC1.4_0062_Sea_ECD-R-20_02.0Hs_14.0Tp_S03.out	6.40E+03	5.60E+04	1.19E+04	5.6E+04	-4.67E-01	5.66E+00	7.55E+01
TwHt1MMxy	Minimum	DLC1.1_0016_Sea_04.0V0_01.4Hs_08.9Tp_S06.out	4.60E+00	-2.81E+00	2.02E+02	5.33E+00	7.01E-01	4.24E+00	3.64E+02
TwHt1MMxy	Maximum	DLC1.1_0104_Sea_14.0V0_03.0Hs_12.0Tp_S05.out	8.04E+03	1.09E+05	-1.68E+03	1.09E+05	-5.41E-01	9.43E+00	1.16E+02

Extreme events for Line 1:

Parameter	Type	File	Anch1Ten (kN)	Anch1Ang (deg)	Fair1Ten (kN)	Fair1Ang (deg)	WaveElev (m)	WindVxi (m/sec)	Time (sec)
Anch1Ten	Minimum	DLC1.4_0033_Sea_ECD+R_02.4Hs_17.6Tp_S05.out	4.10E+02	0.00E+00	6.44E+02	5.04E+01	1.20E-01	1.22E+01	6.93E+01
Anch1Ten	Maximum	DLC1.5_0774_Sea_EWSV+24.0_05.5Hs_18.3Tp_S06.out	1.19E+03	0.00E+00	1.43E+03	3.33E+01	4.24E-01	2.40E+01	3.00E+01
Anch1Ang	Minimum	DLC1.1_0001_Sea_04.0V0_01.4Hs_08.9Tp_S01.out	1.07E+03	0.00E+00	1.33E+03	3.66E+01	3.19E-01	2.13E+00	3.00E+01
Anch1Ang	Maximum	DLC1.1_0001_Sea_04.0V0_01.4Hs_08.9Tp_S01.out	1.07E+03	0.00E+00	1.33E+03	3.66E+01	3.19E-01	2.13E+00	3.00E+01
Fair1Ten	Minimum	DLC1.4_0033_Sea_ECD+R_02.4Hs_17.6Tp_S05.out	4.10E+02	0.00E+00	6.44E+02	5.04E+01	1.99E-01	1.22E+01	6.92E+01
Fair1Ten	Maximum	DLC1.5_0774_Sea_EWSV+24.0_05.5Hs_18.3Tp_S06.out	1.19E+03	0.00E+00	1.43E+03	3.33E+01	4.24E-01	2.40E+01	3.00E+01

Extreme events for Line 2:

Parameter	Type	File	Anch2Ten (kN)	Anch2Ang (deg)	Fair2Ten (kN)	Fair2Ang (deg)	WaveElev (m)	WindVxi (m/sec)	Time (sec)
Anch2Ten	Minimum	DLC1.5_0774_Sea_EWSV+24.0_05.5Hs_18.3Tp_S06.out	9.18E+02	0.00E+00	1.15E+03	3.72E+01	4.24E-01	2.40E+01	3.00E+01
Anch2Ten	Maximum	DLC1.1_0069_Sea_10.0V0_02.2Hs_17.6Tp_S05.out	1.87E+03	2.43E+00	2.13E+03	2.88E+01	1.33E-01	1.03E+01	7.85E+01
Anch2Ang	Minimum	DLC1.1_0001_Sea_04.0V0_01.4Hs_08.9Tp_S01.out	1.13E+03	0.00E+00	1.39E+03	3.57E+01	3.19E-01	2.13E+00	3.00E+01
Anch2Ang	Maximum	DLC1.4_0036_Sea_ECD+R_02.4Hs_17.6Tp_S06.out	1.77E+03	3.07E+00	2.01E+03	2.01E+01	3.49E-01	1.19E+01	7.33E+01
Fair2Ten	Minimum	DLC1.5_0774_Sea_EWSV+24.0_05.5Hs_18.3Tp_S06.out	9.18E+02	0.00E+00	1.15E+03	3.72E+01	4.24E-01	2.40E+01	3.00E+01
Fair2Ten	Maximum	DLC1.1_0069_Sea_10.0V0_02.2Hs_17.6Tp_S05.out	1.87E+03	2.43E+00	2.13E+03	2.87E+01	5.30E-01	9.98E+00	7.73E+01

Extreme events for Line 3:

Parameter	Type	File	Anch3Ten (kN)	Anch3Ang (deg)	Fair3Ten (kN)	Fair3Ang (deg)	WaveElev (m)	WindVxi (m/sec)	Time (sec)
Anch3Ten	Minimum	DLC1.5_0774_Sea_EWSV+24.0_05.5Hs_18.3Tp_S06.out	0.92E+02	0.00E+00	1.13E+03	3.77E+01	4.24E-01	2.40E+01	3.00E+01
Anch3Ten	Maximum	DLC1.1_0069_Sea_10.0V0_02.2Hs_17.6Tp_S05.out	1.90E+03	2.66E+00	2.16E+03	2.85E+01	4.91E-01	1.01E+01	7.73E+01
Anch3Ang	Minimum	DLC1.1_0001_Sea_04.0V0_01.4Hs_08.9Tp_S01.out	1.13E+03	0.00E+00	1.39E+03	3.57E+01	3.19E-01	2.13E+00	3.00E+01
Anch3Ang	Maximum	DLC1.4_0087_Sea_ECD-R_02.4Hs_17.6Tp_S05.out	1.77E+02	2.16E+00	2.01E+02	2.82E+01	8.96E-01	1.19E+01	7.92E+01
Fair3Ten	Minimum	DLC1.5_0774_Sea_EWSV+24.0_05.5Hs_18.3Tp_S06.out	0.92E+02	0.00E+00	1.13E+03	3.77E+01	4.24E-01	2.40E+01	3.00E+01
Fair3Ten	Maximum	DLC1.1_0069_Sea_10.0V0_02.2Hs_17.6Tp_S05.out	1.90E+03	2.66E+00	2.16E+03	2.85E+01	7.32E-01	1.04E+01	7.63E+01

Extreme events for Line 4:

Parameter	Type	File	Anch4Ten (kN)	Anch4Ang (deg)	Fair4Ten (kN)	Fair4Ang (deg)	WaveElev (m)	WindVxi (m/sec)	Time (sec)
Anch4Ten	Minimum	DLC1.4_0033_Sea_ECD+R_02.4Hs_17.6Tp_S05.out	4.10E+02	0.00E+00	6.44E+02	5.04E+01	1.20E-01	1.22E+01	6.93E+01
Anch4Ten	Maximum	DLC1.5_0774_Sea_EWSV+24.0_05.5Hs_18.3Tp_S06.out	1.19E+03	0.00E+00	1.43E+03	3.33E+01	4.24E-01	2.40E+01	3.00E+01
Anch4Ang	Minimum	DLC1.1_0001_Sea_04.0V0_01.4Hs_08.9Tp_S01.out	1.07E+03	0.00E+00	1.33E+03	3.66E+01	3.19E-01	2.13E+00	3.00E+01
Anch4Ang	Maximum	DLC1.1_0001_Sea_04.0V0_01.4Hs_08.9Tp_S01.out	1.07E+03	0.00E+00	1.33E+03	3.66E+01	3.19E-01	2.13E+00	3.00E+01
Fair4Ten	Minimum	DLC1.4_0033_Sea_ECD+R_02.4Hs_17.6Tp_S05.out	4.10E+02	0.00E+00	6.44E+02	5.04E+01	1.99E-01	1.23E+01	6.92E+01
Fair4Ten	Maximum	DLC1.5_0774_Sea_EWSV+24.0_05.5Hs_18.3Tp_S06.out	1.19E+03	0.00E+00	1.43E+03	3.33E+01	4.24E-01	2.40E+01	3.00E+01

Extreme events for Line 5:

Parameter	Type	File	Anch5Ten (kN)	Anch5Ang (deg)	Fair5Ten (kN)	Fair5Ang (deg)	WaveElev (m)	WindVxi (m/sec)	Time (sec)
Anch5Ten	Minimum	DLC1.4_0033_Sea_ECD+R_02.4Hs_17.6Tp_S05.out	4.10E+02	0.00E+00	6.44E+02	5.04E+01	1.20E-01	1.22E+01	6.93E+01
Anch5Ten	Maximum	DLC1.5_0774_Sea_EWSV+24.0_05.5Hs_18.3Tp_S06.out	1.19E+03	0.00E+00	1.43E+03	3.33E+01	4.24E-01	2.40E+01	3.00E+01
Anch5Ang	Minimum	DLC1.1_0001_Sea_04.0V0_01.4Hs_08.9Tp_S01.out	1.07E+03	0.00E+00	1.33E+03	3.66E+01	3.19E-01	2.13E+00	3.00E+01
Anch5Ang	Maximum	DLC1.1_0001_Sea_04.0V0_01.4Hs_08.9Tp_S01.out	1.07E+03	0.00E+00	1.33E+03	3.66E+01	3.19E-01	2.13E+00	3.00E+01
Fair5Ten	Minimum	DLC1.4_0033_Sea_ECD+R_02.4Hs_17.6Tp_S05.out	4.10E+02	0.00E+00	6.44E+02	5.04E+01	1.99E-01	1.23E+01	6.92E+01
Fair5Ten	Maximum	DLC1.5_0774_Sea_EWSV+24.0_05.5Hs_18.3Tp_S06.out	1.19E+03	0.00E+00	1.43E+03	3.33E+01	4.24E-01	2.40E+01	3.00E+01

Extreme events for Line 6:

Parameter	Type	File	Anch6Ten (kN)	Anch6Ang (deg)	Fair6Ten (kN)	Fair6Ang (deg)	WaveElev (m)	WindVxi (m/sec)	Time (sec)
Anch6Ten	Minimum	DLC1.4_0033_Sea_ECD+R_02.4Hs_17.6Tp_S05.out	4.10E+02	0.00E+00	6.44E+02	5.04E+01	1.20E-01	1.22E+01	6.93E+01
Anch6Ten	Maximum	DLC1.5_0774_Sea_EWSV+24.0_05.5Hs_18.3Tp_S06.out	1.19E+03	0.00E+00	1.43E+03	3.33E+01	4.24E-01	2.40E+01	3.00E+01
Anch6Ang	Minimum	DLC1.1_0001_Sea_04.0V0_01.4Hs_08.9Tp_S01.out	1.07E+03	0.00E+00	1.33E+03	3.66E+01	3.19E-01	2.13E+00	3.00E+01
Anch6Ang	Maximum	DLC1.1_0001_Sea_04.0V0_01.4Hs_08.9Tp_S01.out	1.07E+03	0.00E+00	1.33E+03	3.66E+01	3.19E-01	2.13E+00	3.00E+01
Fair6Ten	Minimum	DLC1.4_0033_Sea_ECD+R_02.4Hs_17.6Tp_S05.out	4.10E+02	0.00E+00	6.44E+02	5.04E+01	1.99E-01	1.23E+01	6.92E+01
Fair6Ten	Maximum	DLC1.5_0774_Sea_EWSV+24.0_05.5Hs_18.3Tp_S06.out	1.19E+03	0.00E+00	1.43E+03	3.33E+01	4.24E-01	2.40E+01	3.00E+01

Appendix B. Instabilities

When analyzing the various instabilities for the floating tension leg platform and OC3-Hywind wind turbine systems, note that an extensive study on the instability first encountered in DLC 6.2a has been conducted. In this design load case 6.2a, the rotor is idling with all blades fully feathered at a pitch angle of 90° and with different yaw misalignments ranging from –180° < Yaw < +180°. The charts presented in this section were obtained with a setup similar to DLC 6.2. A constant wind speed of 50 m/s with no shear and still water was used.

Next, constant yaw errors of the nacelle are simulated from –180° < Yaw < +180° in 0.5° steps. All degrees of freedom are activated in the FAST models. For both the TLP and the OC3-Hywind five charts are provided. The first presents the damping ratios for the 6 platform DOFs, the second chart presents the first tower side-to-side and fore-aft DOFs and the drivetrain DOF. The third chart shows the two first flap-wise blade DOFs, the fourth shows the three first edgewise blade DOFs, and the last chart depicts the second modes for the tower and the blades.

Note that the blades in this case are pitched to 90°, so, the flap modes are actually in plane and the edge modes are actually out of plane (reverse to what is normally expected). The drivetrain torsion eliminates one in-plane mode. Therefore, in this case, the charts show 2 flap and 3 edge modes (The 90° blade pitch also explains why one of the tower frequencies shifted so much).

Due to difficulties in clearly identifying each mode—especially for 2nd tower and blade modes—the legend shows the natural frequency at 0° yaw error for each mode. These damping ratios show that, for this particular load case, 8 negatively damped modes for the TLP and 7 negatively damped modes for the OC3-Hywind exist.

Additionally, the charts in B.3 present a section of the time series of the angle of attack α and the lift coefficient c_l at two positions (60% blade length and blade tip) on blade 1 for a yaw misalignment of 40° in a 1-DOF platform yaw model. These diagrams have been created for all three blades at different yaw misalignments for all 1-DOF models where negative damping ratios were found.

B.1. Damping Ratios Tension Leg Platform

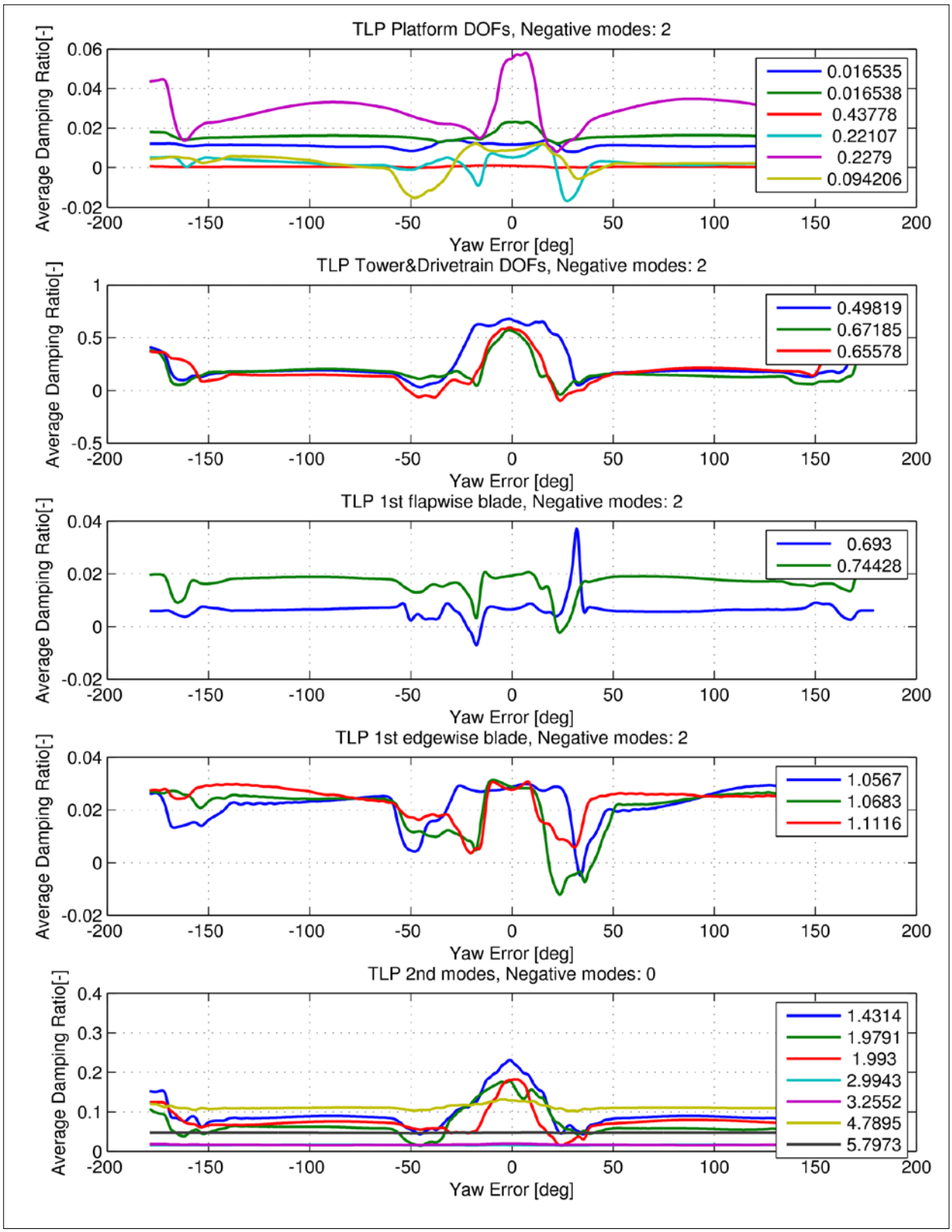

B.2. Damping Ratios OC3-Hywind

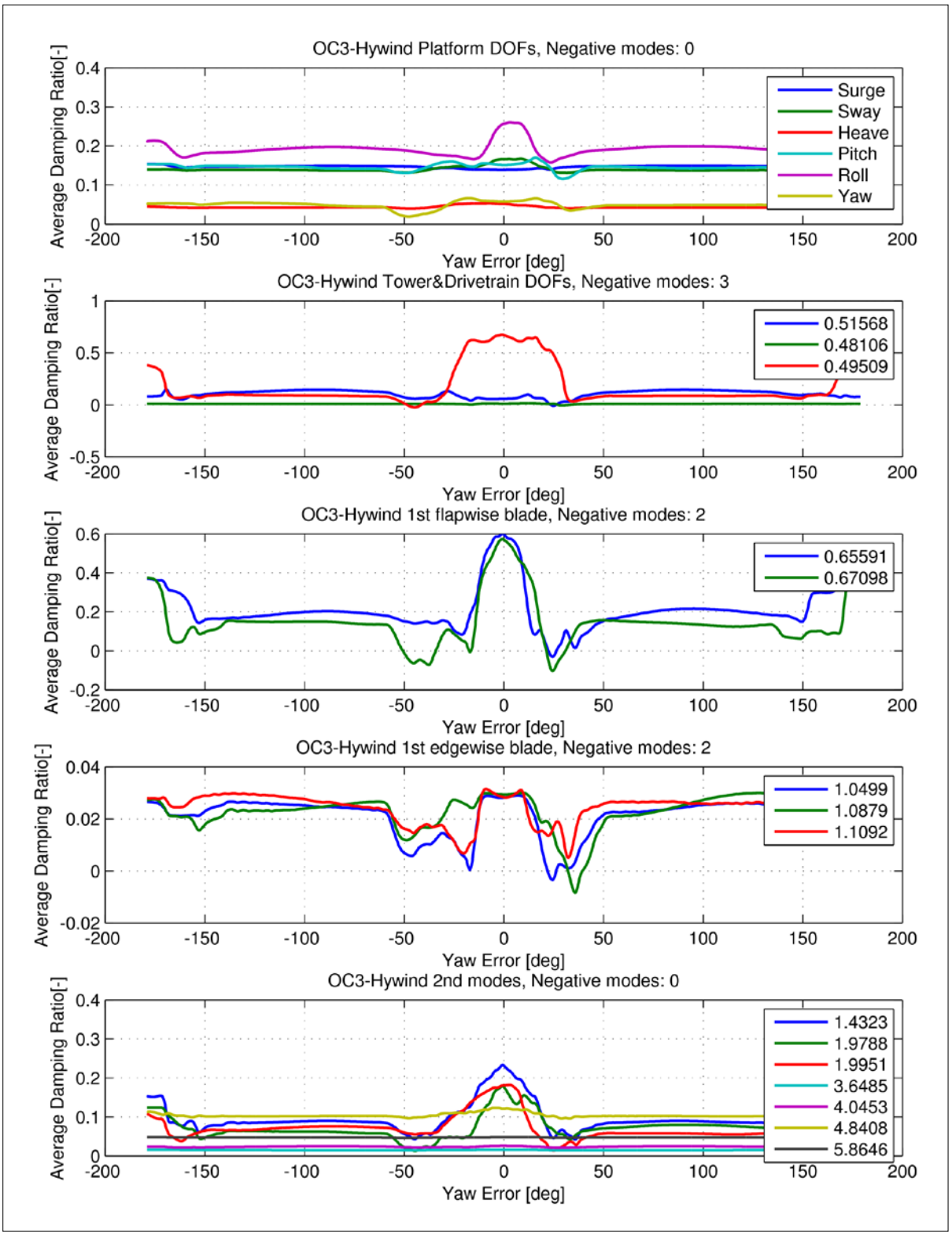

B.3. Angle of Attack

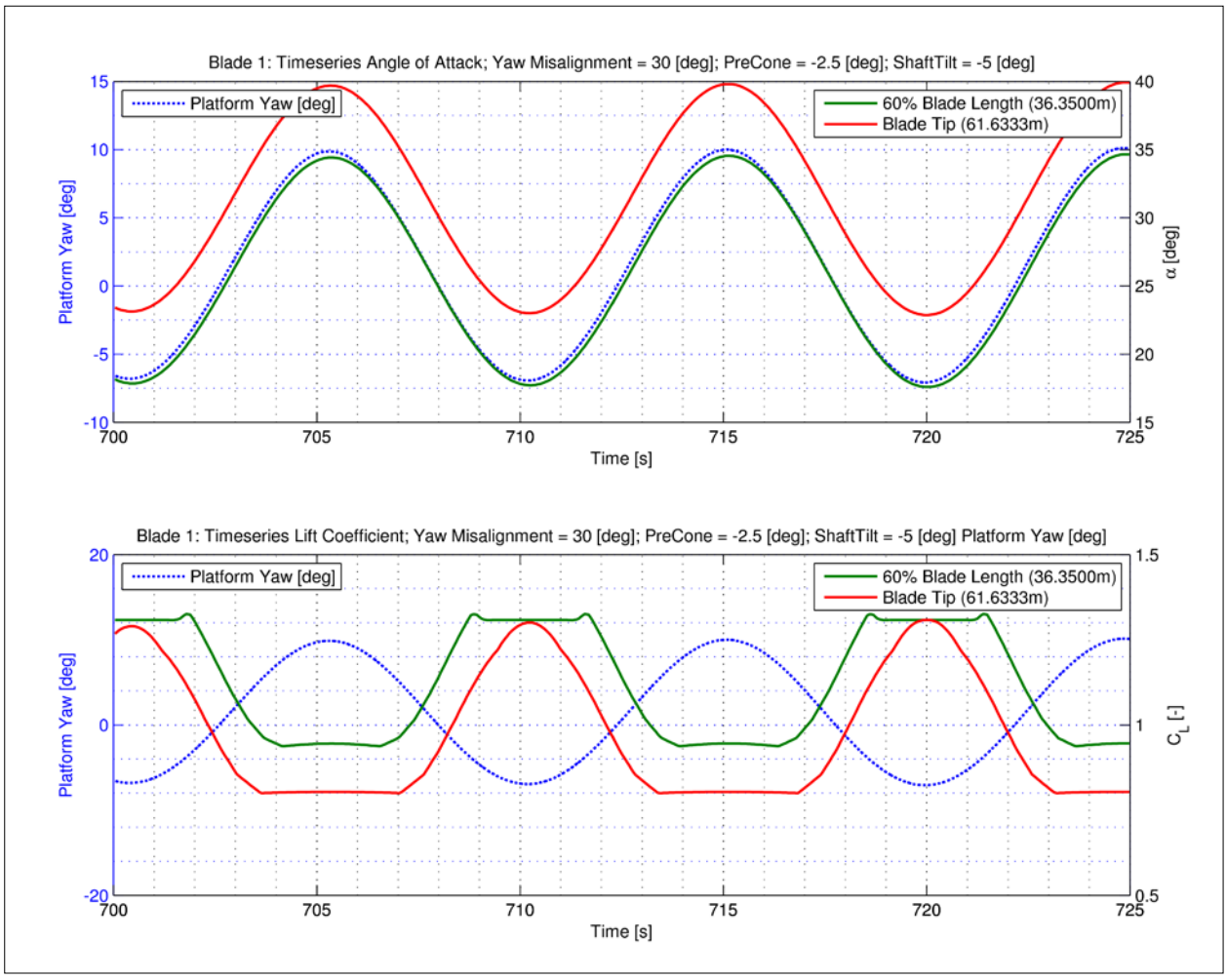

Appendix C. Time Histories

This appendix presents time histories of FAST design load case simulations for the TLP and OC3-Hywind concepts for certain output parameters. The diagrams have been created with the postprocessor MCrunch. In general, time histories are very useful tools used to analyze extreme events and instabilities; they also help to compare the behavior of different designs under distinctive environmental conditions (e.g., wind gusts, high waves). The following charts help to better explain certain wind-triggered and wave-triggered effects described in the report.

C.1. Low-Speed Shaft Moment Design Load Case 1.4

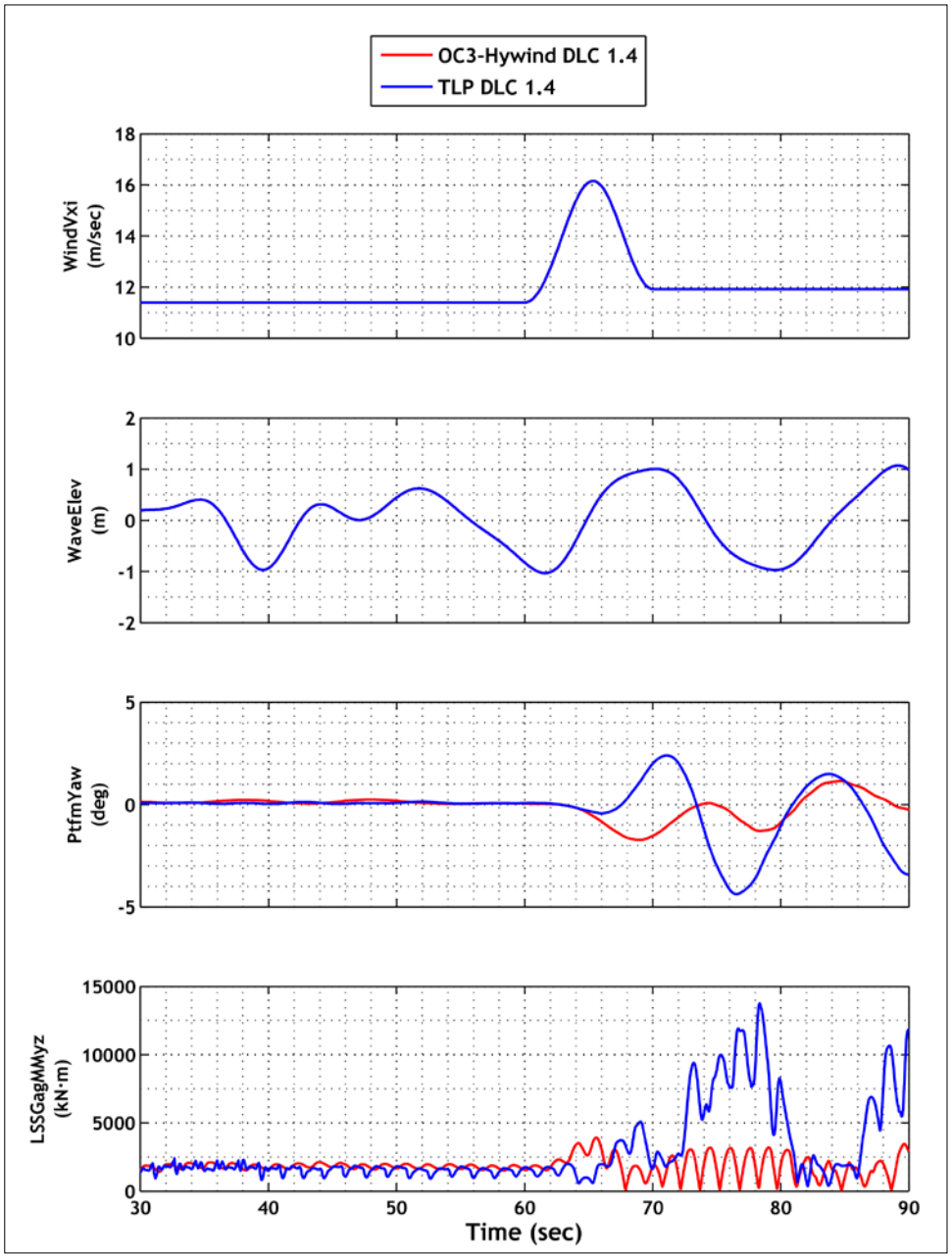

C.2. Blade 1 Root Moment Design Load Case 1.4

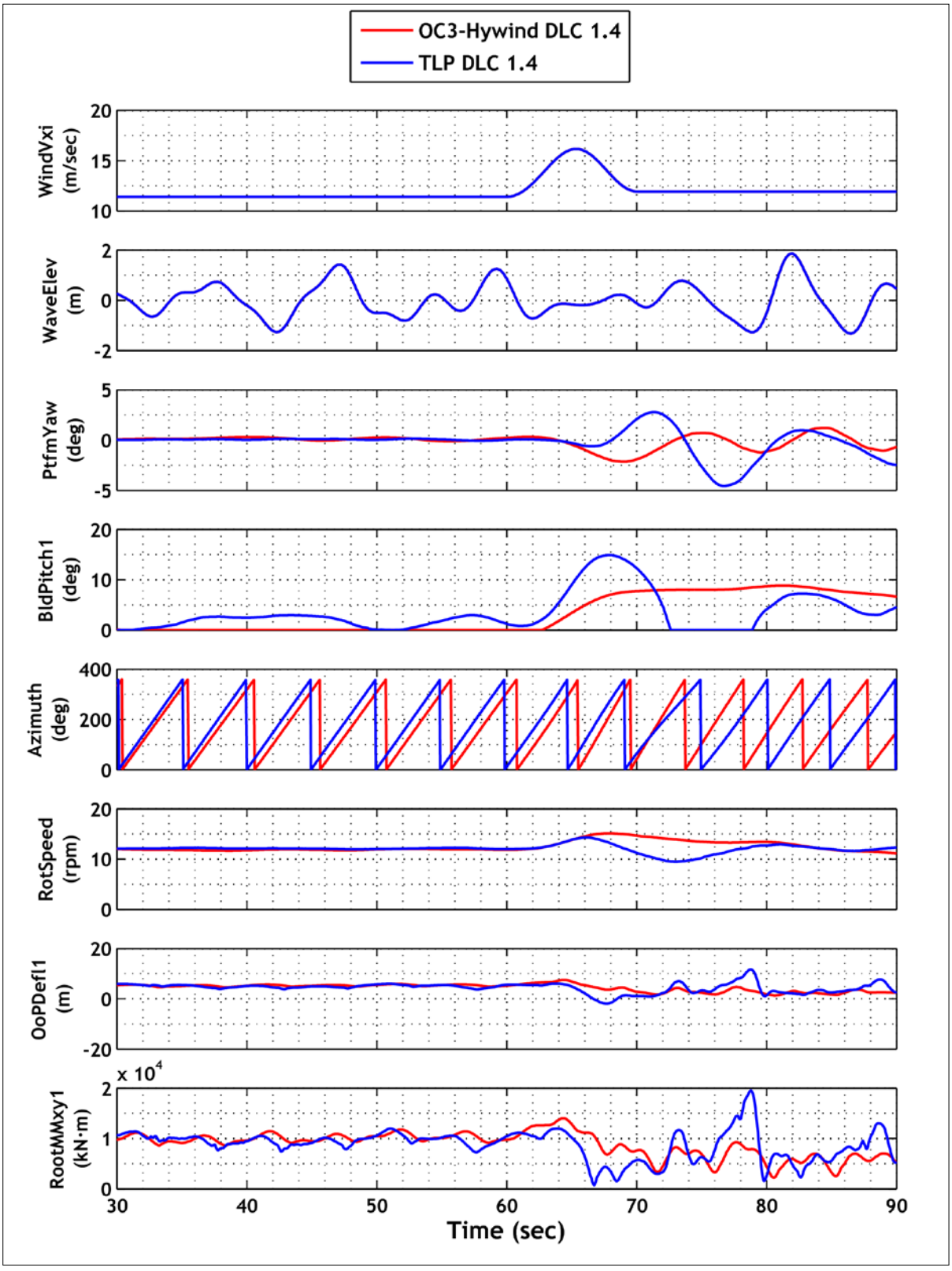

C.3. Tower-Top Displacements Design Load Case 1.3

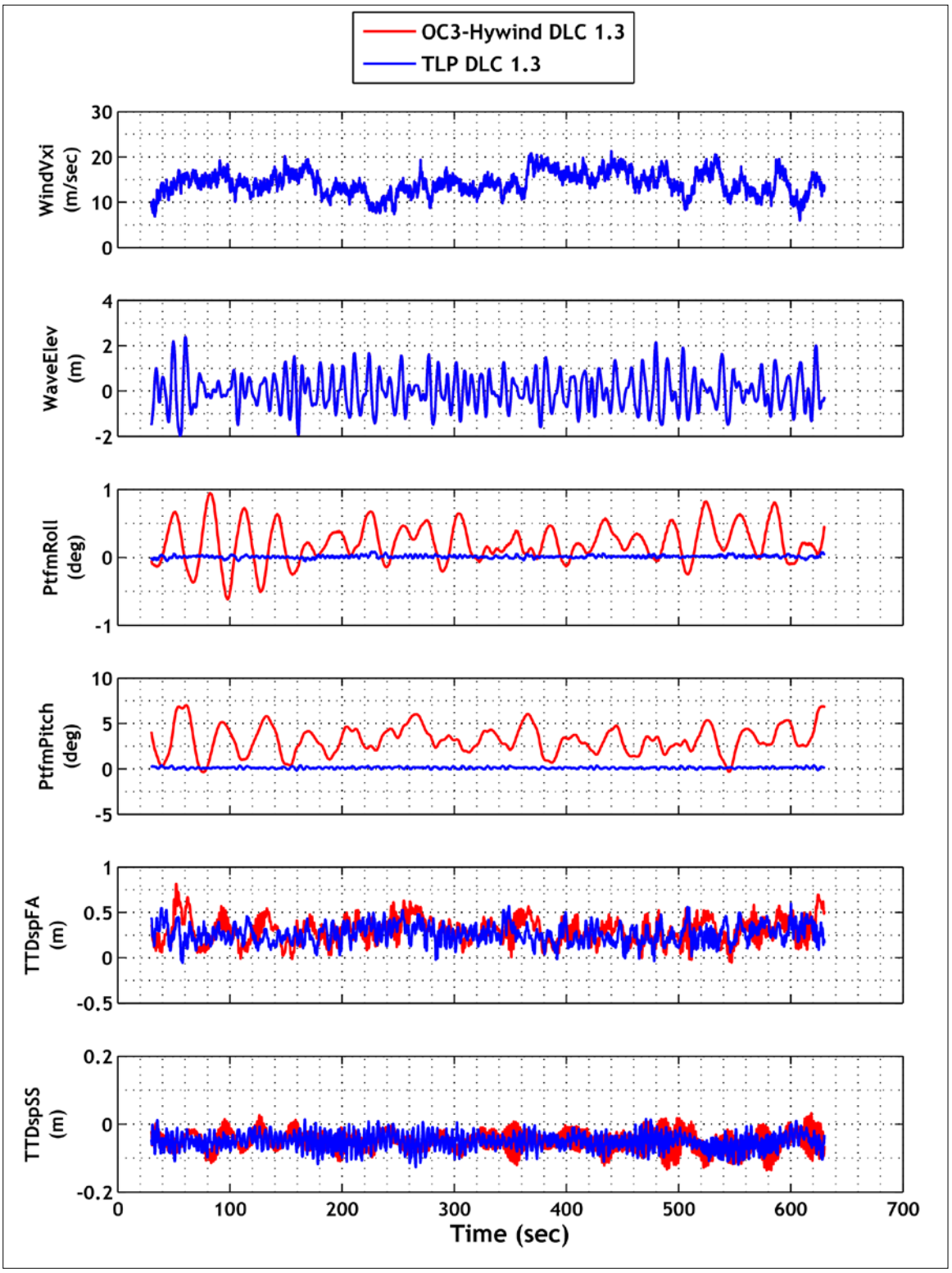

REPORT DOCUMENTATION PAGE

Form Approved
OMB No. 0704-0188

PLEASE DO NOT RETURN YOUR FORM TO THE ABOVE ORGANIZATION.

1. REPORT DATE *(DD-MM-YYYY)*	2. REPORT TYPE	3. DATES COVERED *(From - To)*
February 2010	Subcontract Report	April 2009

4. TITLE AND SUBTITLE
Model Development and Loads Analysis of an Offshore Wind Turbine on a Tension Leg Platform, with a Comparison to Other Floating Turbine Concepts

5a. CONTRACT NUMBER
DE-AC36-08-GO28308

5b. GRANT NUMBER

5c. PROGRAM ELEMENT NUMBER

6. AUTHOR(S)
D. Matha

5d. PROJECT NUMBER
NREL/SR-500-45891

5e. TASK NUMBER
WE101161

5f. WORK UNIT NUMBER

7. PERFORMING ORGANIZATION NAME(S) AND ADDRESS(ES)
University of Colorado - Boulder
c/o Professor Gary Pawles, Dept. of Mechanical Engineering
427 UCB
Boulder, CO 80309-0427

8. PERFORMING ORGANIZATION REPORT NUMBER
KXEA-3-33606-3

9. SPONSORING/MONITORING AGENCY NAME(S) AND ADDRESS(ES)
National Renewable Energy Laboratory
1617 Cole Blvd.
Golden, CO 80401-3393

10. SPONSOR/MONITOR'S ACRONYM(S)
NREL

11. SPONSORING/MONITORING AGENCY REPORT NUMBER
NREL/SR-500-45891-

12. DISTRIBUTION AVAILABILITY STATEMENT
National Technical Information Service
U.S. Department of Commerce
5285 Port Royal Road
Springfield, VA 22161

13. SUPPLEMENTARY NOTES
NREL Technical Monitor: Jason Jonkman

14. ABSTRACT *(Maximum 200 Words)*
This report presents results of the analysis of a 5-MW wind turbine located on a floating offshore tension leg platform (TLP) that was conducted using the fully coupled time-domain aero-hydro-servo-elastic design code FAST with AeroDyn and HydroDyn. The report also provides a description of the development process of the TLP model. The model has been verified via comparisons to frequency-domain calculations. Important differences have been identified between the frequency-domain and time-domain simulations, and have generated implications for the conceptual design process. An extensive loads and stability analysis for ultimate and fatigue loads according to the procedure of the IEC 61400-3 offshore wind turbine design standard was performed with the verified TLP model. This report compares the loads for the wind turbine on the TLP to those of an equivalent land-based turbine. Major instabilities for the TLP are identified and described.

15. SUBJECT TERMS
floating; offshore platform; tension leg platform; aero hydro-servo elastic; design code FAST; offshore wind turbine design

16. SECURITY CLASSIFICATION OF:			17. LIMITATION OF ABSTRACT	18. NUMBER OF PAGES	19a. NAME OF RESPONSIBLE PERSON
a. REPORT	b. ABSTRACT	c. THIS PAGE			19b. TELEPHONE NUMBER (*Include area code*)
Unclassified	Unclassified	Unclassified	UL		

Standard Form 298 (Rev. 8/98)
Prescribed by ANSI Std. Z39.18

F1146-E(10/2008)